New Techniques and Technologies for Remote Sensing of Volcanic Ash and SO_2 Gas

Fred Prata

Climate and Atmosphere Department, NILU, Norway

NILU Norsk institutt for luftforskning

Overview

Types of volcanic activity

Remote sensing of “volcanic clouds”

Ash detection – IR techniques

Examples

SO2 gas detection – IR techniques

The emphasis will be on the use of remote sensing to measure and assess these effects

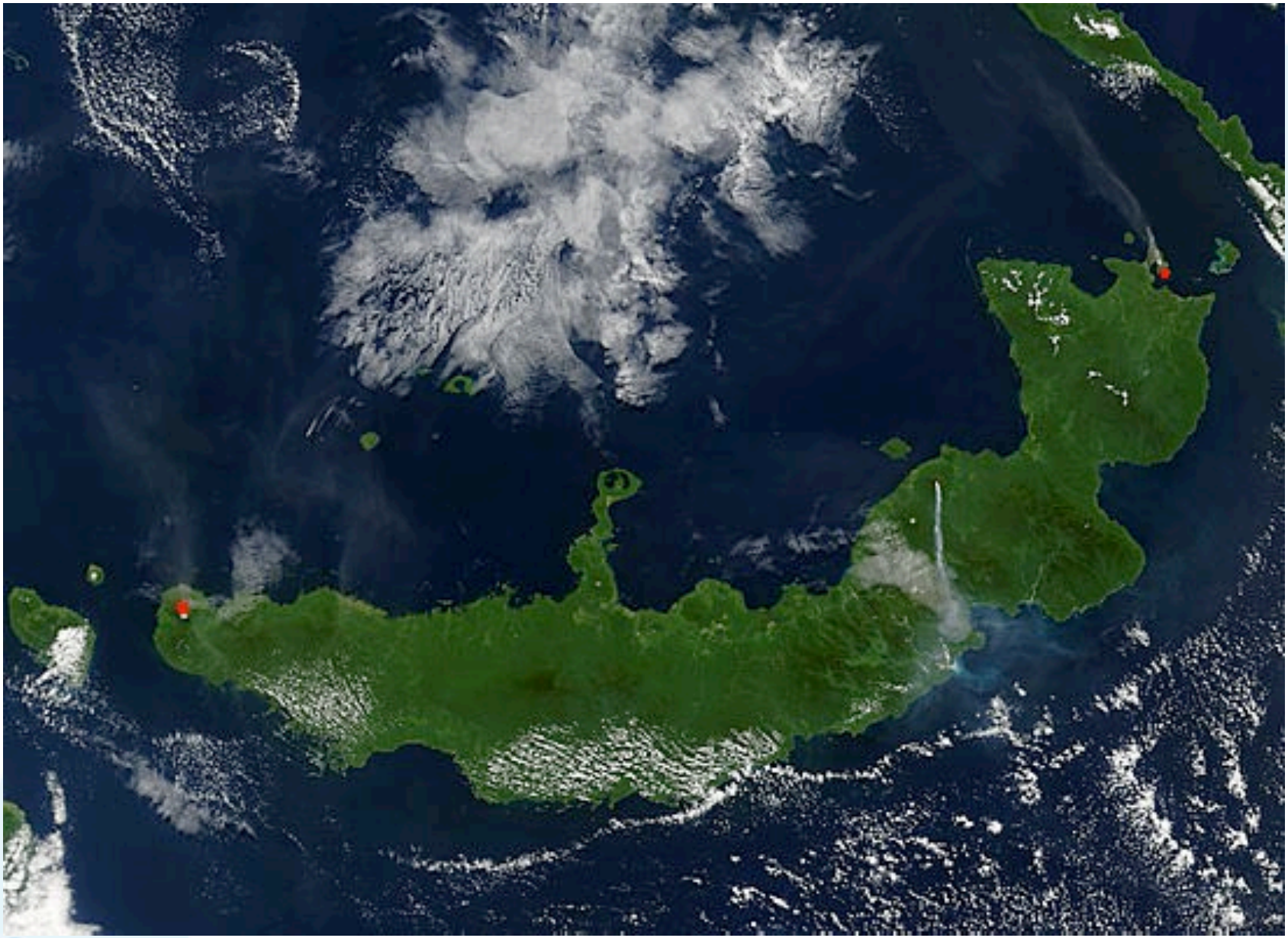

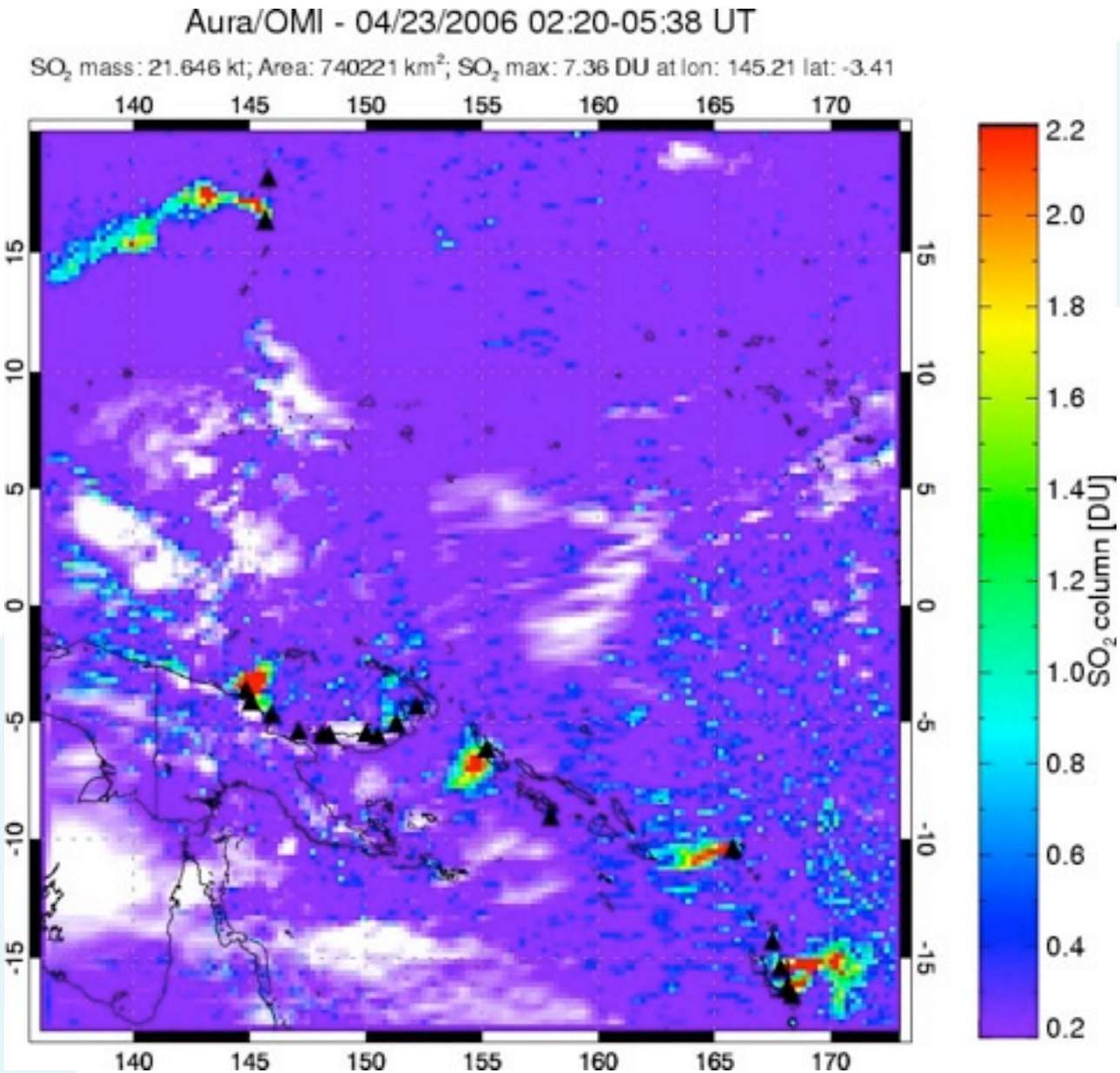
Aura/OMI - 04/23/2006 02:20-05:38 UT
SO2 mass: 21.646 kt; Area: 740221 km2; SO2 max: 7.36 DU at lon: 145.21 lat: -3.41
140
145
150
155
160
165
170
15
10
5
0
-5
-10
-15
2.2
2.0
1.8
1.6
1.4
1.2
1.0
0.8
0.6
0.4
0.2
SO2 column [DU]

The Volcanic Explosivity Index (VEI)

VEI	Description	Volume (m^3)	Height (km)	Type	Number
0	Non-explosive	10^4	0.1	Hawaiian	699
1	Small	10^6	1	Strombolian	845
2	Moderate	10^7	5	Vulcanian	3477
3	Moderate-large	10^8	15	Vulcanian	869
4	Large	10^9	25	Plinian	278
5	Very large	10^{10}	>25	Ultra-Plinian	84
6		10^{11}	>25	Ultra-Plinian	39
7		10^{12}	>25	Ultra-Plinian	4
8		10^{13}	>25	Ultra-Plinian	1?

VEI~2
Every 2 weeks

VEI~6
Krakatau

VEI~5
MtStHelens

VEI~7
Tambora

Local effects

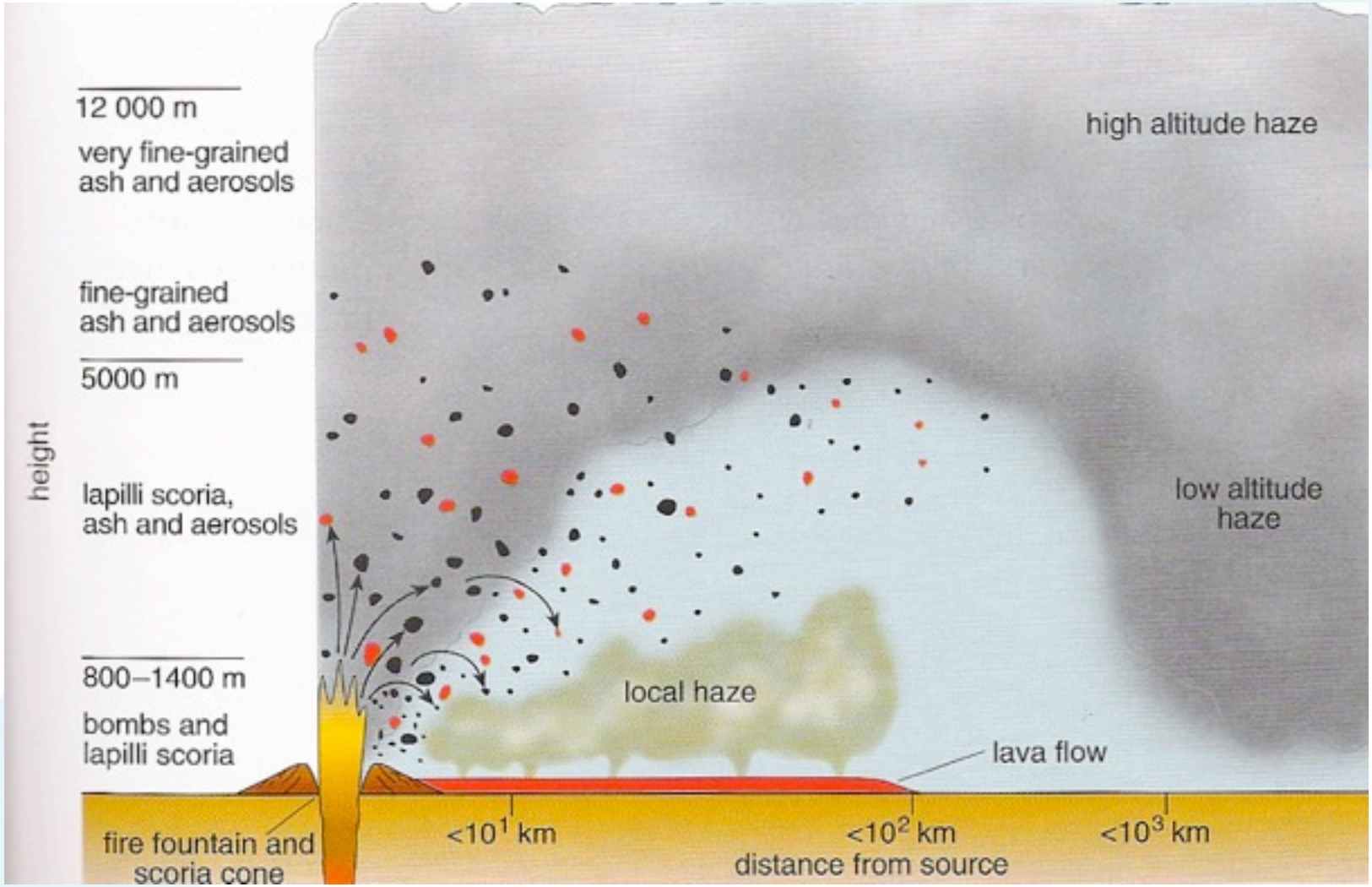

Volcanoes and Climate

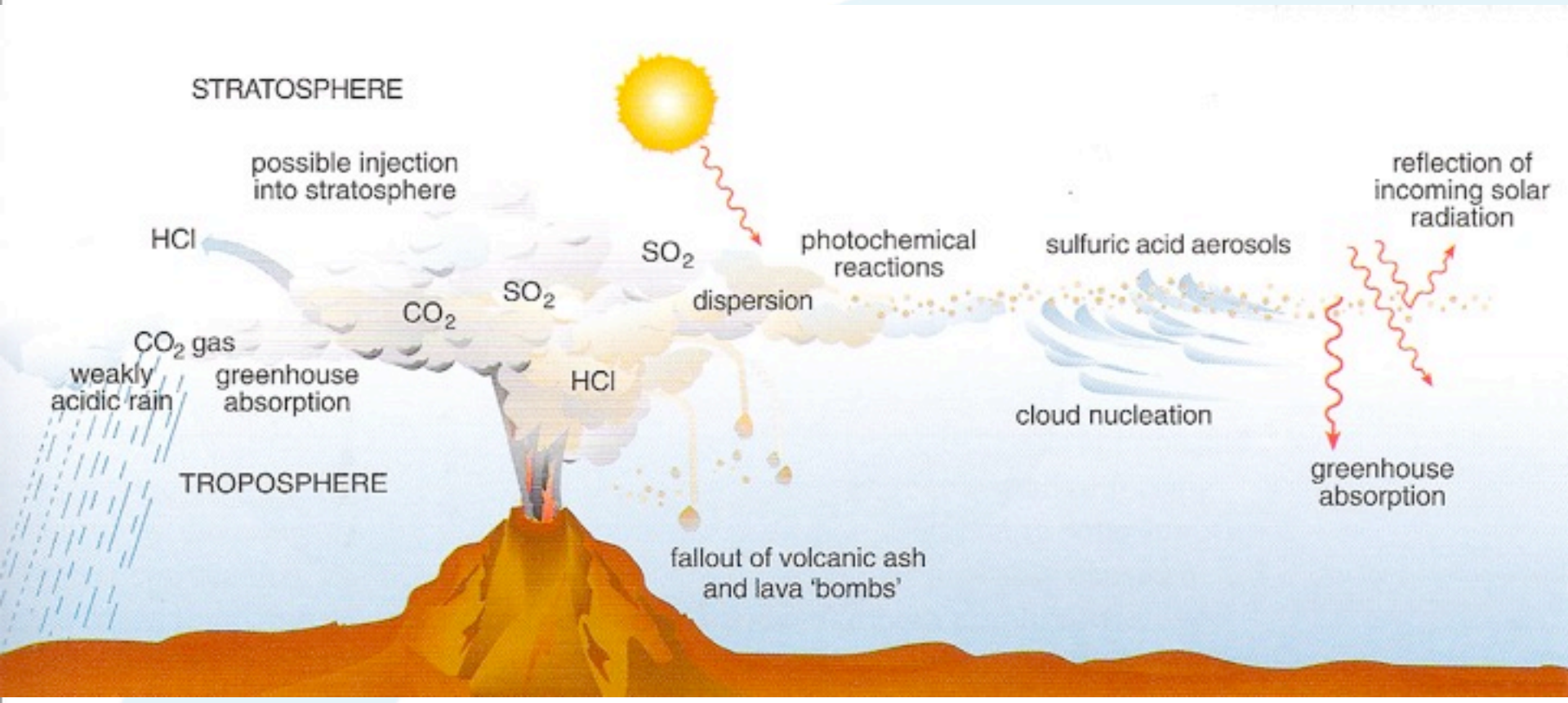

Cooling Effects

~18 Tg

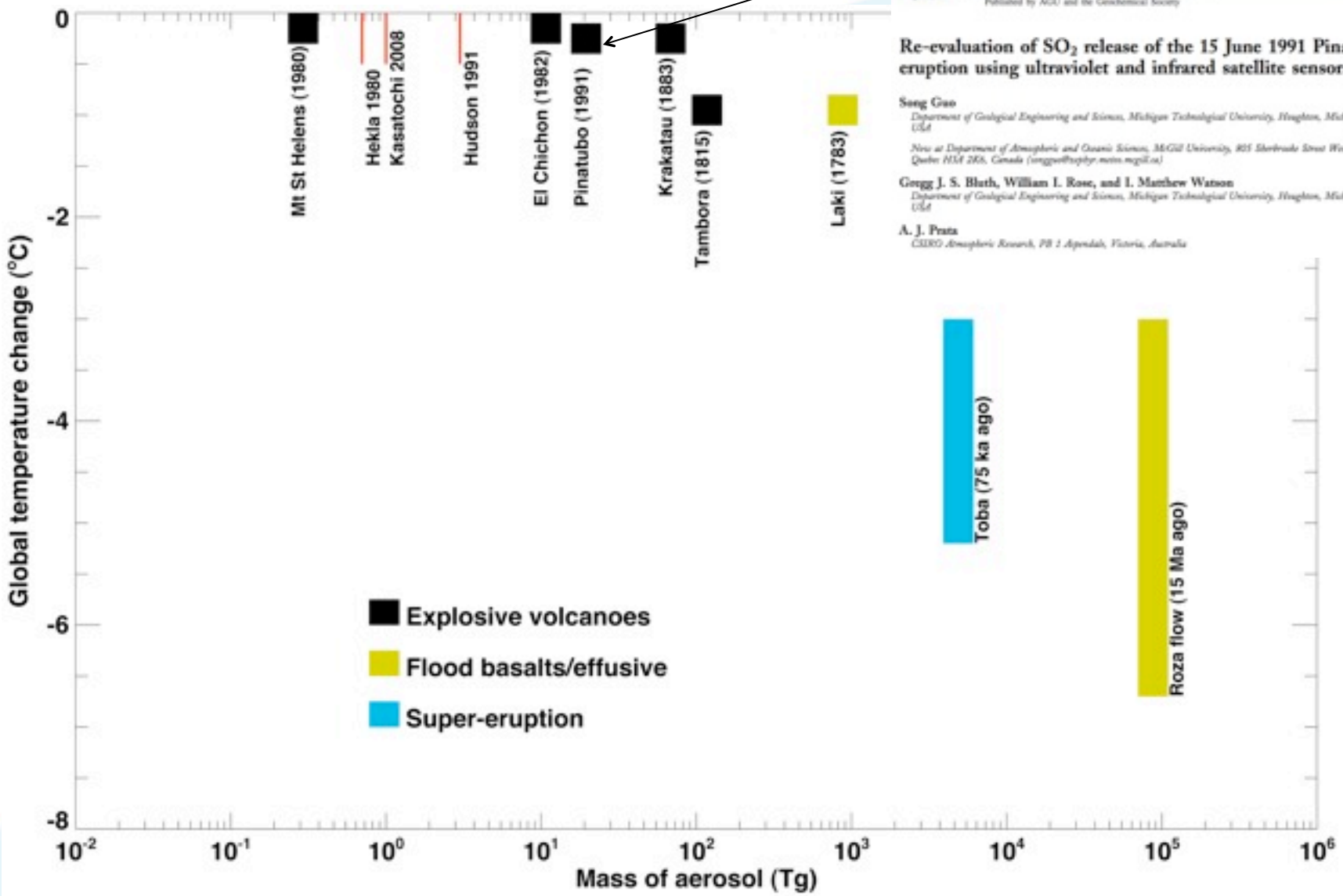

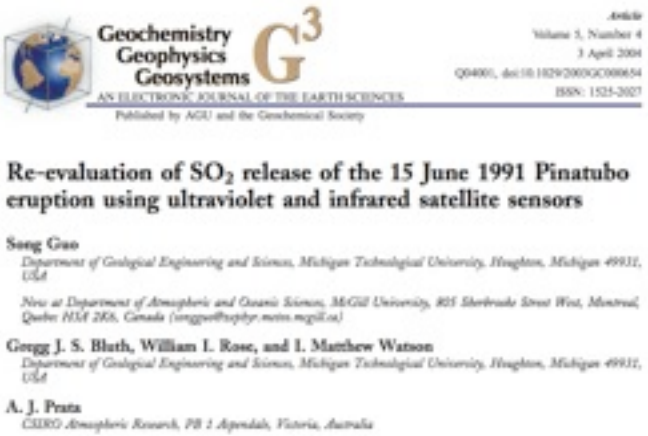
Geochemistry Geophysics Geosystems G3

AN ELECTRONIC JOURNAL OF THE EARTH SCIENCES

Re-evaluation of SO_2 release of the 15 June 1991 Pinatubo eruption using ultraviolet and infrared satellite sensors

Song Guo

Gregg J. S. Bluth, William I. Rose, and I. Matthew Watson

A. J. Prata

Aviation Hazards

- Plugged cooling holes
- Erosion of edges
- Ash build-up

Eruptions Affecting North Pacific Air Routes During the 1990's

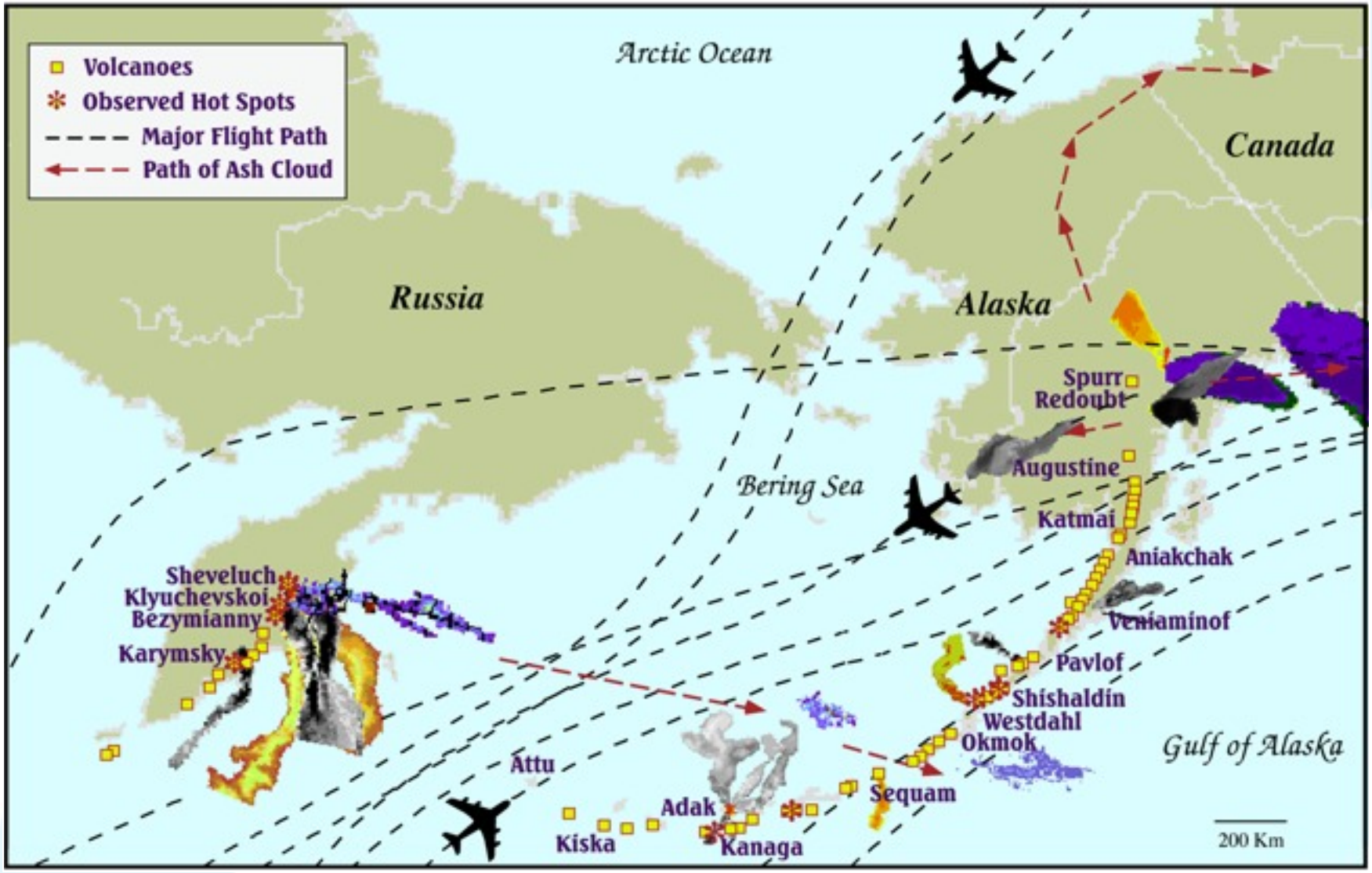

Growth in aviation traffic

Region	Annual average growth rate of passengers (percentage) 2001-2005	
Europe	2.3	4.5
Africa	3.3	5.0
Middle East	6.4	4.0
Asia and Pacific	4.1	7.5
North America	1.8	5.0
Latin America and Caribbean	2.9	4.5
World	2.7	6.0

Freight & mail
(% change in ton-km)

Source: International Civil Aviation Organisation

Global aviation threat

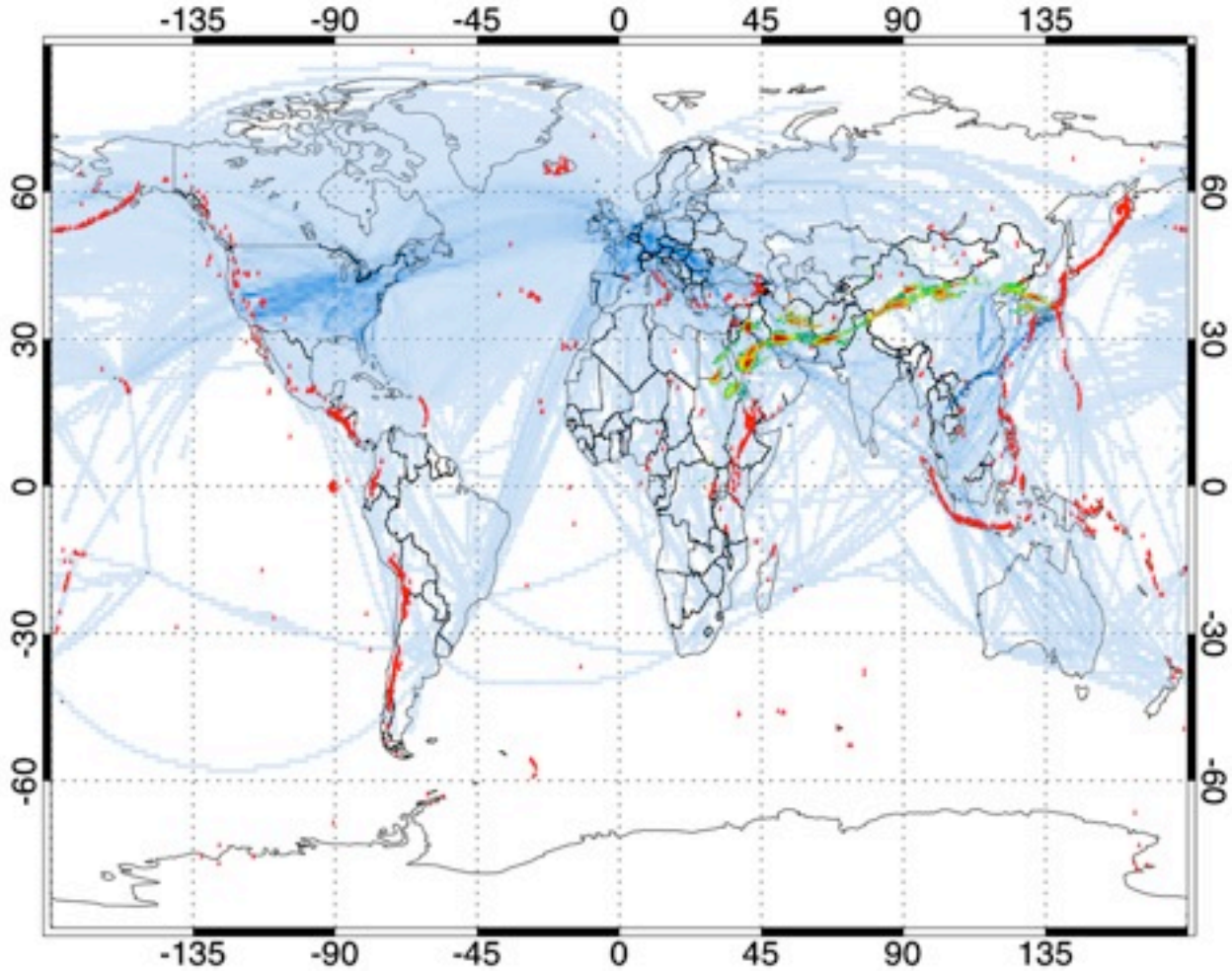

Remote sensing of volcanic clouds

OMI - SO_2, aerosols, BrO

TES - SO_2, HCl

MLS - strat. SO_2, HCl

MODIS - SO_2, ash, sulfate

AIRS - UTLS SO_2, aerosols, SO_2 profile?

CALIPSO - cloud height, aerosol type

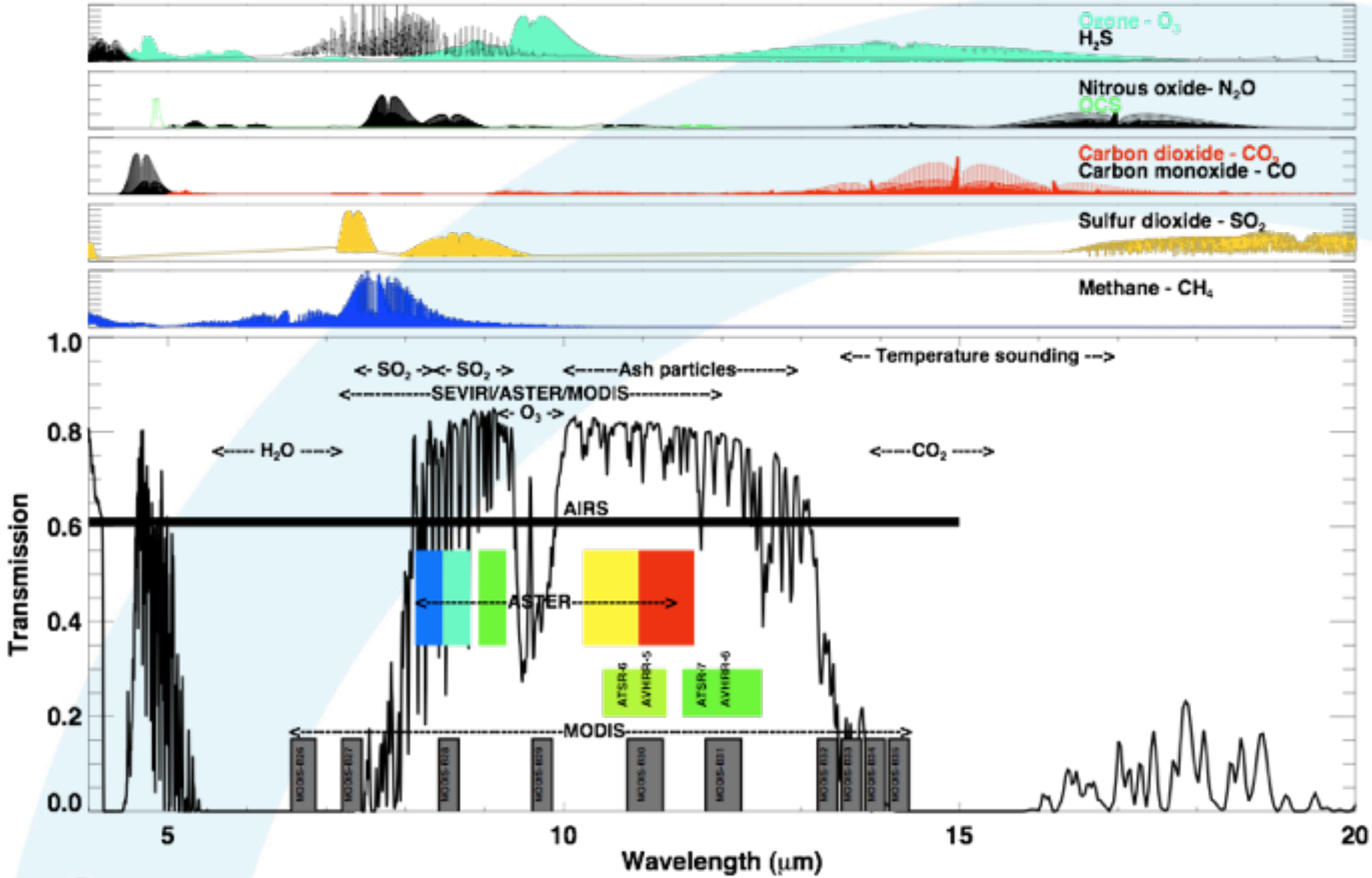
Ozone - O_3
H_2S
Nitrous oxide- N_2O
OCS
Carbon dioxide - CO_2
Carbon monoxide - CO
Sulfur dioxide - SO_2
Methane - CH_4
<- SO_2 -><- SO_2 ->
<------Ash particles------->
<-- Temperature sounding -->
<----------SEVIRI/ASTER/MODIS---------->
<- O_3 ->
<---- H_2O ---->
<----CO_2 ---->
AIRS
<----------ASTER---------->
ATSR-6
AVHRR-5
ATSR-7
AVHRR-6
<----------MODIS---------->
Transmission
1.0
0.8
0.6
0.4
0.2
0.0
5
10
15
20
Wavelength (μm)

Detection

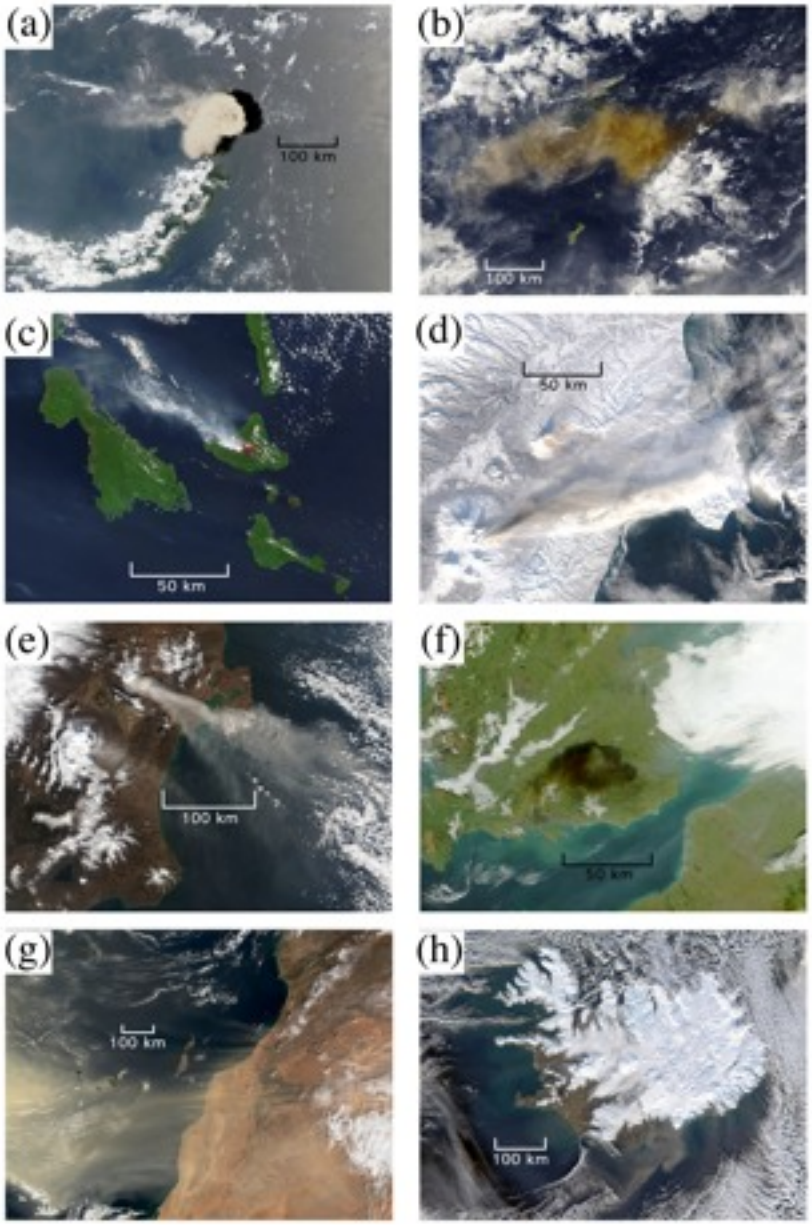

Volcanic ash – Detection and discrimination

Prata, A. J., 1989, Infrared radiative transfer calculations for volcanic ash,
Geophys. Res. Lett., 16(11), 1293–1296

$$T_{11} - T_{12} < 0$$

"reverse absorption" algorithm

$$\Delta T = \Delta T_c [X - X^{\beta}],$$

$$X = 1 - \frac{\Delta T_4}{\Delta T_c},$$

$$\Delta T = T_4 - T_5, \quad \Delta T_c = T_s - T_c, \quad \Delta T_4 = T_s - T_4.$$

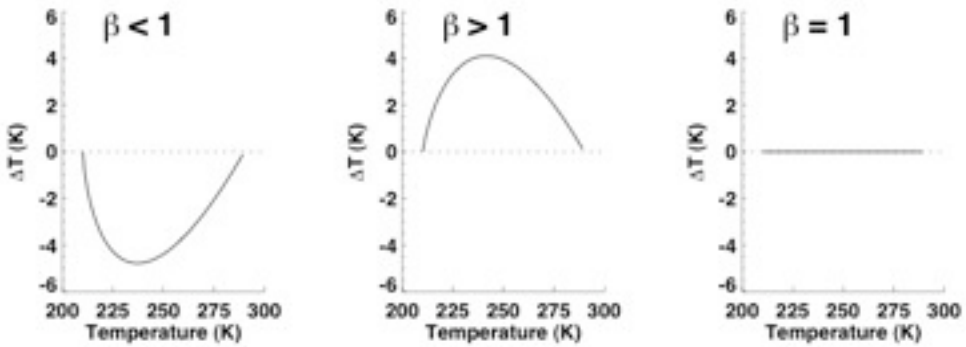

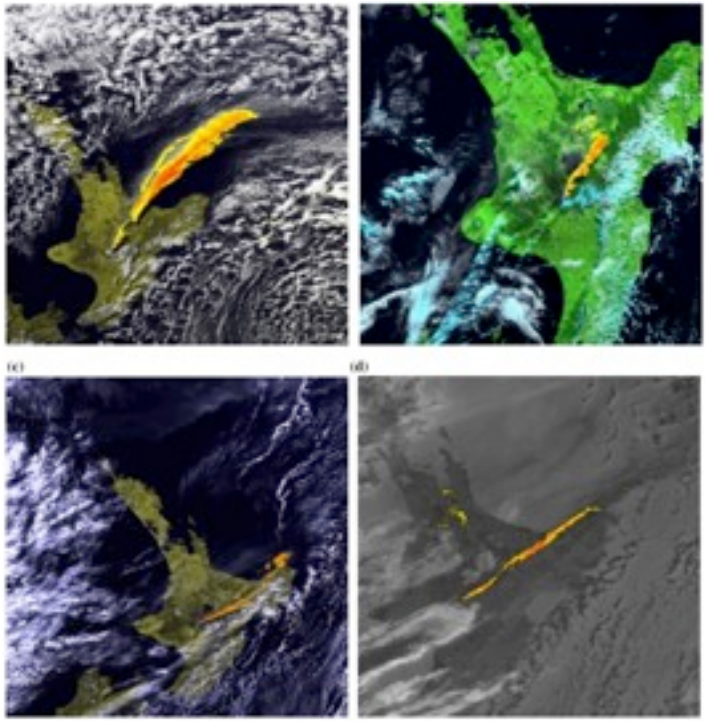

Operational use of the
“reverse absorption” algorithm

Kasatochi eruption

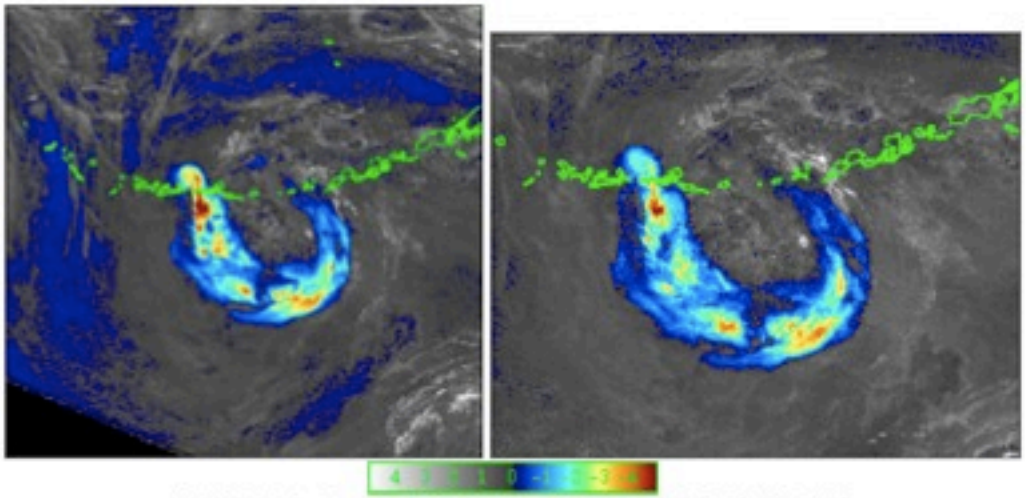

AVHRR 4m5 – Left: NOAA-15 2008/08/08 16:41 UTC
AVHRR 4m5 – Right: NOAA-16 2008/08/08 17:09 UTC

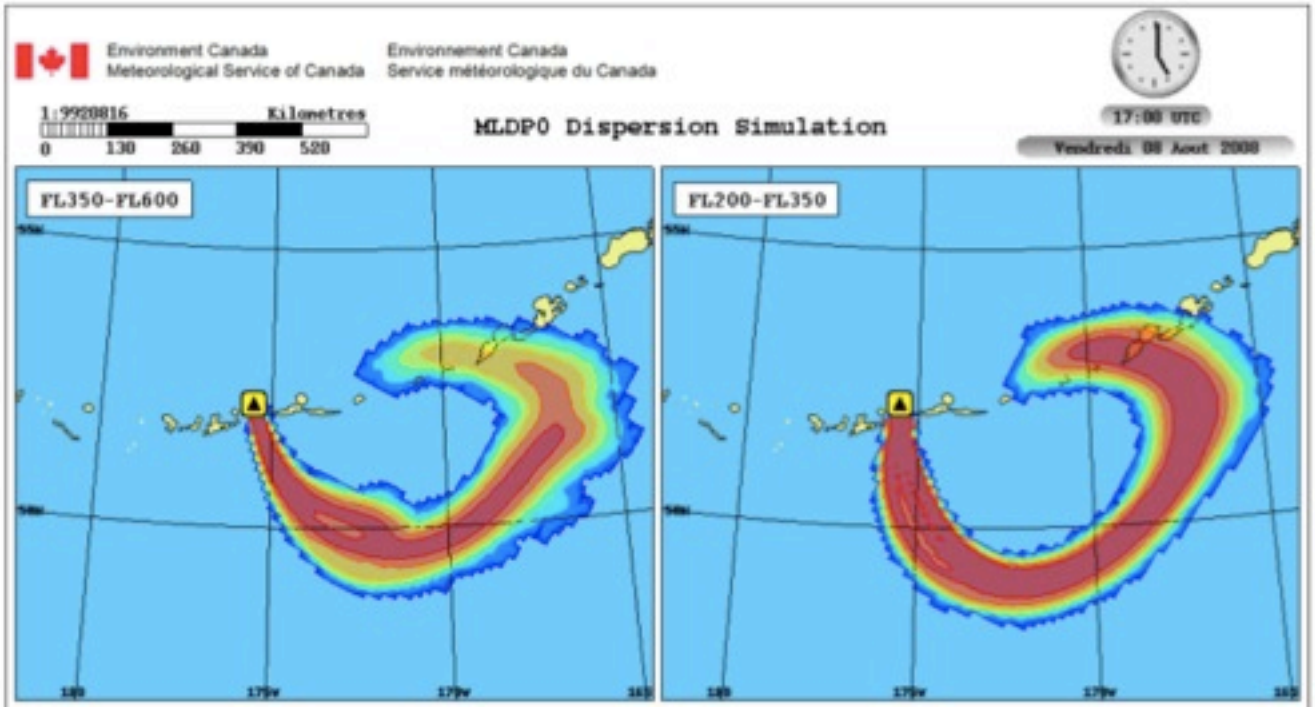

Quantitative products

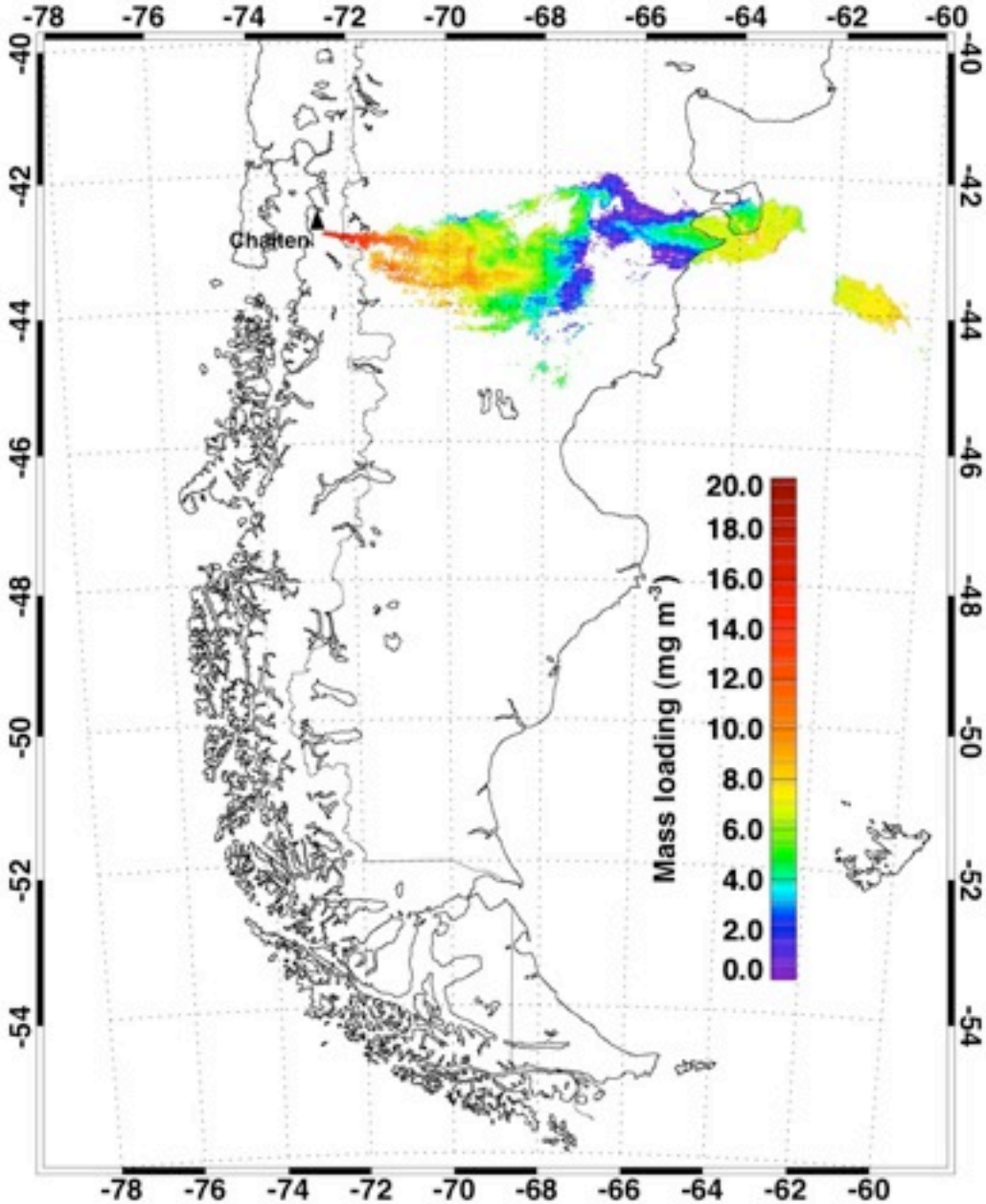

Ash Index

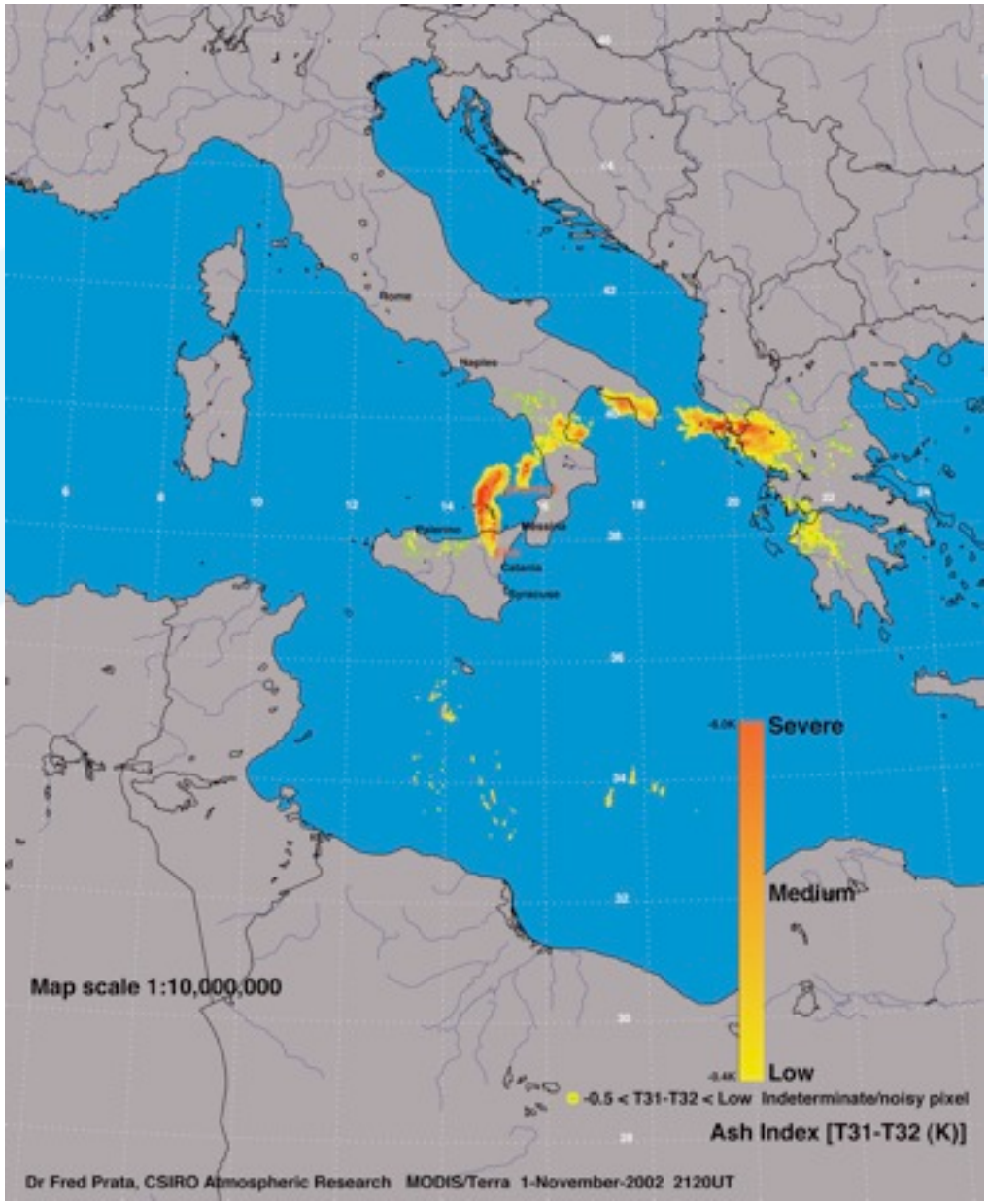
Severe
Medium
Low
Map scale 1:10,000,000
-0.5 < T31-T32 < Low Indeterminate/noisy pixel
Ash Index [T31-T32 (K)]
Dr Fred Prata, CSIRO Atmospheric Research MODIS/Terra 1-November-2002 2120UT

Ash Index for Eyjafjallajokull

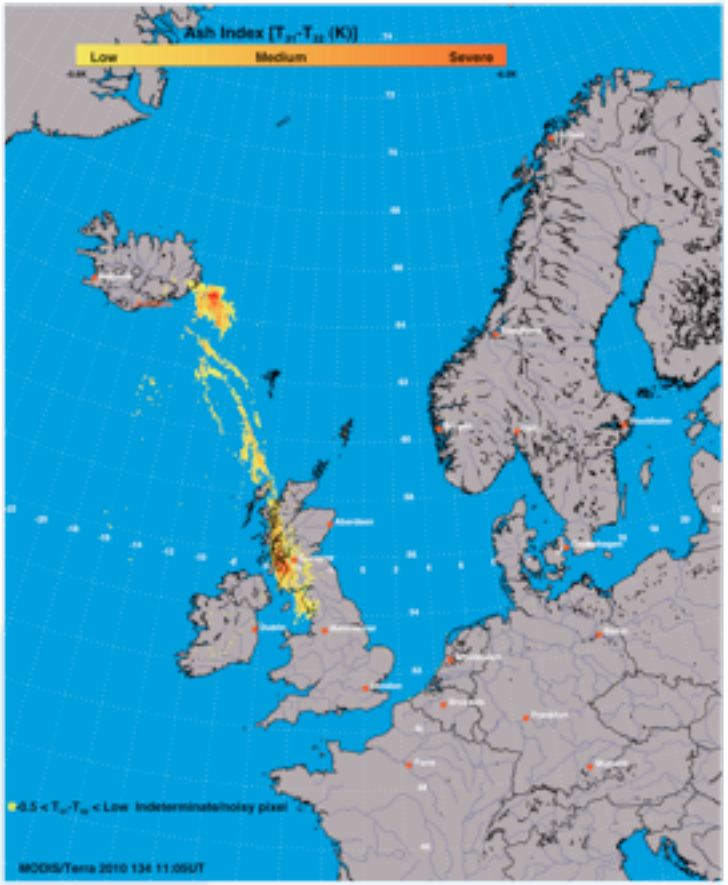

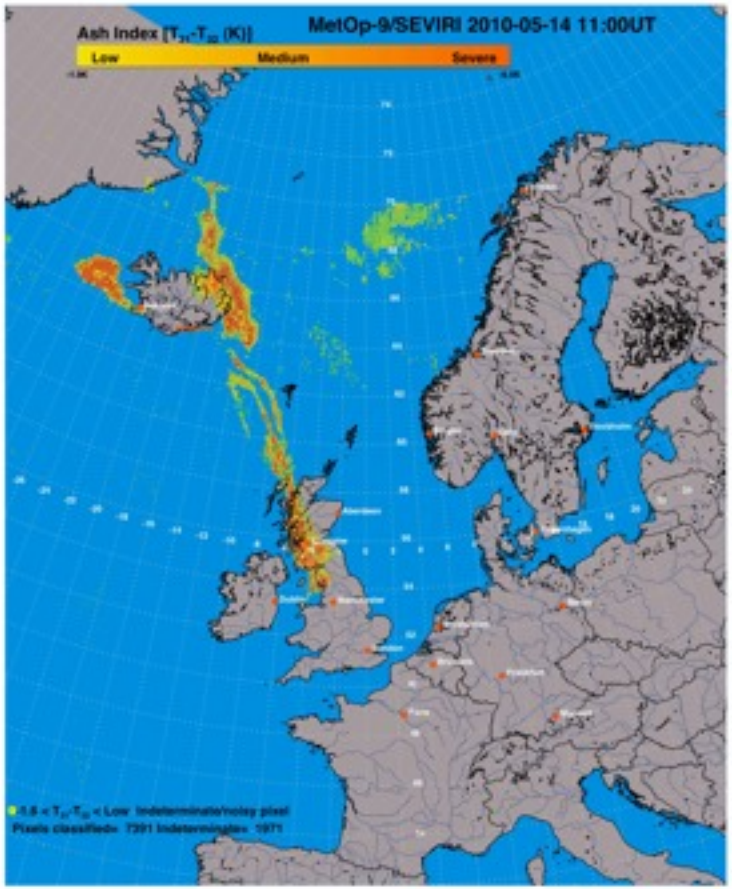

Summary of Ash Detection Methods

Table 1 Summary of ash detection algorithms and techniques used with satellite infrared (IR) and visible channel data

Name	Principle	Reference
RA	2-band IR (11 and 12 μm)	Prata (1989a, b)
Ratio	2-band IR (11 and 12 μm)	Holasek and Rose (1991)
4-band	IR + visible	Mosher (2000)
TVAP	3-band IR (3.9, 11 and 12 μm)	Ellrod et al. (2003)
PCI	Multi-band principal components	Hillger and Clark (2002a, b)
WVC	2-band IR + water vapour correction	Yu et al. (2002)
RAT	3-band IR (3.5, 11, 12 μm)	Pergola et al. (2004)
3-band	3-band (IR and visible)	Pavolonis et al. (2006)

RA = Reverse absorption; TVAP = Three band volcanic ash product; PCI = Principle components; RAT = Ratio method; WVC = Water vapor correction method

Prata, A. J., 2009, Satellite detection of hazardous volcanic clouds and the risk to global air traffic, ***Nat. Haz., 51, 303–324.***

VAAC	GEO Satellite(s)	Temporal Refresh	Spectral Capabilities	Next Generation GEO Satellite
Anchorage	GOES-11	30 minutes	Split-window	GOES-R (2015)
Buenos Aires	GOES-12 GOES-13 MSG	15 minutes 180 minutes 15 minutes	No split-window No split-window Advanced	GOES-R (2015) and **MTG (~2018)**
Darwin	MTSAT FY2D FY2E	60 minutes 60 minutes 60 minutes	Split-window Split-window Split-window	GOES-R like from JMA (2020?) and **FY4A from China (2014)**
London	MSG	15 minutes	Advanced	**MTG (~2018)**
Montreal	GOES-11 GOES-13	30 minutes 15 or 30 minutes	Split-window No split-window	GOES-R (2015)
Tokyo	MTSAT FY2D FY2E	30 minutes 60 minutes 60 minutes	Split-window Split-window Split-window	GOES-R like from JMA (2020?) and **FY4A from China (2014)**
Toulouse	MSG	5 or 15 minutes	Advanced	**MTG (~2018)**
Washington	GOES-11 GOES-12 GOES-13 MSG	30 minutes 15 minutes 15 or 30 minutes 15 minutes	Split-window No split-window No split-window Advanced	GOES-R (2015) and **MTG (~2018)**
Wellington	MTSAT GOES-11	60 minutes 180 minutes	Split-window Split-window	GOES-R like from JMA (2020?) and GOES-R (2015)

Table 1: An overview of the geostationary satellite capabilities is shown as a function of Volcanic Ash Advisory Center (VAAC). The table summarizes the temporal and spectral capabilities (those relevant to volcanic ash remote sensing) of each instrument that covers each VAAC area of responsibility. In addition, future geostationary satellite capabilities are summarized. Next generation satellites that include a hyperspectral sounding capability are shown in bold.

NILU

A closer Look at Ash Detection using SEVIRI

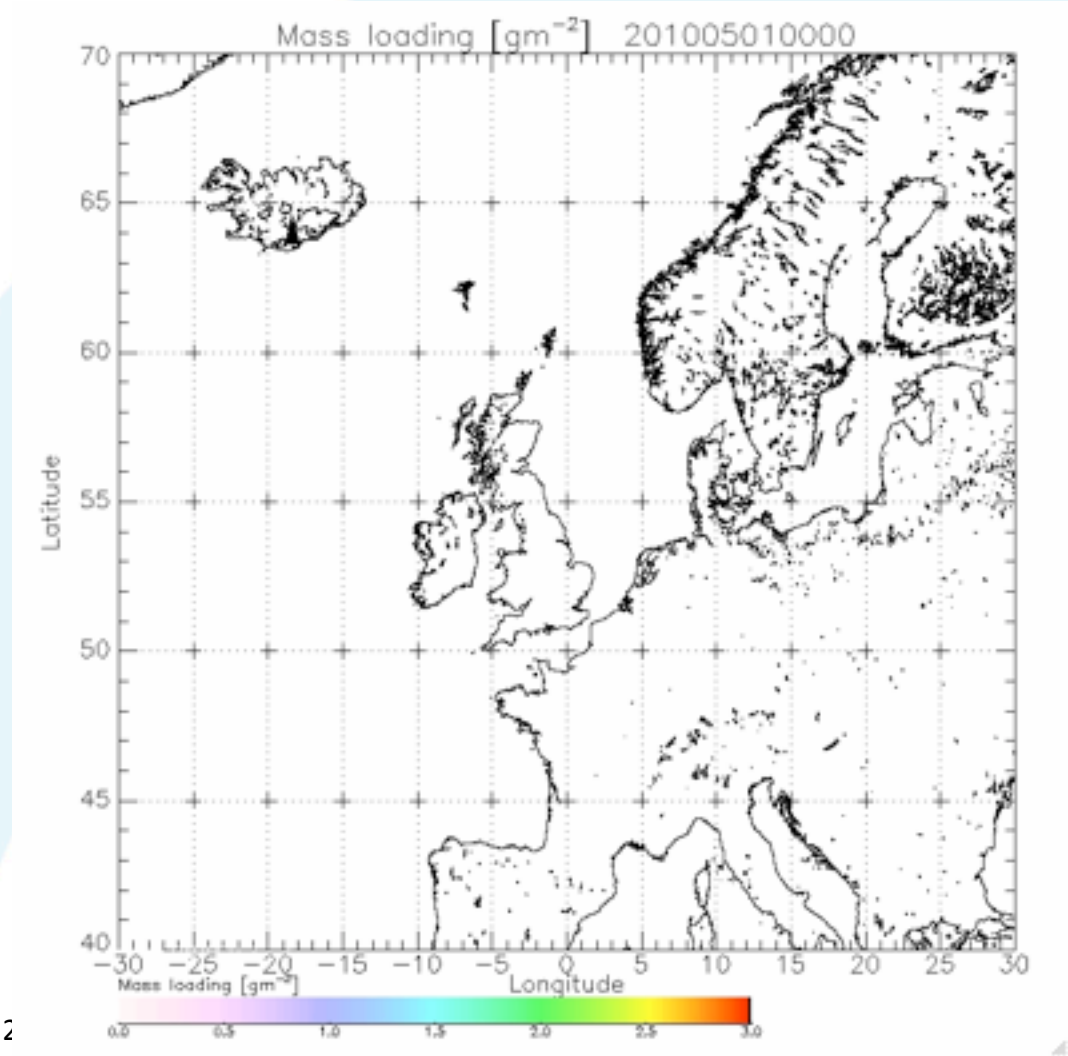

SEVIRI

IR channels

6.3 µm
7.4 µm
8.6 µm
9.7 µm
10.8 µm
12.0 µm
13.2 µm

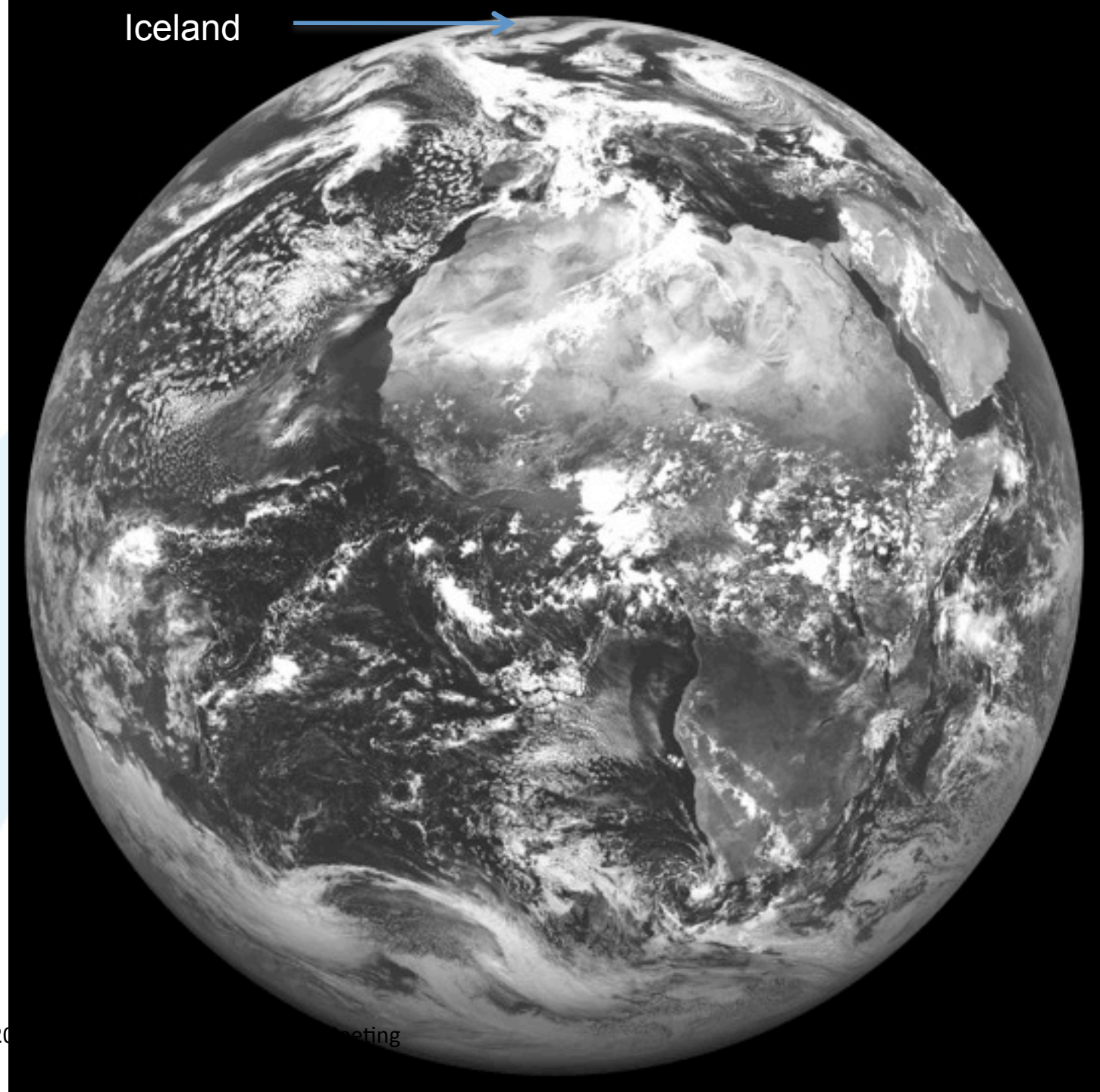

SEVIRI T_{12}

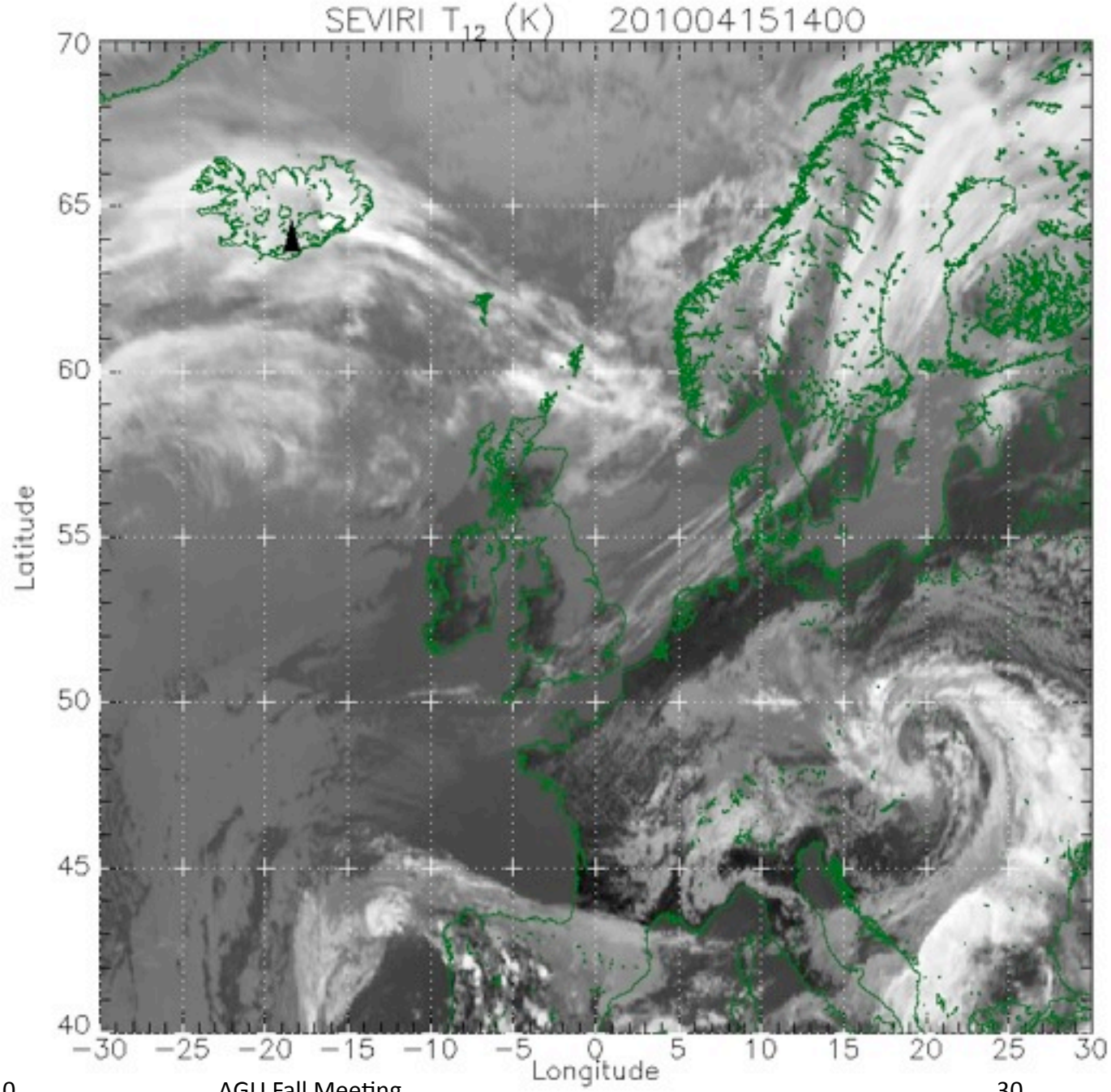
SEVIRI T_{12} (K) 201004151400
Latitude
70
65
60
55
50
45
40
−30 −25 −20 −15 −10 −5 0 5 10 15 20 25 30
Longitude

SEVIRI $T_{11}-T_{12}$

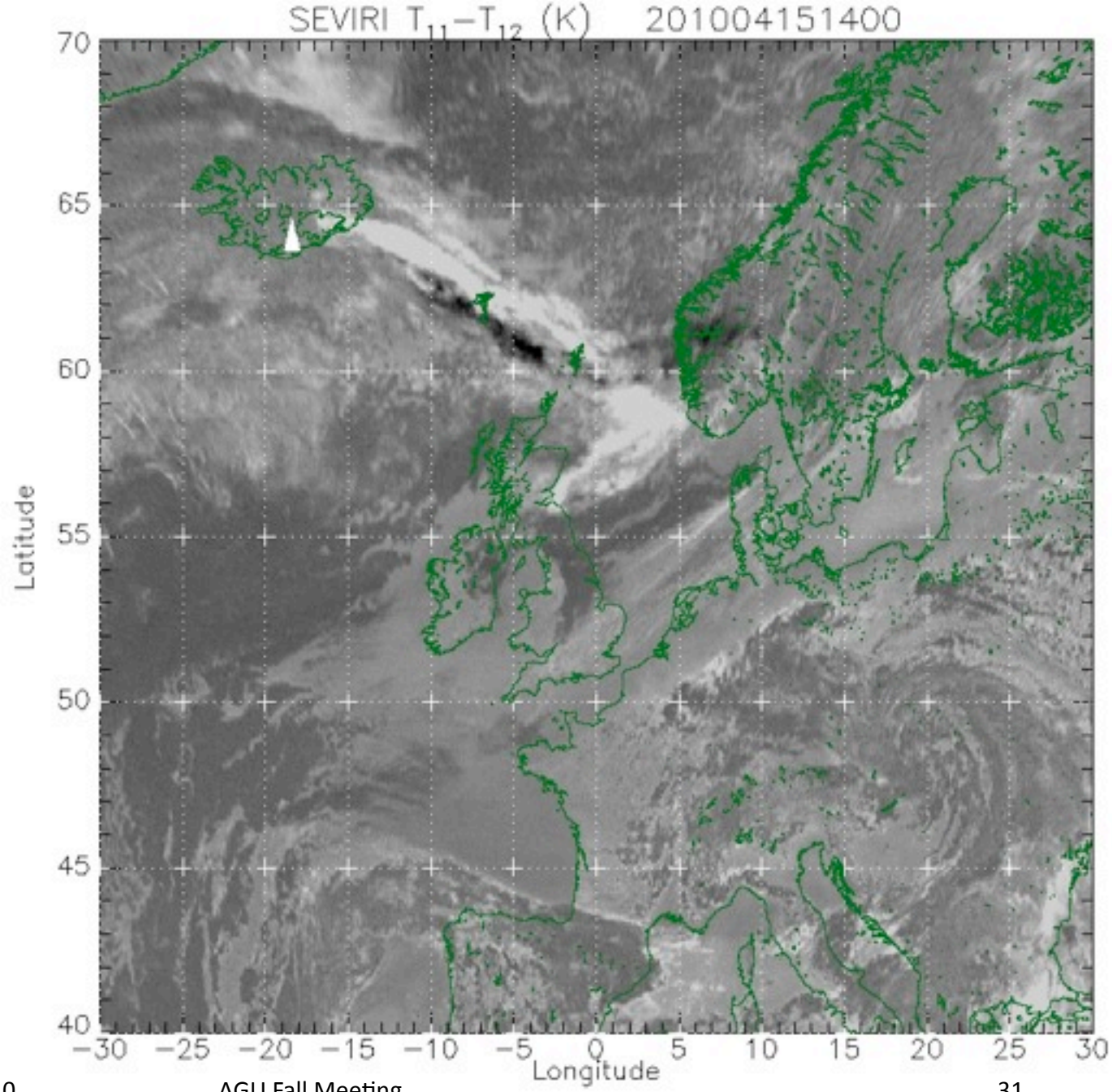

Computer Lab Example

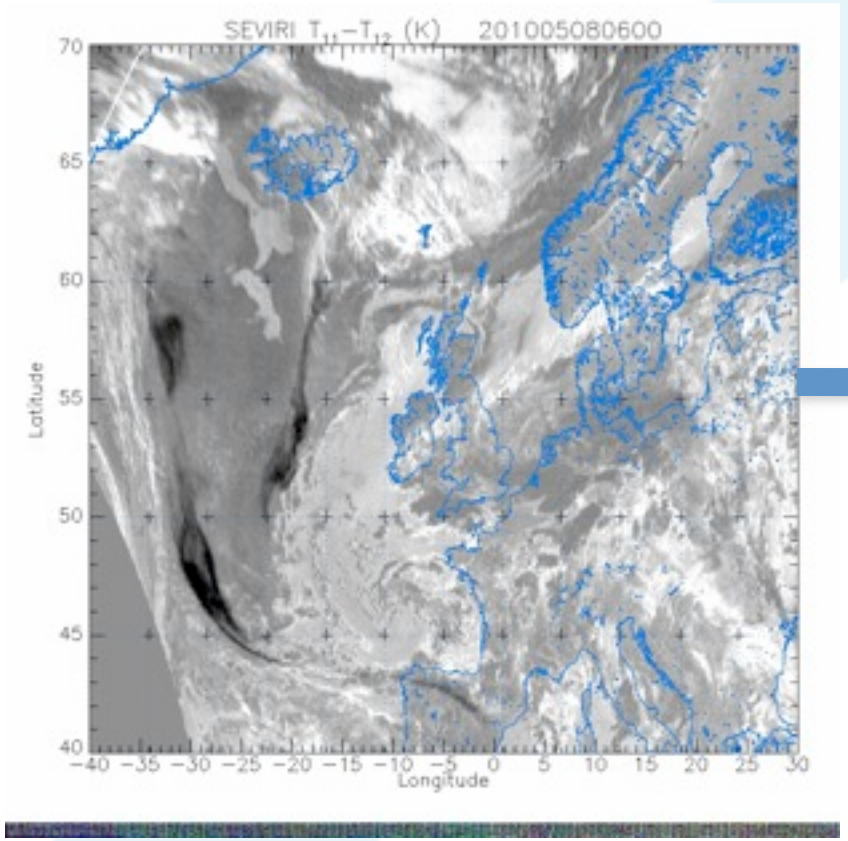

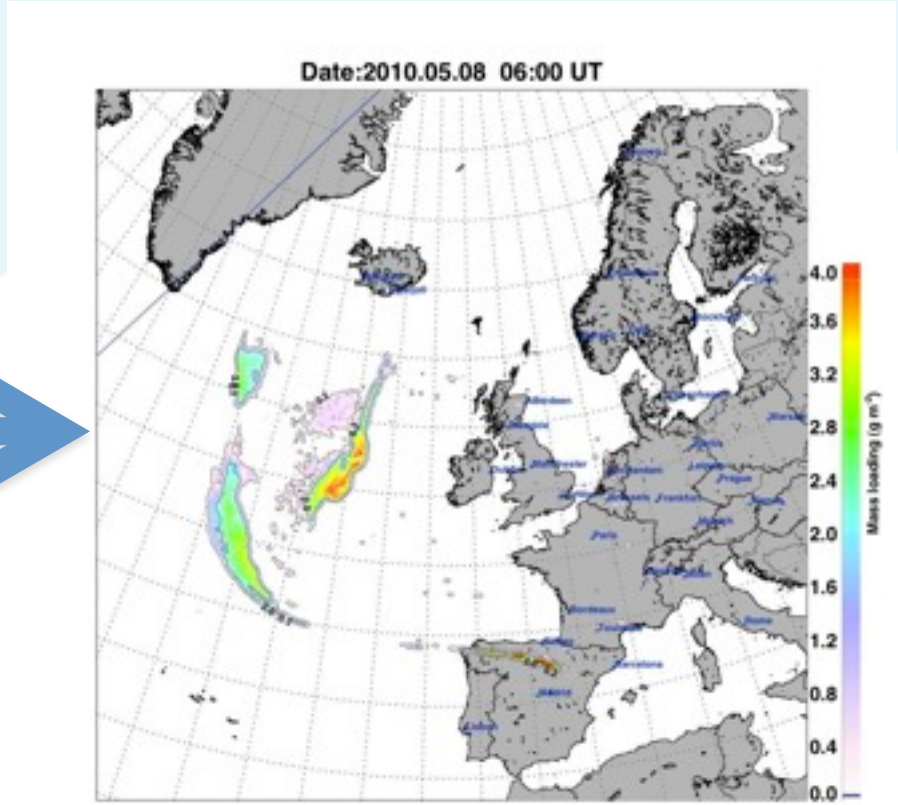

Parametric equations

$$T_4 = \epsilon_4 T_c + (1 - \epsilon_4) T_s$$

$$T_5 = \epsilon_5 T_c + (1 - \epsilon_5) T_s$$

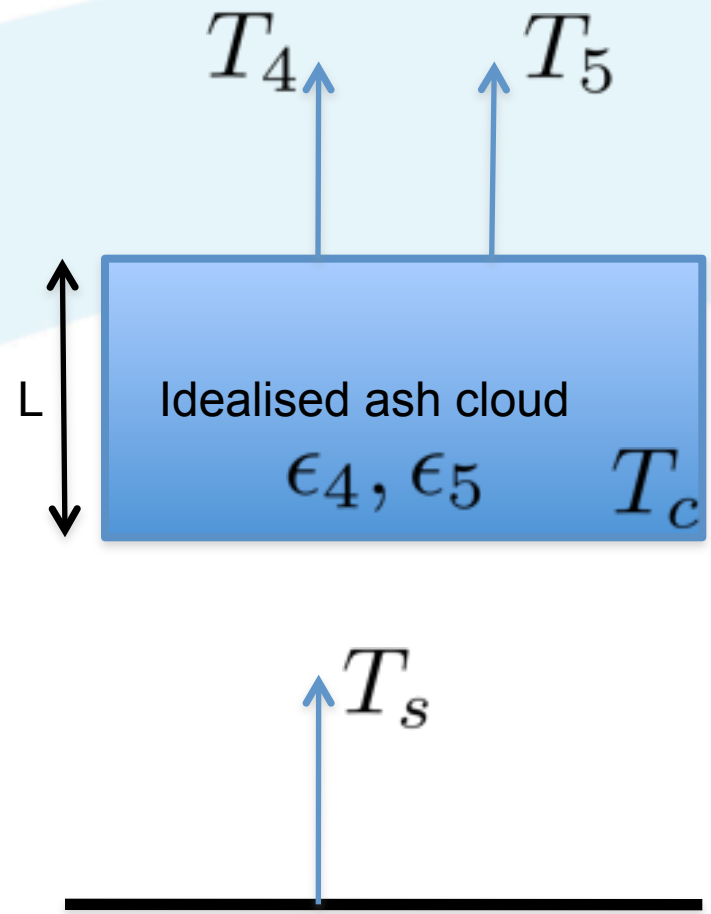

Solve these for:

$$\Delta T = T_4 - T_5$$

Denoting:

$$\Delta T_4 = T_s - T_4$$

$$\Delta T_{tcon} = T_s - T_c$$

$$\left.\begin{aligned} \Psi &= 1 - \frac{\Delta T_4}{\Delta T_{tcon}} \\ \epsilon_i &= 1 - \exp(-k_i L) \end{aligned}\right\} \quad \Psi_i = 1 - \epsilon_i$$

"like" cloud optical depth

$$\beta = \frac{k_j}{k_i} \qquad \lambda_j > \lambda_i$$

Particle microphysics - radius

Solution

$$\Delta T = \Delta T_{tcon}(\Psi - \Psi^{\beta})$$

$$\beta > 1 \qquad ice/water - cloud$$

$$\beta < 1 \qquad ash - cloud$$

Note that: $\Psi < 1$

Solving for radius and optical depth

Given T_4 and Ψ it is possible to construct "theoretical curves" that suggest the behaviour of "real" measurements on a plot of T_4 vs ΔT

Volcanic ash – Detection and discrimination

Prata, A. J., 1989, Infrared radiative transfer calculations for volcanic ash,
Geophys. Res. Lett., 16(11), 1293–1296

$$T_{11} - T_{12} < 0$$

"reverse absorption" algorithm

$$\Delta T = \Delta T_c [X - X^{\beta}],$$

$$X = 1 - \frac{\Delta T_4}{\Delta T_c},$$

$$\Delta T = T_4 - T_5, \quad \Delta T_c = T_s - T_c, \quad \Delta T_4 = T_s - T_4.$$

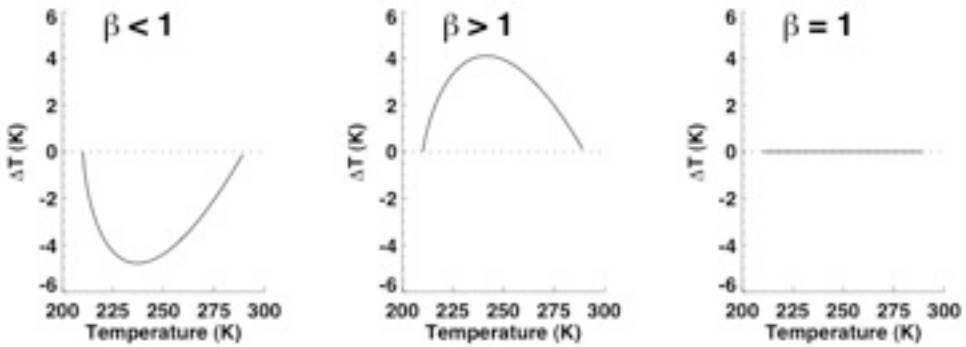

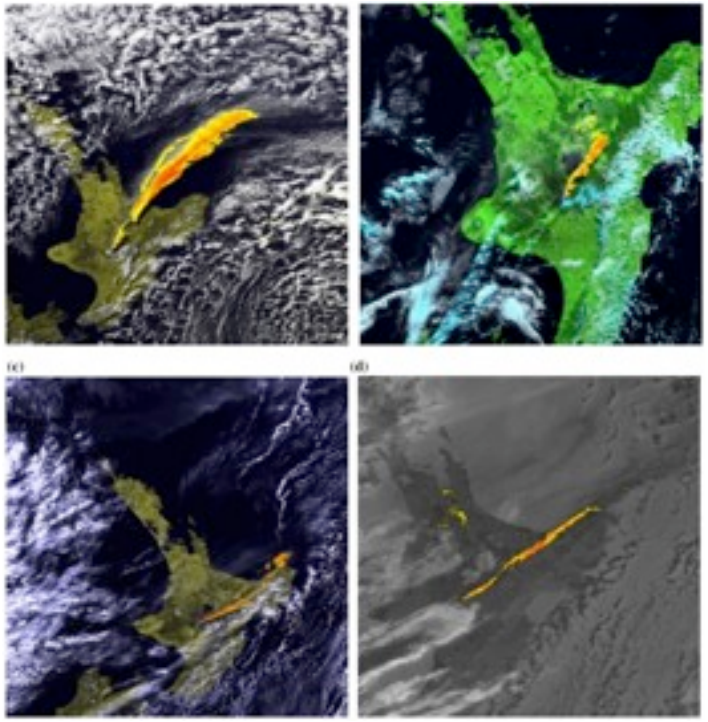

Theory and Measurement

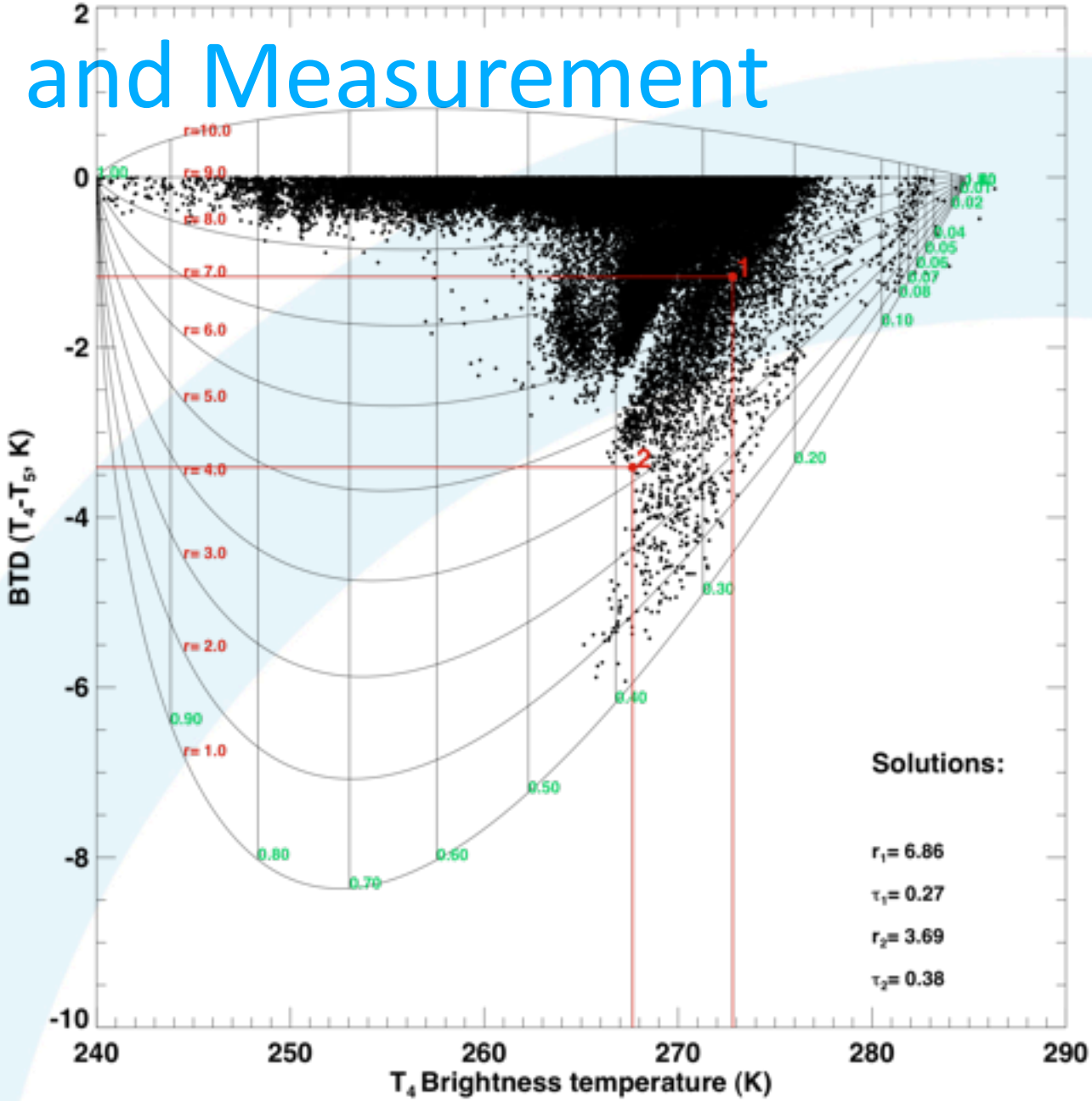

Calculating the mass loading (gm^{-2})

$$M_l = \frac{4}{3}\rho\frac{r\tau}{Q_{ext}}$$

ρ	Density	Units: kg m^{-3}
Q_{ext}	Extinction efficiency	none
τ	Optical depth	none
r	Effective radius	µm

Eyjafjallajökull, April/May 2010

Methodology

- Data source: SEVIRI 12-channel 15-minute data for 30W-30E, 40N-70N, from 14.04.2010 to 24.05.2010. Only use IR channels.
- Automatically detect pixels affected by ash
- Apply water vapour correction
- Apply parallax correction
- Retrieve effective particle radius, IR optical depth and mass loading (g m^{-2})
- Validate
- Determine concentrations using coincident CALIOP space-based lidar measurements

Some problems with ash detection

Water vapour makes T_{11}-T_{12} > 0

Correction applied based on Yu et al. (2003)

Clear land at night gives T_{11}-T_{12} < 0

No good correction algorithm available

Mixed pixels

Difficult to correct for without sub-pixel data

Improvement possible for some pixels by using spatial information

Retrieval scheme

Solve the RT equation with scattering for a plane-parallel cloud:

$$\mu \frac{\partial I}{\partial \tau}(\tau, \mu) = I(\tau, \mu) - (1 - \varpi_o) B(T) \frac{\varpi_o}{2} \int_{-1}^{1} P(\mu; \mu') I(\tau, \mu') d\mu'$$

Boundary conditions:

$$I(0, -\mu) = 0$$

$$I(\tau_1, +\mu) = B(T_s)$$

Solution:

$$I(\tau, \mu_i) = \sum_j L_j W_j(\mu_i) exp(-k_j \tau) + B(T)$$

Microphysics

Refractive index as a function of wavelength.
Spherical particles.
Mie scattering equation solver

Modified-gamma and log-normal size distributions

$$\frac{dn(r)}{dr} = \frac{Nb^7}{6!} r^6 exp(-br)$$

$$\frac{dn(r)}{dr} = \frac{N}{r\sigma\sqrt{2\pi}} exp\left\{\frac{-(Ln[r] - Ln[r_o])^2}{2\sigma^2}\right\}$$

Efficiency factors for polydispersions:

$$\hat{Q}_f = \frac{\int_o^\infty \pi r^2 Q_f(\frac{2\pi r}{\lambda}, m) \frac{dn(r)}{dr} dr}{\int_o^\infty \pi r^2 \frac{dn(r)}{dr} dr}$$

Refractive indices

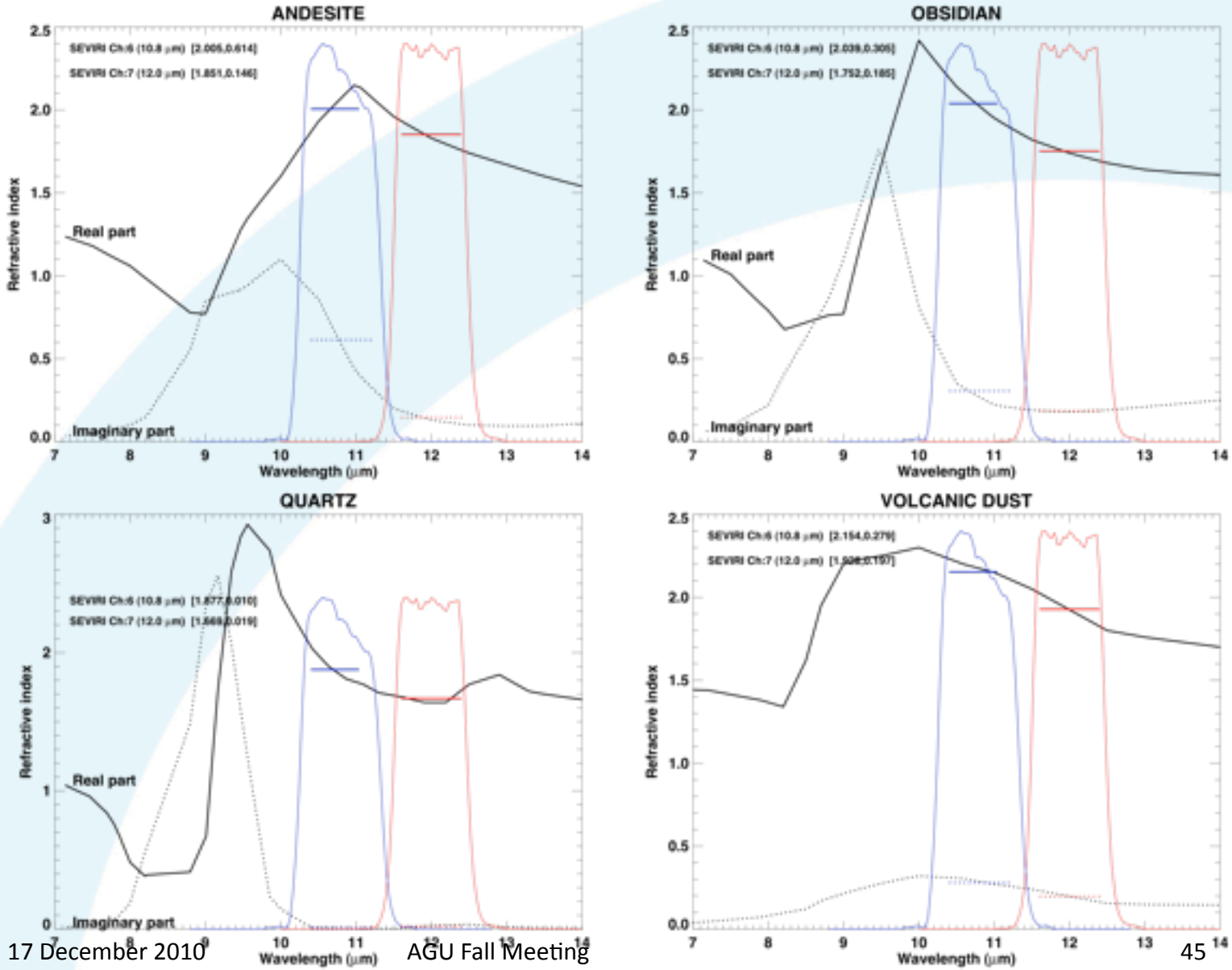

Procedure

Run Mie code for particle sizes from 0.2 to 32 µm in steps of 0.2 µm

Run RT code for all particle sizes, optical depths from 0.02 to 8, in steps of 0.02, 16 streams, and cloud-top and surface temperatures from Tc±10 K, Ts ±10 K

Generate very large look-up table containing simulated top-of-atmosphere (no water vapour) brightness temperatures

at 10.8, 12.0 µm

Use ash-identified pixels with measured BTs at

10.8 and 12.0 µm to find "best fit" to

simulations.

(Sometimes several values found).

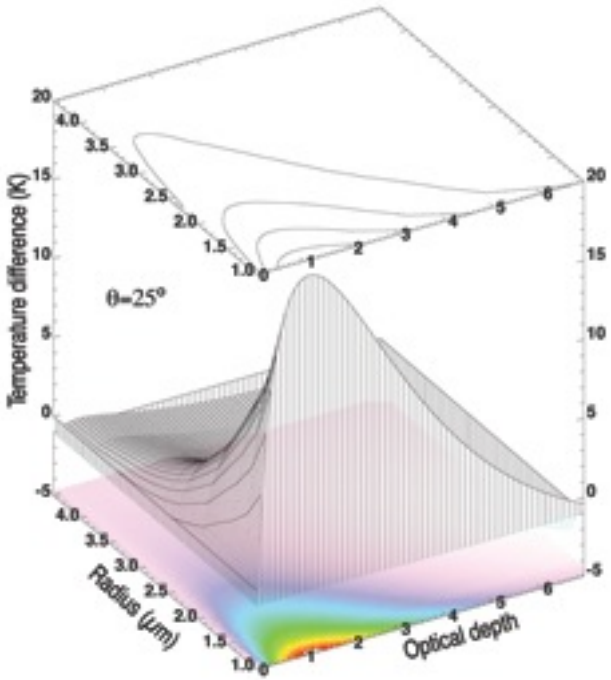

16 April 20:00 UT

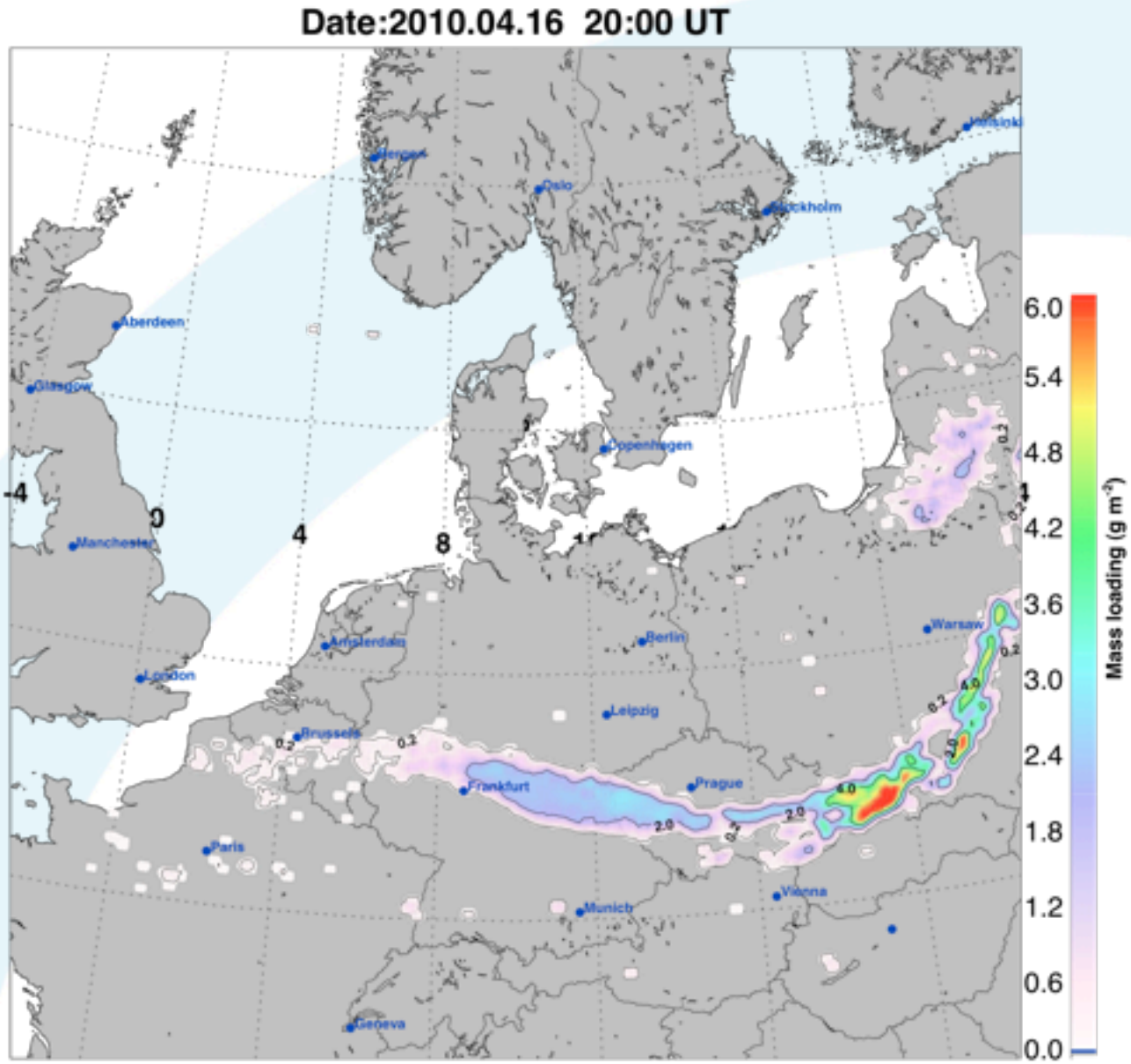

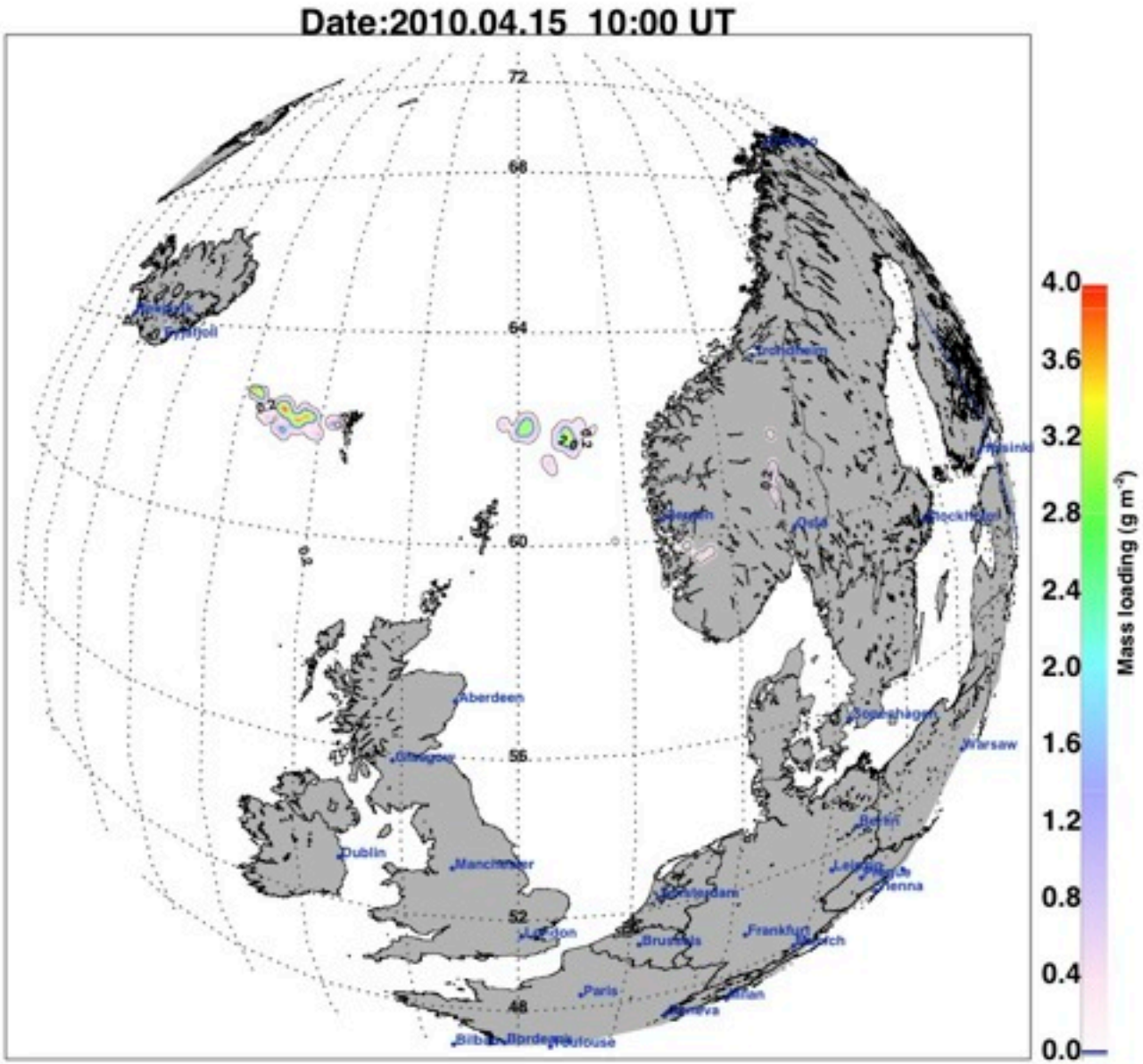
Date:2010.04.15 10:00 UT
72
68
64
60
56
52
48
Aberdeen
Glasgow
Dublin
Manchester
London
Amsterdam
Brussels
Frankfurt
Paris
Geneva
Milan
Vienna
Warsaw
Berlin
Copenhagen
Oslo
Stockholm
Helsinki
Trondheim
Toulouse
4.0
3.6
3.2
2.8
2.4
2.0
1.6
1.2
0.8
0.4
0.0
Mass loading (g m^{-2})

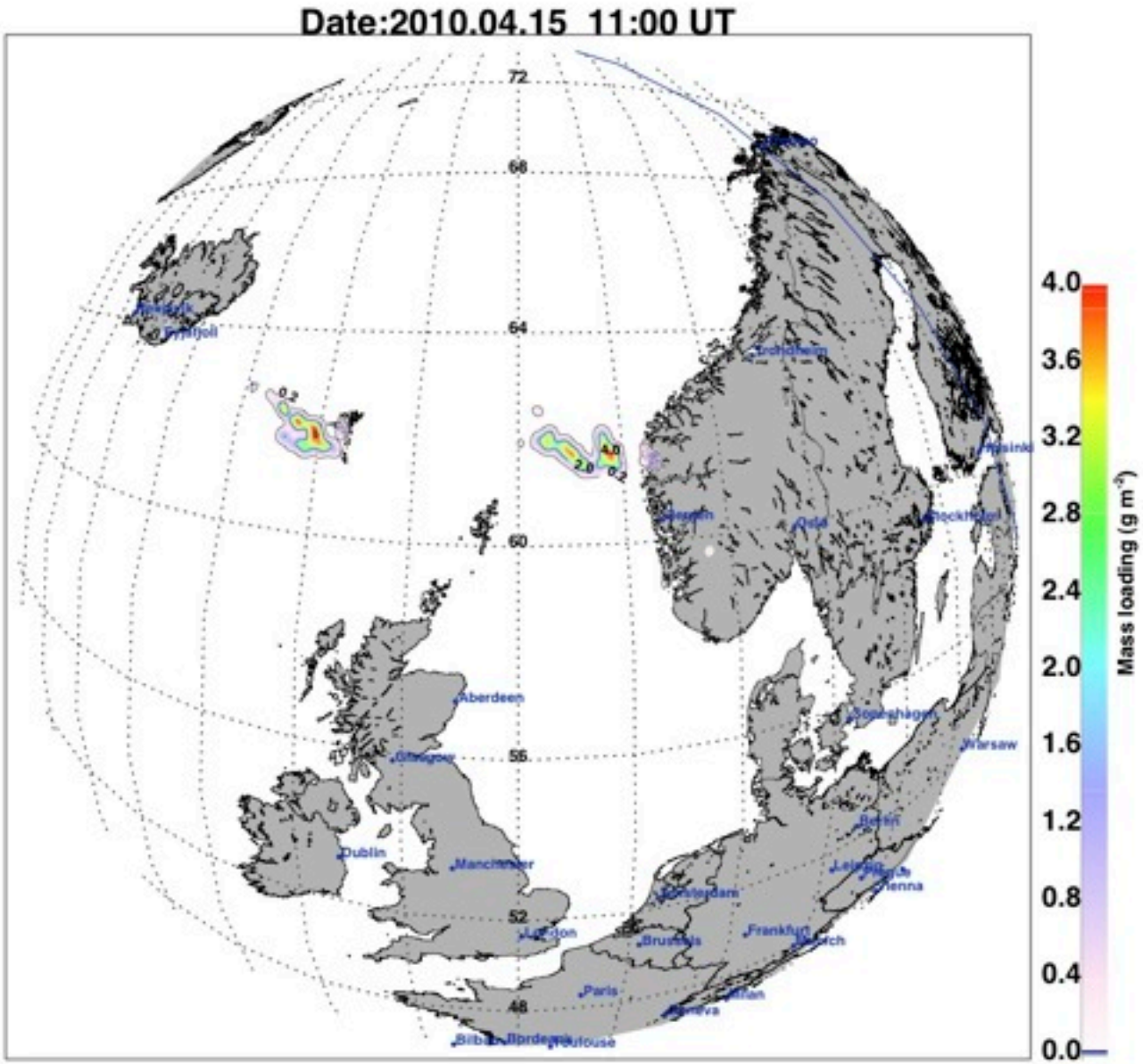
Date:2010.04.15 11:00 UT
72
68
64
60
56
52
48
Aberdeen
Glasgow
Dublin
Manchester
London
Amsterdam
Brussels
Paris
Frankfurt
Zurich
Milan
Geneva
Vienna
Warsaw
Berlin
Copenhagen
Oslo
Stockholm
Helsinki
Trondheim
Bergen
Toulouse
4.0
3.6
3.2
2.8
2.4
2.0
1.6
1.2
0.8
0.4
0.0
Mass loading (g m^{-2})

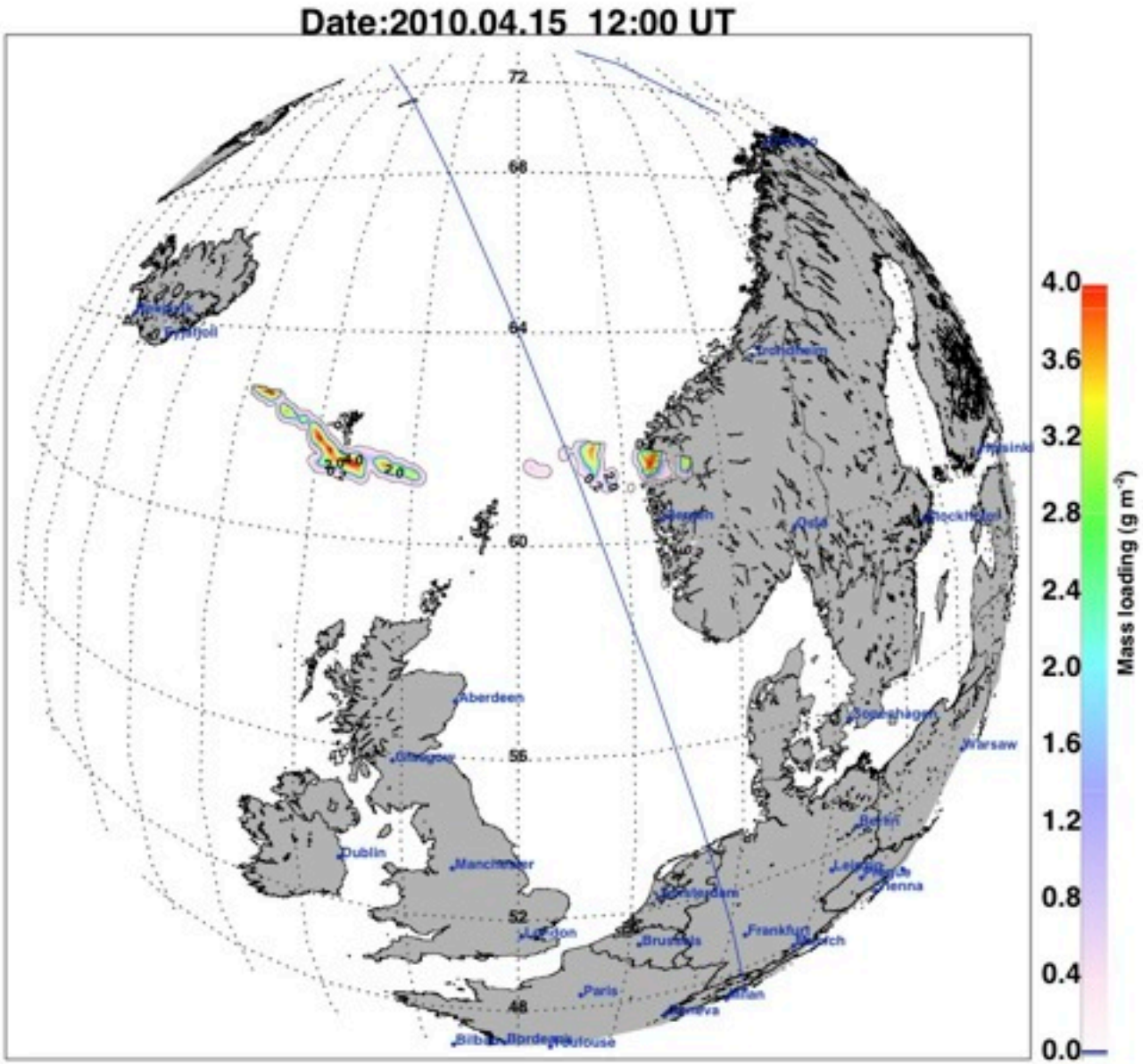
Date:2010.04.15 12:00 UT
72
68
64
60
56
52
48
Aberdeen
Glasgow
Dublin
Manchester
London
Amsterdam
Brussels
Paris
Frankfurt
Zurich
Milan
Geneva
Toulouse
Bilbao
Ilprdeen
Copenhagen
Warsaw
Berlin
Leipzig
Prague
Vienna
Stockholm
Oslo
Helsinki
Trondheim
Bergen
Reykjavik
Thorshavn
4.0
3.6
3.2
2.8
2.4
2.0
1.6
1.2
0.8
0.4
0.0
Mass loading (g m^{-2})

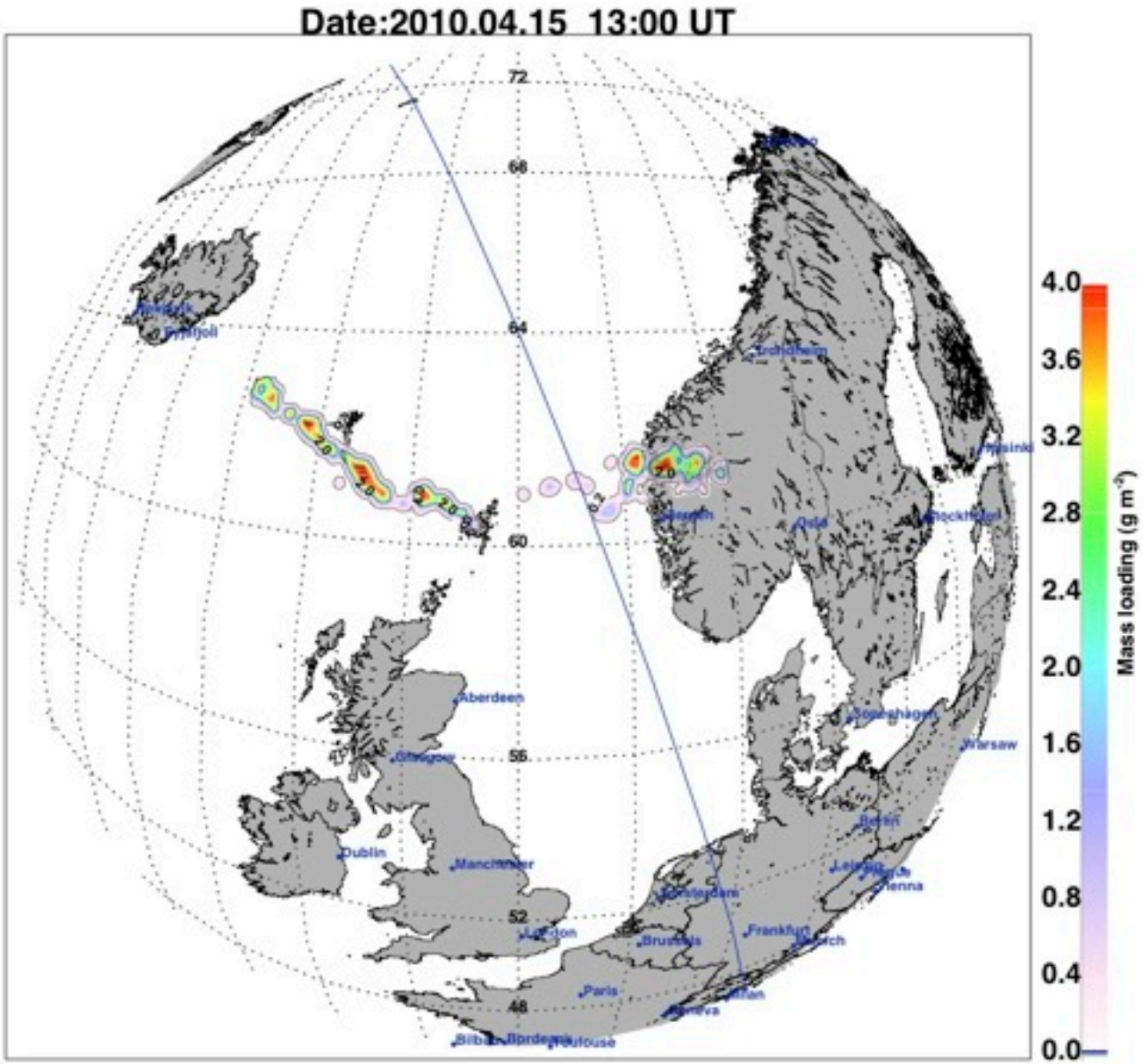
Date:2010.04.15 13:00 UT
Mass loading (g m^{-2})
4.0
3.6
3.2
2.8
2.4
2.0
1.6
1.2
0.8
0.4
0.0
72
68
64
60
56
52
48
Aberdeen
Glasgow
Dublin
Manchester
London
Paris
Brussels
Amsterdam
Frankfurt
Zurich
Milan
Geneva
Toulouse
Copenhagen
Warsaw
Berlin
Leipzig
Vienna
Oslo
Stockholm
Helsinki
Trondheim

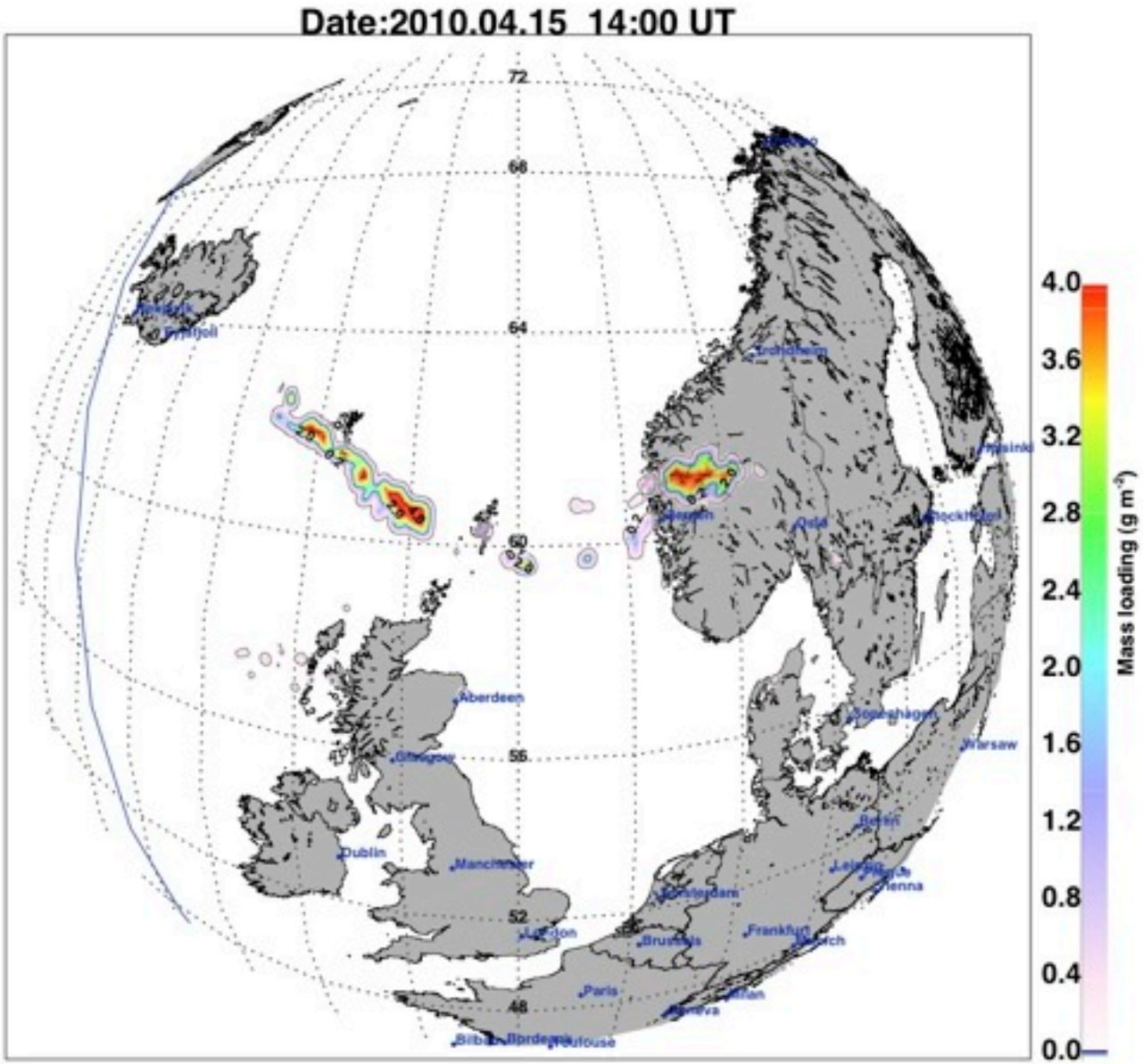
Date:2010.04.15 14:00 UT
72
68
64
60
56
52
48
Aberdeen
Glasgow
Dublin
Manchester
London
Paris
Brussels
Frankfurt
Zurich
Milan
Geneva
Vienna
Warsaw
Berlin
Copenhagen
Stockholm
Oslo
Helsinki
Trondheim
Bergen
Reykjavik
Bilbao
Bordeaux
Toulouse
4.0
3.6
3.2
2.8
2.4
2.0
1.6
1.2
0.8
0.4
0.0
Mass loading (g m^{-2})

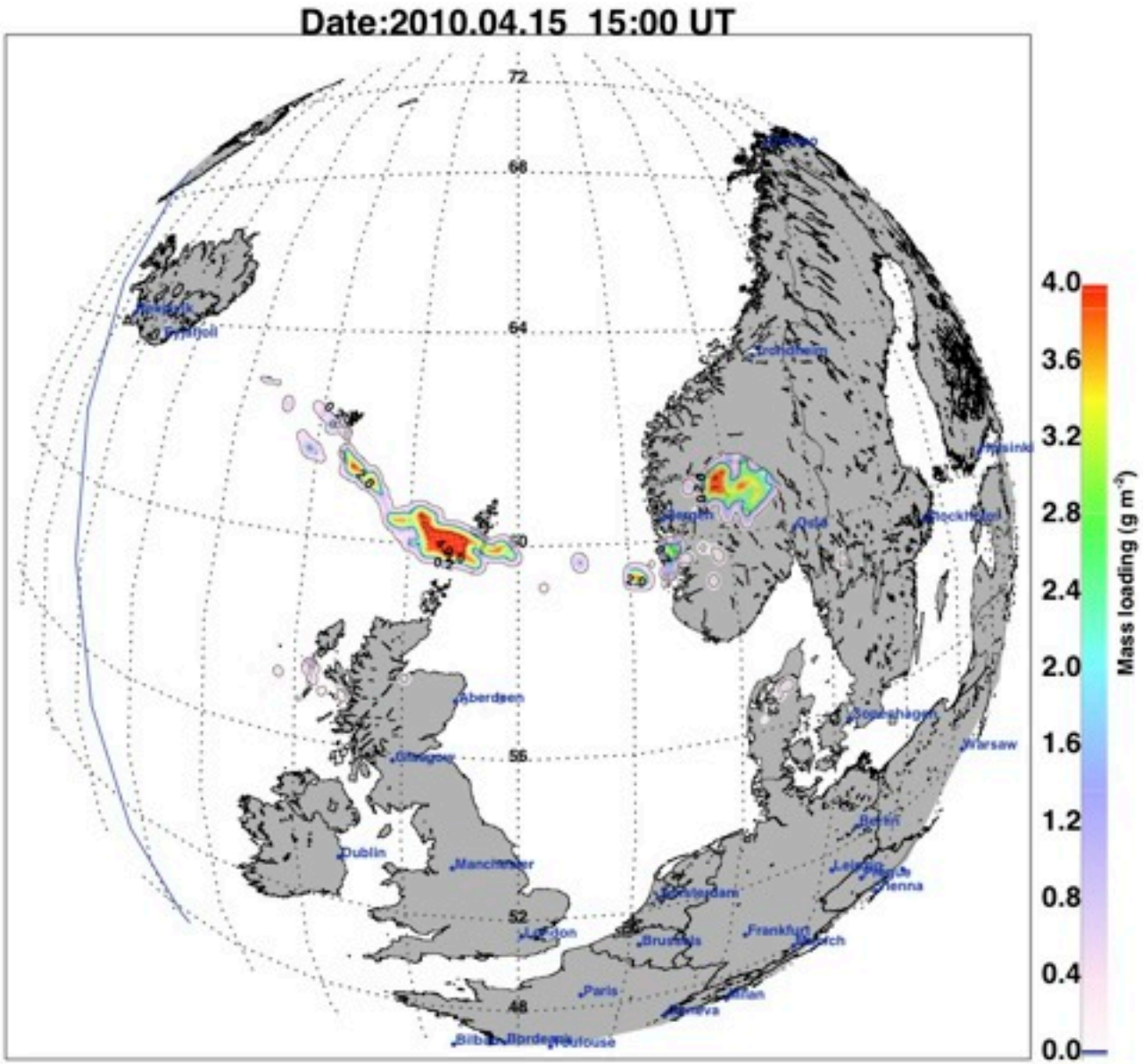
Date:2010.04.15 15:00 UT
72
68
64
60
56
52
48
Aberdeen
Glasgow
Dublin
Manchester
London
Amsterdam
Brussels
Paris
Frankfurt
Zurich
Milan
Geneva
Toulouse
Copenhagen
Warsaw
Berlin
Leipzig
Vienna
Stockholm
Oslo
Helsinki
Trondheim
Bergen
Reykjavik
Prestjon
4.0
3.6
3.2
2.8
2.4
2.0
1.6
1.2
0.8
0.4
0.0
Mass loading (g m-2)

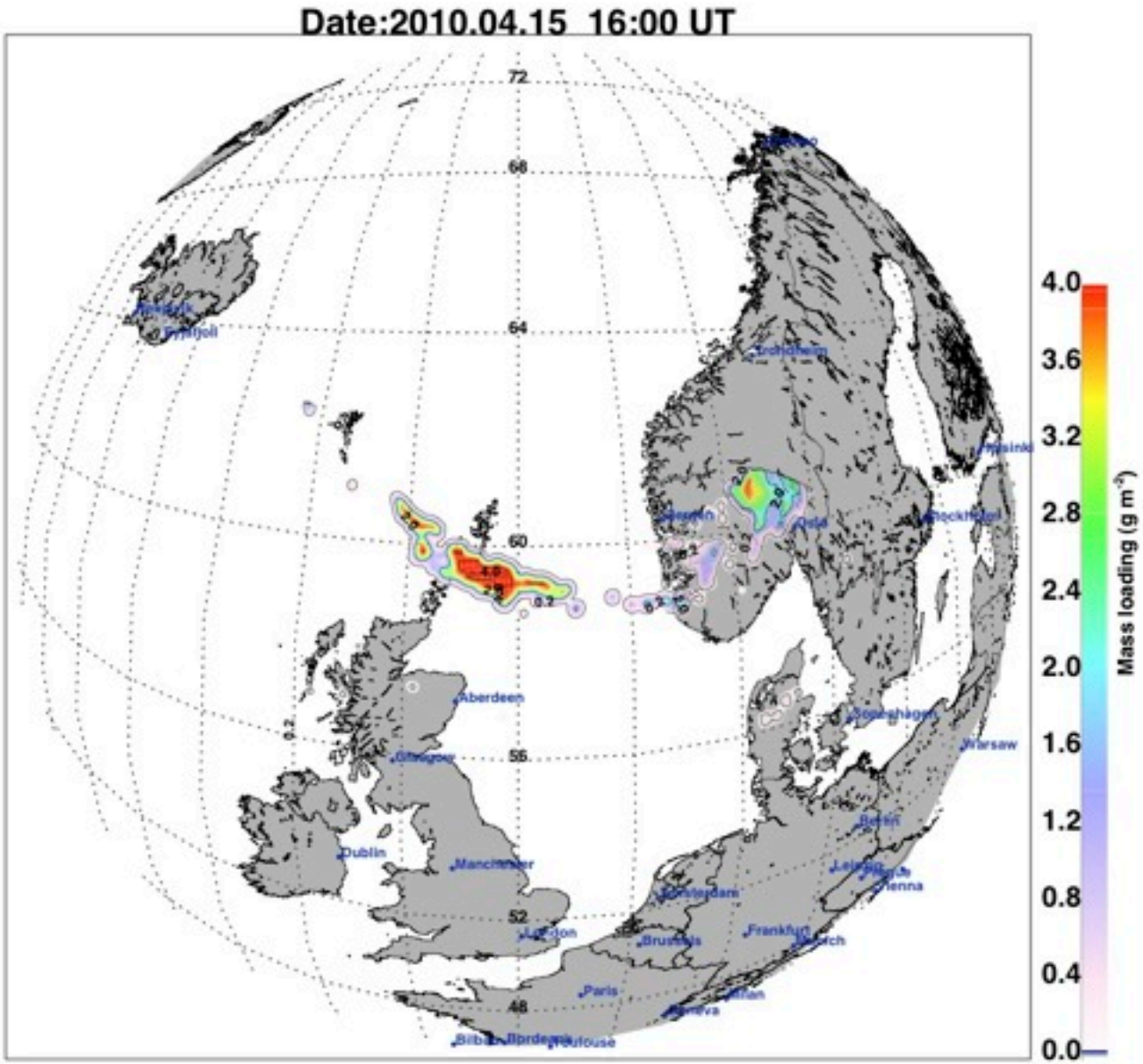
Date:2010.04.15 16:00 UT
72
68
64
60
56
52
48
Aberdeen
Glasgow
Dublin
Manchester
London
Paris
Brussels
Frankfurt
Zurich
Milan
Geneva
Toulouse
Bilbao
Amsterdam
Leipzig
Prague
Vienna
Berlin
Copenhagen
Warsaw
Stockholm
Oslo
Gothenburg
Trondheim
Bergen
Reykjavik
Helsinki
4.0
3.6
3.2
2.8
2.4
2.0
1.6
1.2
0.8
0.4
0.0
Mass loading (g m^{-2})

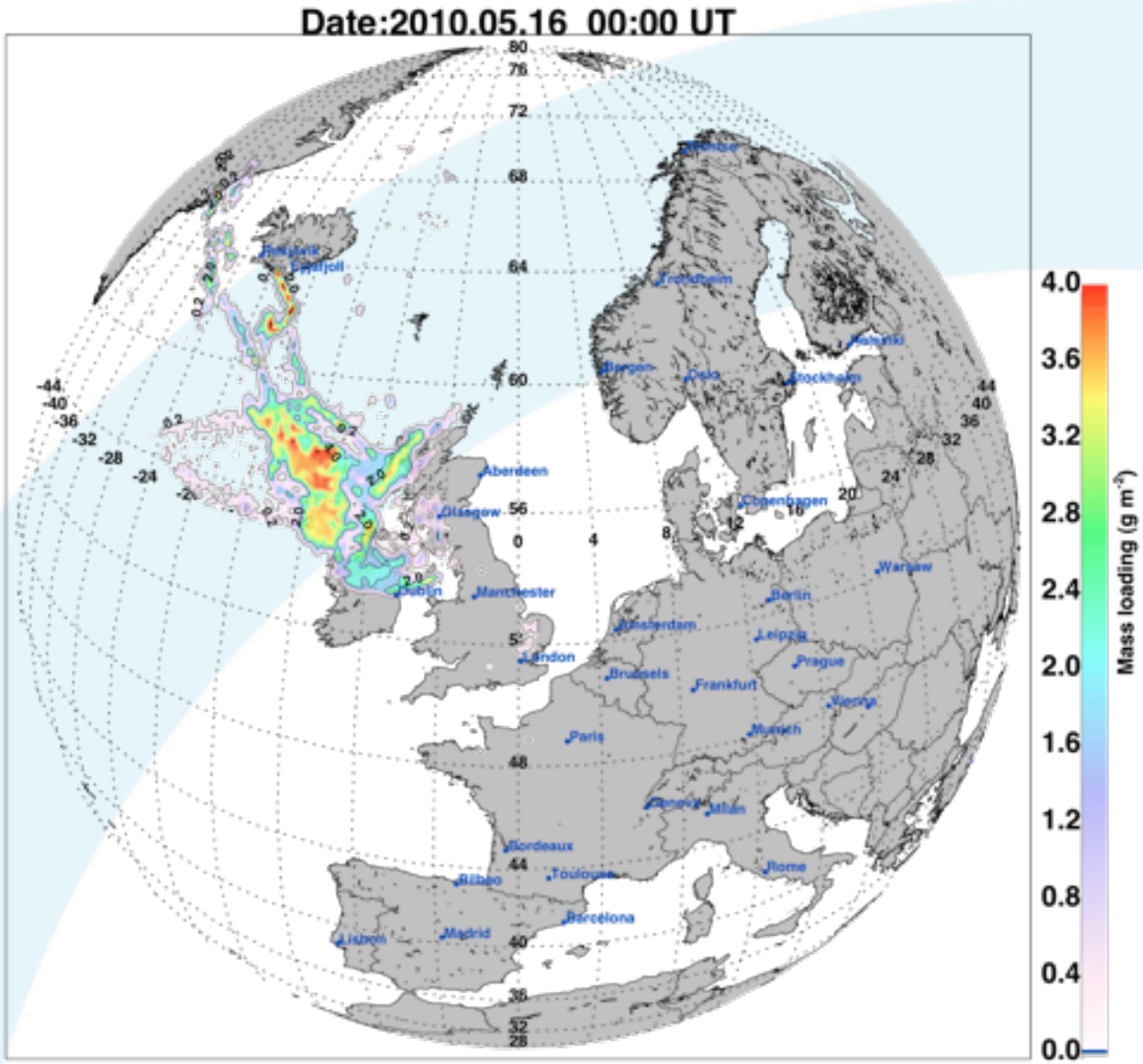
Date:2010.05.16 00:00 UT
Mass loading (g m^{-2})
4.0
3.6
3.2
2.8
2.4
2.0
1.6
1.2
0.8
0.4
0.0
Reykjavik
Eyjafjoll
Trondheim
Bergen
Oslo
Stockholm
Helsinki
Aberdeen
Glasgow
Copenhagen
Dublin
Manchester
Warsaw
Berlin
Amsterdam
Leipzig
London
Prague
Brussels
Frankfurt
Vienna
Paris
Munich
Geneva
Milan
Bordeaux
Toulouse
Rome
Bilbao
Barcelona
Lisbon
Madrid

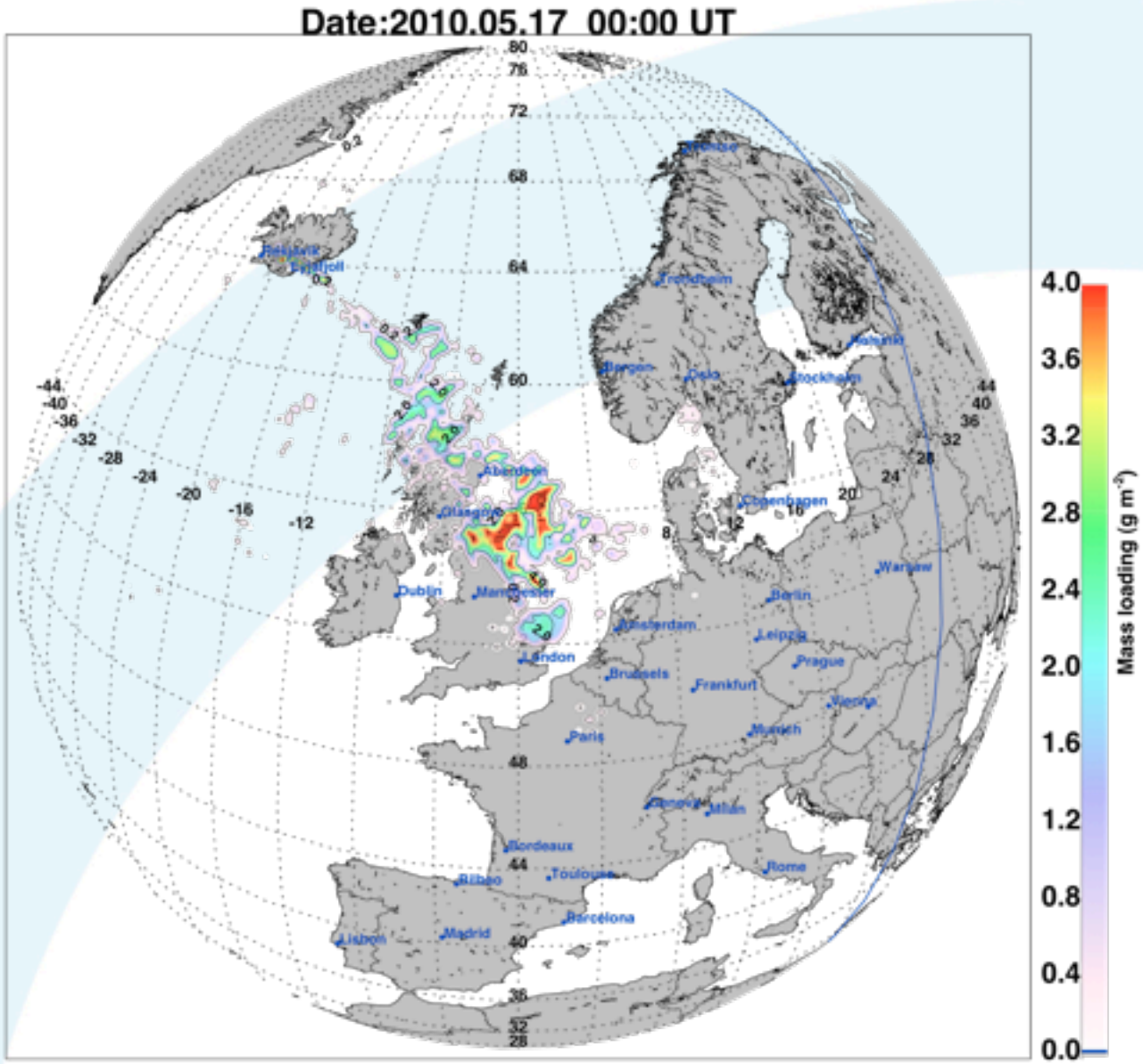
Date:2010.05.17 00:00 UT
Mass loading (g m^{-2})
4.0
3.6
3.2
2.8
2.4
2.0
1.6
1.2
0.8
0.4
0.0
Reykjavik
Eyjafjoll
Trondheim
Bergen
Oslo
Stockholm
Helsinki
Aberdeen
Glasgow
Copenhagen
Dublin
Manchester
Warsaw
Berlin
Amsterdam
Leipzig
London
Prague
Brussels
Frankfurt
Vienna
Paris
Munich
Geneva
Milan
Bordeaux
Toulouse
Rome
Bilbao
Barcelona
Lisbon
Madrid

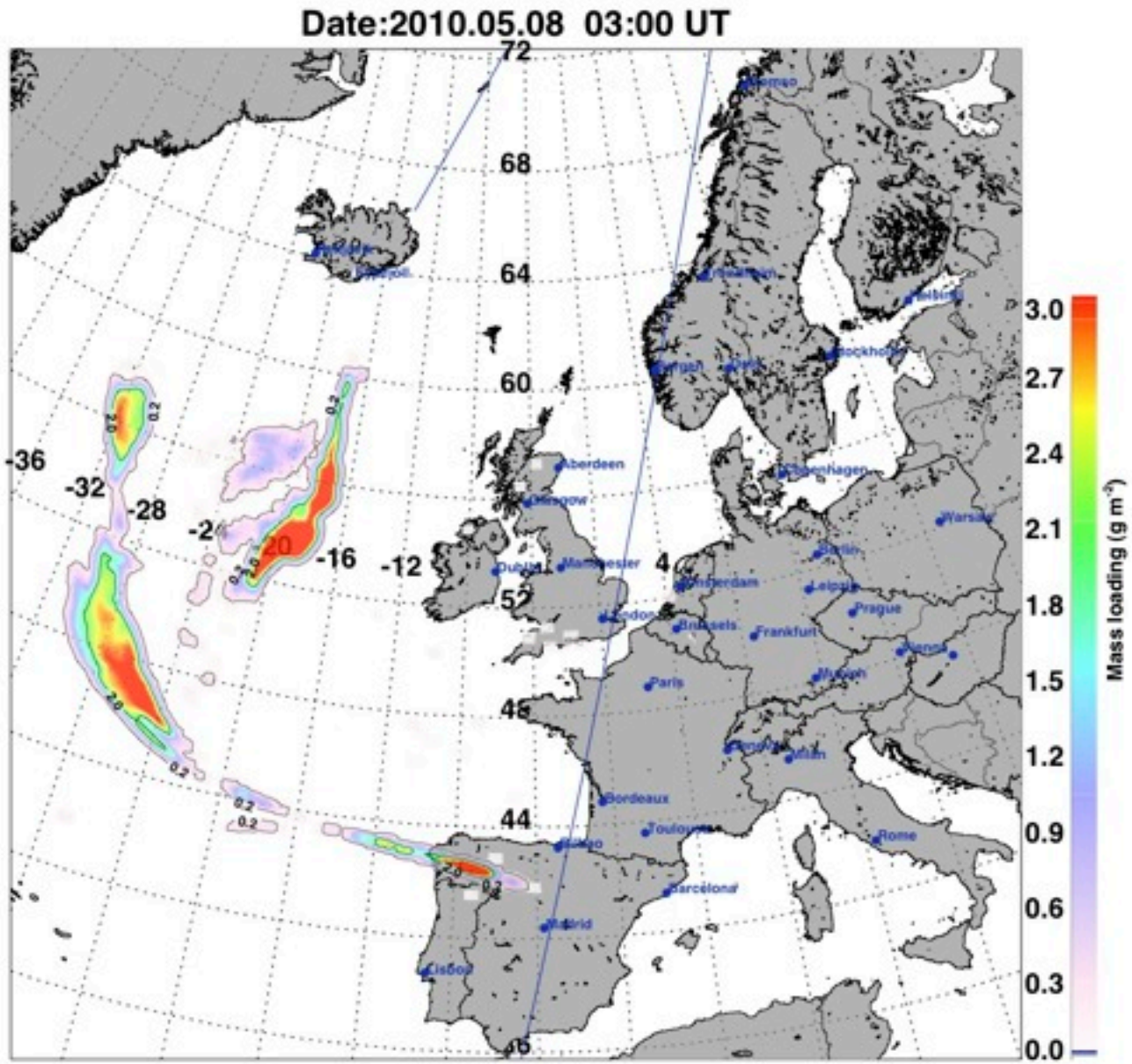
Date:2010.05.08 03:00 UT
Mass loading (g m^{-2})
3.0
2.7
2.4
2.1
1.8
1.5
1.2
0.9
0.6
0.3
0.0
72
68
64
60
52
48
44
-36
-32
-28
-24
-20
-16
-12
4
Aberdeen
Glasgow
Dublin
Manchester
London
Amsterdam
Brussels
Frankfurt
Leipzig
Prague
Warsaw
Berlin
Copenhagen
Stockholm
Helsinki
Paris
Bordeaux
Toulouse
Rome
Barcelona
Madrid
Lisbon
Porto

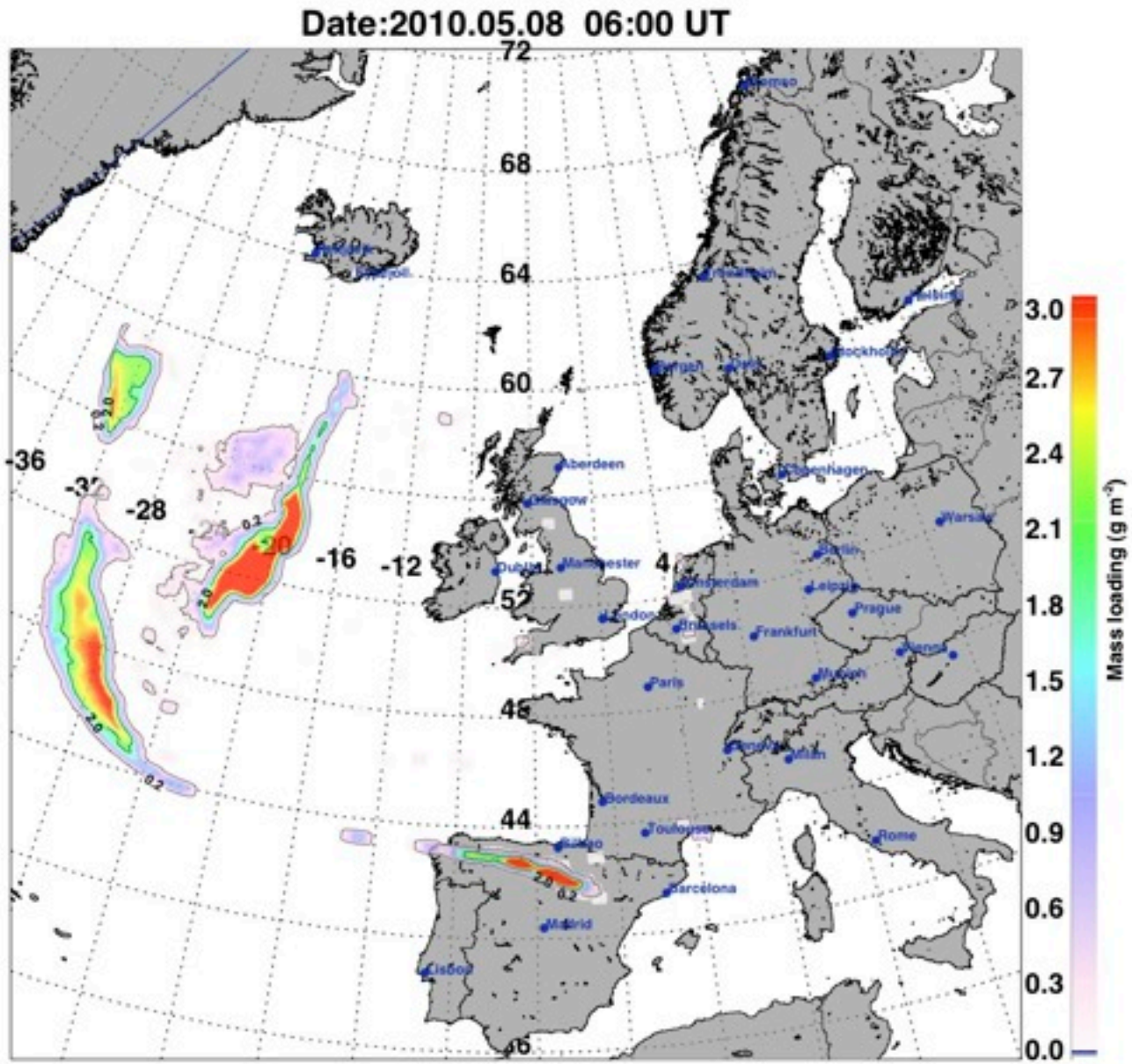
Date:2010.05.08 06:00 UT
Mass loading (g m^{-2})
3.0
2.7
2.4
2.1
1.8
1.5
1.2
0.9
0.6
0.3
0.0
72
68
64
60
52
48
44
-36
-28
-16
-12
4
Aberdeen
Glasgow
Dublin
Manchester
London
Amsterdam
Brussels
Frankfurt
Leipzig
Prague
Warsaw
Berlin
Copenhagen
Stockholm
Helsinki
Oslo
Paris
Munich
Vienna
Zurich
Bordeaux
Toulouse
Rome
Barcelona
Madrid
Lisboa
Bilbao

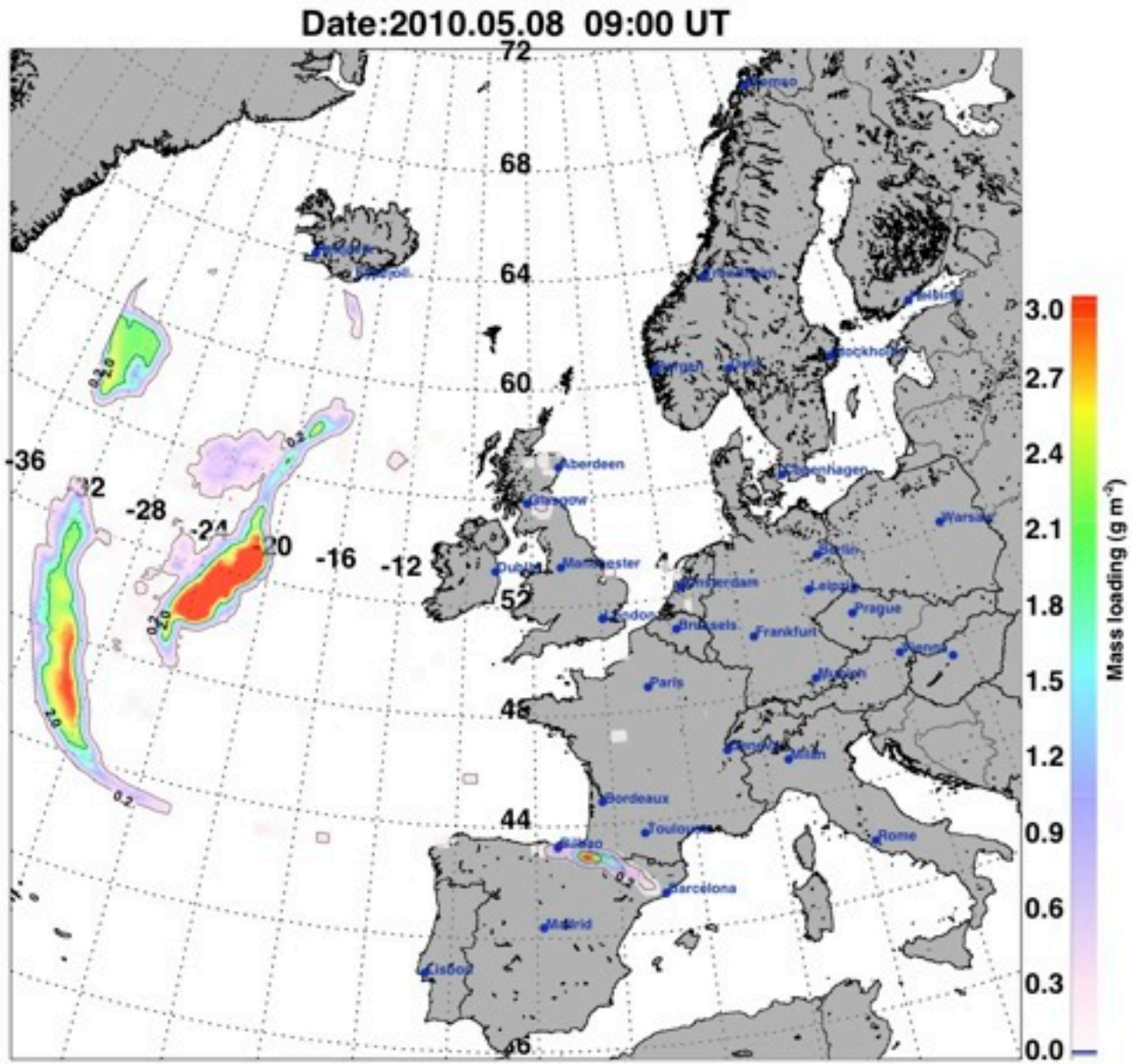
Date:2010.05.08 09:00 UT
72
68
64
60
52
46
44
-36
-32
-28
-24
-20
-16
-12
Aberdeen
Glasgow
Dublin
Manchester
London
Amsterdam
Brussels
Frankfurt
Leipzig
Prague
Warsaw
Berlin
Copenhagen
Stockholm
Helsinki
Paris
Munich
Vienna
Bordeaux
Toulouse
Rome
Barcelona
Madrid
Lisbon
Mass loading (g m-2)
3.0
2.7
2.4
2.1
1.8
1.5
1.2
0.9
0.6
0.3
0.0

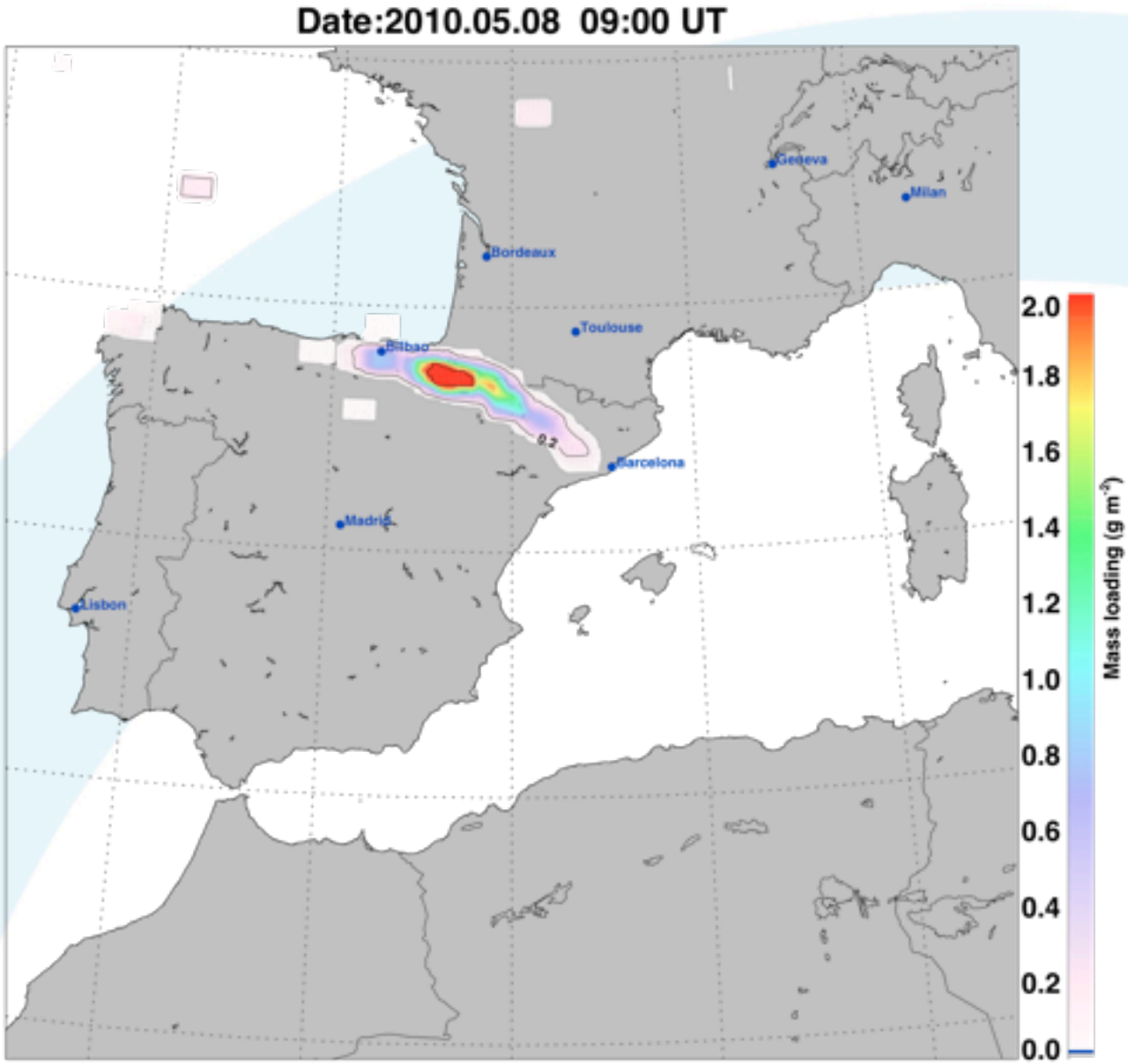
Date:2010.05.08 09:00 UT
Geneva
Milan
Bordeaux
Toulouse
Bilbao
Barcelona
Madrid
Lisbon
2.0
1.8
1.6
1.4
1.2
1.0
0.8
0.6
0.4
0.2
0.0
Mass loading (g m^{-2})

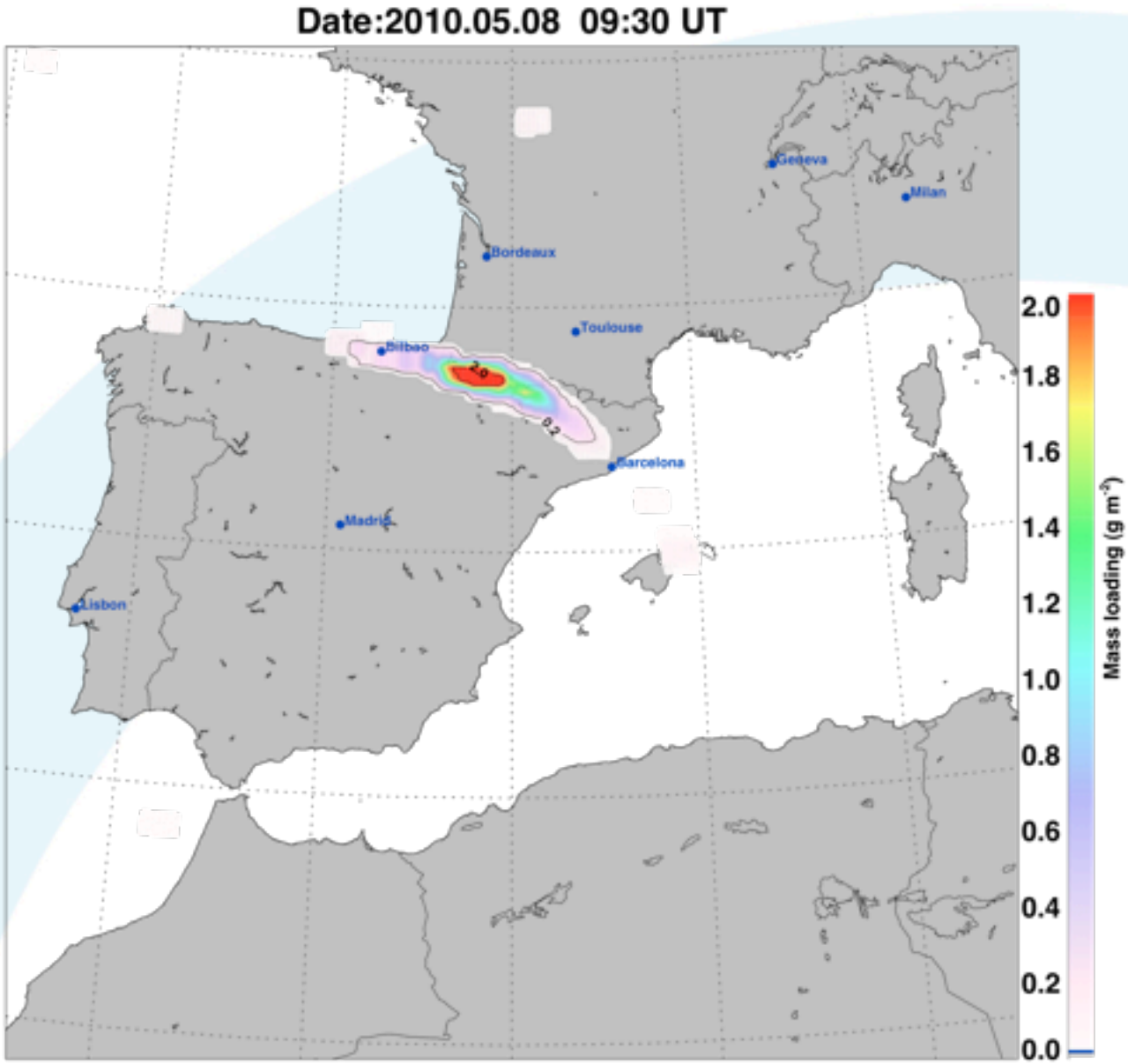
Date:2010.05.08 09:30 UT
Geneva
Milan
Bordeaux
Toulouse
Bilbao
Barcelona
Madrid
Lisbon
2.0
0.2
2.0
1.8
1.6
1.4
1.2
1.0
0.8
0.6
0.4
0.2
0.0
Mass loading (g m^{-2})

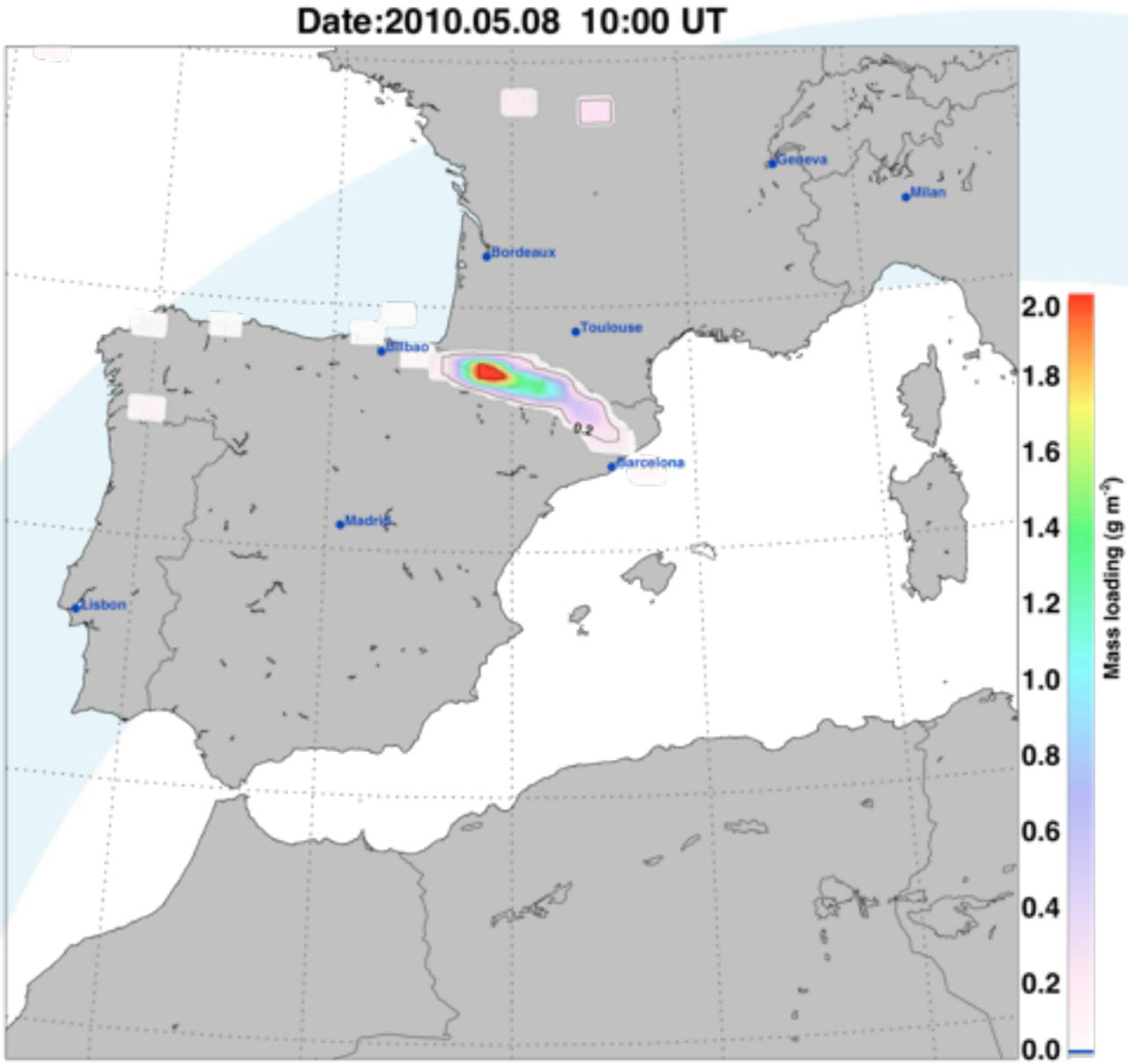
Date:2010.05.08 10:00 UT
Geneva
Milan
Bordeaux
Toulouse
Bilbao
Barcelona
Madrid
Lisbon
0.2
2.0
1.8
1.6
1.4
1.2
1.0
0.8
0.6
0.4
0.2
0.0
Mass loading (g m^{-2})

Sun photometer at Barcelona

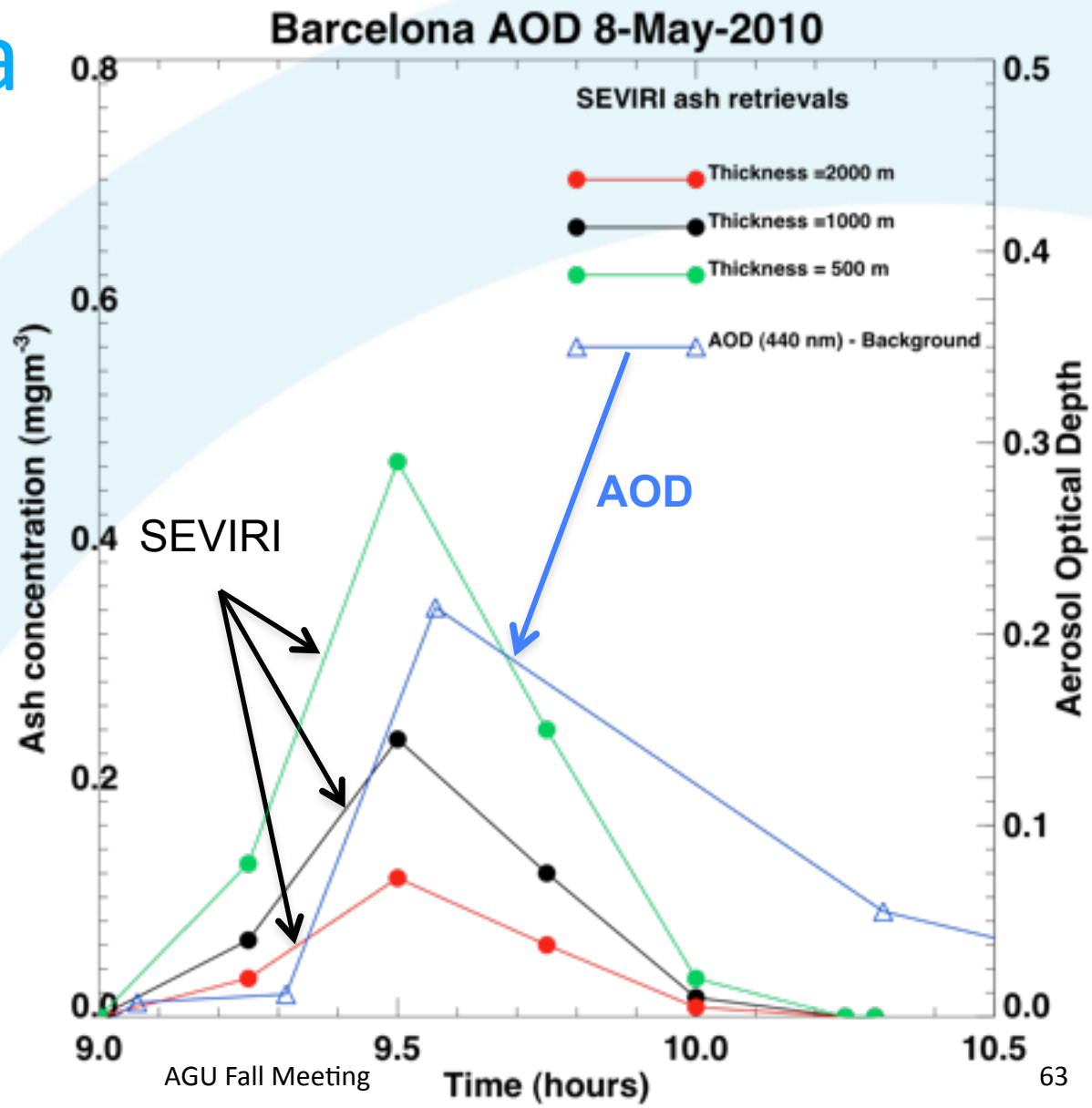

Date:2010.04.15 13:30 UT

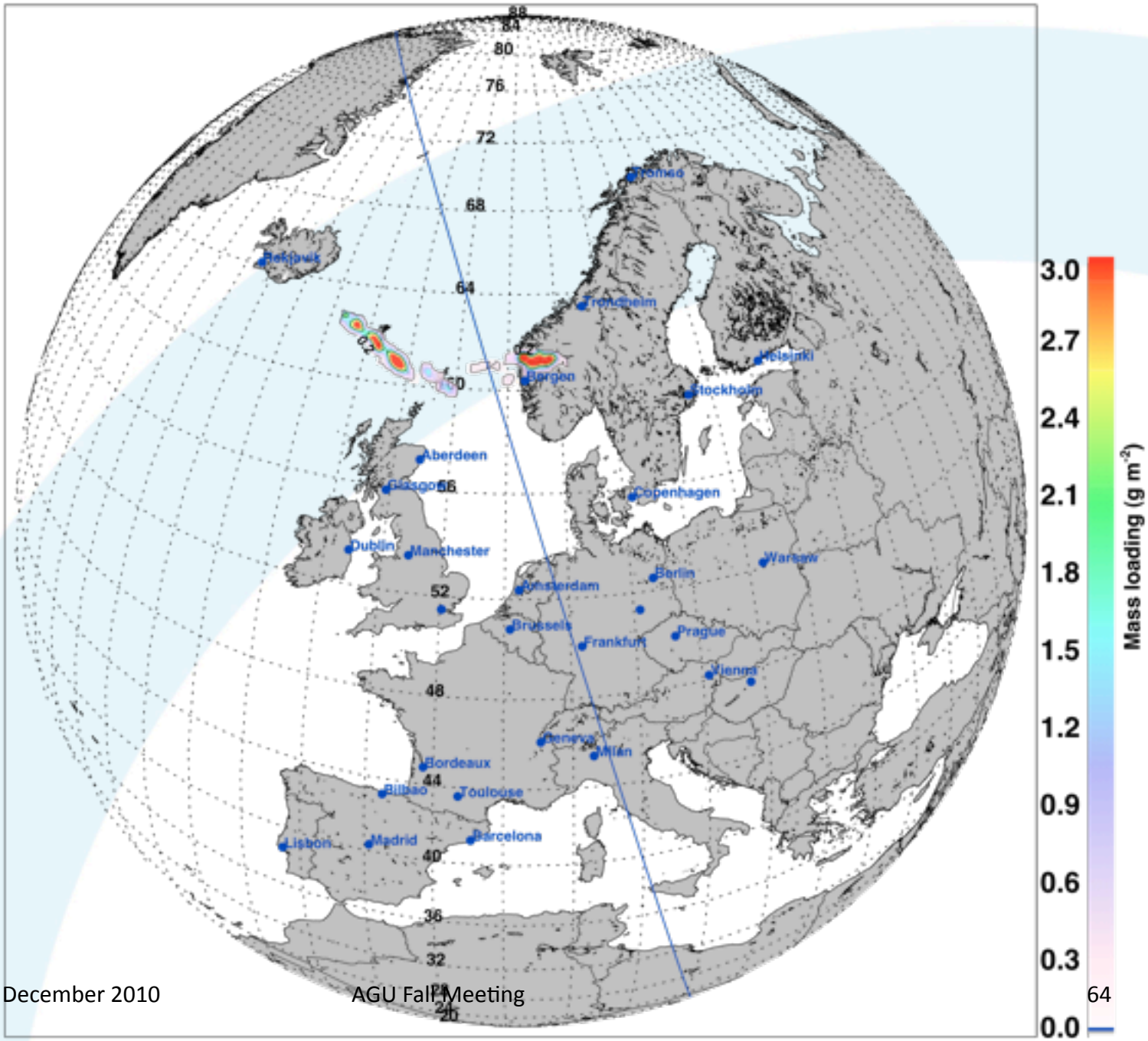

15 April 2010 - Daytime

CALIPSO

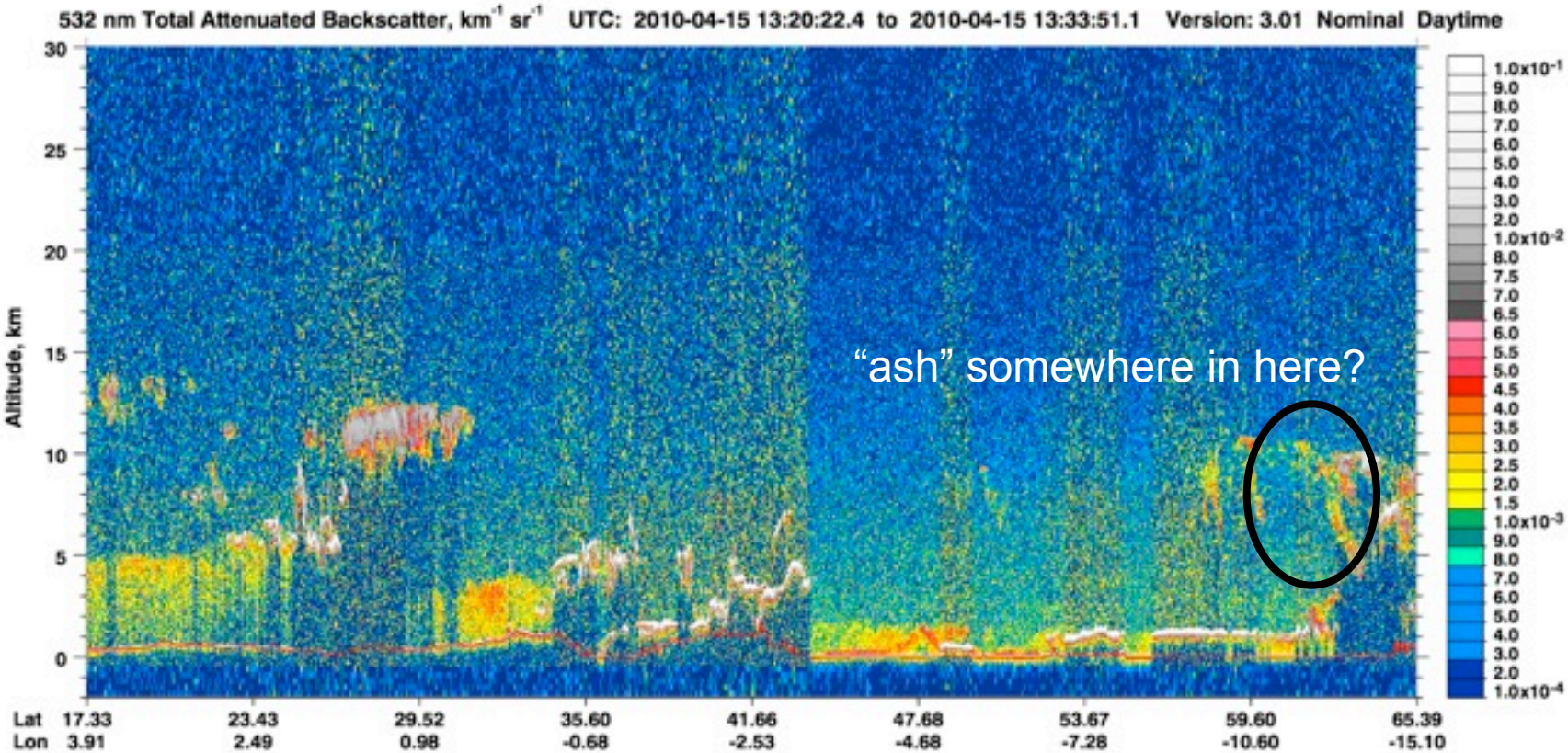

CALIOP "curtain" 532 nm Total Backscatter

Date:2010.05.12 03:30 UT

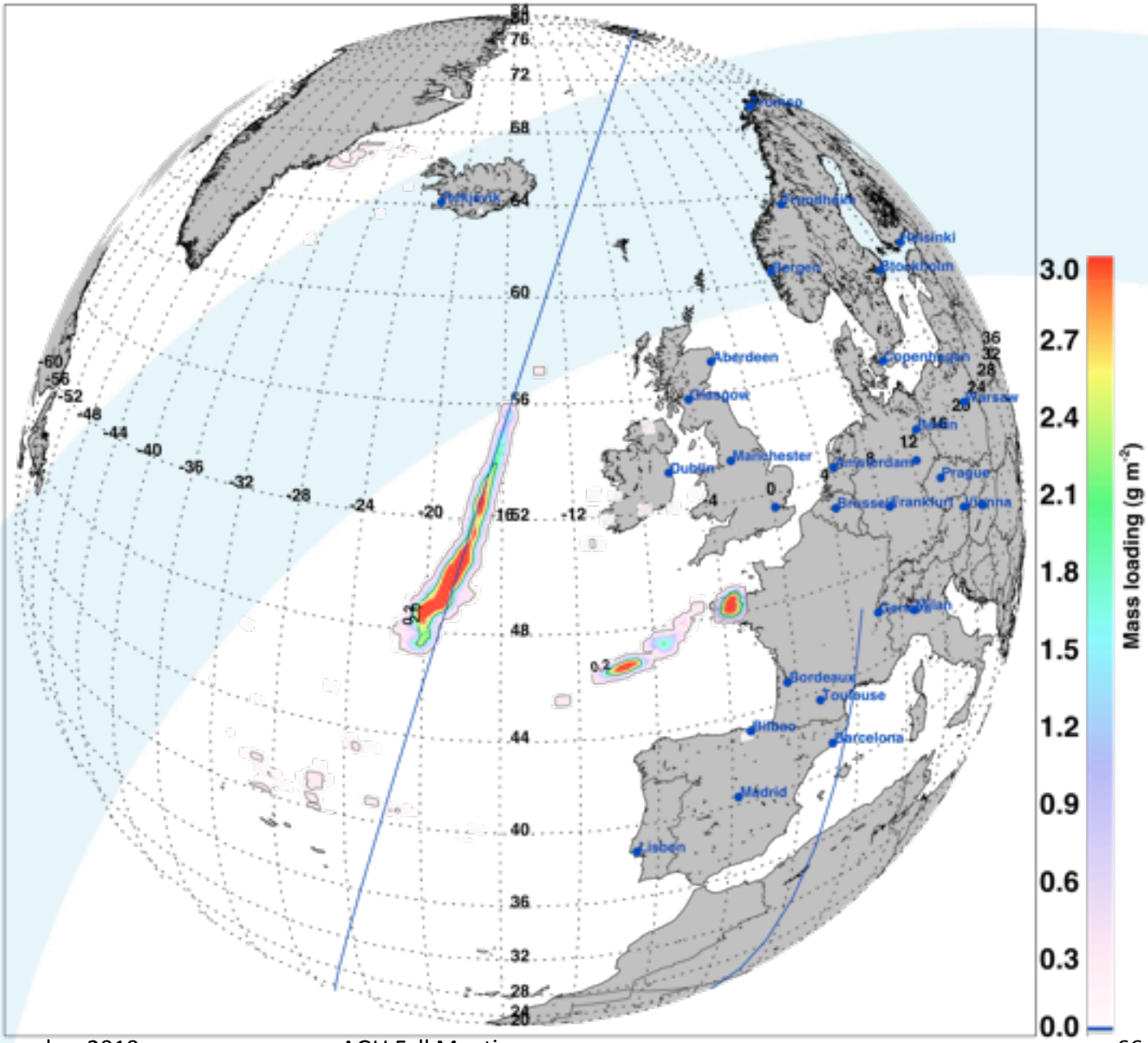

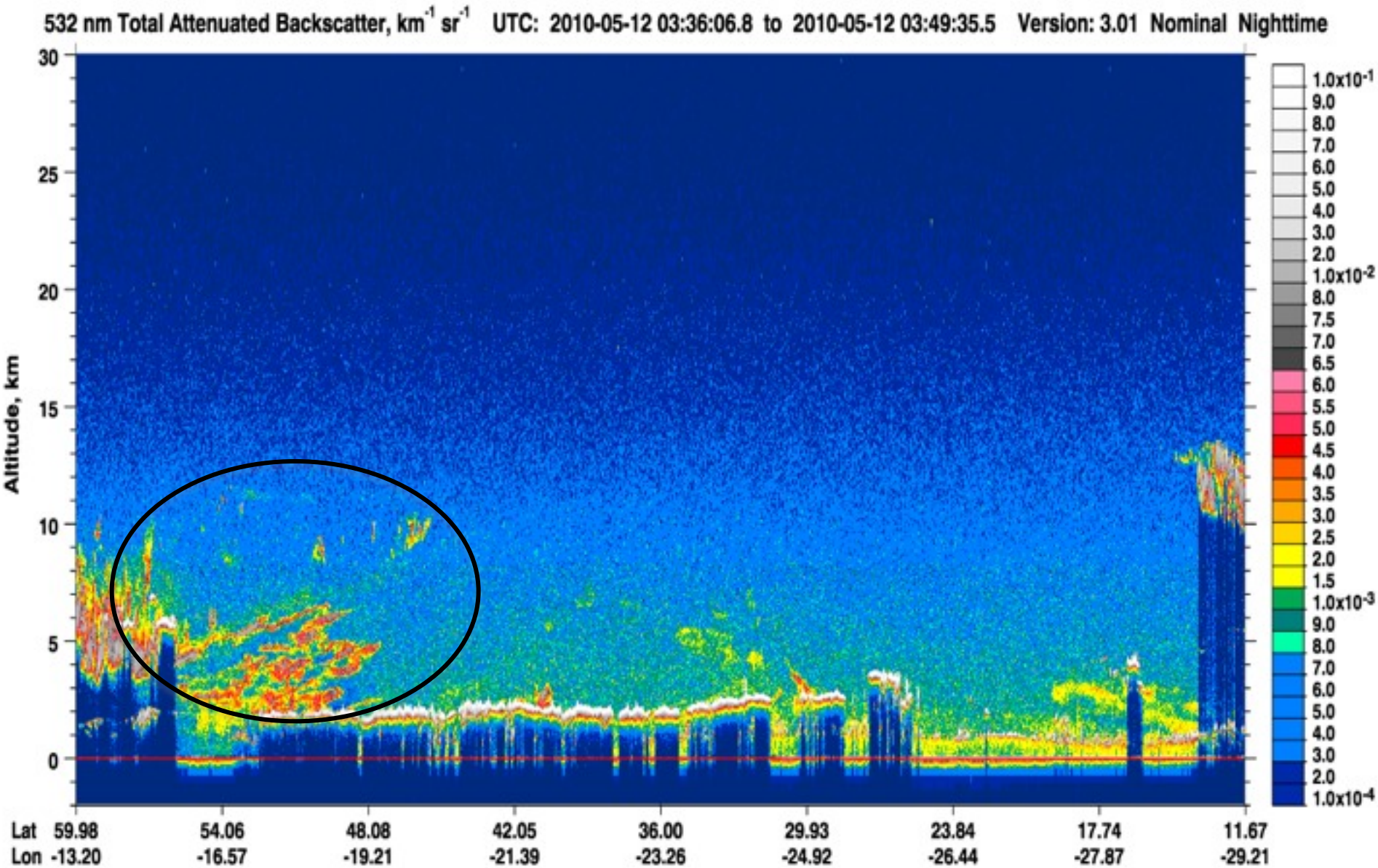
532 nm Total Attenuated Backscatter, km-1 sr-1 UTC: 2010-05-12 03:36:06.8 to 2010-05-12 03:49:35.5 Version: 3.01 Nominal Nighttime
Altitude, km
30
25
20
15
10
5
0
Lat 59.98 54.06 48.08 42.05 36.00 29.93 23.84 17.74 11.67
Lon -13.20 -16.57 -19.21 -21.39 -23.26 -24.92 -26.44 -27.87 -29.21
1.0x10-1
9.0
8.0
7.0
6.0
5.0
4.0
3.0
2.0
1.0x10-2
8.0
7.5
7.0
6.5
6.0
5.5
5.0
4.5
4.0
3.5
3.0
2.5
2.0
1.5
1.0x10-3
9.0
8.0
7.0
6.0
5.0
4.0
3.0
2.0
1.0x10-4

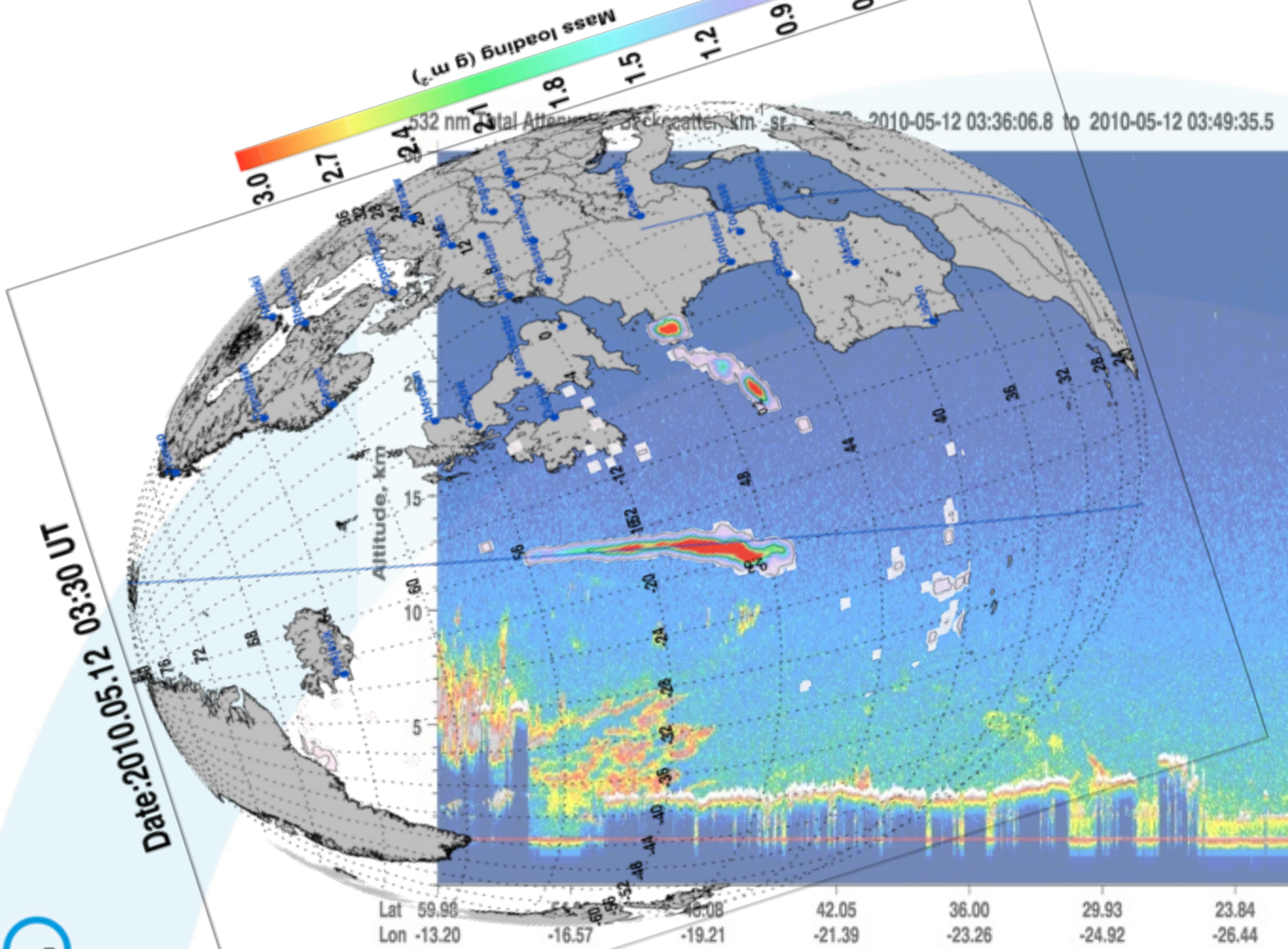
Date:2010.05.12 03:30 UT
Mass loading (g m⁻³)
3.0
2.7
2.4
2.1
1.8
1.5
1.2
0.9
0.6
532 nm Total Attenuated Backscatter, km⁻¹ sr⁻¹
2010-05-12 03:36:06.8 to 2010-05-12 03:49:35.5
Altitude, km
Lat 59.98 48.08 42.05 36.00 29.93 23.84
Lon -13.20 -16.57 -19.21 -21.39 -23.26 -24.92 -26.44

For a single aerosol type the mass loading may be written:

$$m_l = \int_{z_1}^{z_2} \rho(z) dz$$

If we assume that the concentration profile is constant over the layer then:

$$\rho = \frac{m_l}{\Delta z}$$

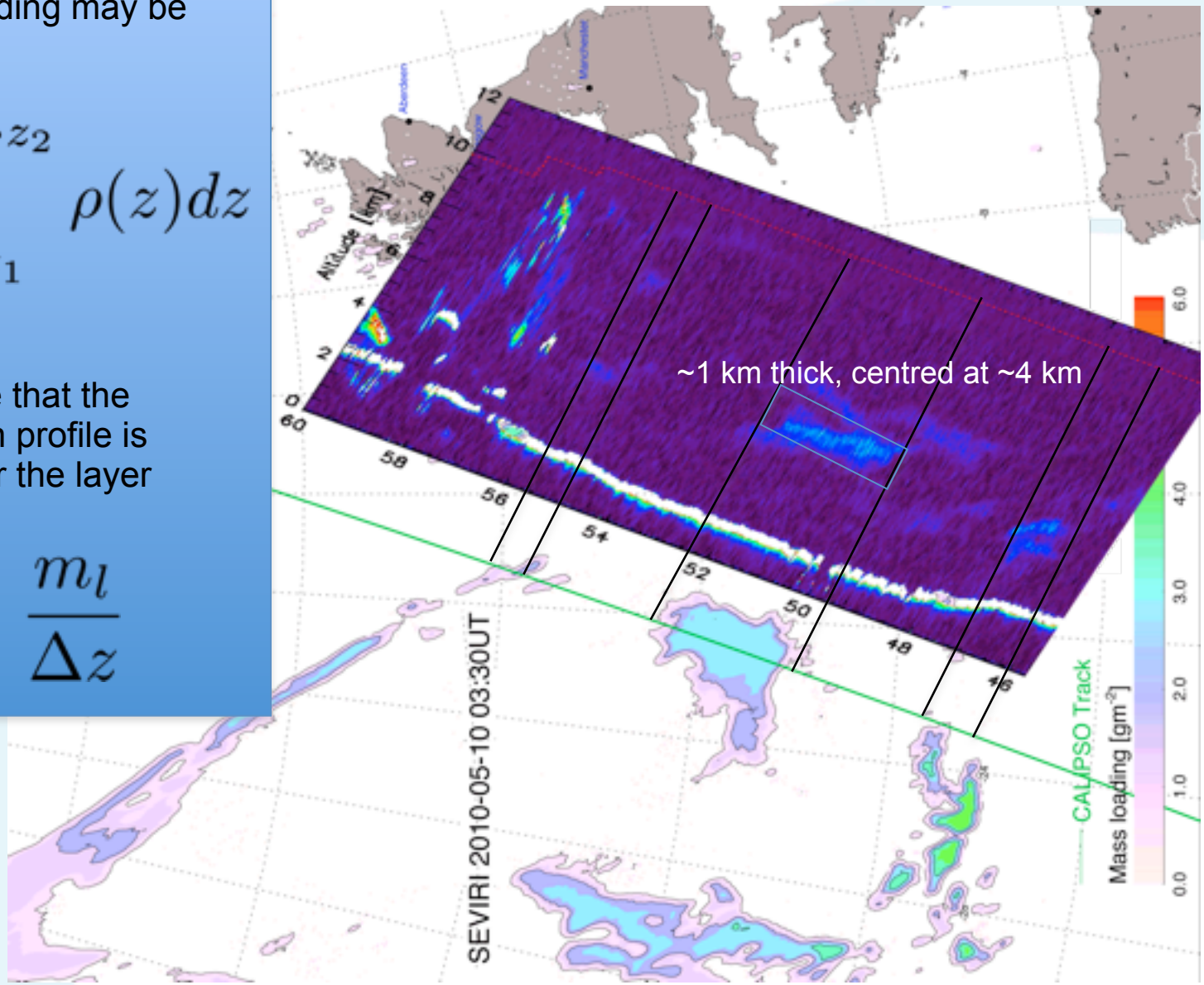

$$m_l = \int_{z_1}^{z_2} \rho(z)dz$$

$m_l \sim 0.4$ g m^{-2}

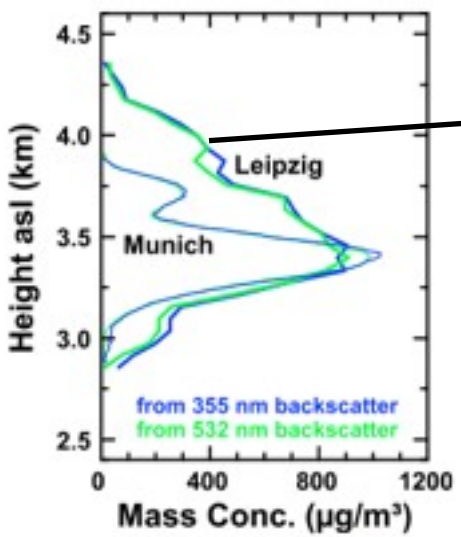

Figure 4. Mass concentrations estimated from the 355 and 532 nm backscatter profiles in Figure 3.

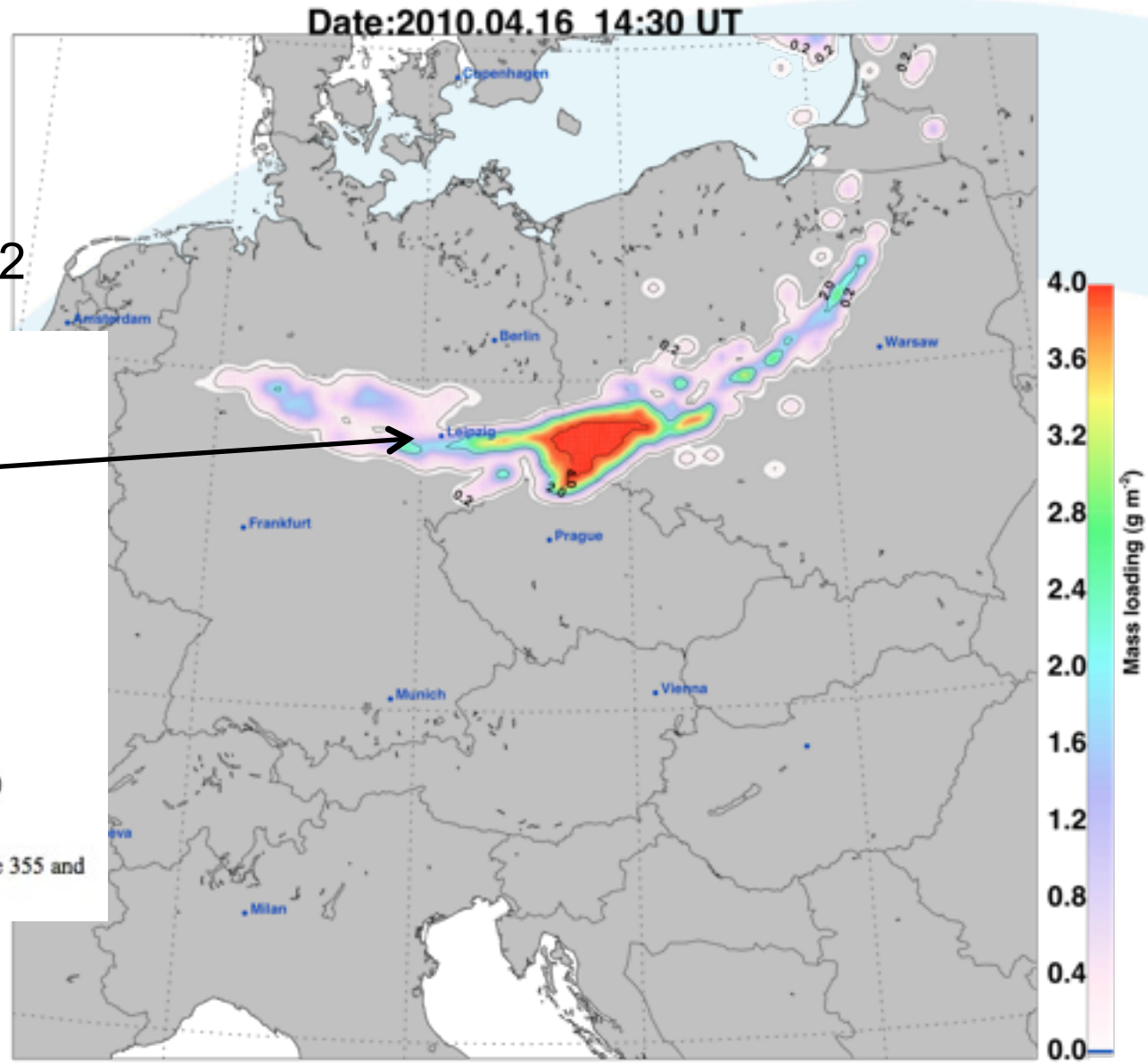

$m_l \sim 0.2\ g\ m^{-2}$

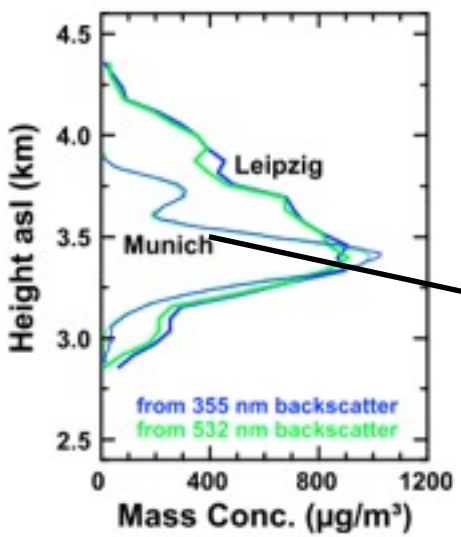

Figure 4. Mass concentrations estimated from the 355 and 532 nm backscatter profiles in Figure 3.

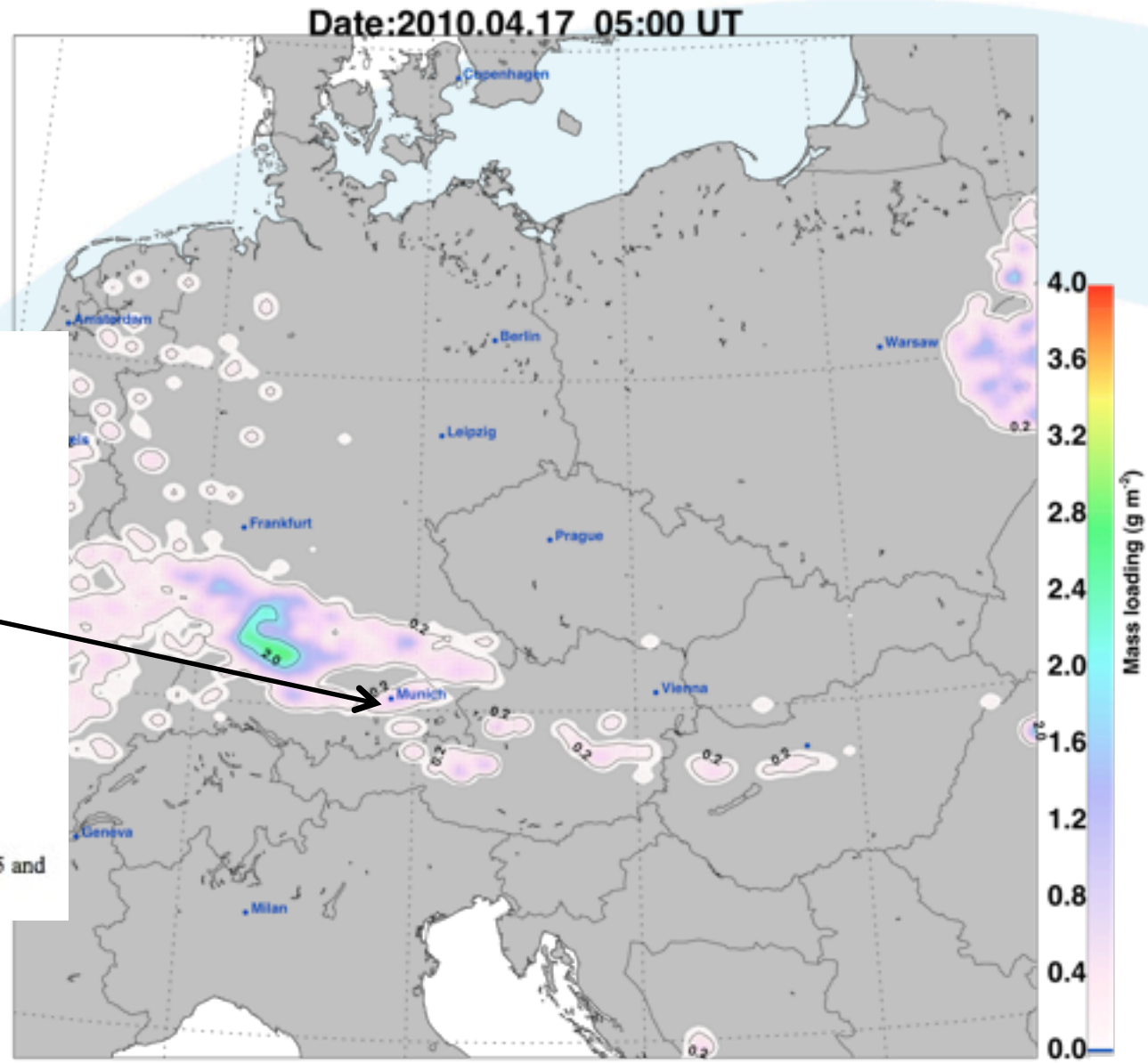

Visualisation

Courtesy: Vince Realmuto, JPL

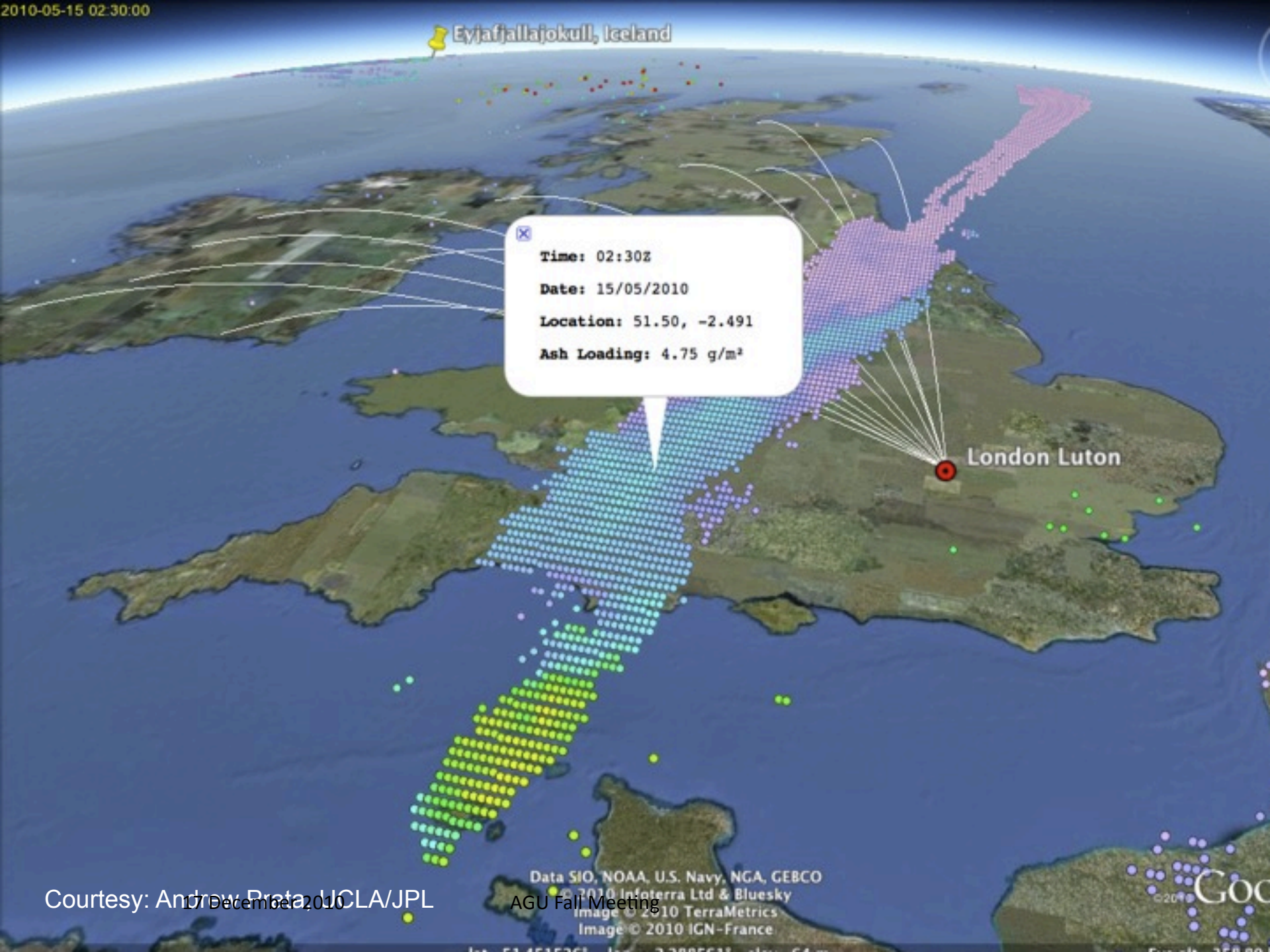

Courtesy: Andrew Prata, UCLA/JPL

Courtesy: Andrew Prata, UCLA/JPL

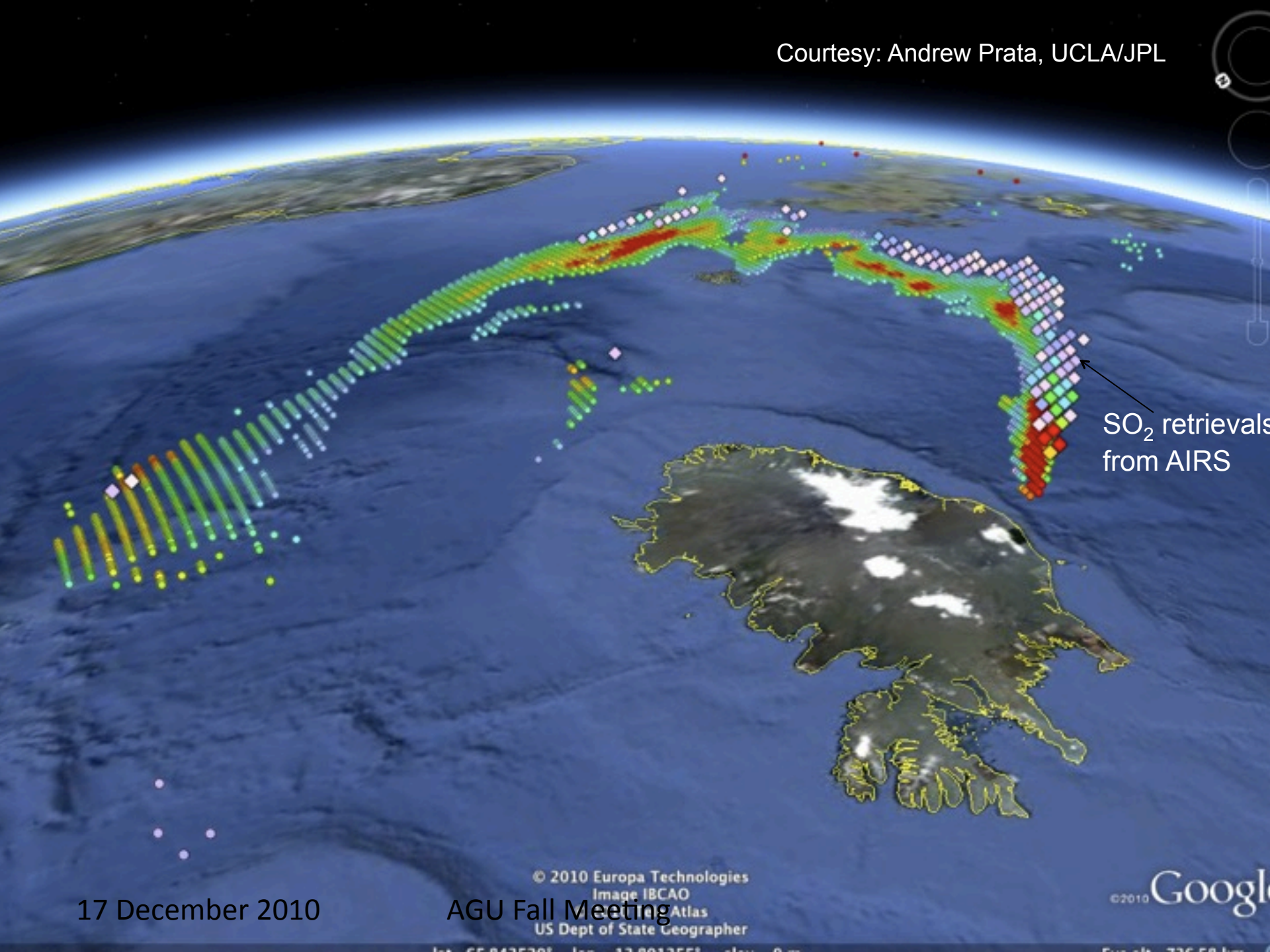

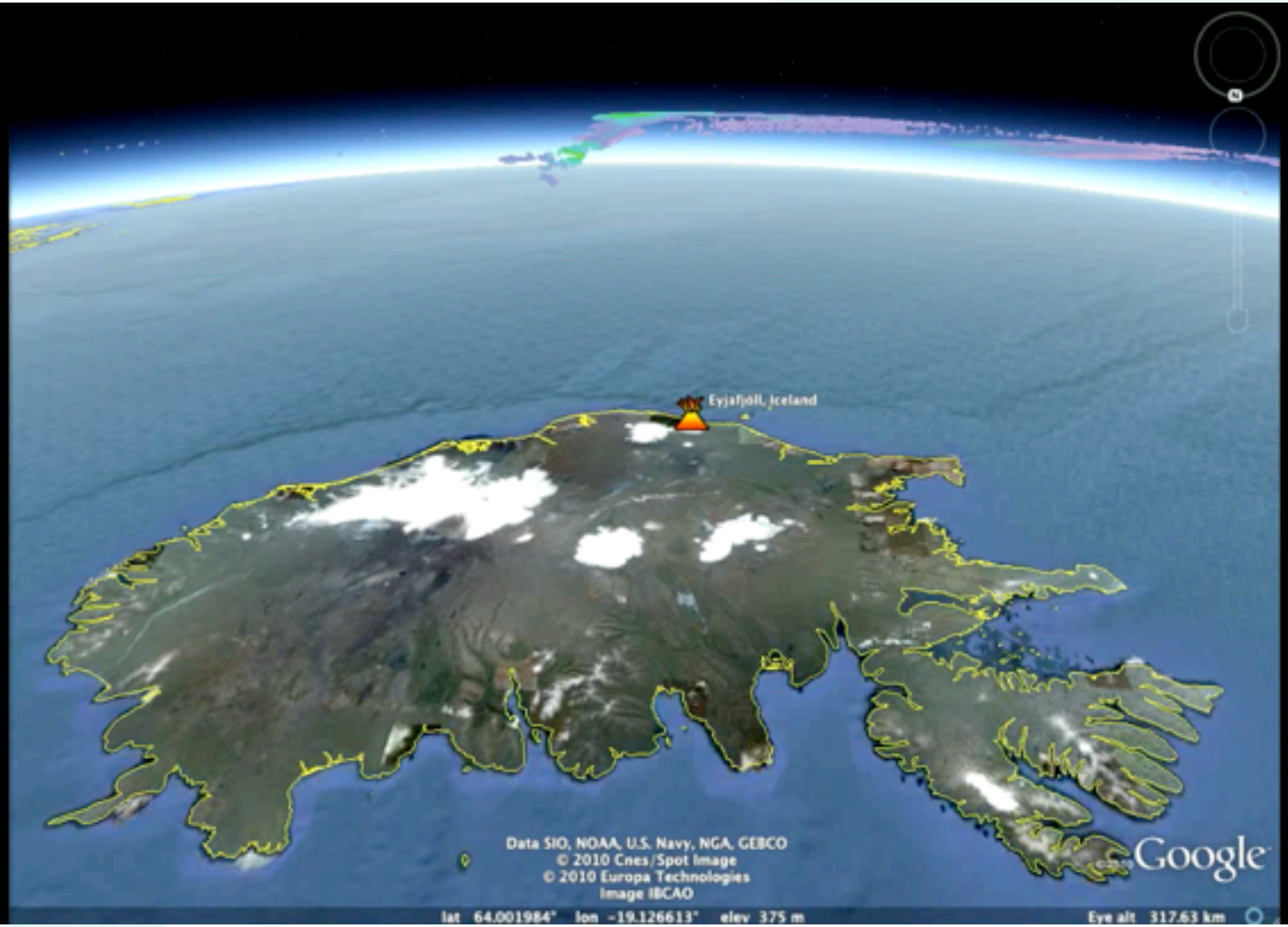
Eyjafjöll, Iceland
Data SIO, NOAA, U.S. Navy, NGA, GEBCO
© 2010 Cnes/Spot Image
© 2010 Europa Technologies
Image IBCAO
lat 64.001984° lon -19.126613° elev 375 m
Eye alt 317.63 km
Google

SEVIRI

Soufriere Hills
11-12 February 2010

36 hrs at 15 min resolution

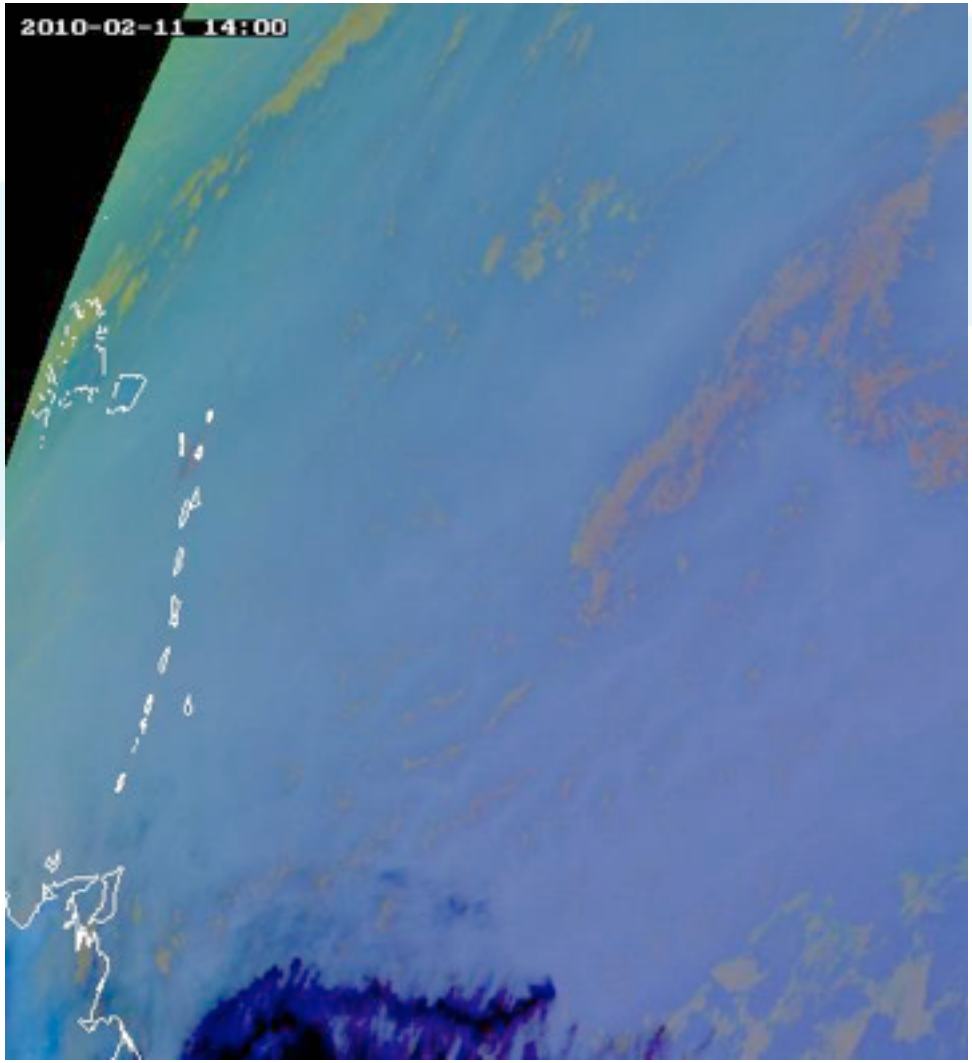

SEVIRI – triple detection

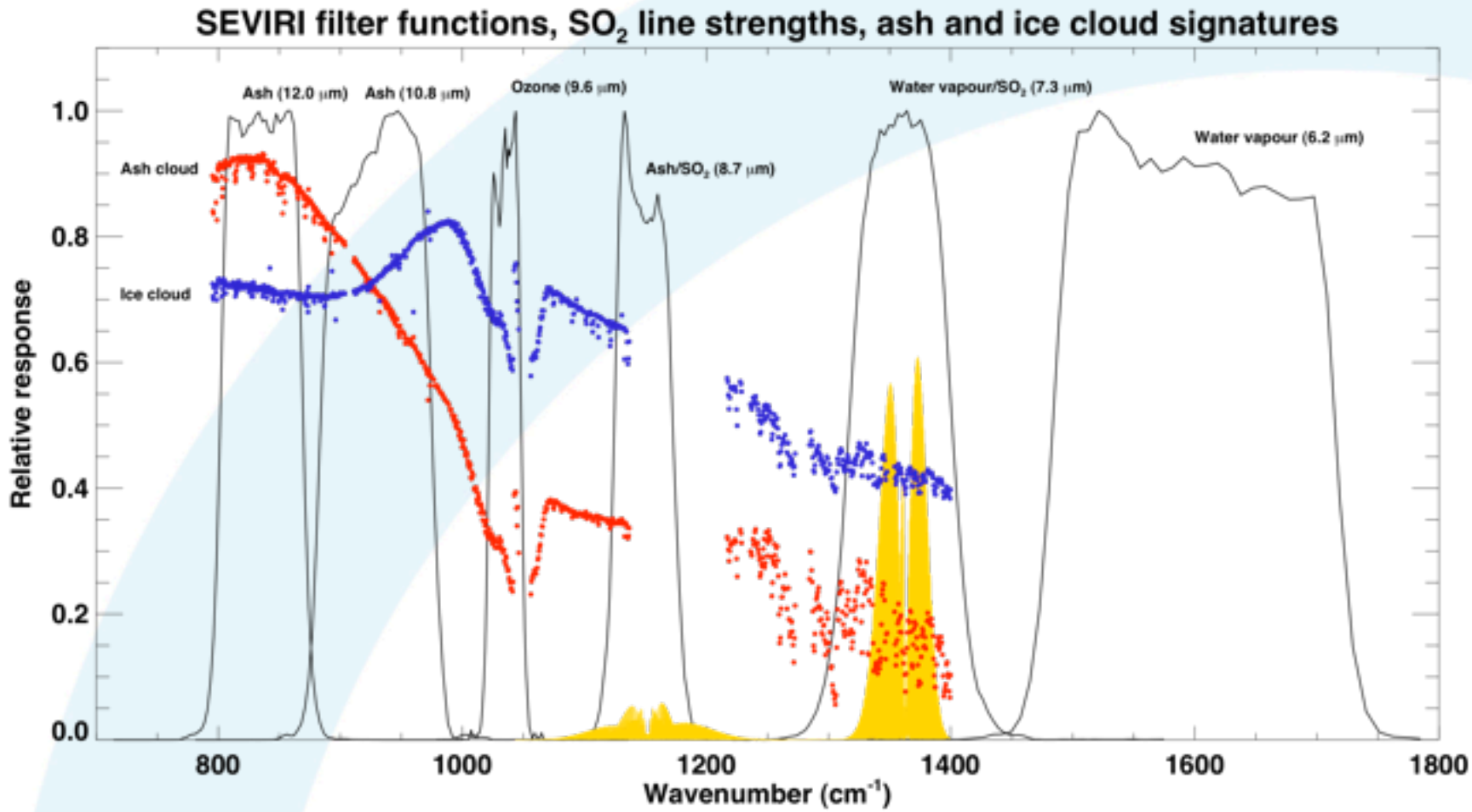

SEVIRI – triple detection

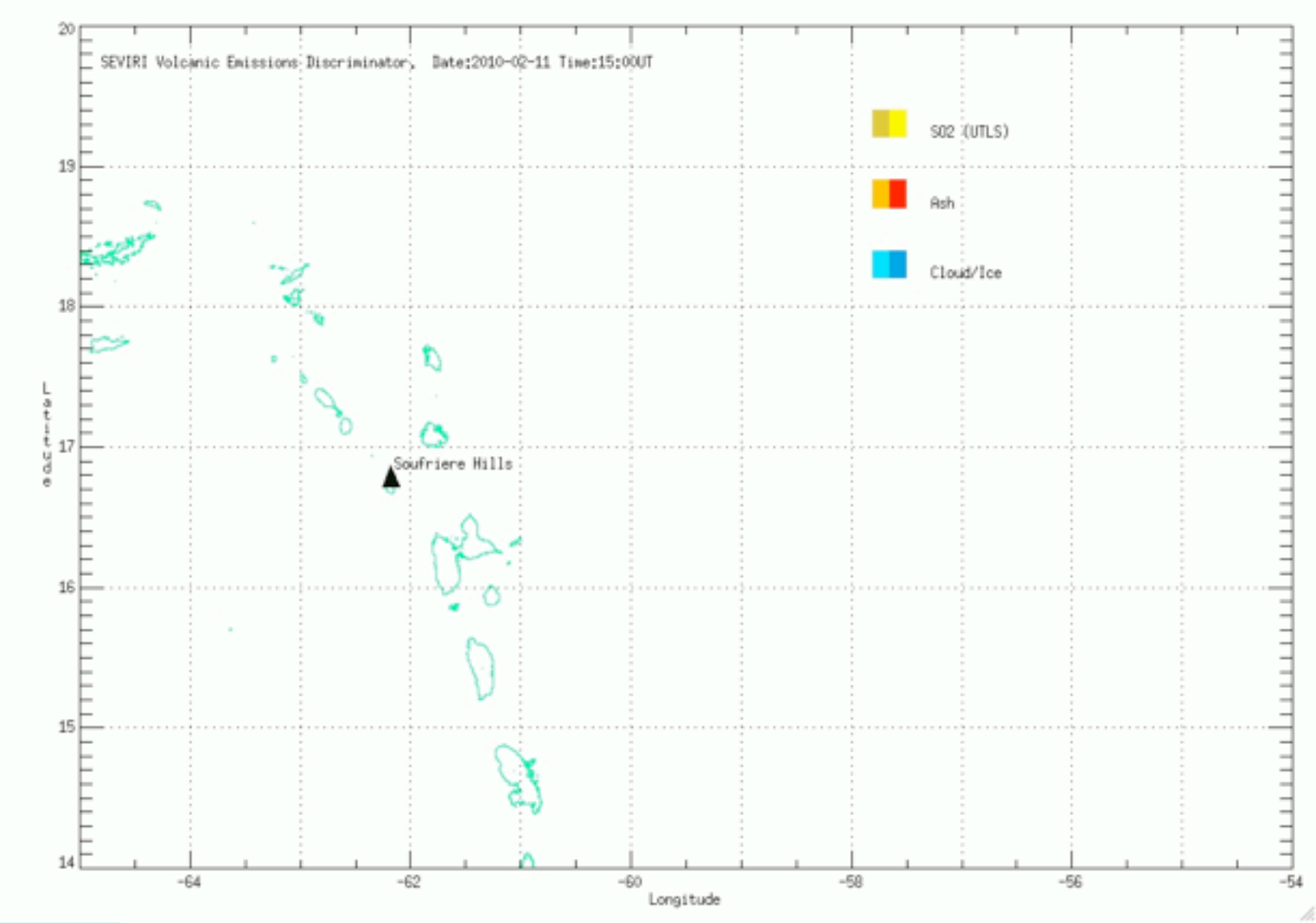

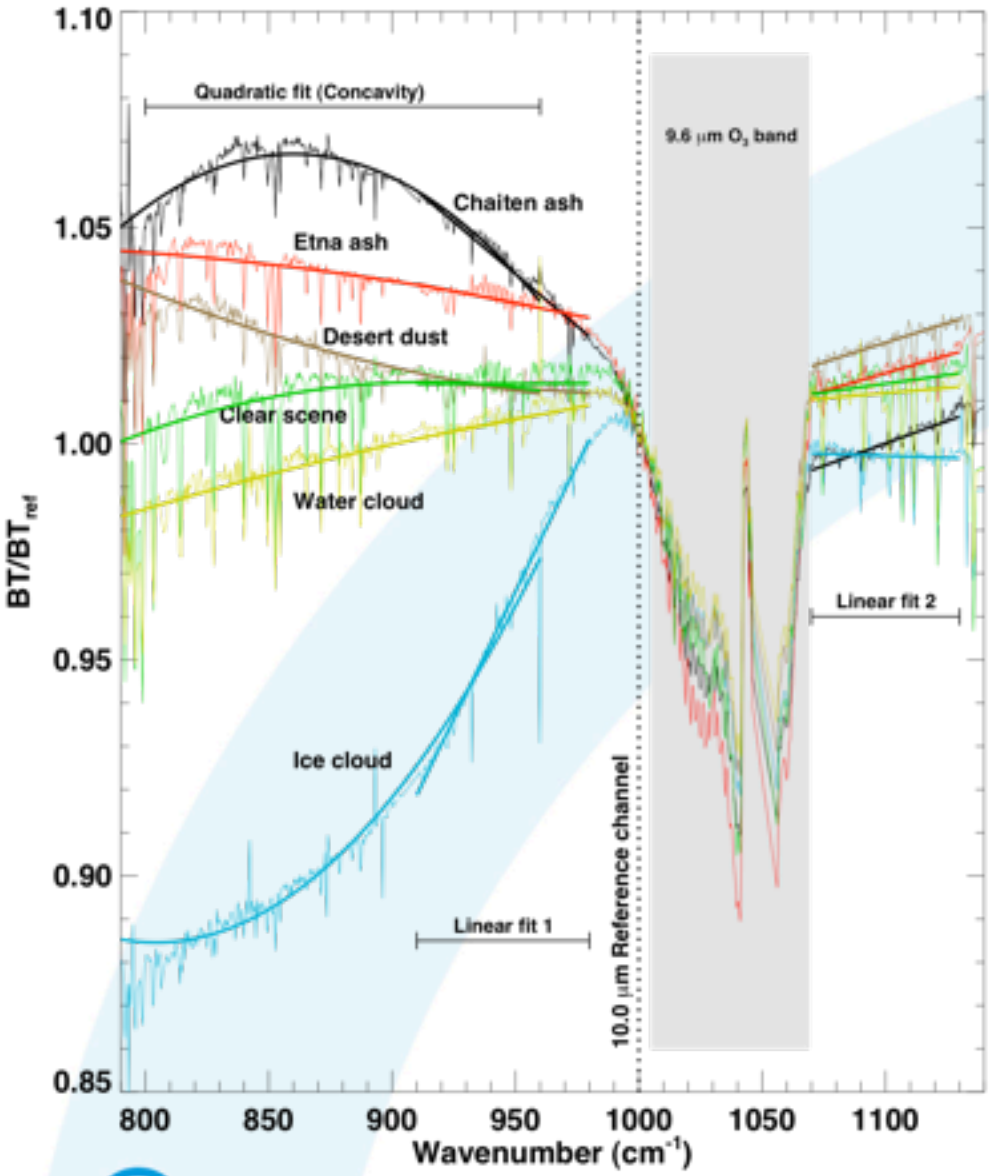
Quadratic fit (Concavity)
9.6 μm O3 band
Chaiten ash
Etna ash
Desert dust
Clear scene
Water cloud
Ice cloud
Linear fit 1
Linear fit 2
10.0 μm Reference channel
BT/BTref
Wavenumber (cm-1)
1.10
1.05
1.00
0.95
0.90
0.85
800
850
900
950
1000
1050
1100

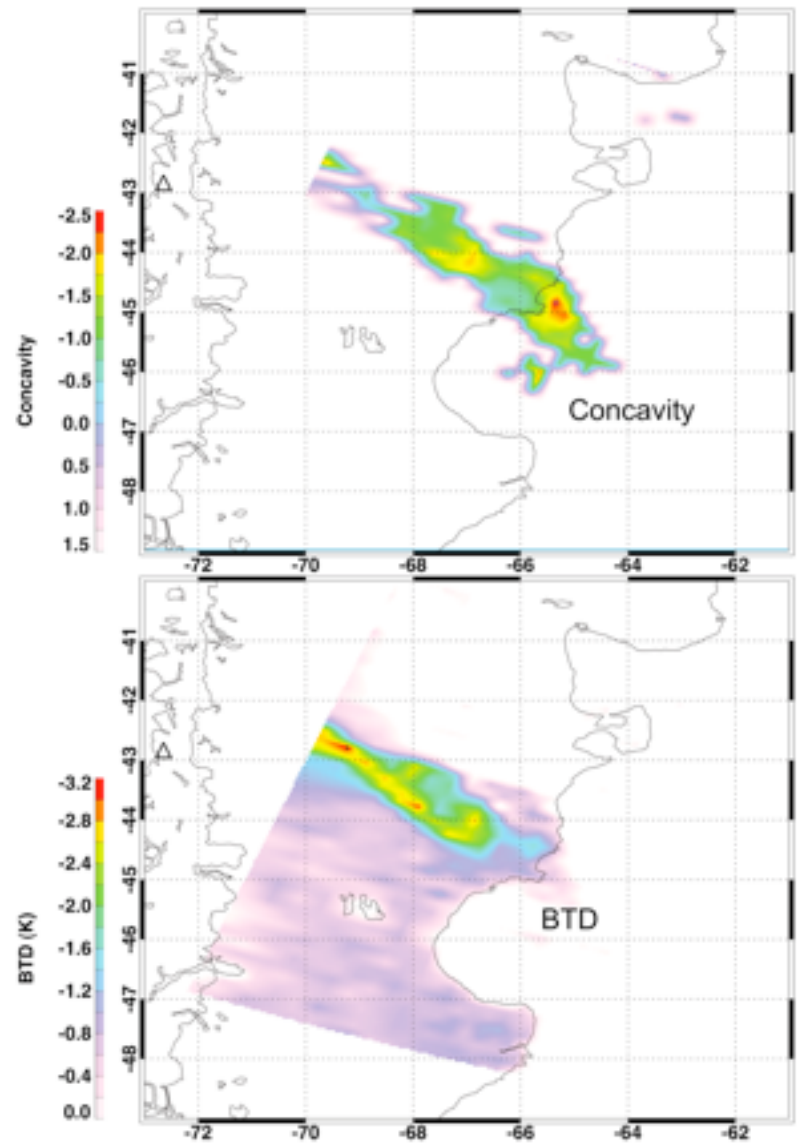
Concavity
Concavity
BTD
BTD (K)
-2.5
-2.0
-1.5
-1.0
-0.5
0.0
0.5
1.0
1.5
-3.2
-2.8
-2.4
-2.0
-1.6
-1.2
-0.8
-0.4
0.0
-41
-42
-43
-44
-45
-46
-47
-48
-72
-70
-68
-66
-64
-62

Linear 1 – SO_2

Contents lists available at ScienceDirect

Remote Sensing of Environment

journal homepage: www.elsevier.com/locate/rse

The infrared spectral signature of volcanic ash determined from high-spectral resolution satellite measurements

G. Gangale [a], A.J. Prata [b,*], L. Clarisse [c]

[a] Dipartimento di Ingegneria dei Materiali e dell'Ambiente, Università di Modena e Reggio Emilia, Italy
[b] Climate and Atmosphere Department, Norwegian Institute for Air Research, PO Box 100, 2027 Kjeller, Norway
[c] Spectroscopie de l'Atmosphère, Service de Chimie Quantique Photophysique, Université Libre de Bruxelles, Brussels, Belgium

ARTICLE INFO

Article history:
Received 22 June 2009
Received in revised form 21 September 2009
Accepted 23 September 2009
Available online xxxx

Keywords:
Volcanic ash
Radiative transfer
Infrared remote sensing

ABSTRACT

High-spectral resolution infrared spectra of the earth's atmosphere and surface are routinely available from satellite sensors, such as the Atmospheric Infrared Sounder (AIRS) and the Infrared Atmospheric Sounding Interferometer (IASI). We exploit the spectral content of AIRS data to demonstrate that airborne volcanic ash has a unique signature in the infrared (8–12 μm) that can be used to infer particle size, infrared opacity and composition. The spectral signature is interpreted with the aid of a radiative transfer model utilizing the optical properties of andesite, rhyolite and quartz. Based on the infrared spectral signature, a new volcanic ash detection algorithm is proposed that can discriminate volcanic ash from other airborne substances and we show that the algorithm depends on particle size, optical depth and composition. The new algorithm has an improved sensitivity to optically thin ash clouds, and hence can detect them for longer (~4 days) and at greater distances from the source(~5000 km).

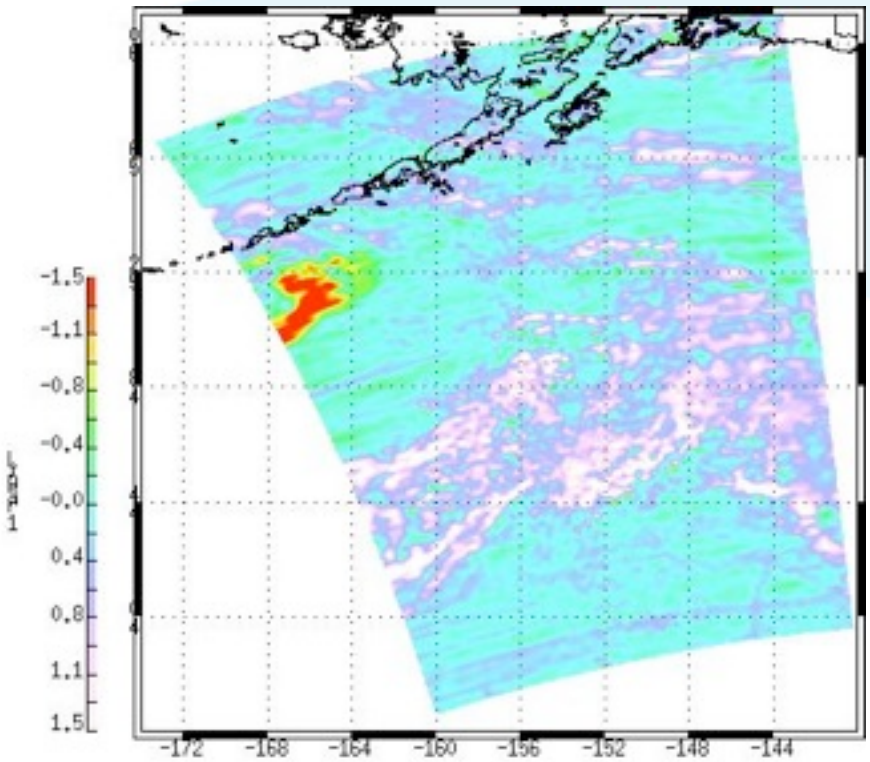

Linear 2 – SO_2

Contents lists available at ScienceDirect

Remote Sensing of Environment

journal homepage: www.elsevier.com/locate/rse

The infrared spectral signature of volcanic ash determined from high-spectral resolution satellite measurements

G. Gangale [a], A.J. Prata [b,*], L. Clarisse [c]

[a] Dipartimento di Ingegneria dei Materiali e dell'Ambiente, Università di Modena e Reggio Emilia, Italy
[b] Climate and Atmosphere Department, Norwegian Institute for Air Research, PO Box 100, 2027 Kjeller, Norway
[c] Spectroscopie de l'Atmosphère, Service de Chimie Quantique Photophysique, Université Libre de Bruxelles, Brussels, Belgium

ARTICLE INFO

Article history:
Received 22 June 2009
Received in revised form 21 September 2009
Accepted 23 September 2009
Available online xxxx

Keywords:
Volcanic ash
Radiative transfer
Infrared remote sensing

ABSTRACT

High-spectral resolution infrared spectra of the earth's atmosphere and surface are routinely available from satellite sensors, such as the Atmospheric Infrared Sounder (AIRS) and the Infrared Atmospheric Sounding Interferometer (IASI). We exploit the spectral content of AIRS data to demonstrate that airborne volcanic ash has a unique signature in the infrared (8–12 μm) that can be used to infer particle size, infrared opacity and composition. The spectral signature is interpreted with the aid of a radiative transfer model utilizing the optical properties of andesite, rhyolite and quartz. Based on the infrared spectral signature, a new volcanic ash detection algorithm is proposed that can discriminate volcanic ash from other airborne substances and we show that the algorithm depends on particle size, optical depth and composition. The new algorithm has an improved sensitivity to optically thin ash clouds, and hence can detect them for longer (~4 days) and at greater distances from the source(~5000 km).

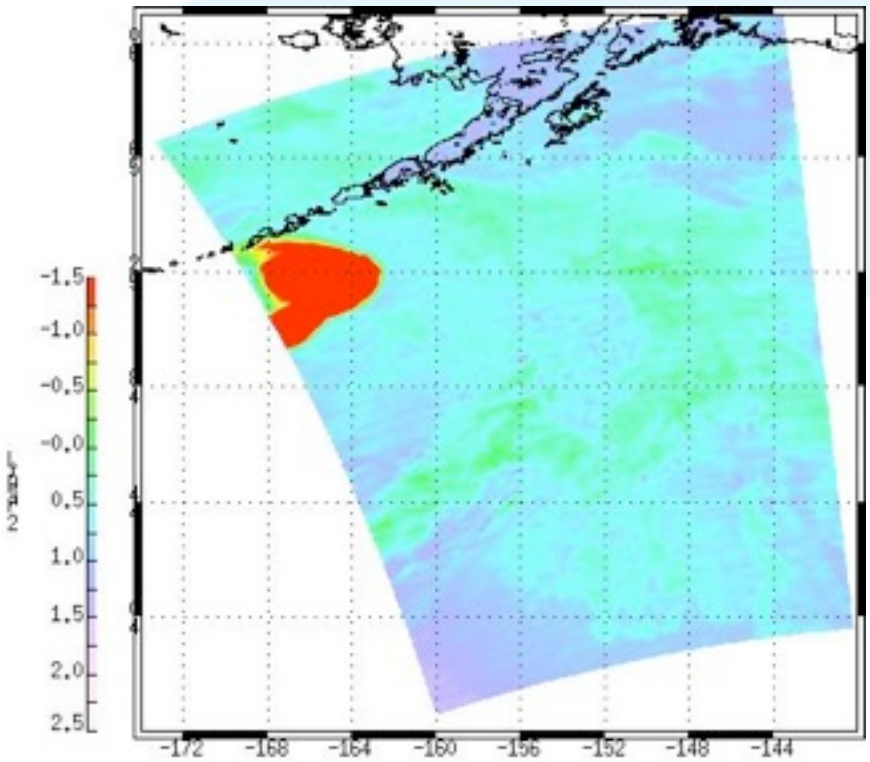

Concavity

Contents lists available at ScienceDirect

Remote Sensing of Environment

journal homepage: www.elsevier.com/locate/rse

The infrared spectral signature of volcanic ash determined from high-spectral resolution satellite measurements

G. Gangale [a], A.J. Prata [b,*], L. Clarisse [c]

[a] Dipartimento di Ingegneria dei Materiali e dell'Ambiente, Università di Modena e Reggio Emilia, Italy
[b] Climate and Atmosphere Department, Norwegian Institute for Air Research, PO Box 100, 2027 Kjeller, Norway
[c] Spectroscopie de l'Atmosphère, Service de Chimie Quantique Photophysique, Université Libre de Bruxelles, Brussels, Belgium

ARTICLE INFO

Article history:
Received 22 June 2009
Received in revised form 21 September 2009
Accepted 23 September 2009
Available online xxxx

Keywords:
Volcanic ash
Radiative transfer
Infrared remote sensing

ABSTRACT

High-spectral resolution infrared spectra of the earth's atmosphere and surface are routinely available from satellite sensors, such as the Atmospheric Infrared Sounder (AIRS) and the Infrared Atmospheric Sounding Interferometer (IASI). We exploit the spectral content of AIRS data to demonstrate that airborne volcanic ash has a unique signature in the infrared (8–12 μm) that can be used to infer particle size, infrared opacity and composition. The spectral signature is interpreted with the aid of a radiative transfer model utilizing the optical properties of andesite, rhyolite and quartz. Based on the infrared spectral signature, a new volcanic ash detection algorithm is proposed that can discriminate volcanic ash from other airborne substances and we show that the algorithm depends on particle size, optical depth and composition. The new algorithm has an improved sensitivity to optically thin ash clouds, and hence can detect them for longer (~4 days) and at greater distances from the source(~5000 km).

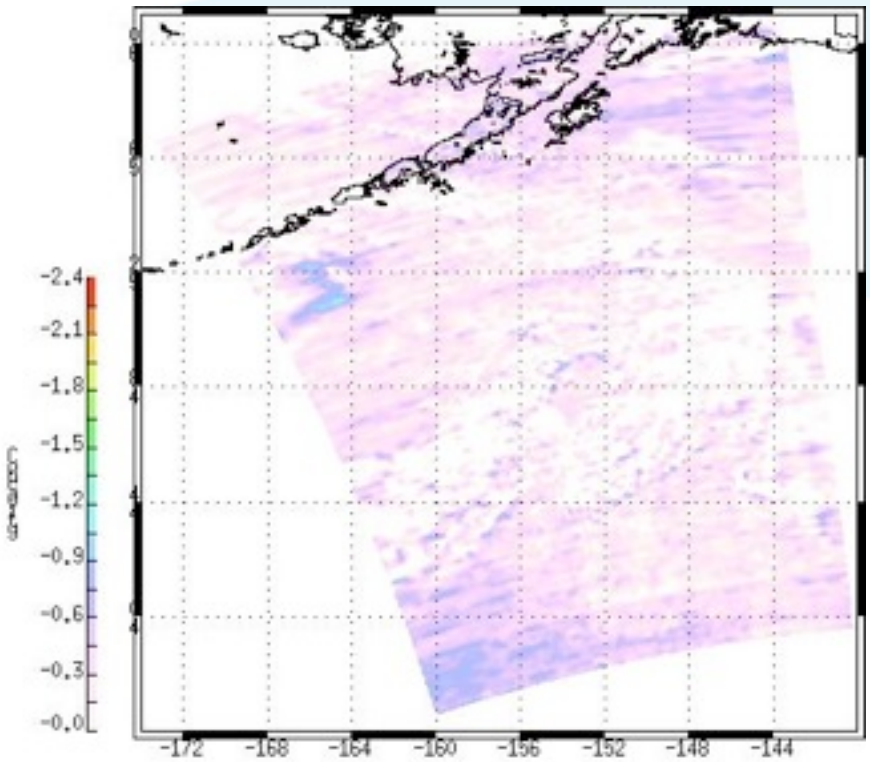

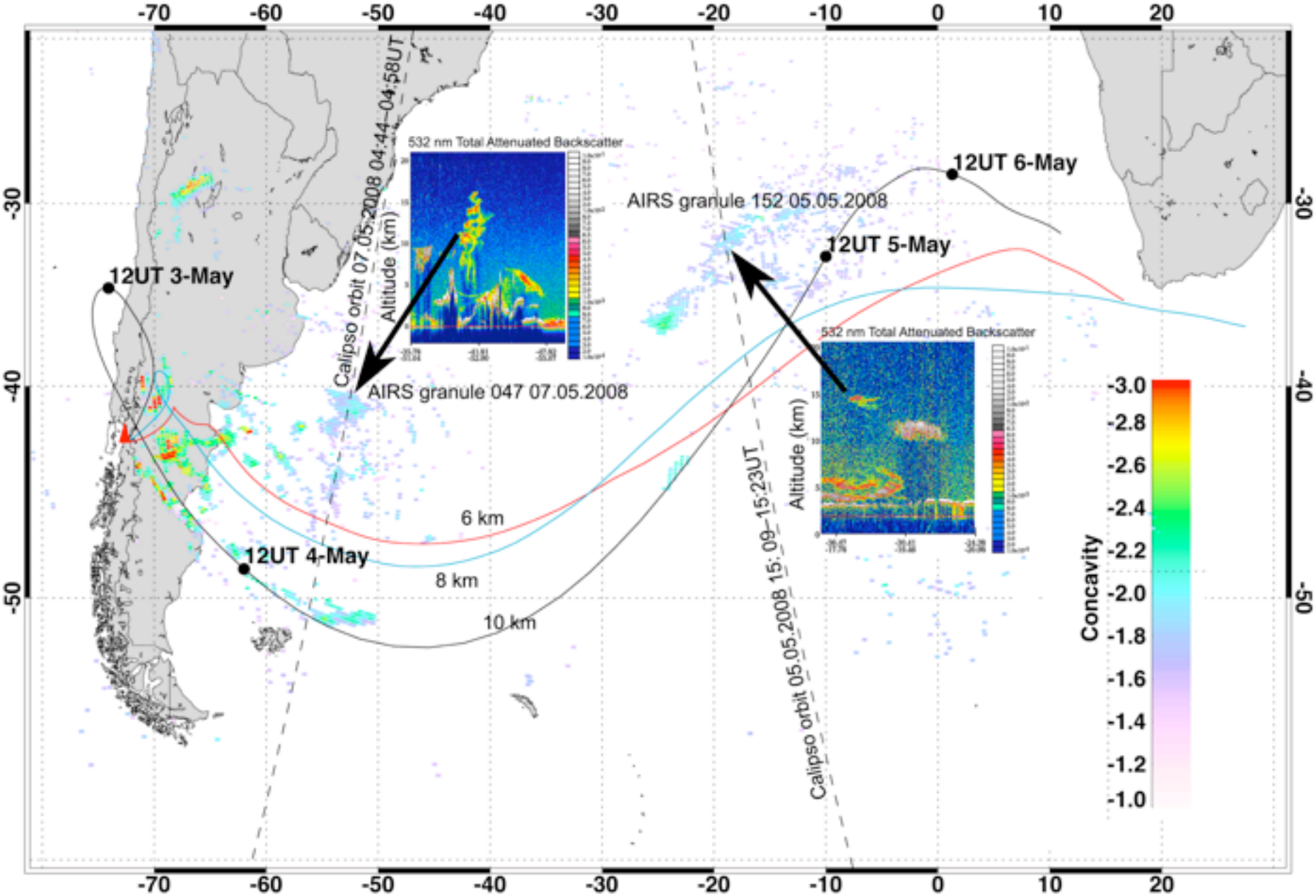
532 nm Total Attenuated Backscatter
Altitude (km)
Calipso orbit 07.05.2008 04:44–04:58UT
AIRS granule 047 07.05.2008
AIRS granule 152 05.05.2008
12UT 3-May
12UT 4-May
12UT 5-May
12UT 6-May
6 km
8 km
10 km
532 nm Total Attenuated Backscatter
Altitude (km)
Calipso orbit 05.05.2008 15:09–15:23UT
Concavity
-3.0
-2.8
-2.6
-2.4
-2.2
-2.0
-1.8
-1.6
-1.4
-1.2
-1.0
-70
-60
-50
-40
-30
-20
-10
0
10
20

Collocation of ash and SO_2

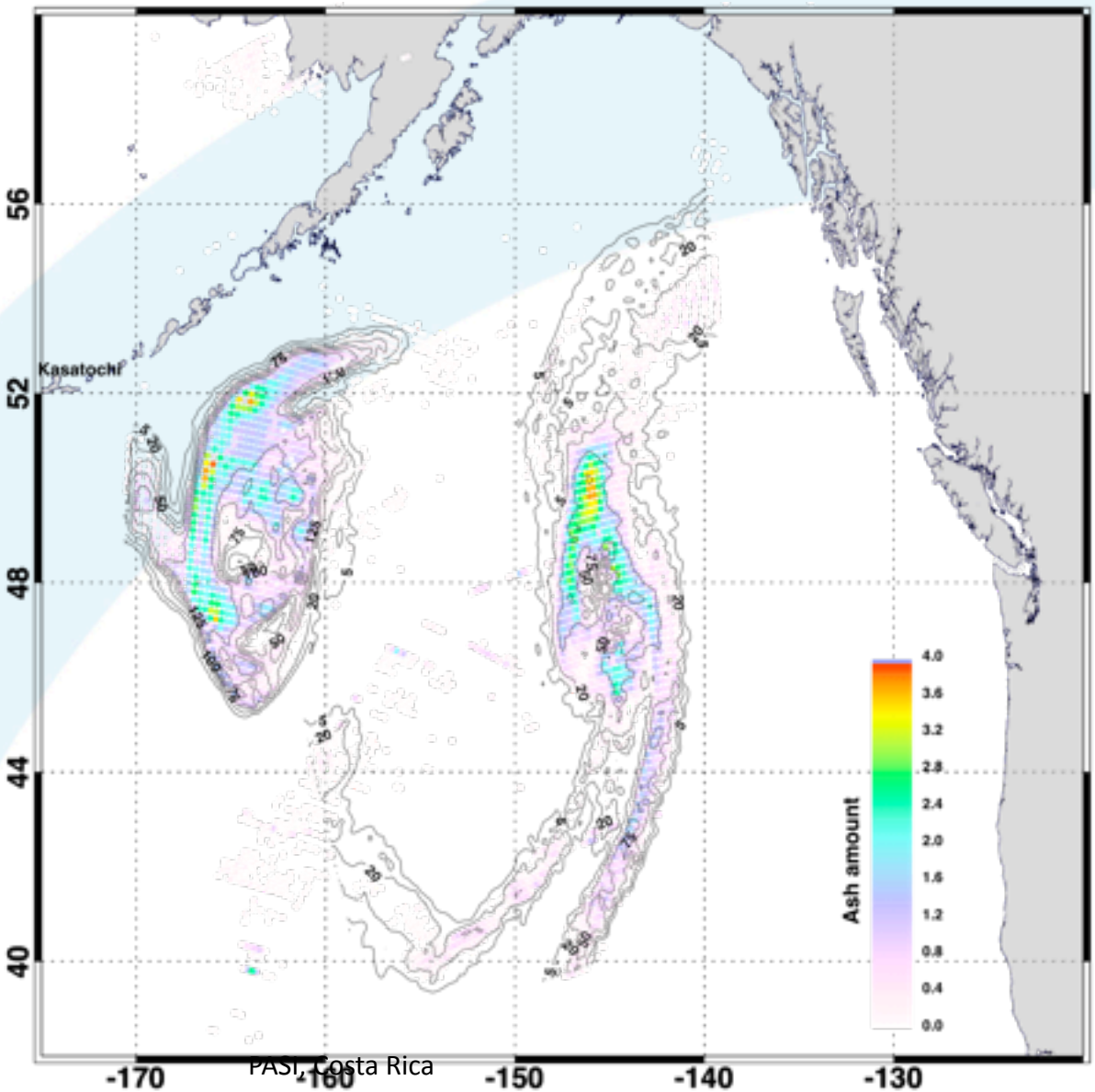

Chaitén, Chile

First rhyolitic ash eruption in the satellite era (~30 years)

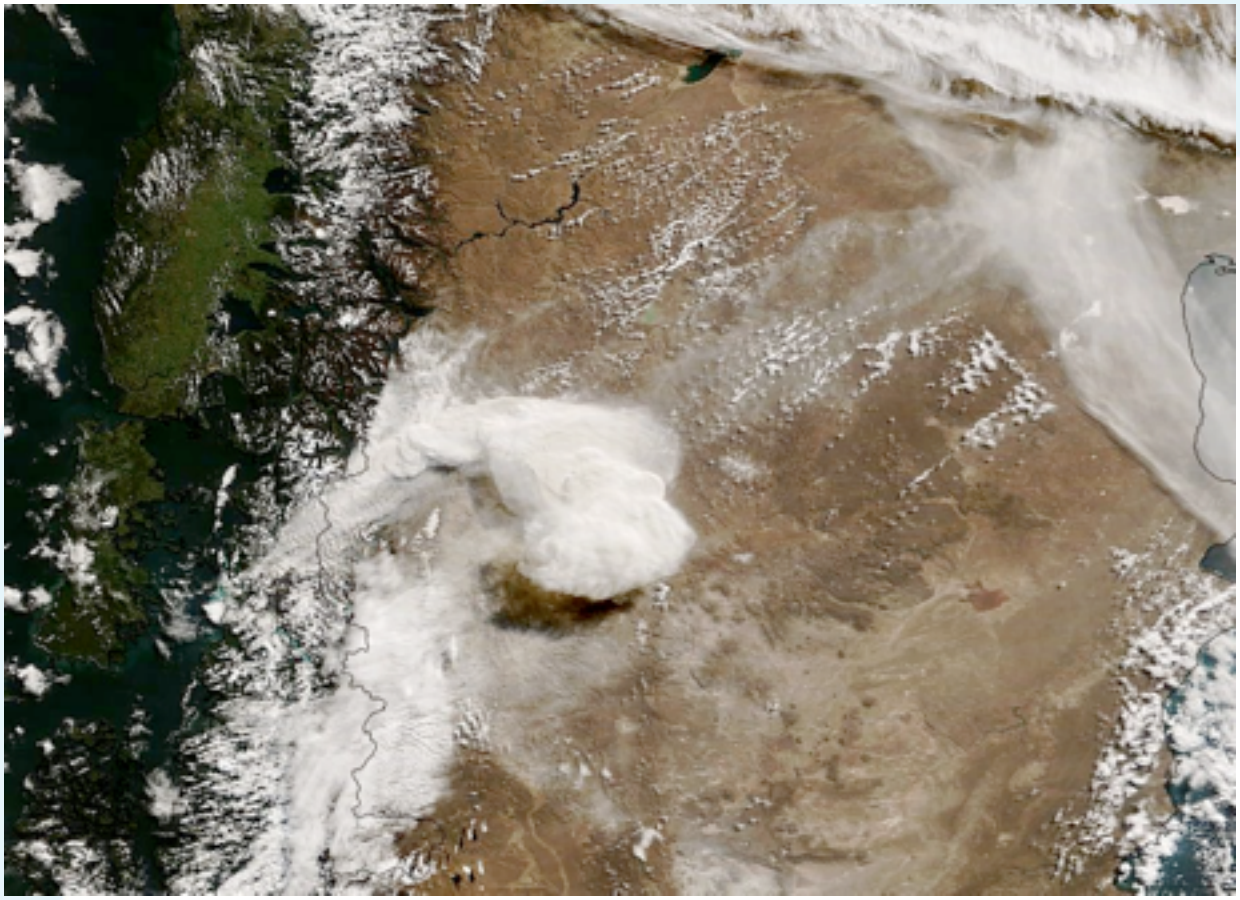

S.A. Carn, J.S. Pallister, L. Lara, J. Ewert, G. Villarosa, M. Fromm, S. Watt, A.J. Prata, D.M. Pyle, T.A. Mather, N. Matthews, R.S. Martin, A. Pavez, R. Aguilera, R. Thomas, W. Rison, P. Krehbiel, J. Johnson, A. Folch, D. Basualto, T.J. Casadevall, M. Guffanti, C. Benitez, J.G. Viramonte, 2008, The awakening of Chaitén volcano, Chile, ***EOS Trans. (to appear).***

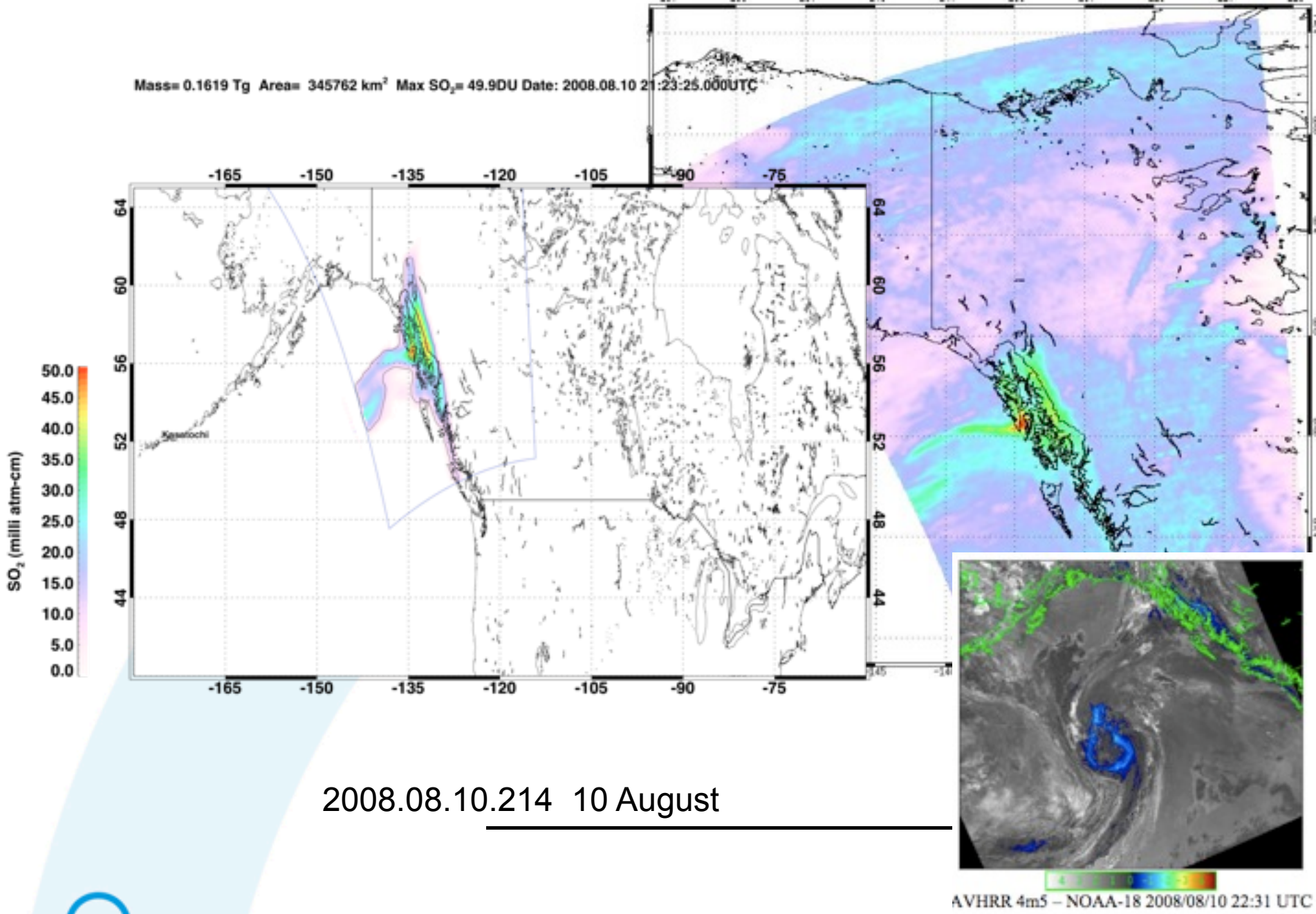

2008.08.10.214 10 August

Sensitivity to particle size and

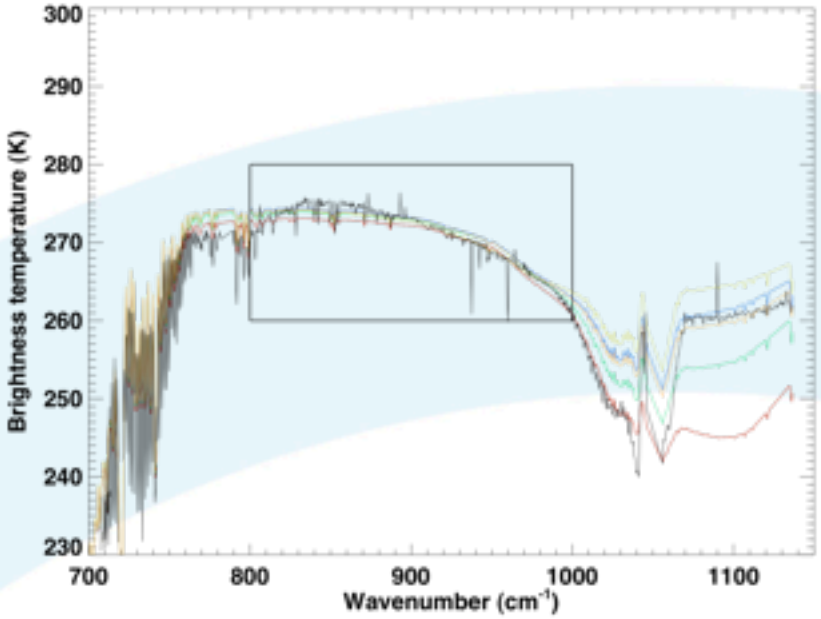

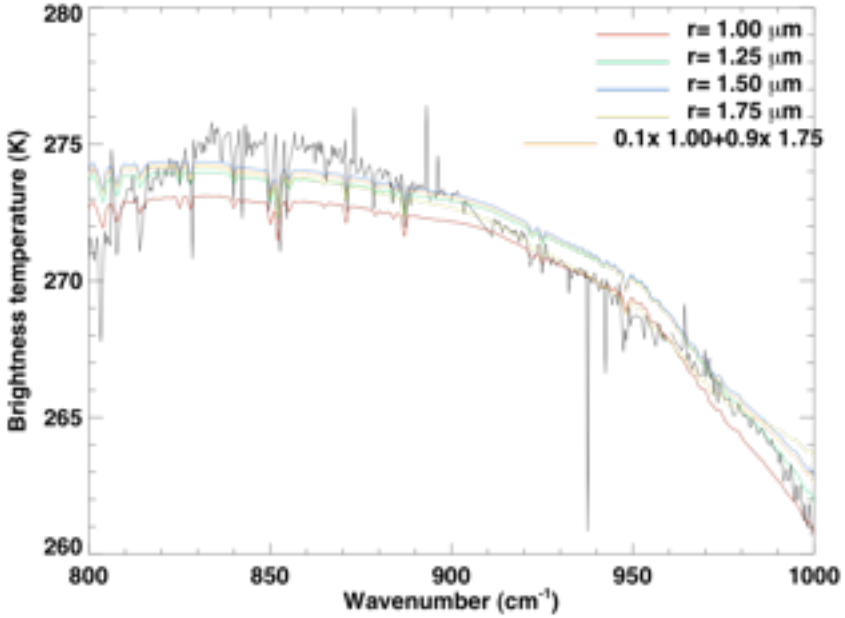

IASI

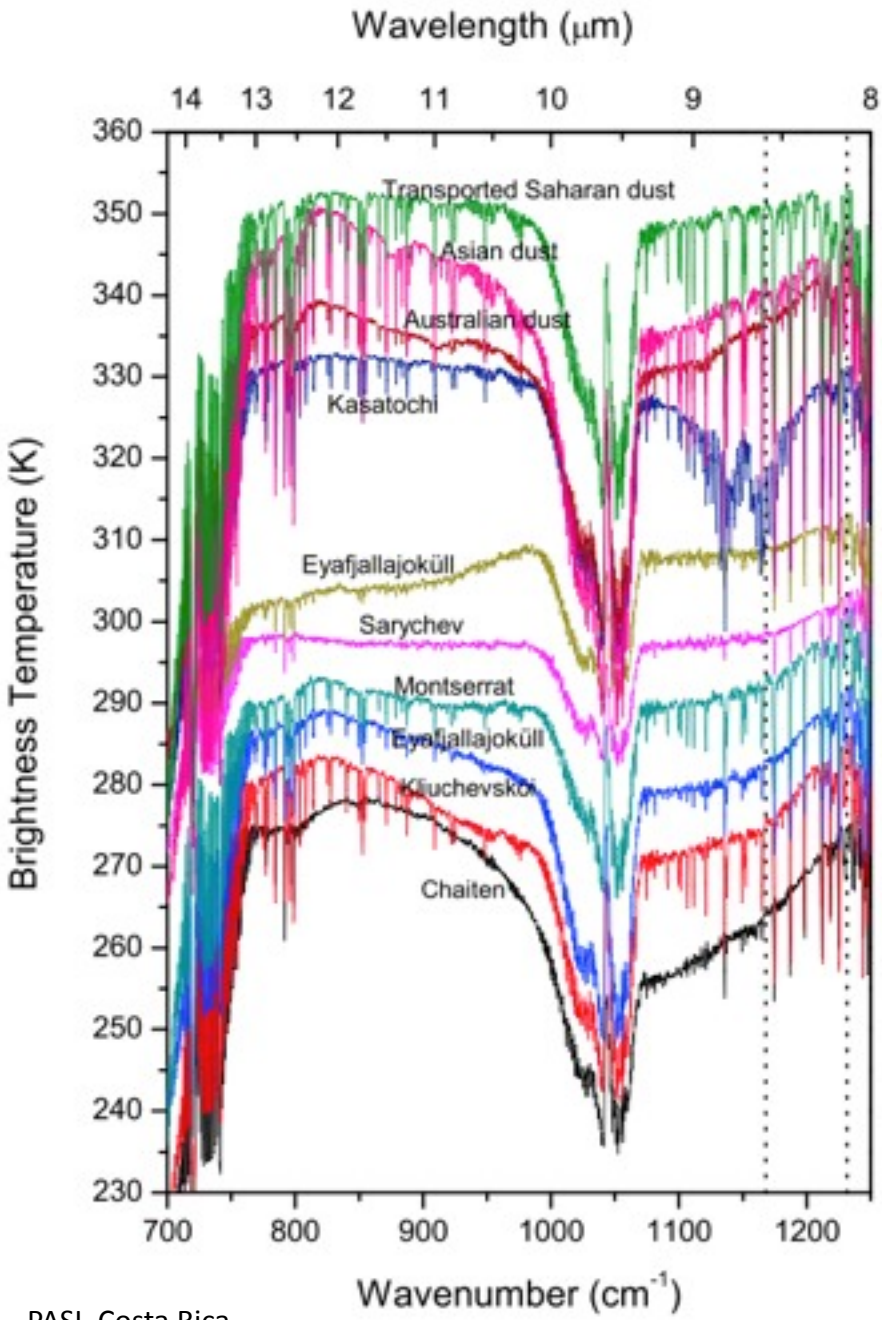
Wavelength (μm)
14
13
12
11
10
9
8
Brightness Temperature (K)
360
350
340
330
320
310
300
290
280
270
260
250
240
230
Transported Saharan dust
Asian dust
Australian dust
Kasatochi
Eyafjallajoküll
Sarychev
Montserrat
Eyafjallajoküll
Kliuchevskoi
Chaiten
700
800
900
1000
1100
1200
Wavenumber (cm-1)

Papers …

GEOPHYSICAL RESEARCH LETTERS, VOL. 37, L19806, doi:10.1029/2010GL044828, 2010

A correlation method for volcanic ash detection using hyperspectral infrared measurements

Lieven Clarisse,[1] Fred Prata,[2] Jean-Lionel Lacour,[1] Daniel Hurtmans,[1] Cathy Clerbaux,[1,3] and Pierre-François Coheur[1]

Received 23 July 2010; revised 26 August 2010; accepted 27 August 2010; published 12 October 2010.

[1] Remote satellite detection of airborne volcanic ash is important for mitigating hazards to aviation and for calculating plume altitudes. Infrared sounders are essential for detecting ash, as they can distinguishing aerosol type and can be used day and night. While broadband sensors are mainly used for this purpose, they have inherent limitations. Typically, water and ice can mask volcanic ash, while wind blown dust can yield false detection. High spectral resolution sounders should be able to overcome some of these limitations. However, existing detection methods are not easily applicable to hyperspectral sounders and there is therefore a pressing need for novel techniques. In response, we propose a sensitive and robust volcanic ash detection method for hyperspectral sounders based on correlation coefficients and demonstrate it on IASI observations. We show that the method differentiates ash from clouds and dust. Easy to implement, it could contribute to operational volcanic hazard mitigation. **Citation:** Clarisse, L., F. Prata, J.-L. Lacour, D. Hurtmans, C. Clerbaux, and P.-F. Coheur (2010), A correlation method for volcanic ash detection using hyperspectral infrared measurements, *Geophys. Res. Lett.*, *37*, L19806, doi:10.1029/2010GL044828.

infrared imagers (e.g., MODIS, AVHRR, GOES, SEVIRI). Most of the available algorithms find their origin in the reverse absorption method [*Prata*, 1989; *Tupper et al.*, 2004]. It exploits the differential absorption between channels in the region 10 to 12 μm. While water and ice clouds absorb preferentially towards 12 μm, ash clouds absorb preferentially towards 10 μm. There are a number of limitations to the reverse absorption technique [*Pavolonis et al.*, 2006], such as the fact that water and ice clouds can have a masking effect on the observation of volcanic ash, while wind blown mineral dust can yield false detection (see Figure 1). Several multichannel extensions and new algorithms have been proposed, enhancing both the sensitivity and robustness [see, e.g., *Ellrod et al.*, 2003; *Pergola et al.*, 2008; *Tupper et al.*, 2004; *Pavolonis and Sieglaff*, 2009].

[4] With the advent of the infrared sounders AIRS and IASI, and in the perspective of the planned GMES Sentinel missions for atmospheric composition, hyperspectral sounders are becoming increasingly important. While it is likely that these can overcome some of the limitations of broadband sensors (Figure 1 is a good example of how a spectrometer can discriminate more than an imager), there has been little progress in developing a universal volcanic ash detection

Retrieving radius, concentration, optical depth, and mass of different types of aerosols from high-resolution infrared nadir spectra

Lieven Clarisse,[1,*] Daniel Hurtmans,[1] Alfred J. Prata,[2] Federico Karagulian,[1] Cathy Clerbaux,[3,1] Martine De Mazière,[4] and Pierre-François Coheur[1]

[1]Spectroscopie de l'Atmosphère, Service de Chimie Quantique et Photophysique, Université Libre de Bruxelles (ULB), Brussels, Belgium

[2]Climate and Atmosphere Department, Norwegian Institute for Air Research, P.O. Box 100, 2027 Kjeller, Norway

[3]UPMC University Paris 06, Université Versailles Saint Quentin; CNRS/INSU, LATMOS-IPSL, Paris, France

[4]Belgian Institute for Space Aeronomy, 3 Avenue Circulaire, B-1180 Brussels, Belgium

*Corresponding author: lclariss@ulb.ac.be

Received 15 March 2010; revised 12 May 2010; accepted 18 May 2010; posted 2 June 2010 (Doc. ID 125477); published 23 June 2010

We present a sophisticated radiative transfer code for modeling outgoing IR radiation from planetary atmospheres and, conversely, for retrieving atmospheric properties from high-resolution nadir-observed spectra. The forward model is built around a doubling-adding routine and calculates, in a spherical refractive geometry, the outgoing radiation emitted by the Earth and the atmosphere containing one layer of aerosol. The inverse model uses an optimal estimation approach and can simultaneously retrieve atmospheric trace gases, aerosol effective radius, and concentration. It is different from existing codes, as most forward codes dealing with multiple scattering assume a plane-parallel atmosphere, and as for the retrieval, it does not rely on precalculated spectra, the use of microwindows, or two-step retrievals. The simultaneous retrieval on a broad spectral range exploits the full potential of current state-of-the-art hyperspectral IR sounders, such as AIRS and IASI, and should be particularly useful in studying major pollution events. We present five example retrievals of IASI spectra observed in the range from 800 to 1200 cm^{-1} above dust, volcanic ash, sulfuric acid, ice particles, and biomass burning aerosols.

OCIS codes: 010.1100, 010.0280, 010.5620.

Three year SO_2 measurements from IASI

Lieven Clarisse, Fred Prata, Andreas Richter, Simon Carn, Daniel Hurtmans, Pierre Coheur, Juliette Hadji-Lazaro, Cathy Clerbaux

The SO_2 Pyramid

Upper Troposphere
Lower Stratosphere

-0.5 W/m^2 (± 2)

1Tg ± a lot

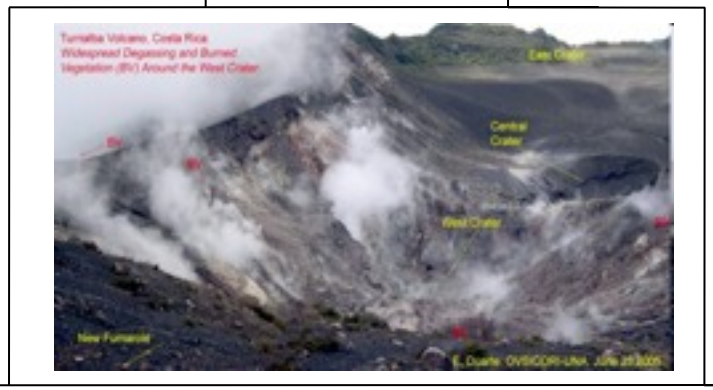

Free troposphere: -0.3 W/m^2

10 ± 5 Tg

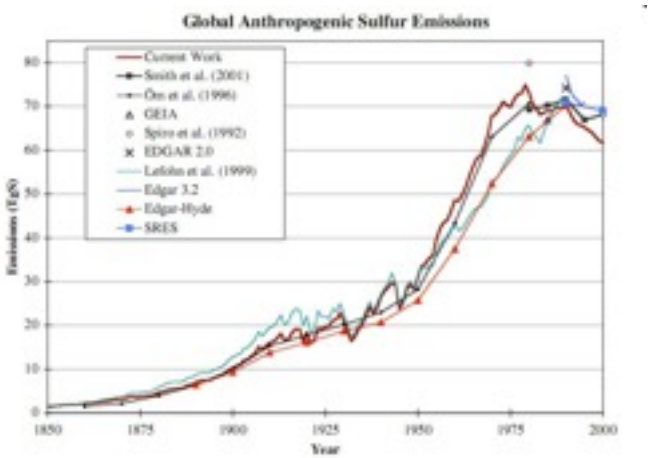

Figure 1–Global sulfur dioxide emissions from this study (thick line) and several other recent estimates (see text). Note that the Lefohn *et al.* estimate does not include all anthropogenic emissions sources. References not shown on the curt are: GEIA (Benkovitz *et al.* 1996); EDGAR 2.0 (Olivier *et al* 1996); EDGAR 3.2 (Olivier and Berdowski, 2001); EDGAR-HYDE (Van Aardenne *et al.* 2001); and SRES (Nakicenovic and Swart 2000).

Boundary Layer: -0.2 W/m^2

70 ± 10 Tg

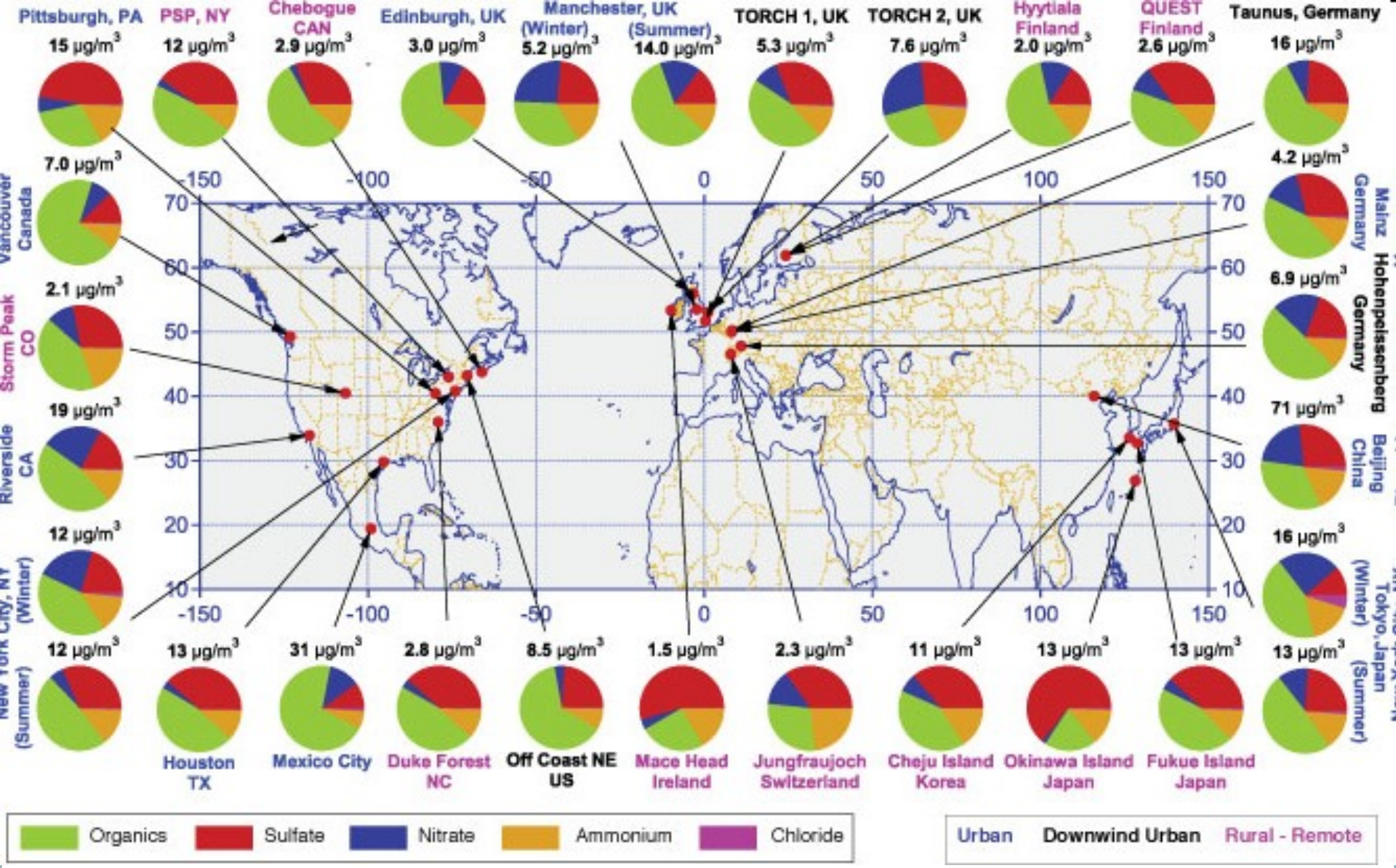

Sulphuric acid
Ammonium sulphate

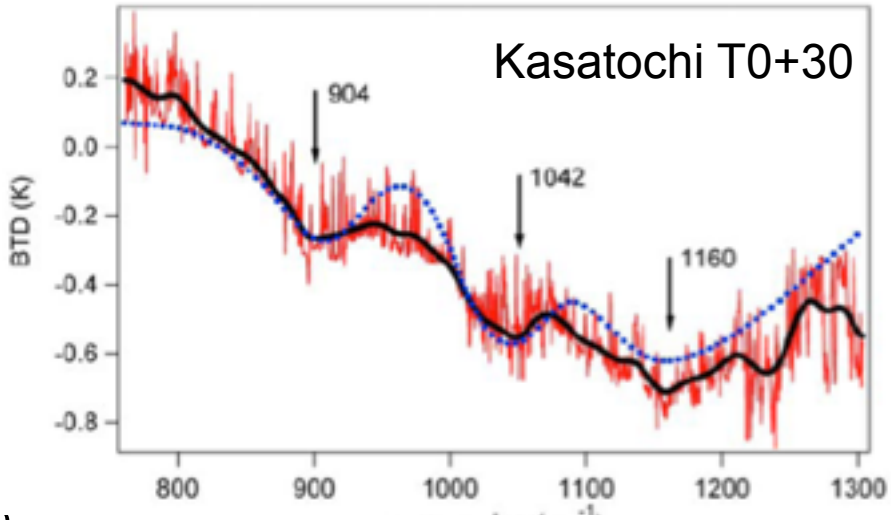
Kasatochi T0+30
BTD (K)
904
1042
1160
0.2
0.0
-0.2
-0.4
-0.6
-0.8
800
900
1000
1100
1200
1300

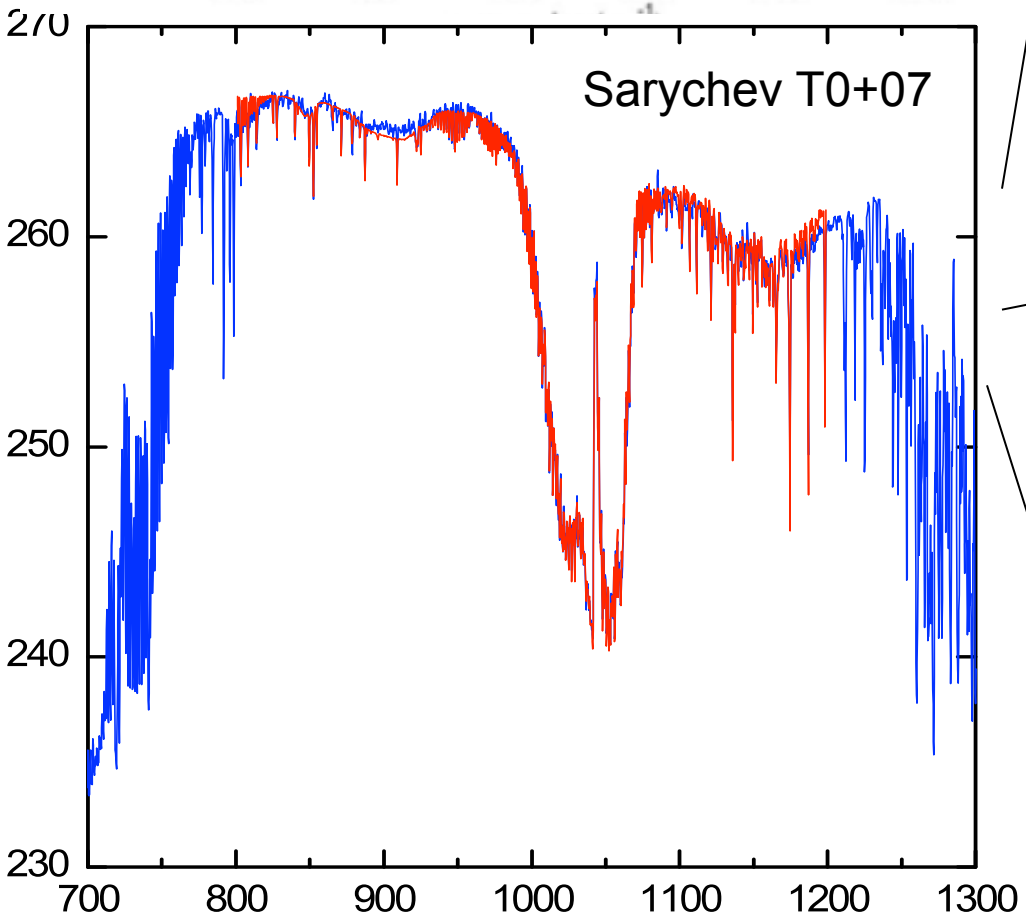
Sarychev T0+07
270
260
250
240
230
700
800
900
1000
1100
1200
1300

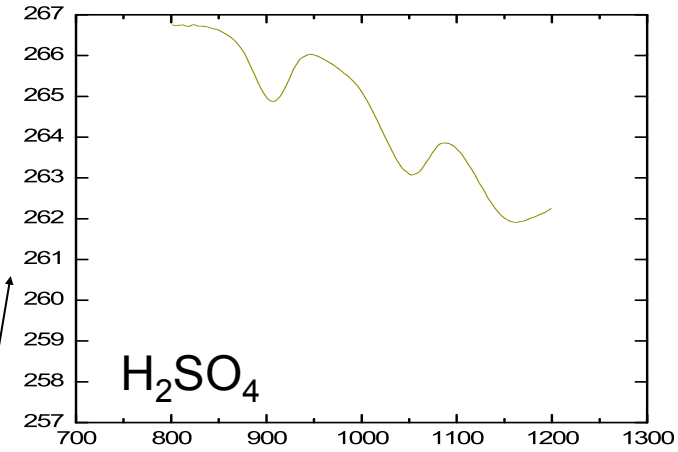
H_2SO_4
267
266
265
264
263
262
261
260
259
258
257
700
800
900
1000
1100
1200
1300

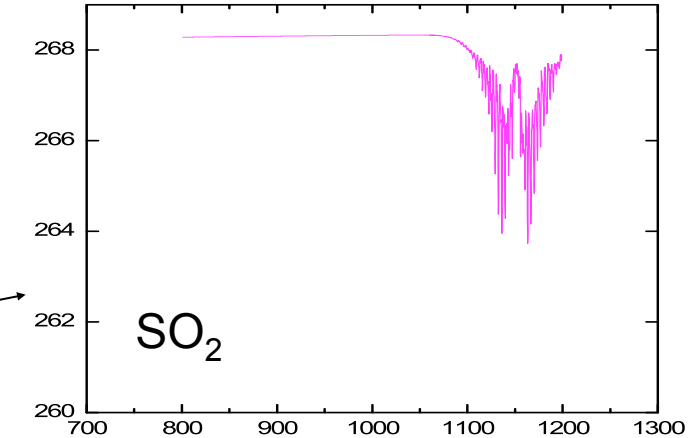
SO_2
268
266
264
262
260
700
800
900
1000
1100
1200
1300

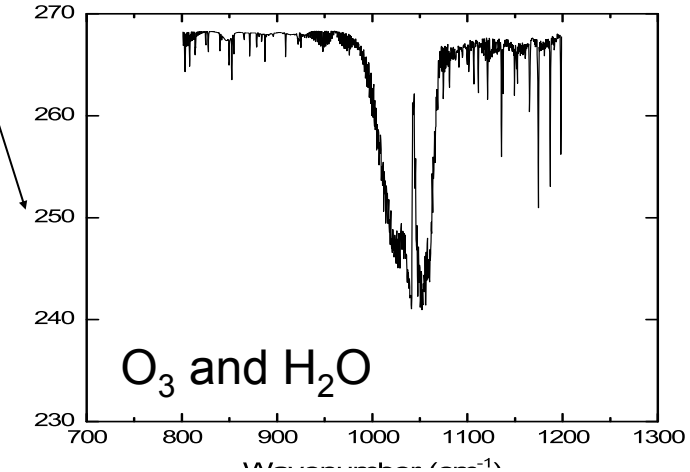
O_3 and H_2O
270
260
250
240
230
700
800
900
1000
1100
1200
1300

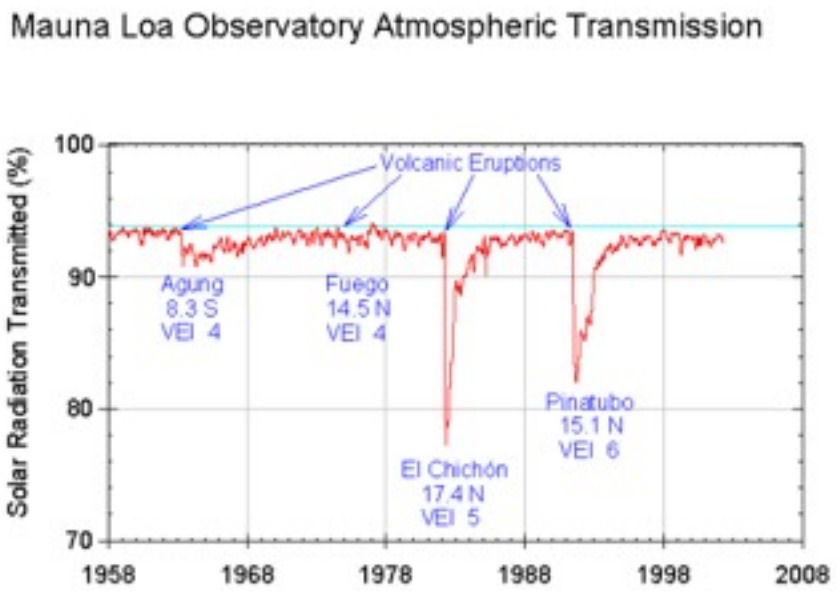
Mauna Loa Observatory Atmospheric Transmission
Solar Radiation Transmitted (%)
100
90
80
70
1958
1968
1978
1988
1998
2008
Volcanic Eruptions
Agung
8.3 S
VEI 4
Fuego
14.5 N
VEI 4
El Chichón
17.4 N
VEI 5
Pinatubo
15.1 N
VEI 6

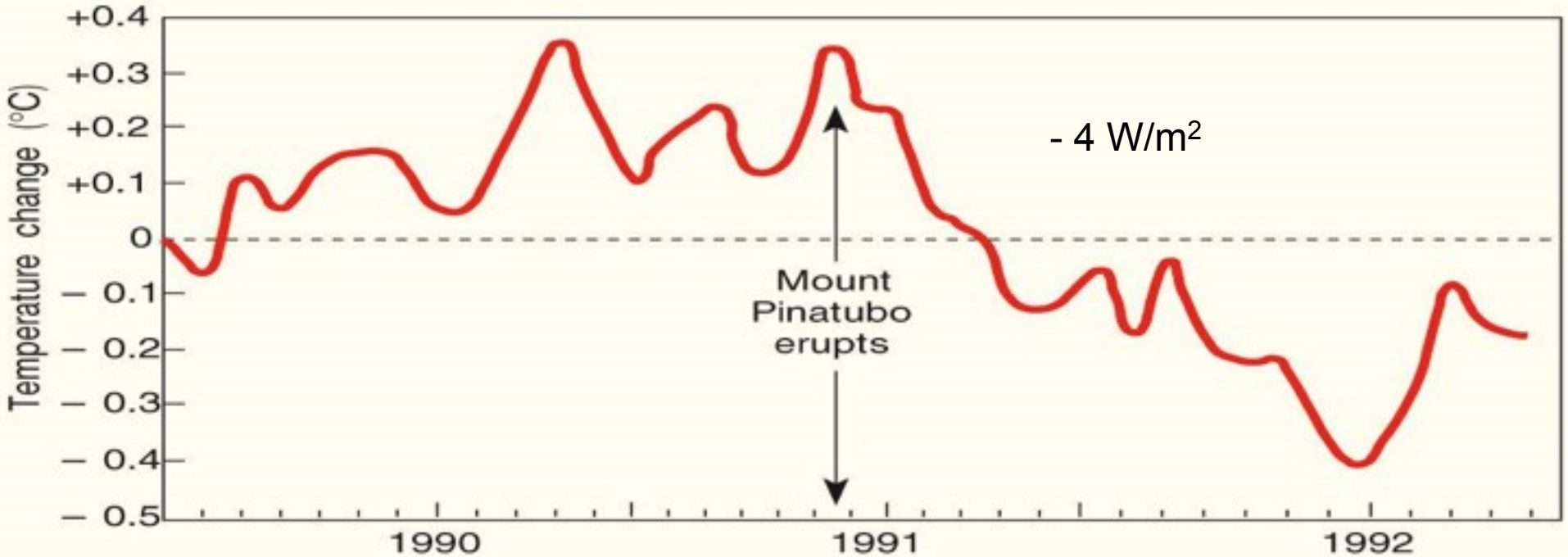
Temperature change (°C)
+0.4
+0.3
+0.2
+0.1
0
– 0.1
– 0.2
– 0.3
– 0.4
– 0.5
1990
1991
1992
Mount
Pinatubo
erupts
- 4 W/m²

TOMS Sulfur dioxide (kt) record

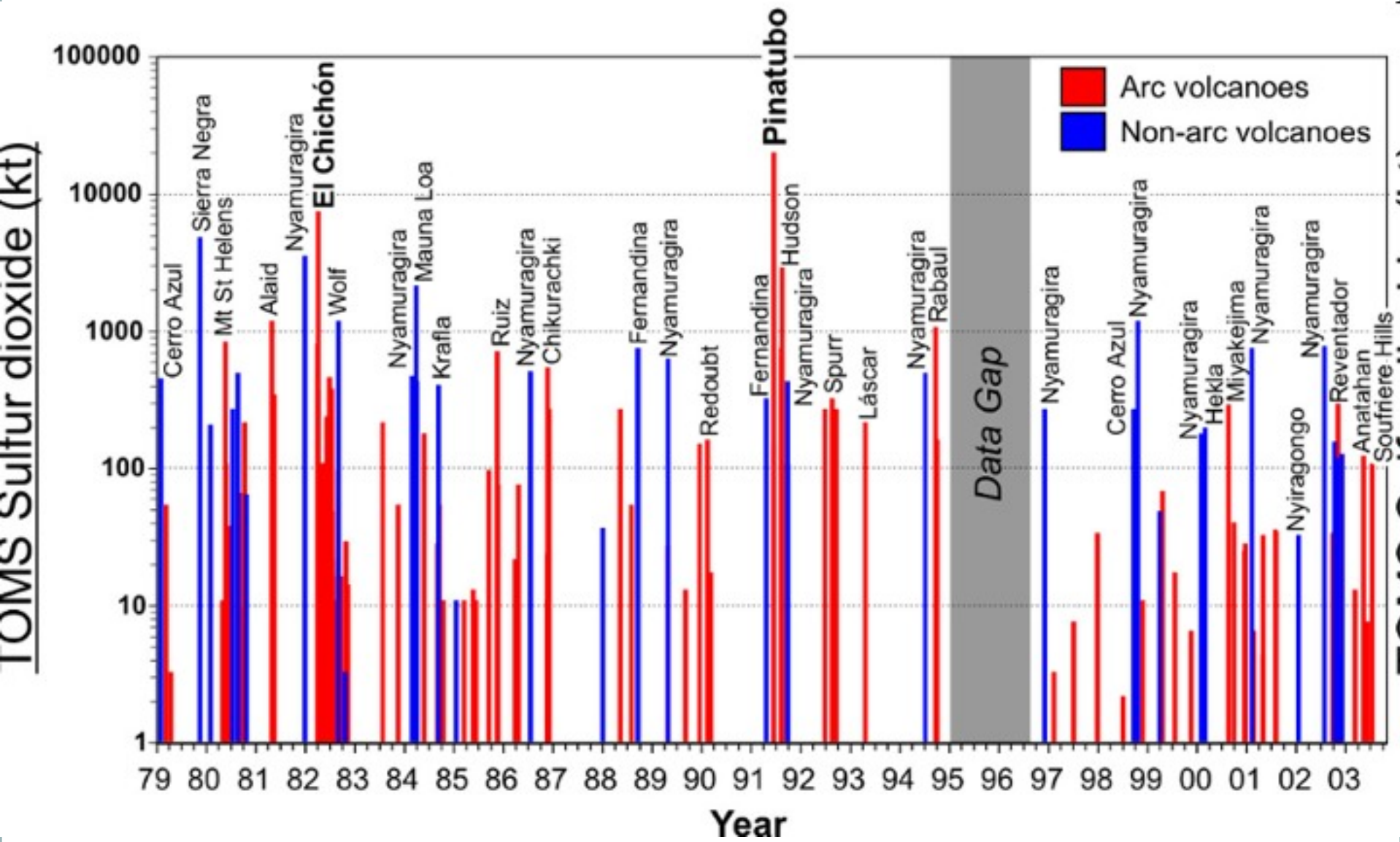

5DU detection limit / 10-30 % error !?

	TOMS UV	GOME2 UV	OMI UV	AIRS IR	IASI IR
Footprint	39x39	80x40	13x24	13x13	12x12
Channels	7	4096	780	2378	8460
Spectral resolution	1.1nm	0.3nm	0.45nm	$1cm^{-1}$	$0.5cm^{-1}$
Detection Limit – DU	5	0.25	0.25	0.25	0.25
Coverage	1	1	1	2	2

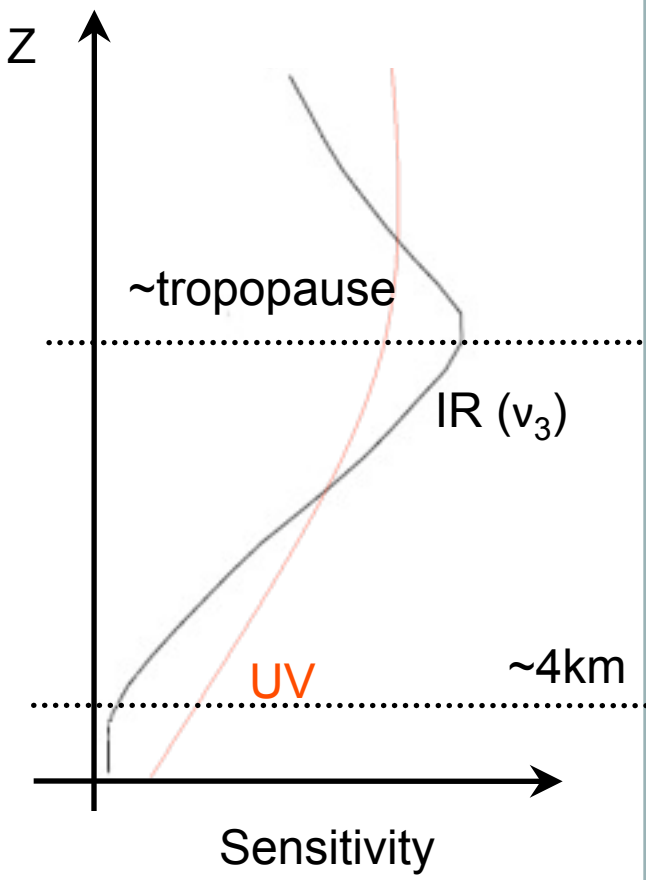

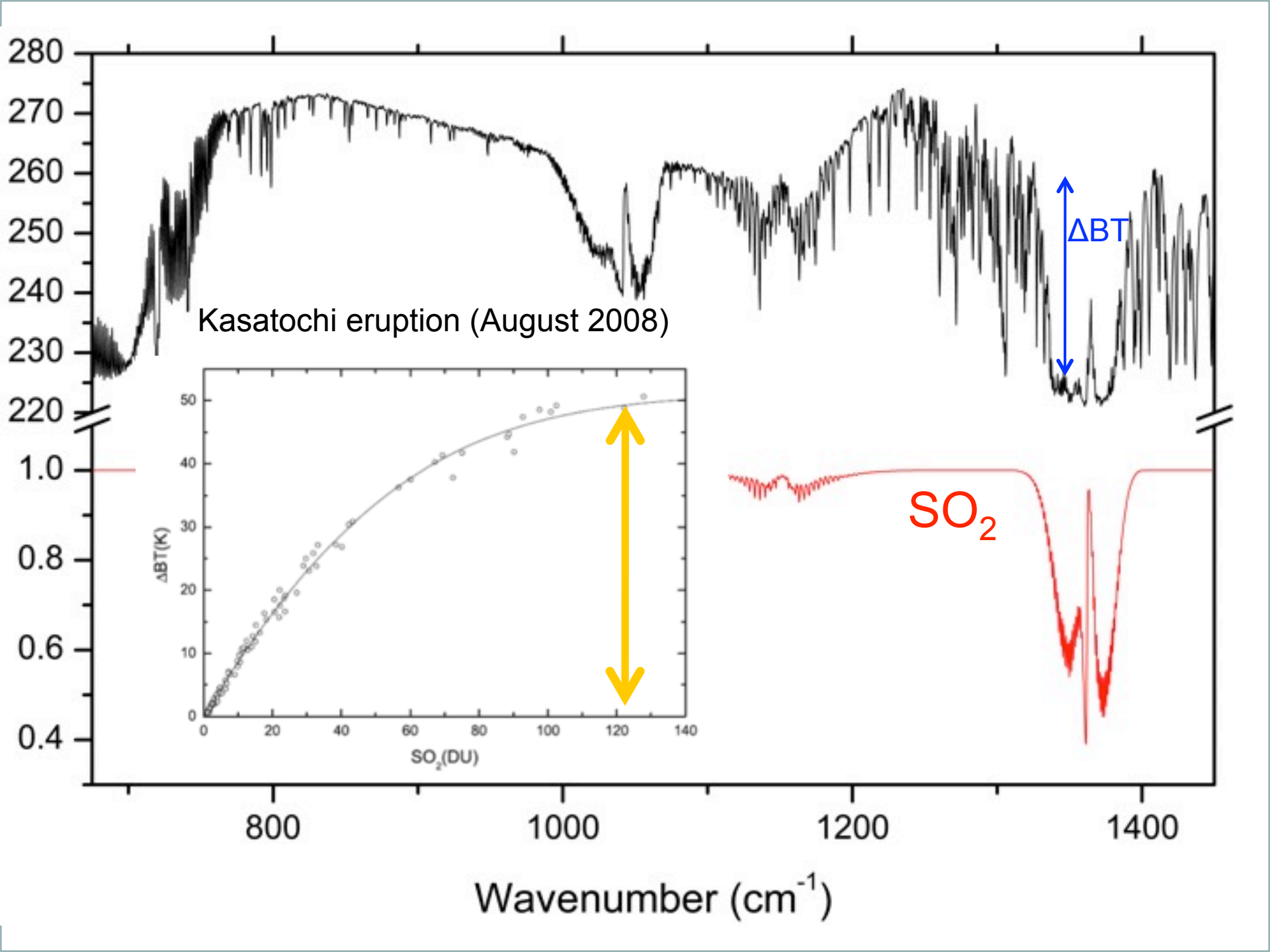
Kasatochi eruption (August 2008)
ΔBT
SO2
ΔBT(K)
SO2(DU)
Wavenumber (cm-1)
280
270
260
250
240
230
220
1.0
0.8
0.6
0.4
800
1000
1200
1400

Rapid SO_2 Retrieval Methodology

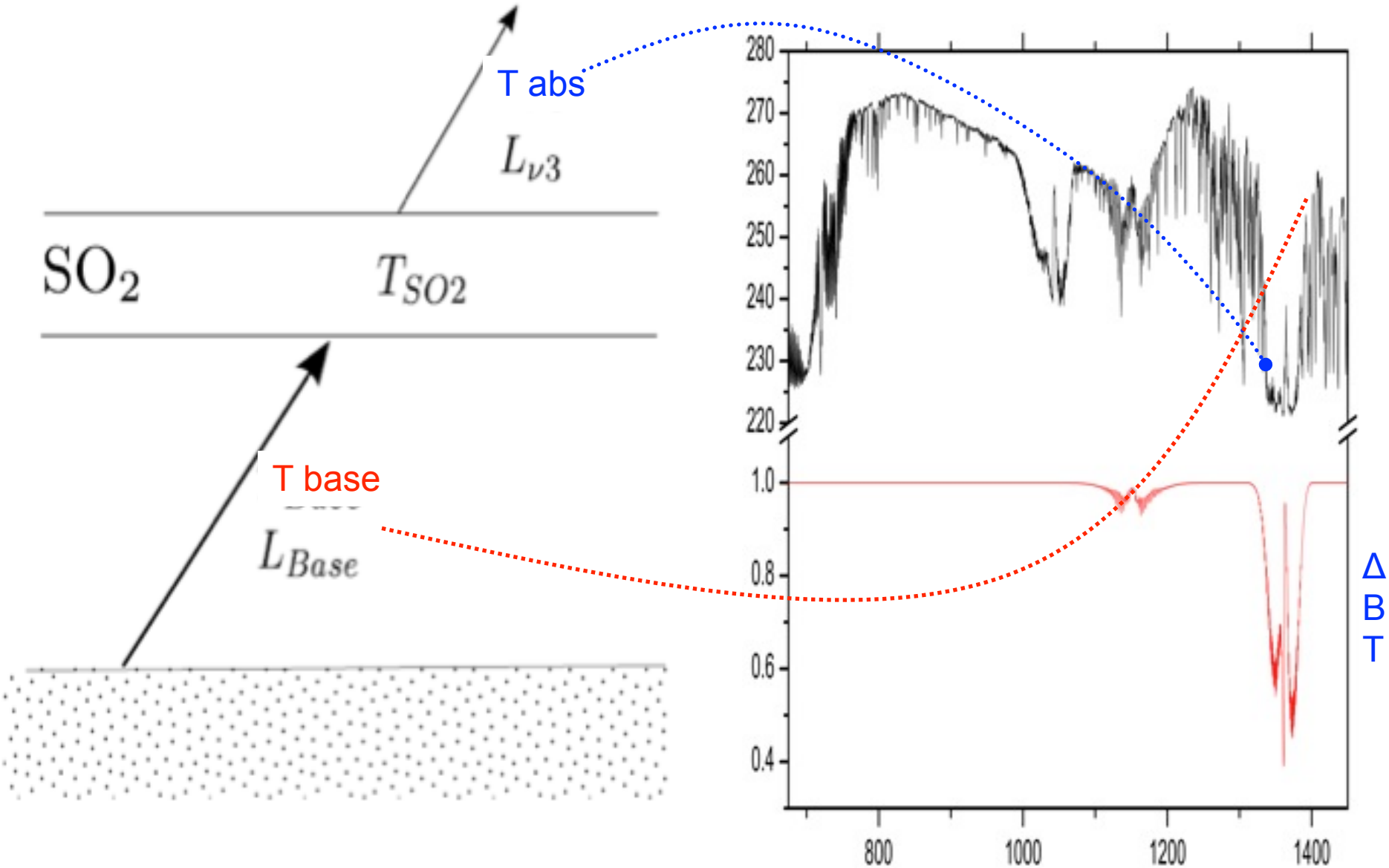

$$C = -\frac{\cos\theta}{c_1}\ln\left(\frac{(\exp(A/T_{\mathrm{B}})-1)(\exp(A/T_{\mathrm{SO2}})-\exp(A/T_{\nu 3}))}{(\exp(A/T_{\nu 3})-1)(\exp(A/T_{\mathrm{SO2}})-\exp(A/T_{\mathrm{B}}))}\right).$$

Rapid SO_2 Retrieval Methodology

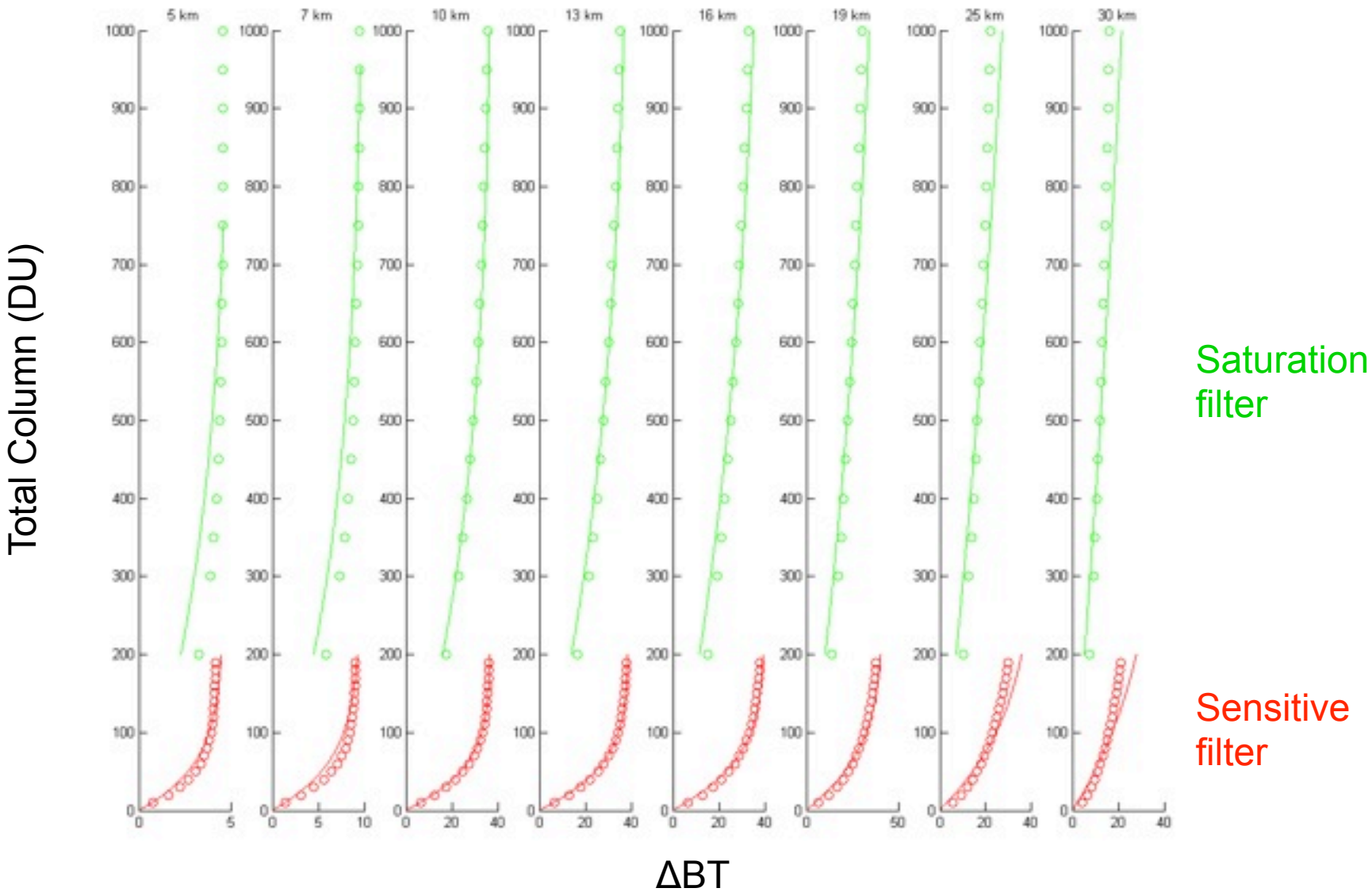

6% theoretical accuracy !

Kasatochi eruption, August 2008

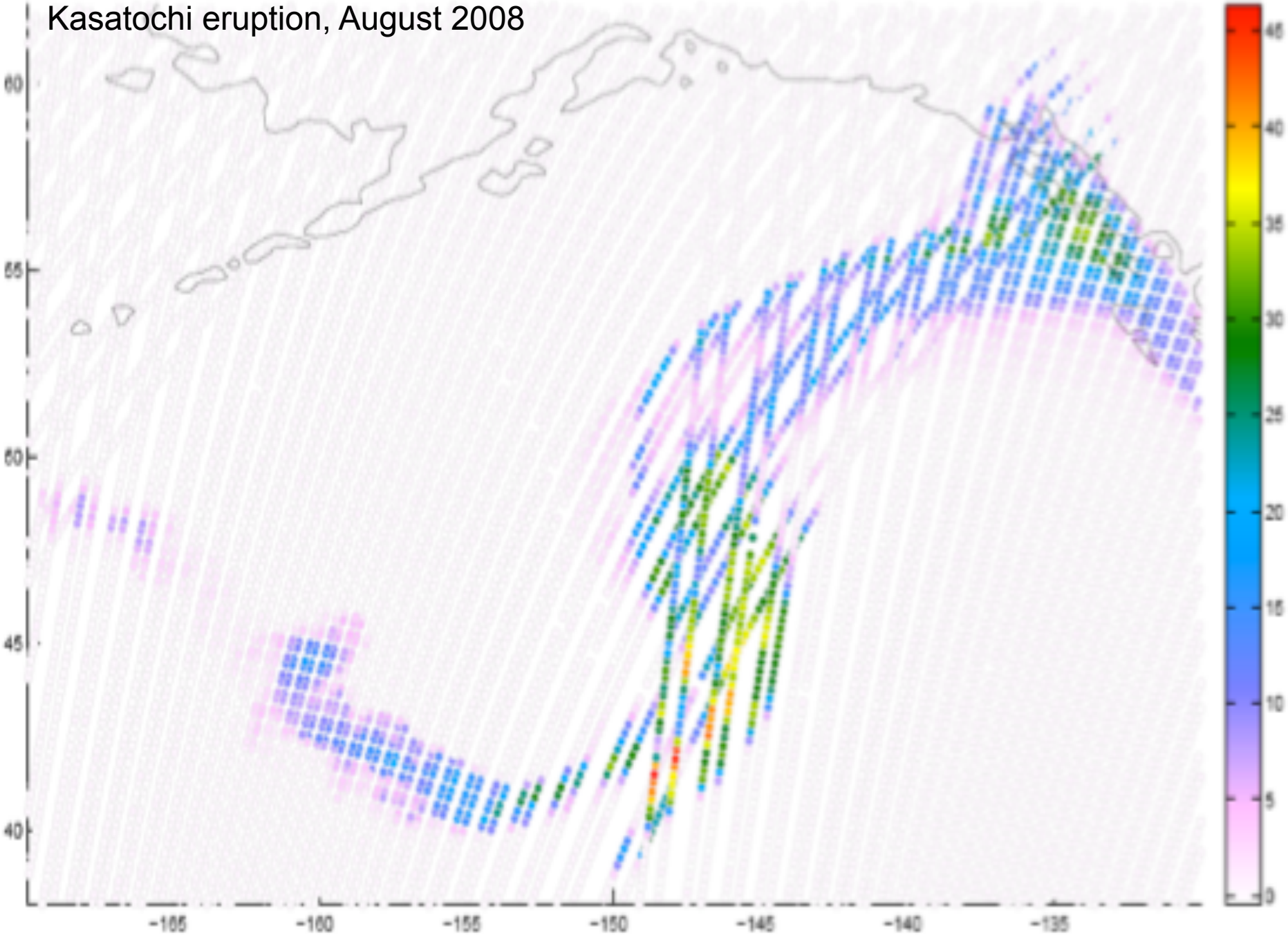

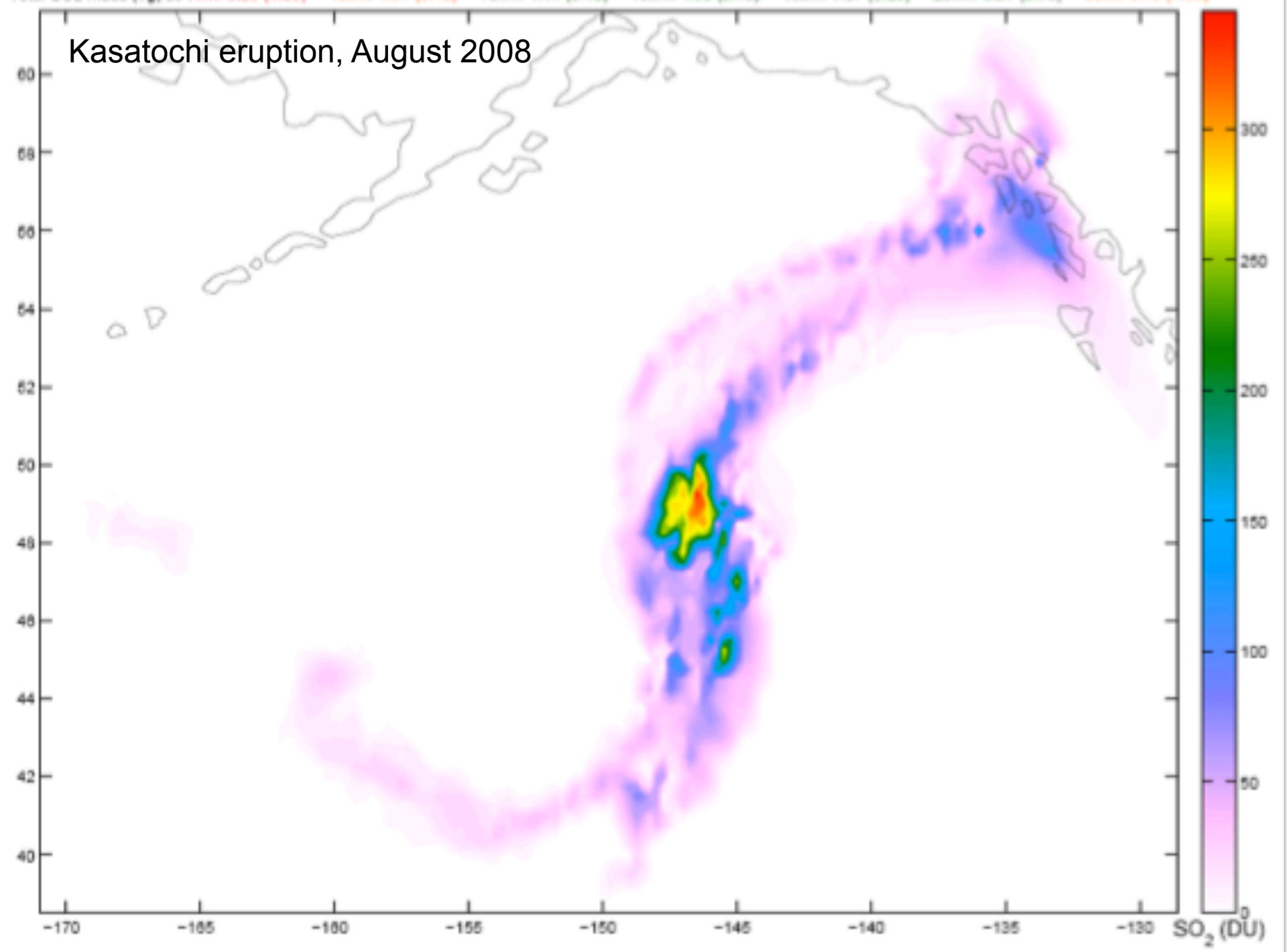
Kasatochi eruption, August 2008
60
58
56
54
52
50
48
46
44
42
40
−170
−165
−160
−155
−150
−145
−140
−135
−130
300
250
200
150
100
50
0
SO_2 (DU)

3 year timeseries of SO_2 from IASI

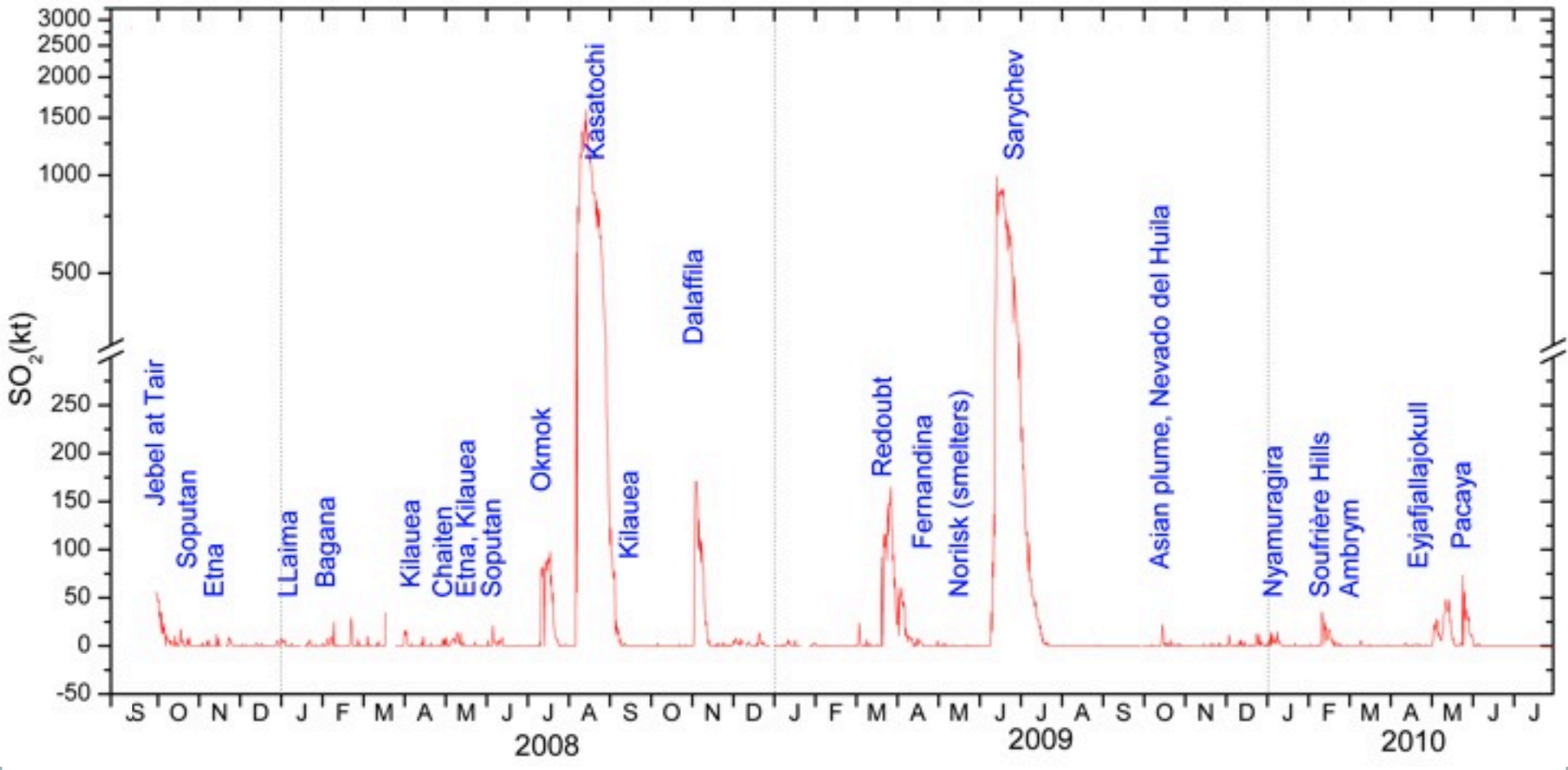

20 % error wrt optimal estimation!!

3 year global UTLS SO_2 from IASI

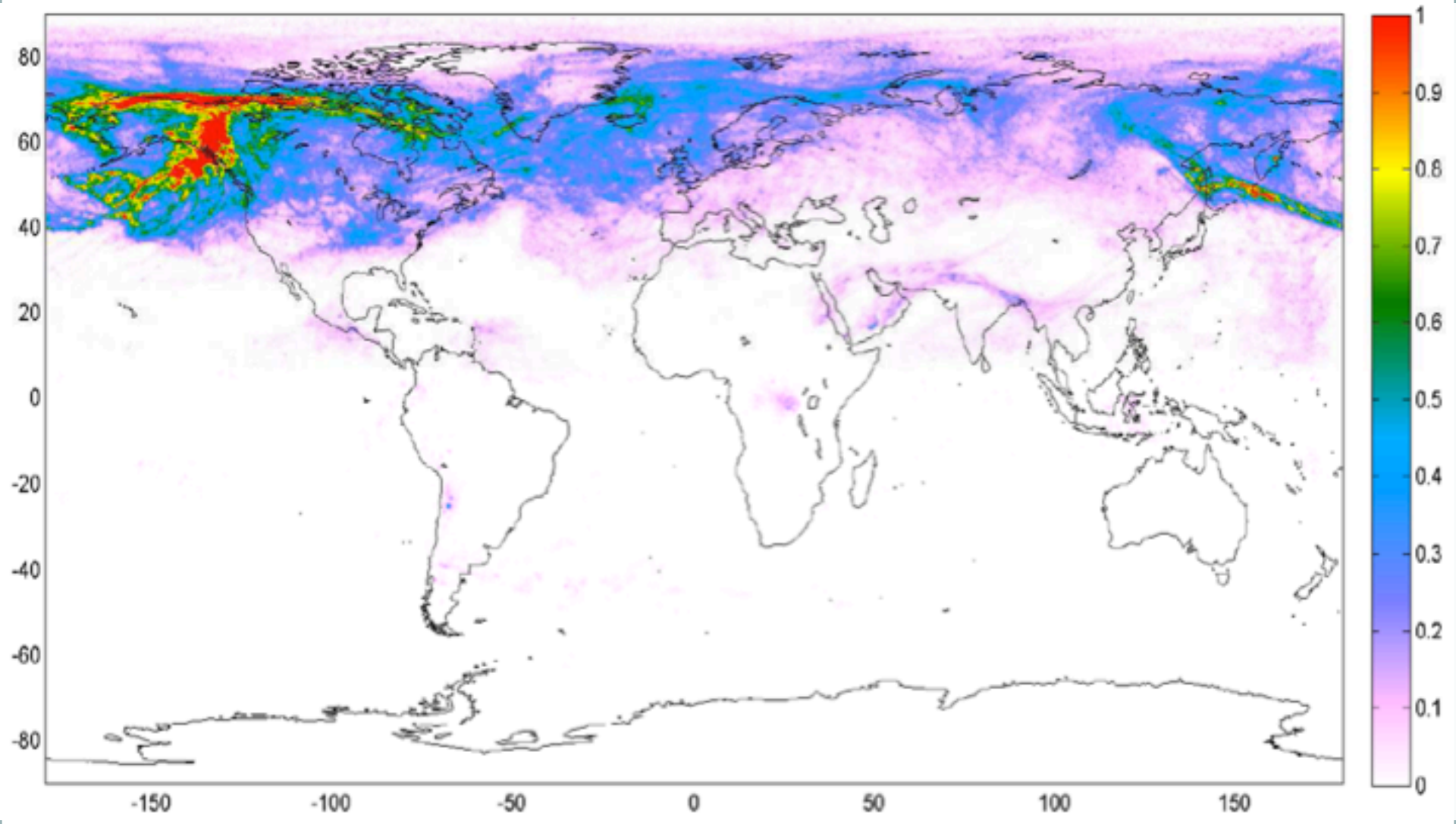

Up to 1 DU on average!

3 year global average SO_2 from IASI (without large eruptions)

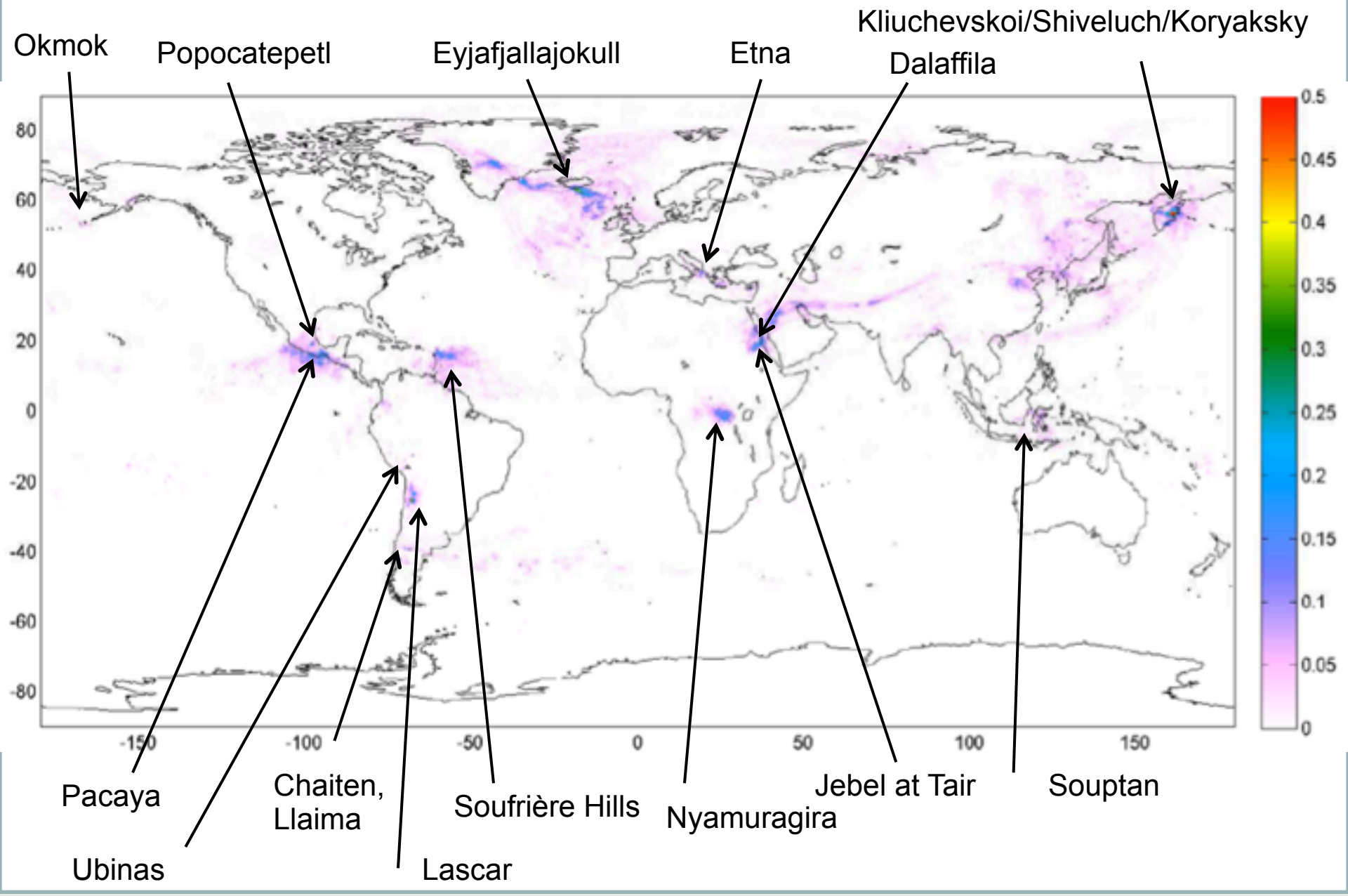

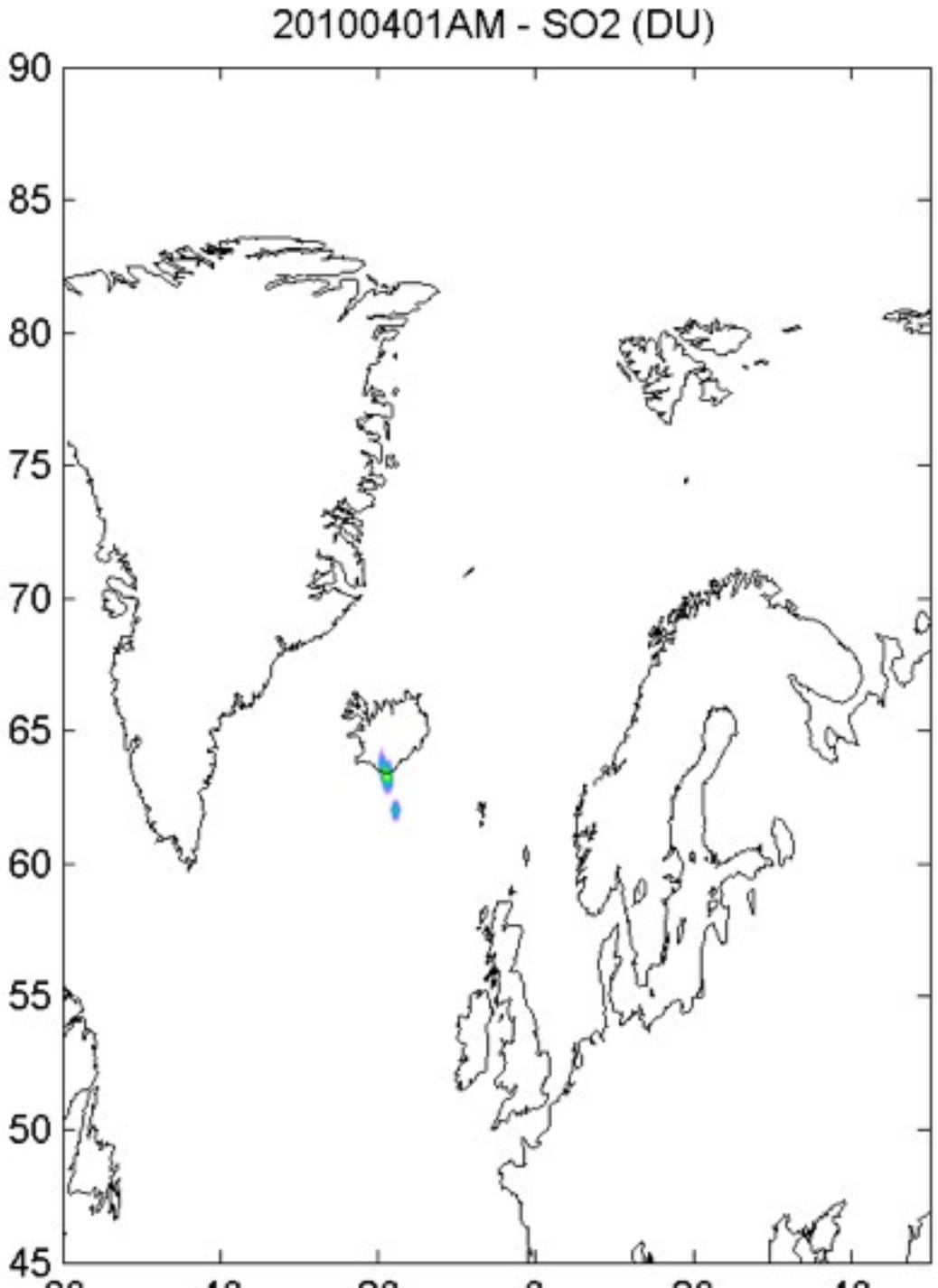
20100401AM - SO2 (DU)
90
85
80
75
70
65
60
55
50
45

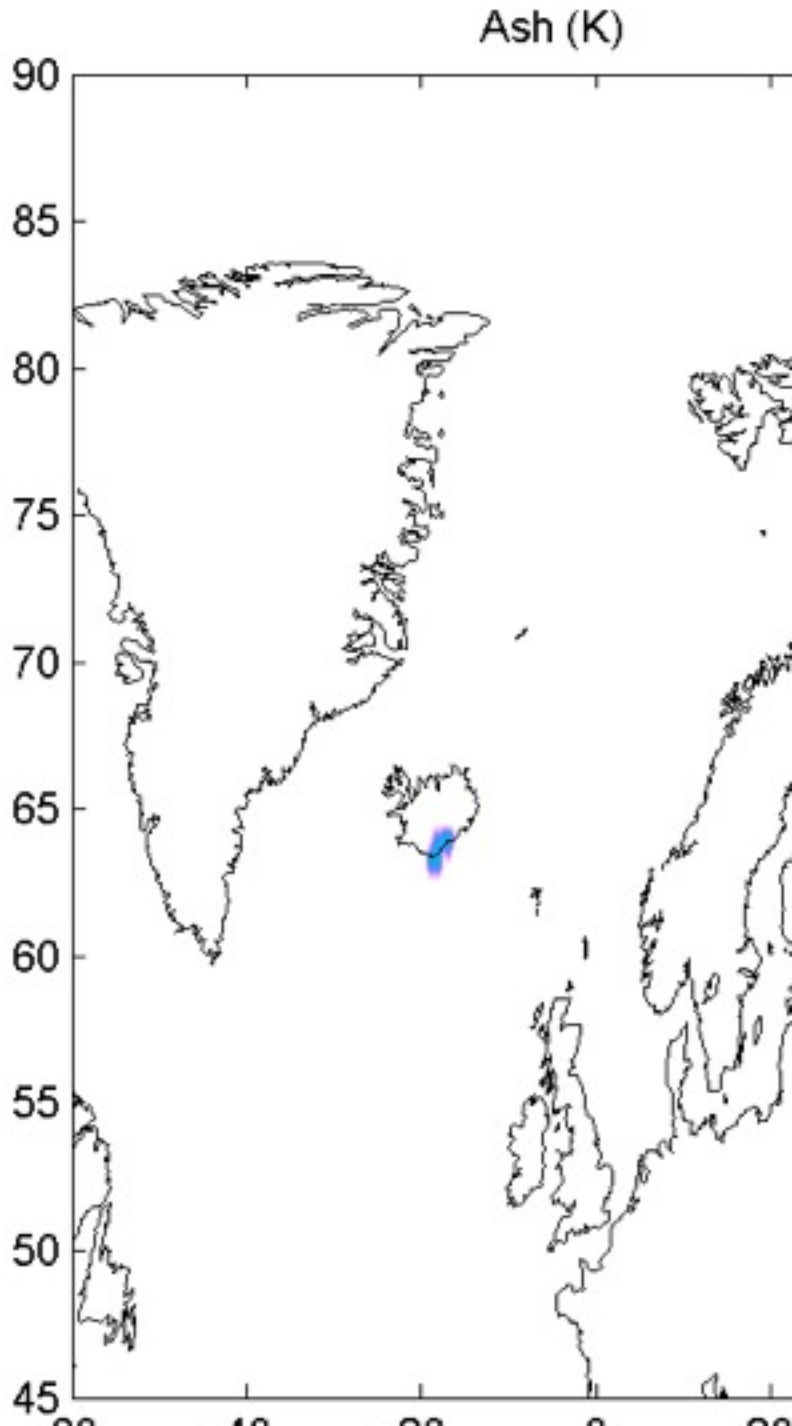
Ash (K)
90
85
80
75
70
65
60
55
50
45

Sarychev eruption

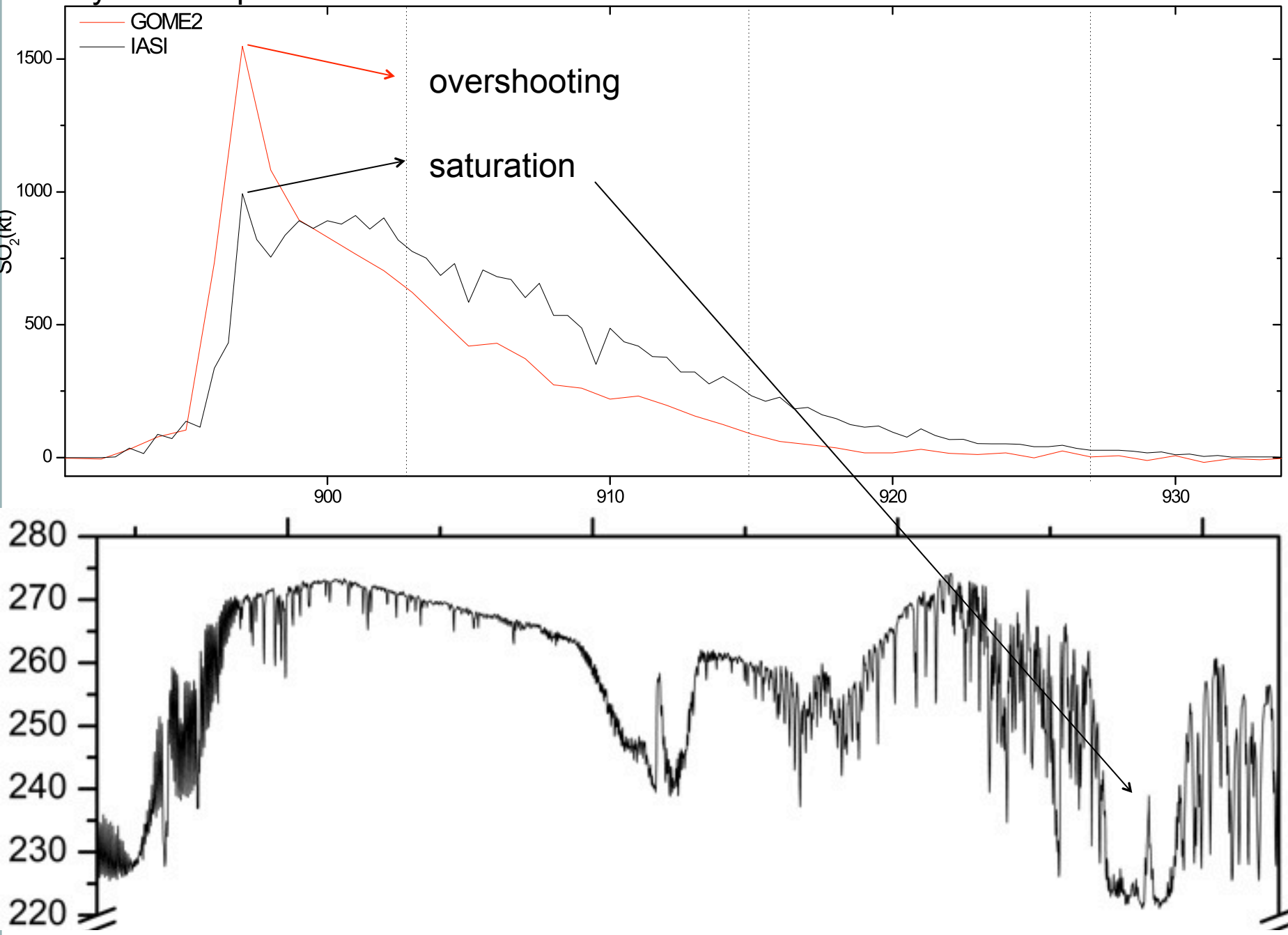

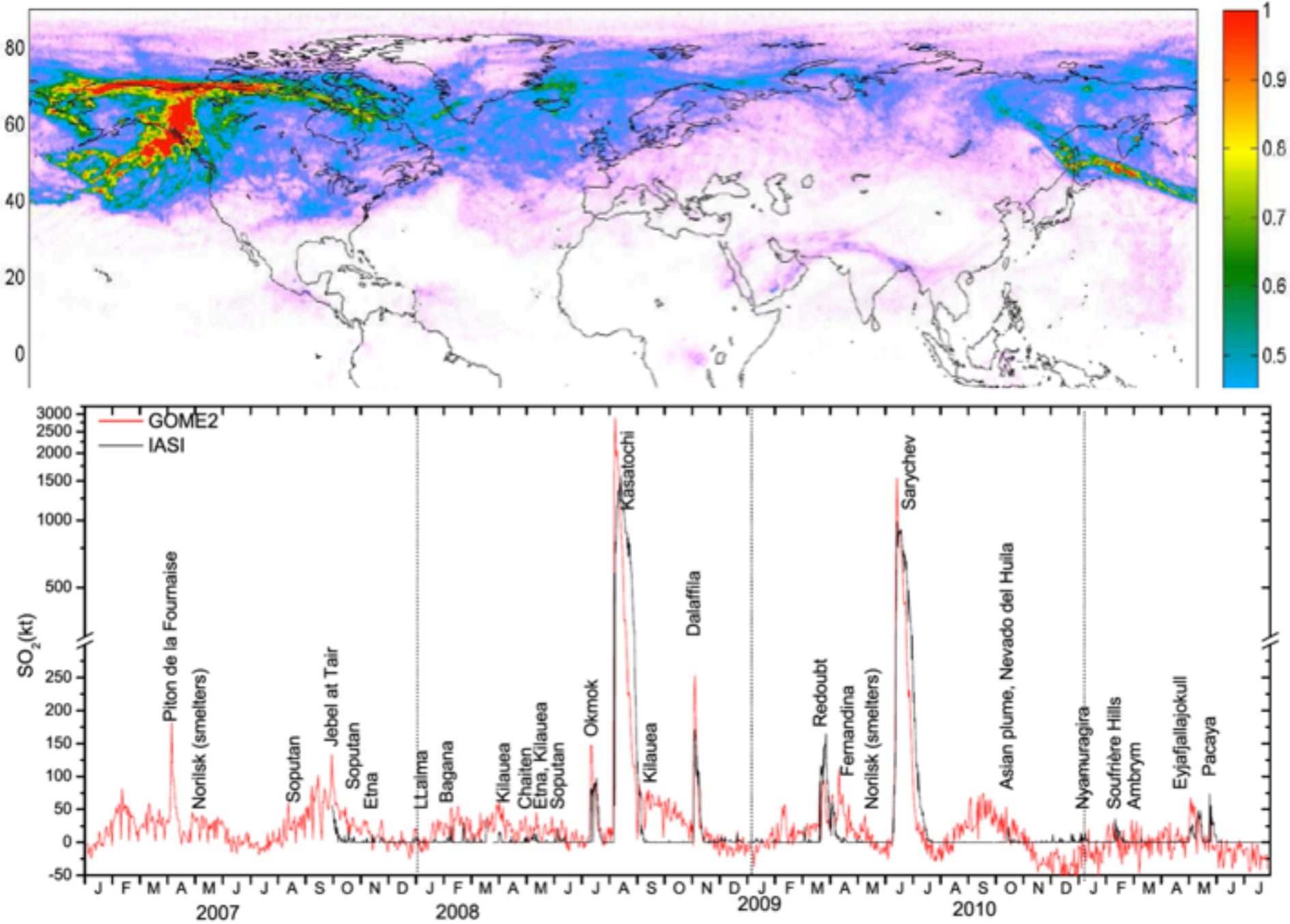

Figure 1: Timeseries 2007-2010 of SO2 (kt) at 12km from IASI and GOME2.

Measuring volcanic SO_2

Explosive volcanism - effects on climate and life

Anthropogenic emissions - decreasing in the developed world but still rising in China/ India/South Africa

Geo-engineering (controversial suggestion to inject S into stratosphere)

Aviation hazard (?)

SO_2 measurements from satellites

INSTRUMENT	From
TOMS	1979
TOVS	1979
MLS	1991
MODIS	1999
ASTER	1999
ACE	*2003*

Some SO_2 clouds detected in TOVS/HIRS data 1980 - 2000

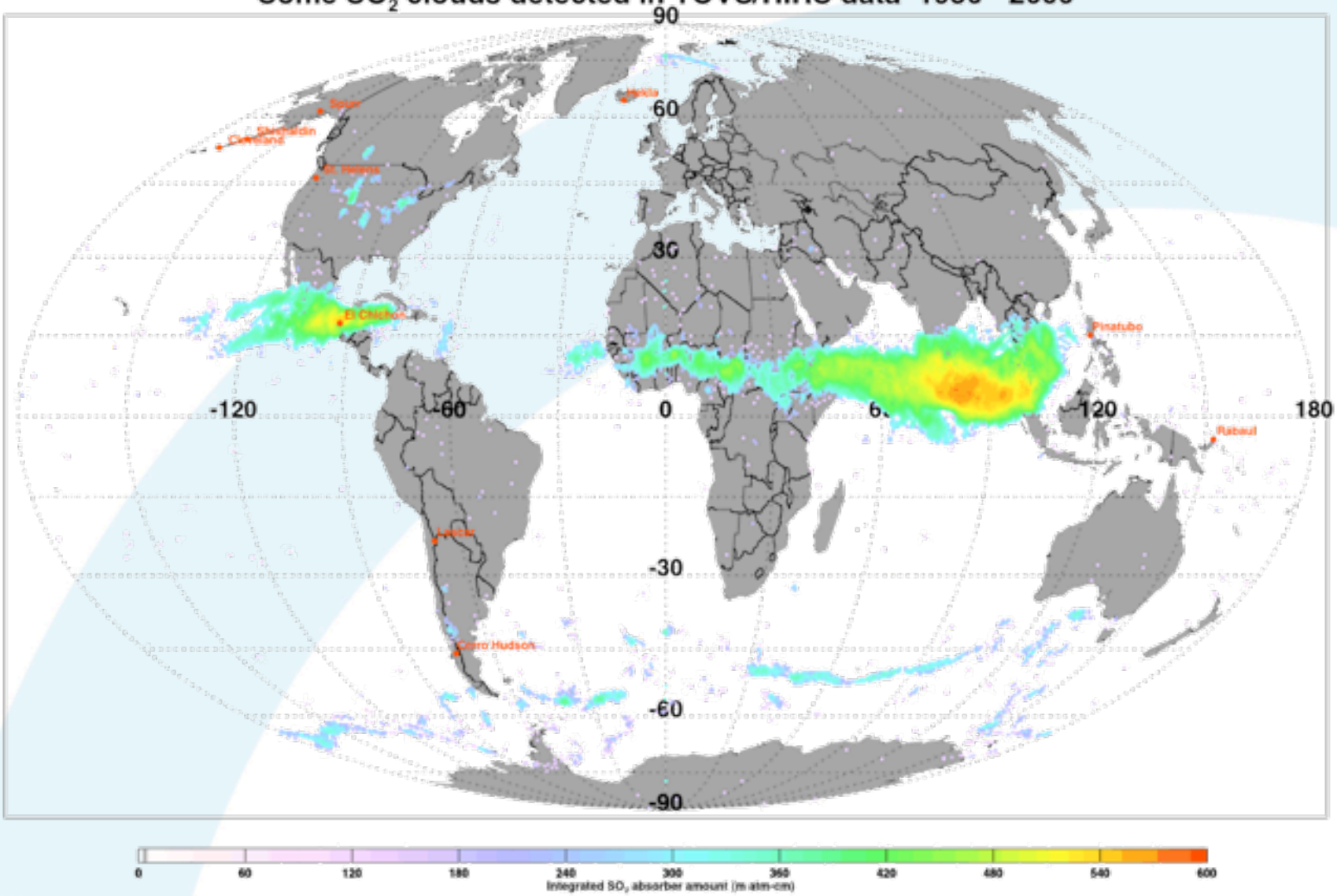

Carn, S., Prata, A. and S. Karlsdottir, 2008, Circumpolar transport of a volcanic cloud from Hekla (Iceland). *J. Geophys. Res.*, 113, D14311, doi:10.1029/2008JD009878.

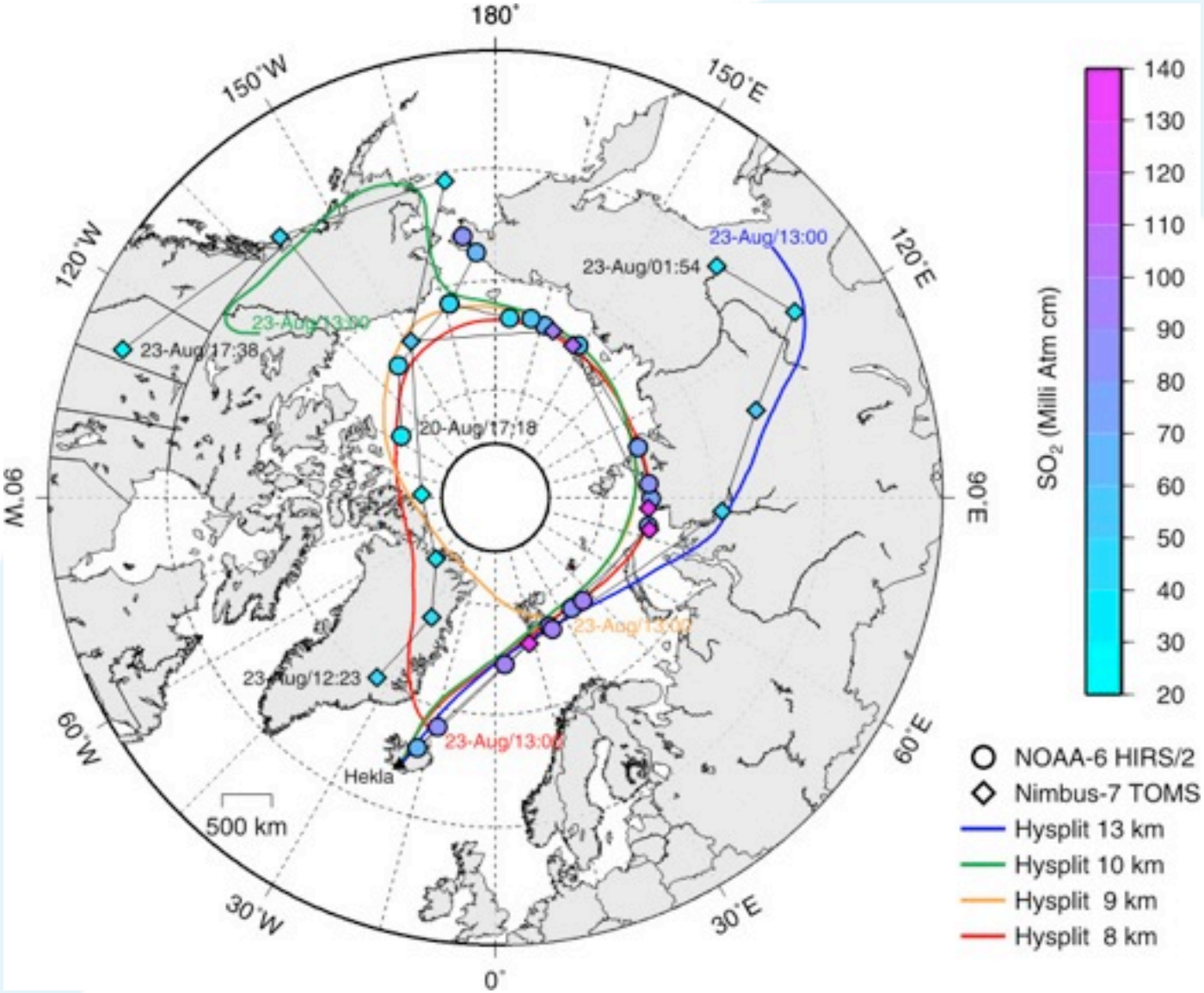

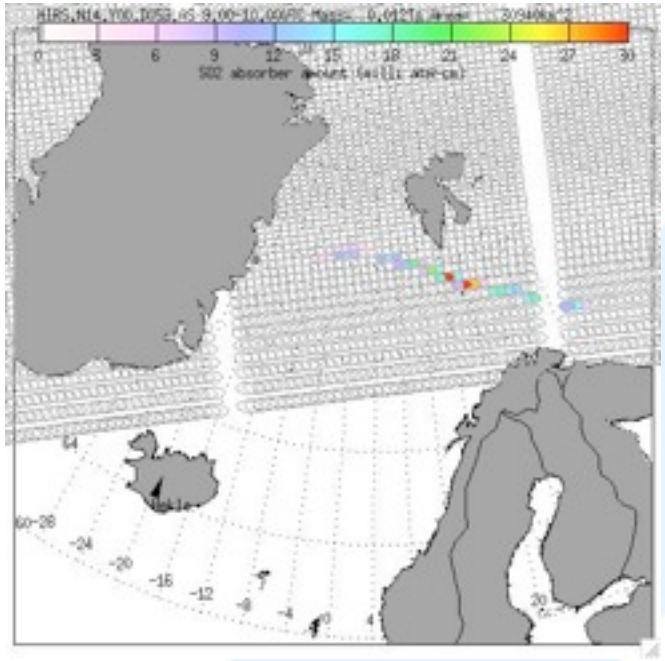

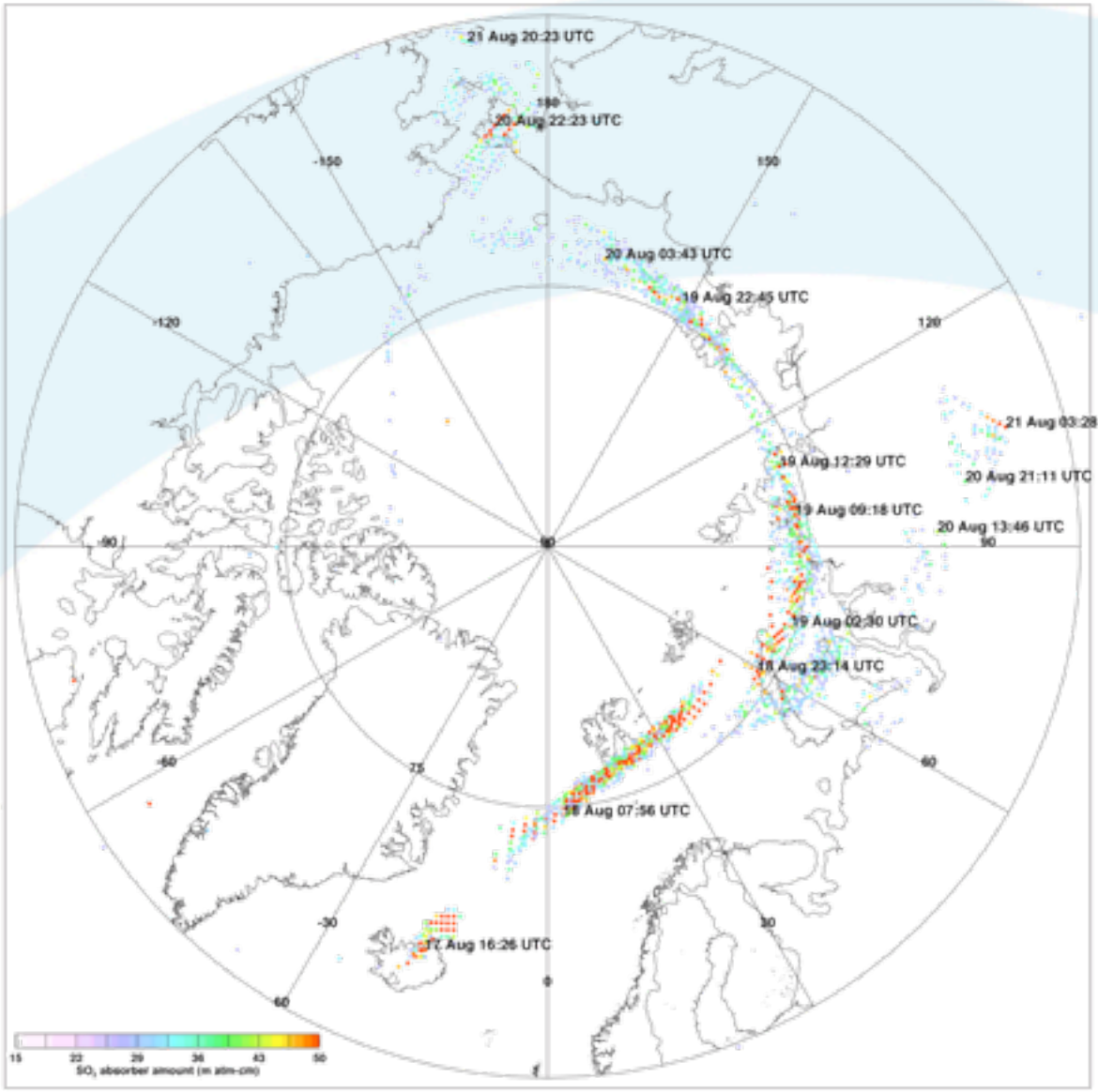

TOVS/ATOVS

S-Watch implementation at the Bureau of Met

VAAC Region - Swatch graphical coverage

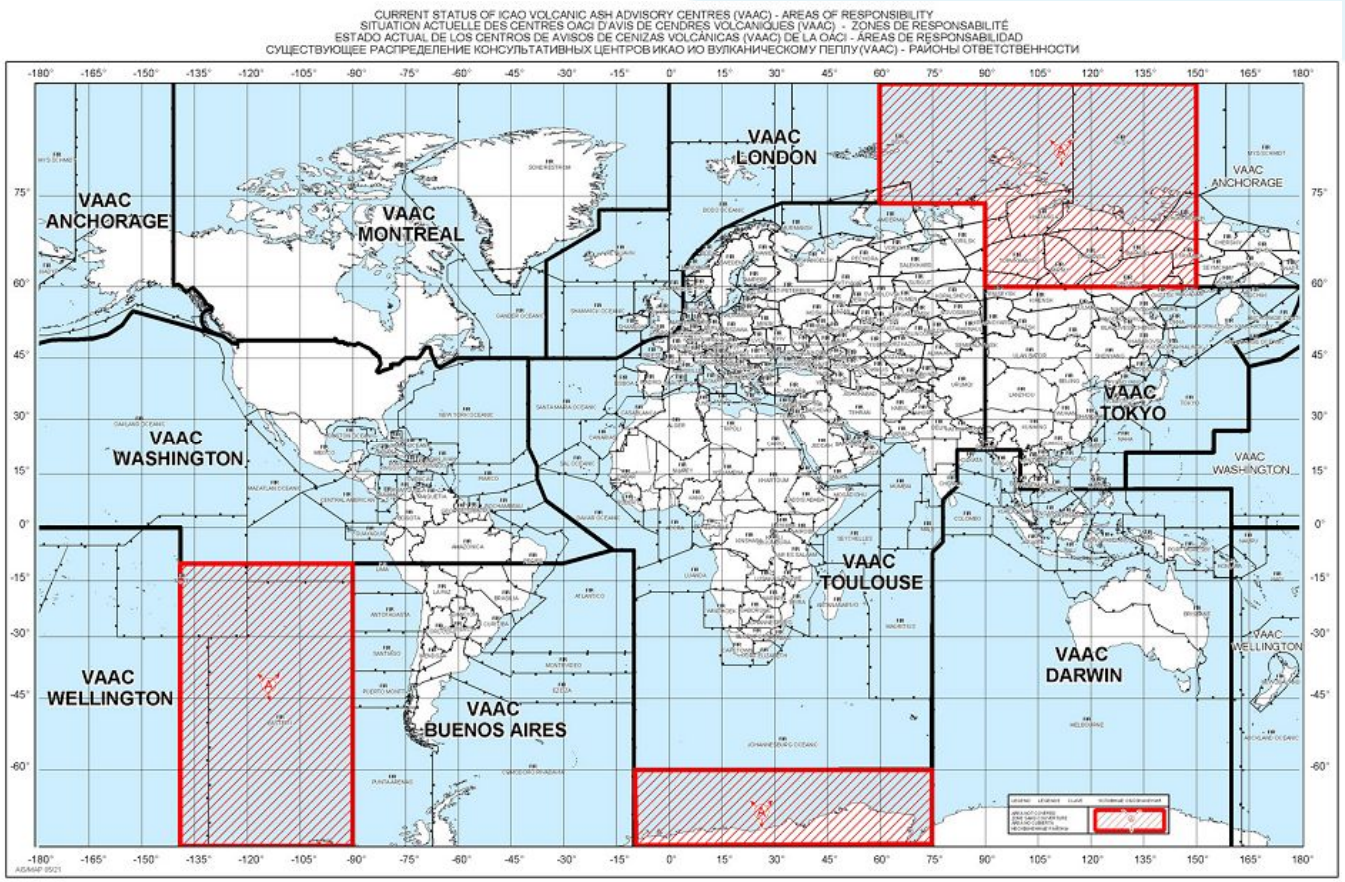

VAAC1=[88,135,-18,20]

VAAC2=[125,170,-35,20]

VAACm=[88,170,-35,20]

Swatch Processor

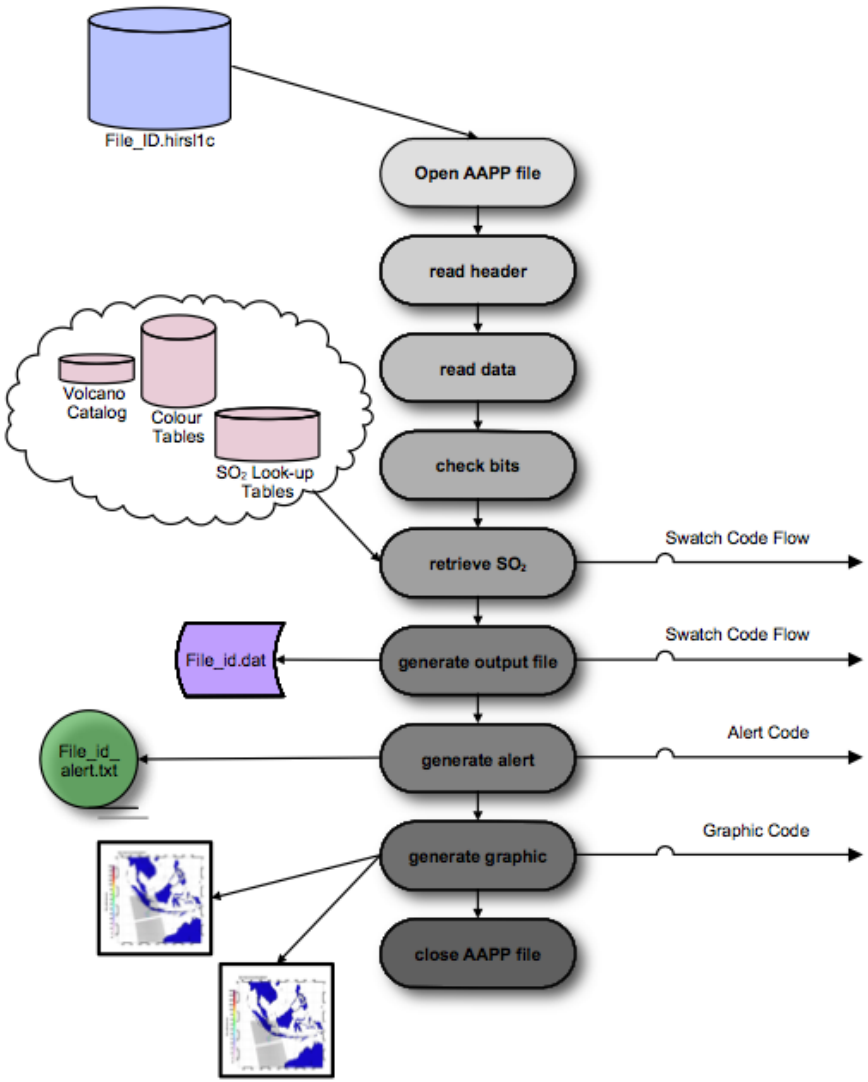

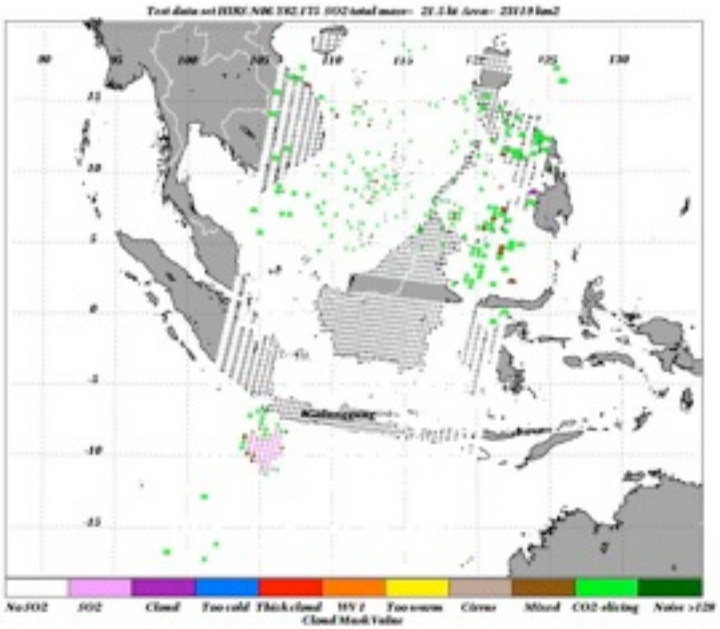

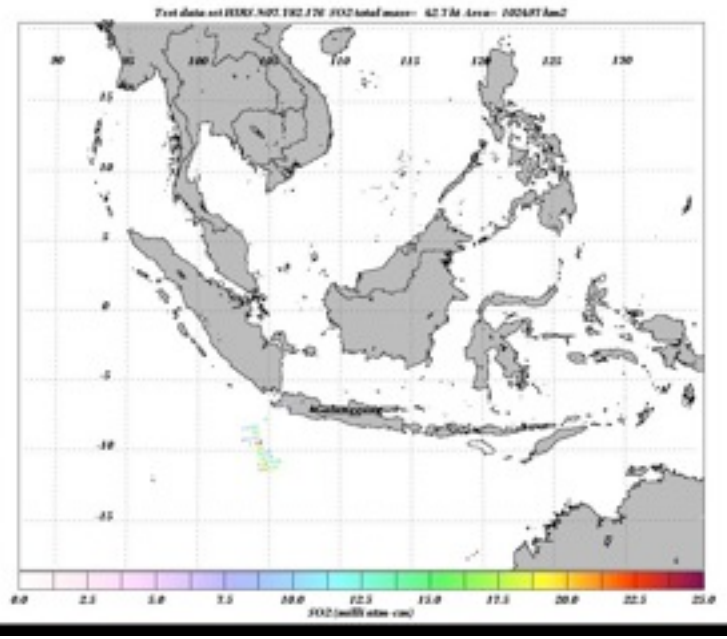

I/O: The Data Output File

Label	Meaning
Lon	Longitude (decimal degrees)
Lat	Latitude (decimal degrees)
T67	BT 6.7 µm (Kelvin)
T73	BT 7.3 µm (Kelvin)
T83	BT 8.3 µm (kelvin)
T11	BT 11 µm (Kelvin)
SO2	SO_2 column (DU)
DT	BT 7.3 µm – BT 7.3 µm interpolated (Kelvin)
D83-11	BT 8.3 µm – BT 11 µm (Kelvin)
T134	BT 13.4 µm (Kelvin)
T137	BT 13.7 µm (Kelvin)
T140	BT 14.0 µm (Kelvin)
T142	BT 14.2 µm (Kelvin)
T145	BT 14.5 µm (Kelvin)
T147	BT 14.7 µm (Kelvin)
Trat	CO_2 slicing ratio
CLD	Cloud flag value
Smass	SO_2 pixel mass (kt)
Area	Pixel area (km^2)

<u>Data Output File</u>

Naming convention:

SO2ndddyyyy.tt.tttt.dat

n=VAAC region (1,2 or m)

ddd=day of year (1-366)

yyyy=Year

tt.tttt=decimal time (hrs, UTC)

Measuring SO_2 from AIRS

JOURNAL OF GEOPHYSICAL RESEARCH, VOL. 112, D20204, doi:10.1029/2006JD007955, 2007

Click Here for Full Article

Retrieval of volcanic SO_2 column abundance from Atmospheric Infrared Sounder data

A. J. Prata[1] and C. Bernardo[2]

Received 23 August 2006; revised 25 June 2007; accepted 16 July 2007; published 19 October 2007.

[1]Norwegian Institute for Air Research, Kjeller, Norw
[2]Auspace Ltd., Mitchell, ACT, Australia.

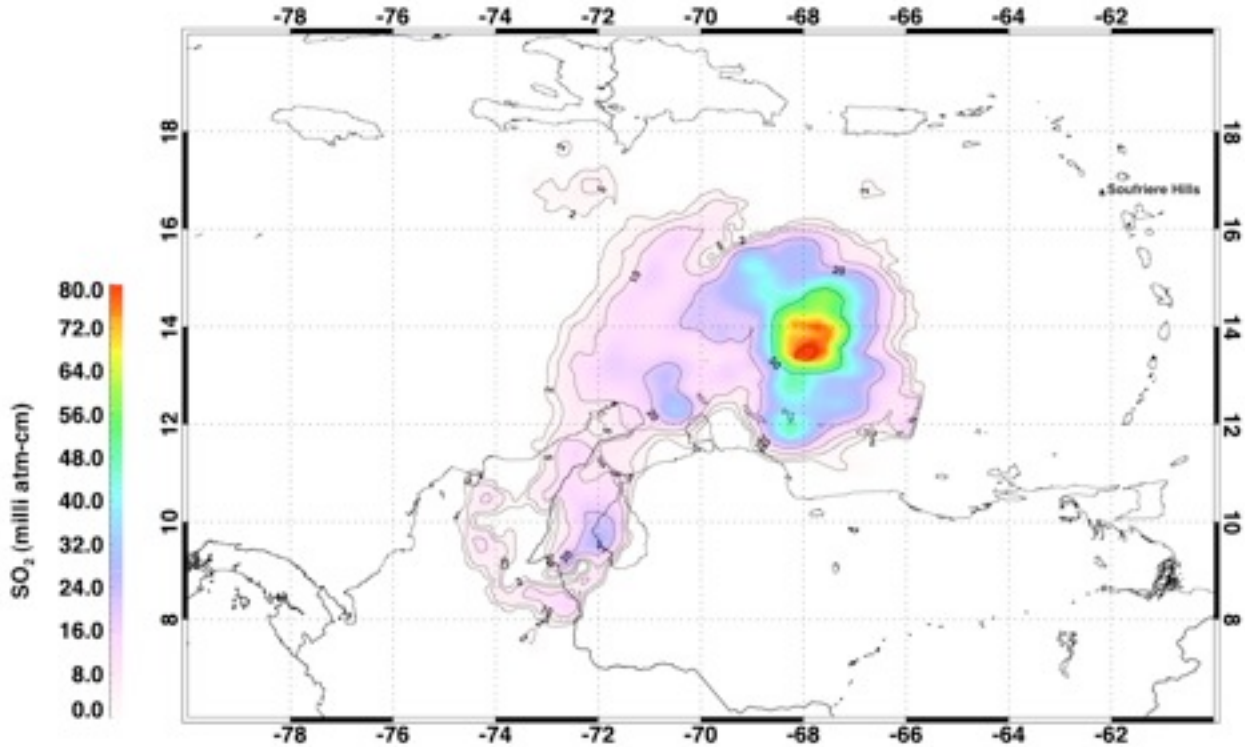

Spectral matching

Many molecules have distinctive absorption bands

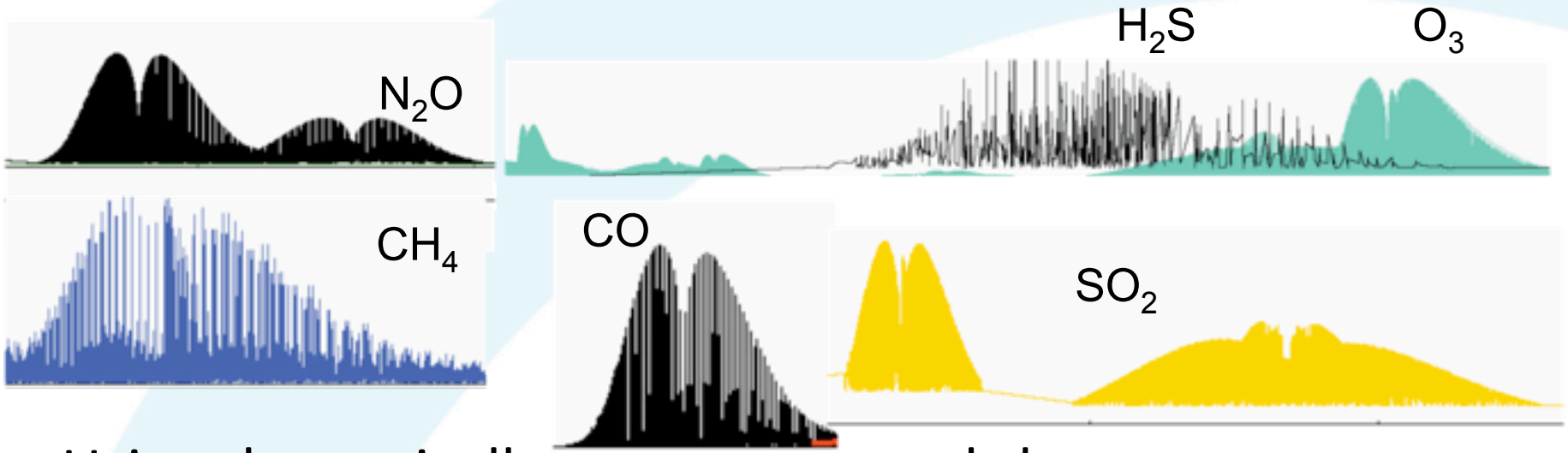

Using theoretically-derived spectral shapes, molecules can be identified by comparing (or matching) the observed shape with theory.

Spectral matching (1)

Radiative transfer equation

$$I_\nu = I_{\nu,s} + \int_0^\infty B_\nu[T(z)] \left(\frac{\partial \tau_\nu[z, q_1(z), q_2(z) \ldots q_n(z)]}{\partial z} \right) dz,$$

Choose absorption region and split integral into 3 parts:

$$\begin{aligned} I_\nu \approx & \int_0^{z_1} B_\nu[T(z)] \left(\frac{\partial \tau_\nu[z, q_2(z) \ldots q_n(z)]}{\partial z} \right) dz && \text{Below gas layer} \\ + & \int_{z_1}^{z_2} B_\nu[T(z)] \left(\frac{\partial \tau_\nu[z, q_1(z), q_2(z) \ldots q_n(z)]}{\partial z} \right) dz && \text{In gas layer} \\ + & \int_{z_2}^{\infty} B_\nu[T(z)] \left(\frac{\partial \tau_\nu[z, q_2(z) \ldots q_n(z)]}{\partial z} \right) dz. && \text{Above gas layer} \end{aligned}$$

Spectral matching (2)

$$I'_\nu = I_{\nu,0} \exp\left\{-\int_o^\infty k_\nu(z)q(z)dz\right\}$$

Beer-Bougier-Lambert law

$$A_\nu = -\ln\left\{\frac{I'_\nu}{I_{o,\nu}}\right\} = \int_o^\infty k_\nu(z)q(z)dz.$$

Absorbance spectrum

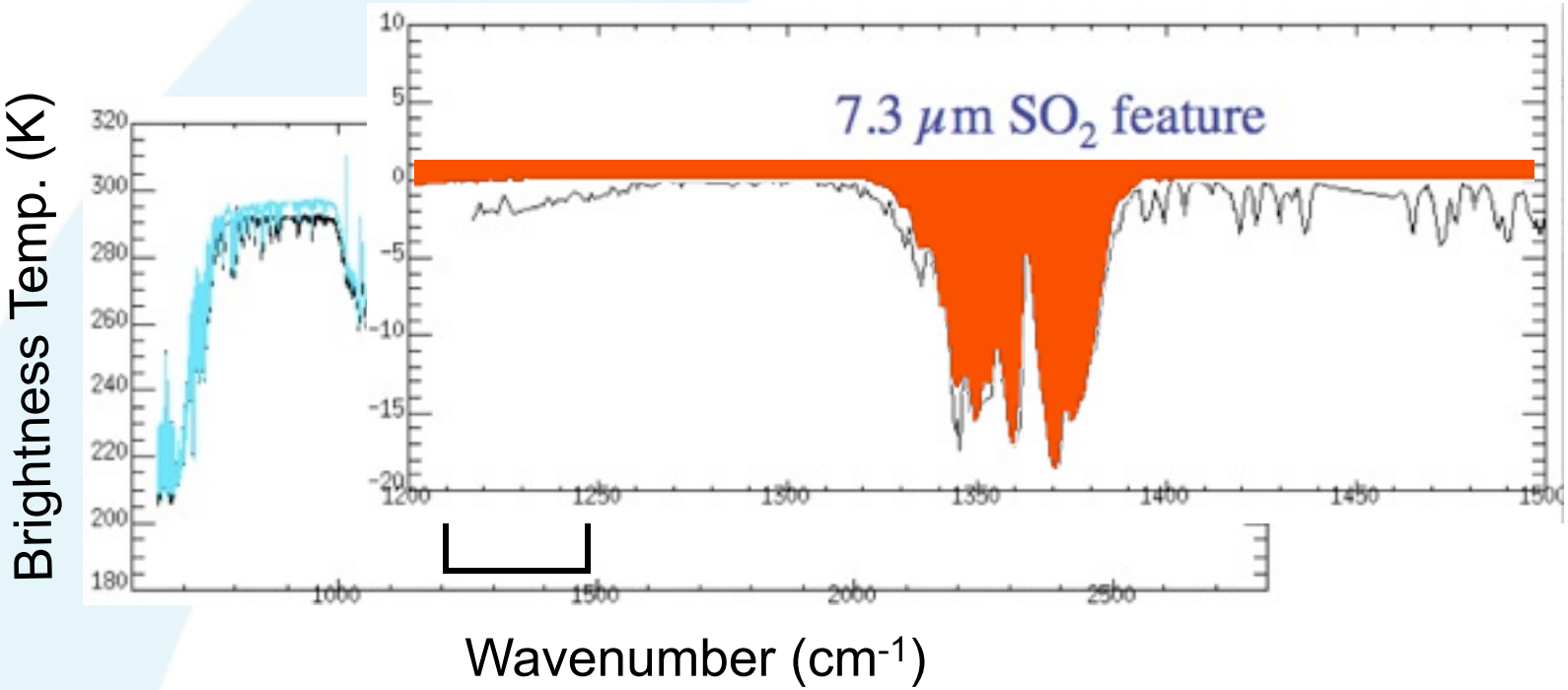

Retrieval

Single Lorentz line

$$A\Delta\nu = \int_{\Delta\nu} \left\{1 - \exp[-\frac{1}{\pi}\int_{z_1}^{z_2} \frac{\alpha q(z)}{(\nu-\nu_0)^2+\alpha^2} dz]\right\} d\nu,$$

$$A\Delta\nu = 2\pi\alpha\psi[L_0(\psi) + L_1(\psi)]\exp\{-\psi\},$$

$$\psi = \frac{Su}{2\pi\alpha},$$

For a band with temperature dependent line strengths and line broadening effects, a radiative transfer model must be used

$$\vec{x} = (\mathbf{K}^T\mathbf{K})^{-1}\mathbf{K}^T\vec{y}.$$

Least squares solution

$\vec{x}$: layer absorber amounts (N layers)

$\vec{y}$: observed absorbances (M wavenumbers)

K: is an MxN matrix of absorption cross sections

AIRS Volcanic SO_2

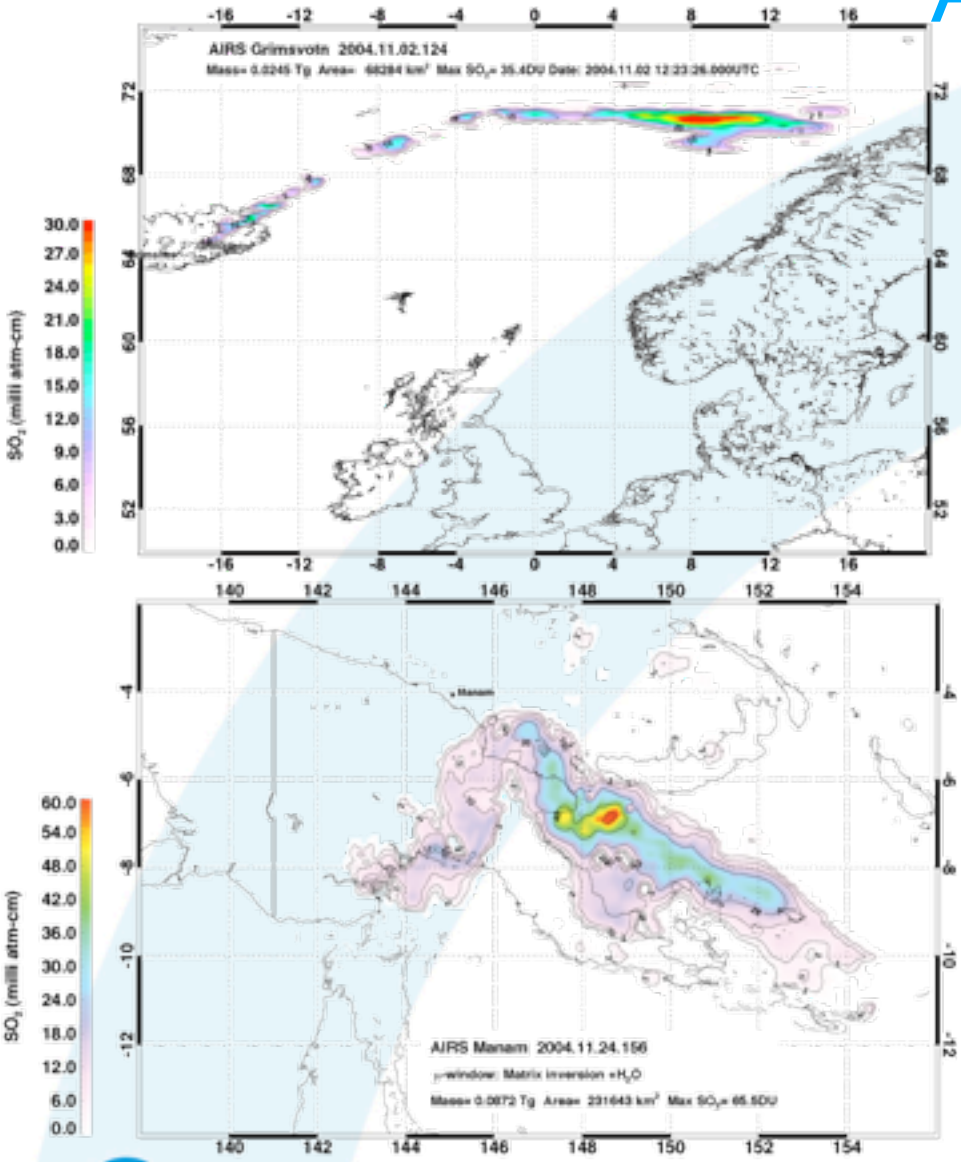

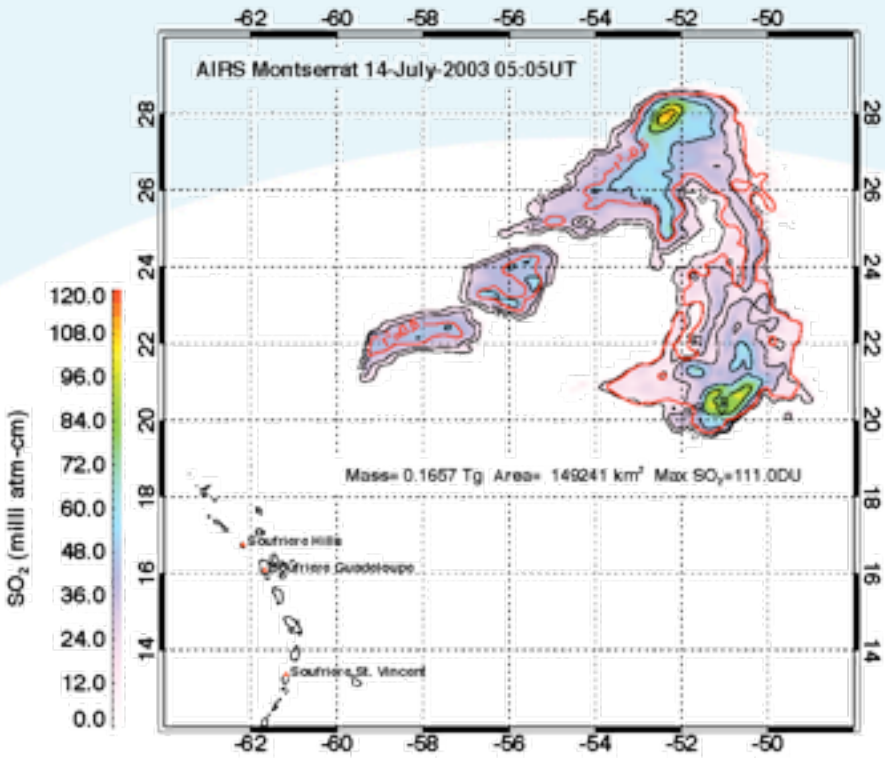

Manam Eruption Jan 28 2005

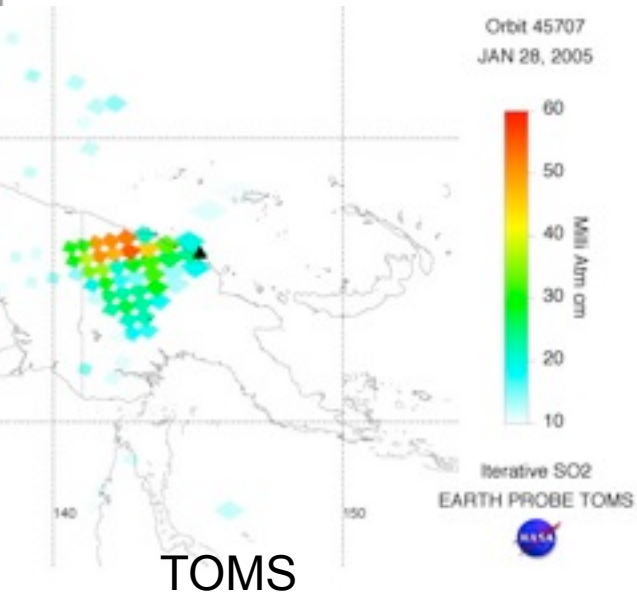

TOMS

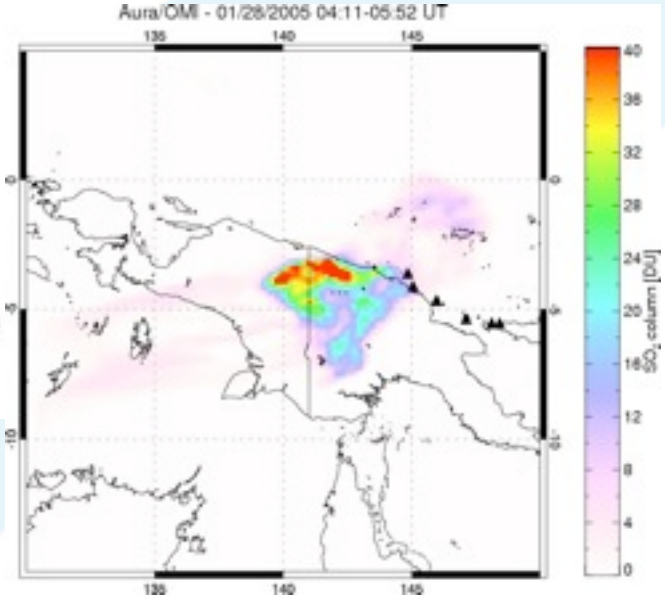

OMI

AIRS

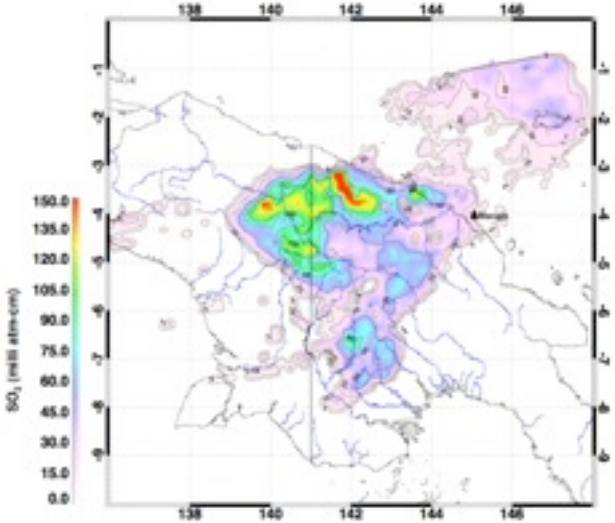

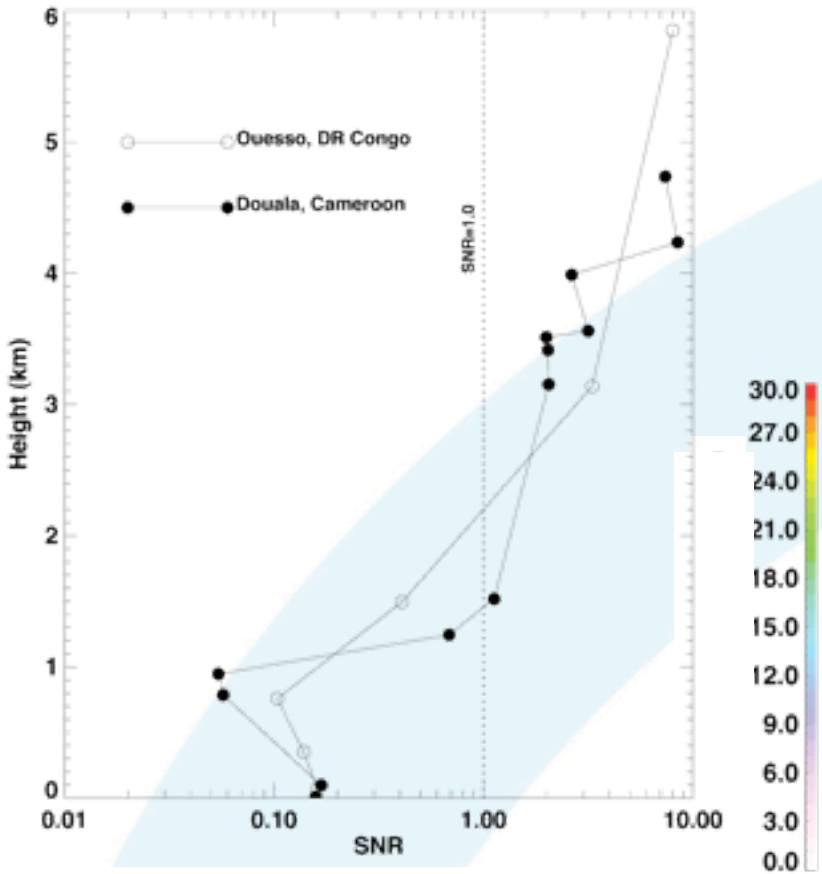

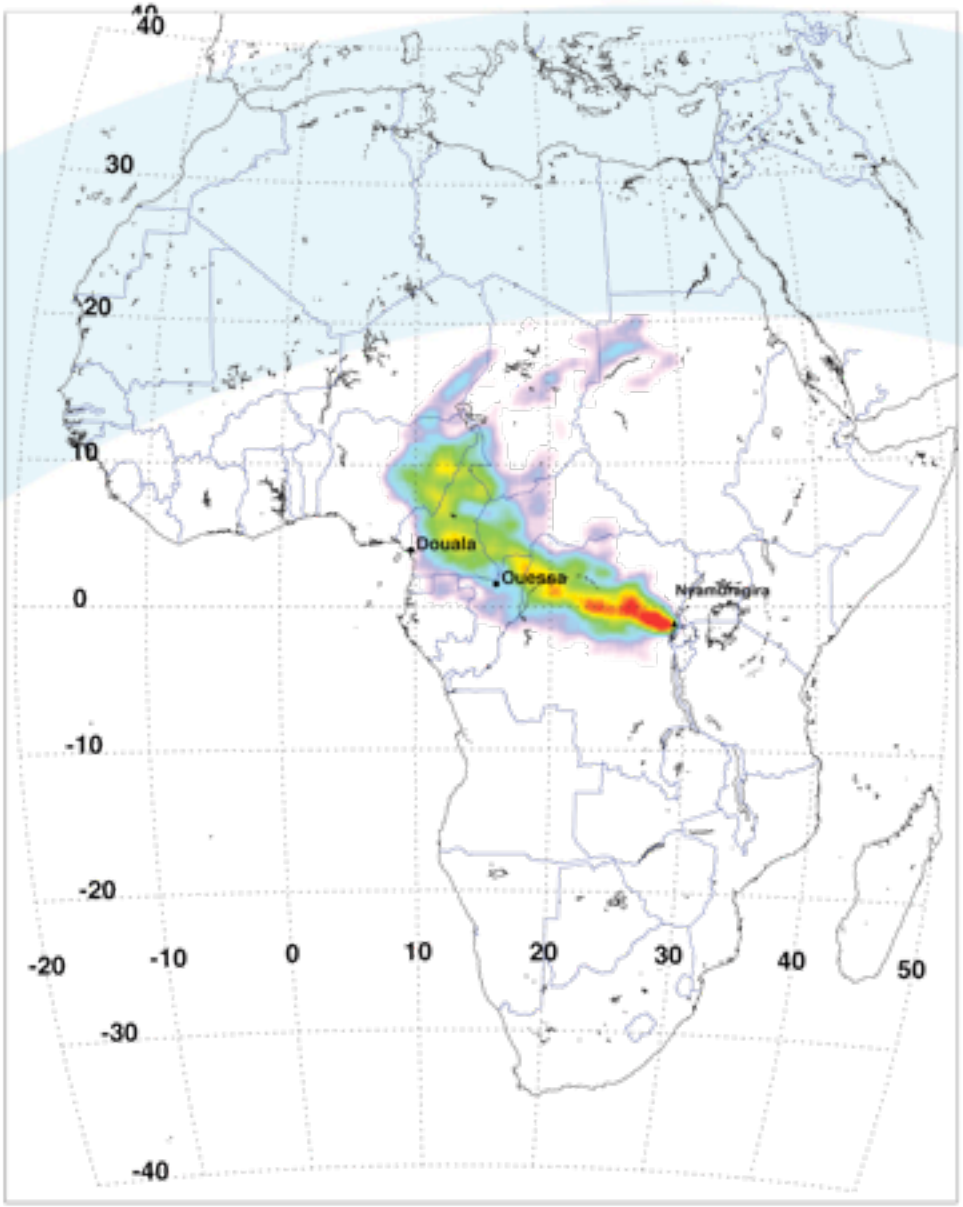

$$SNR = \frac{\sqrt{\frac{1}{\Delta\nu}\int_{\Delta\nu}\Delta S_\nu^2 d\nu}}{NE\Delta I}.$$

$$\Delta S_\nu = |I_{\nu,z'} - I_{\nu,0}|,$$

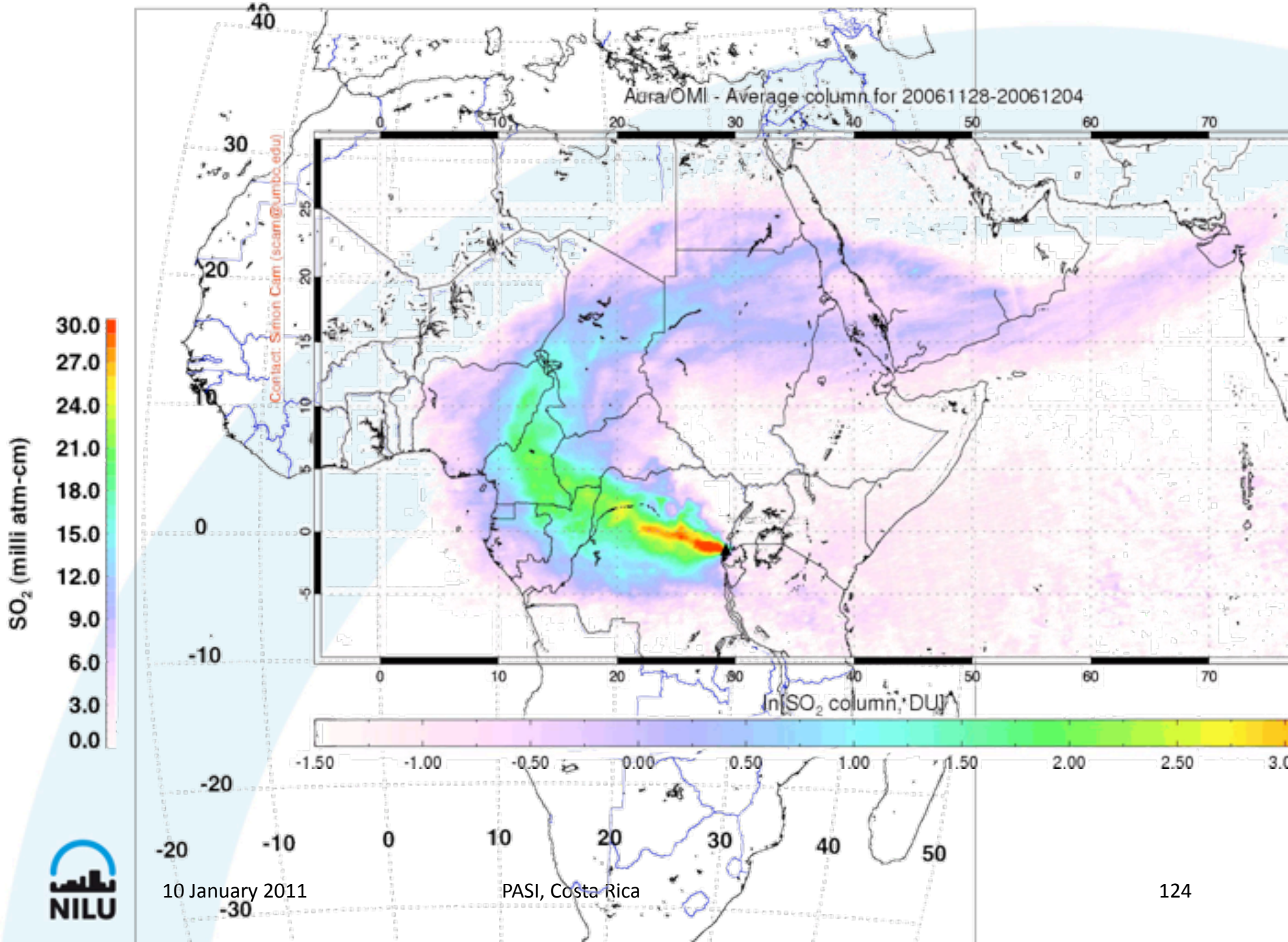
Aura/OMI - Average column for 20061128-20061204
Contact: Simon Carn (scarn@umbc.edu)
ln[SO2 column, DU]
SO2 (milli atm-cm)
30.0
27.0
24.0
21.0
18.0
15.0
12.0
9.0
6.0
3.0
0.0

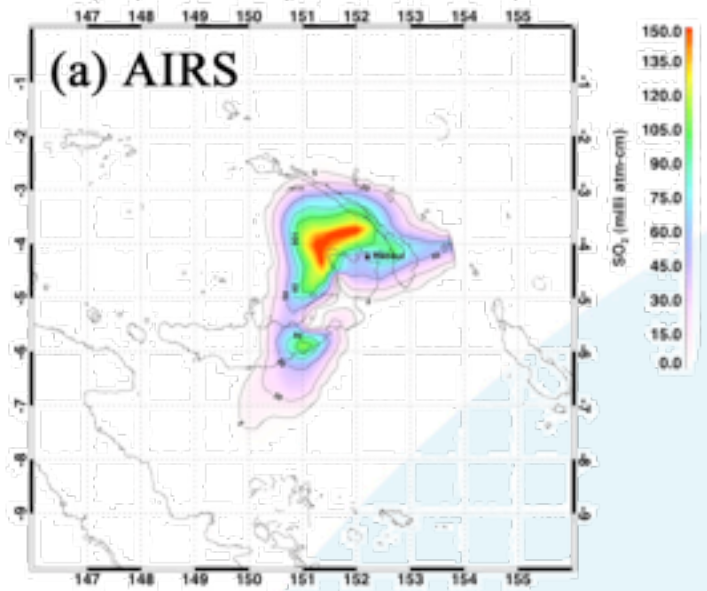
(a) AIRS
SO2 (milli atm-cm)
150.0
135.0
120.0
105.0
90.0
75.0
60.0
45.0
30.0
15.0
0.0

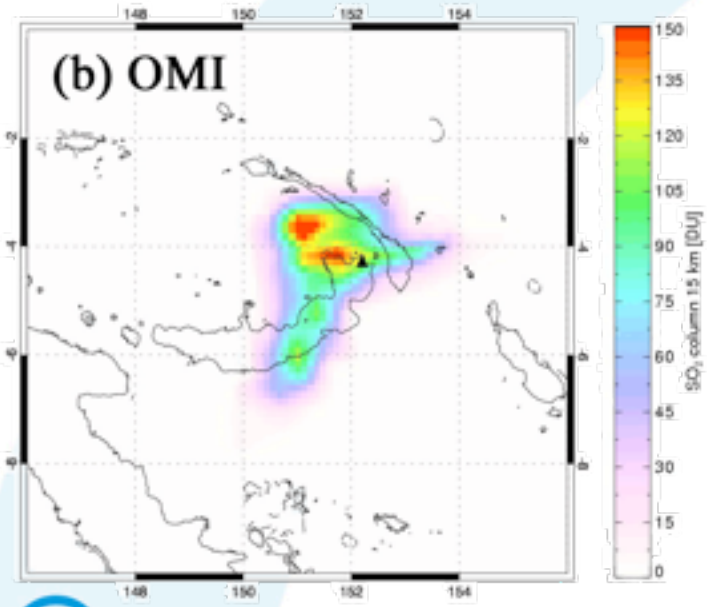
(b) OMI
SO2 column 15 km [DU]
150
135
120
105
90
75
60
45
30
15
0

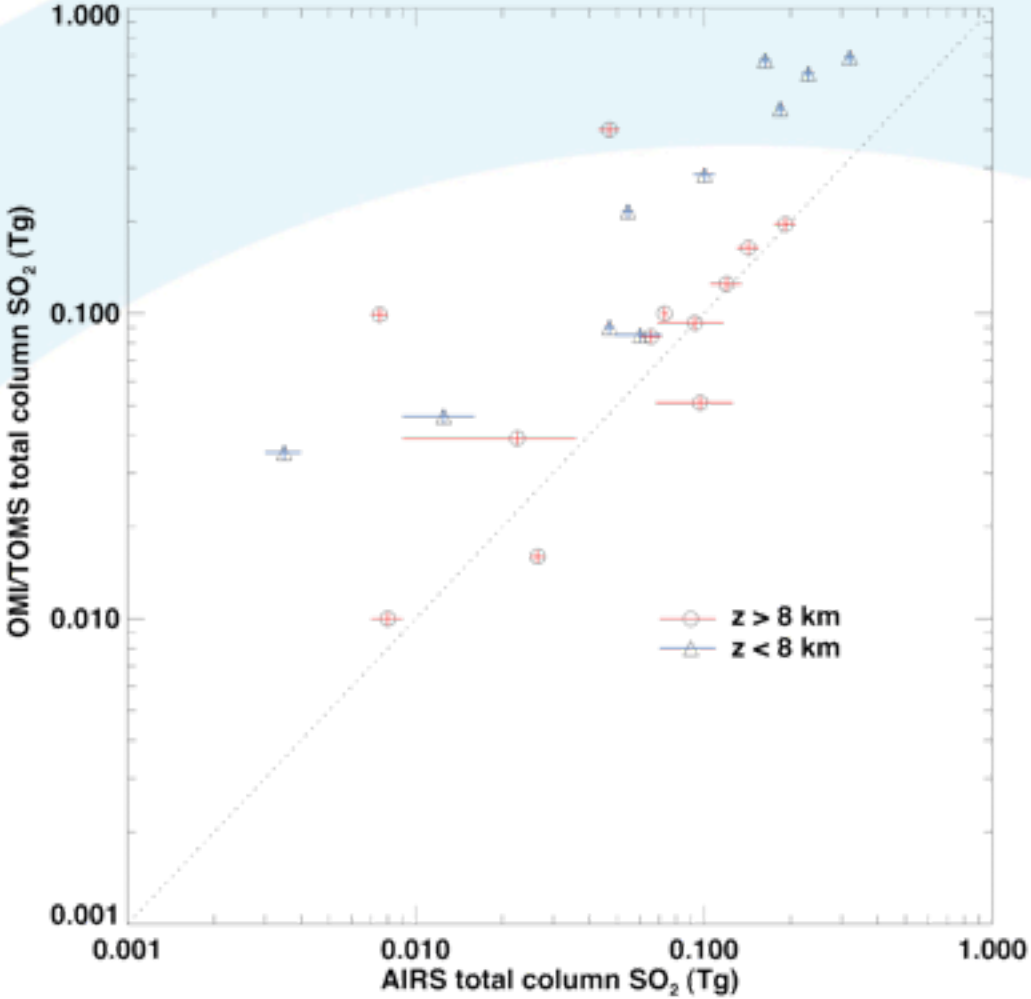
OMI/TOMS total column SO2 (Tg)
AIRS total column SO2 (Tg)
1.000
0.100
0.010
0.001
z > 8 km
z < 8 km

Other spectral regions

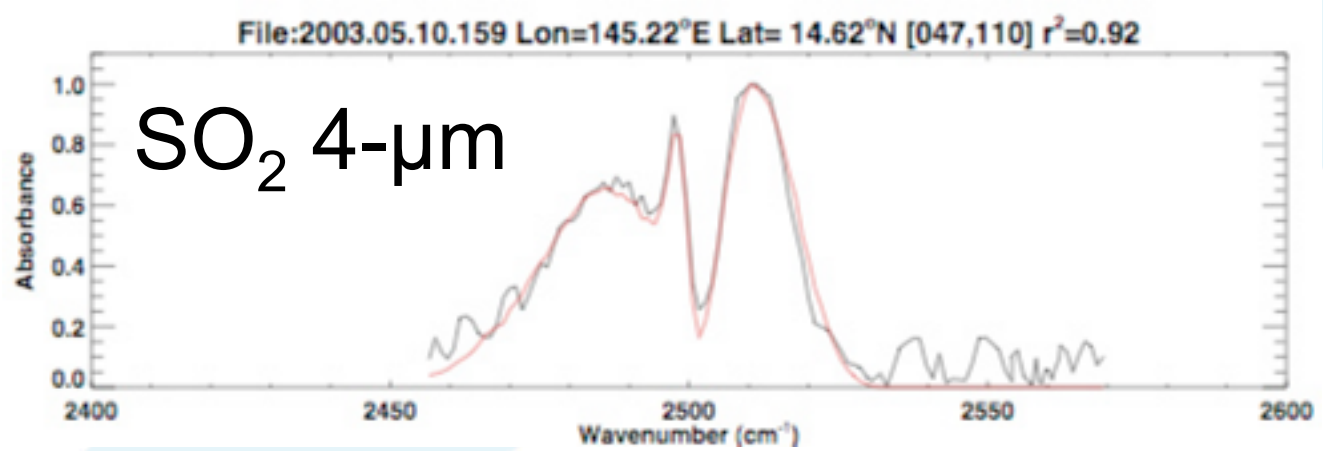

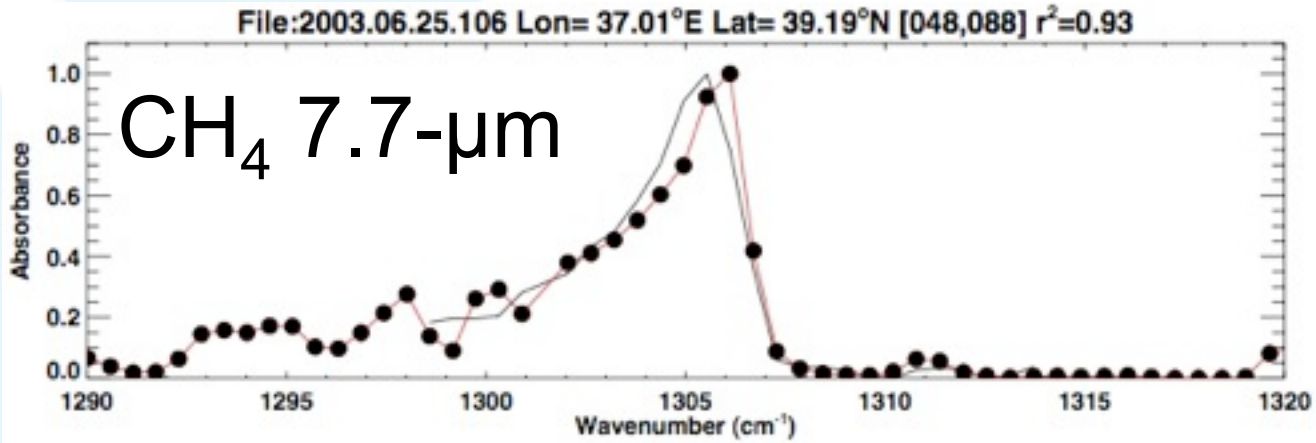

H_2S: 1332–1344 cm^{-1}

Al Mishraq Sulphur fire

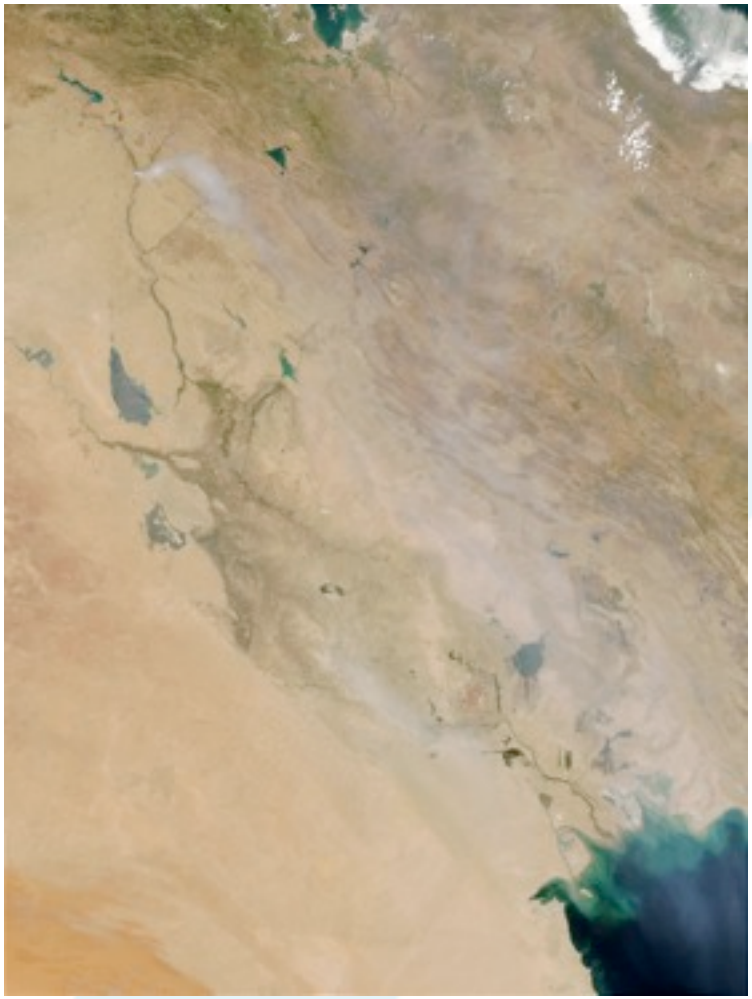

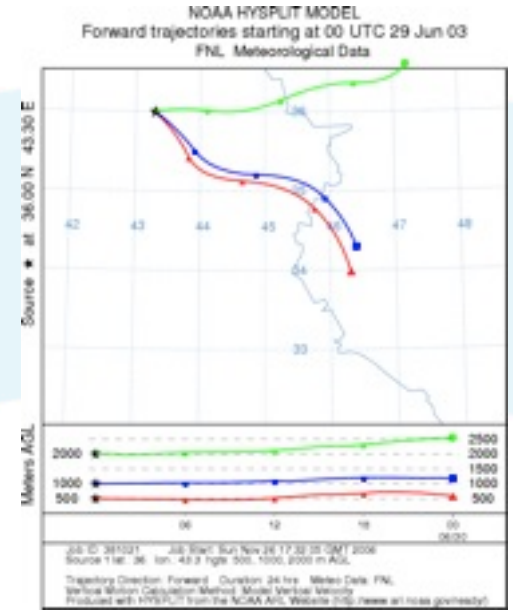

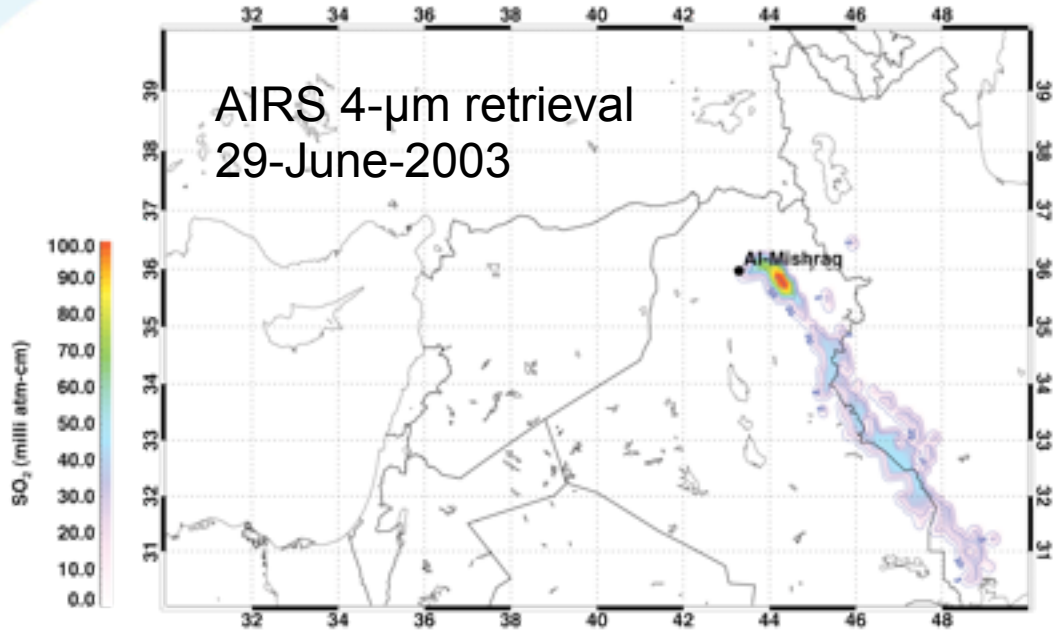

AIRS 4 µm

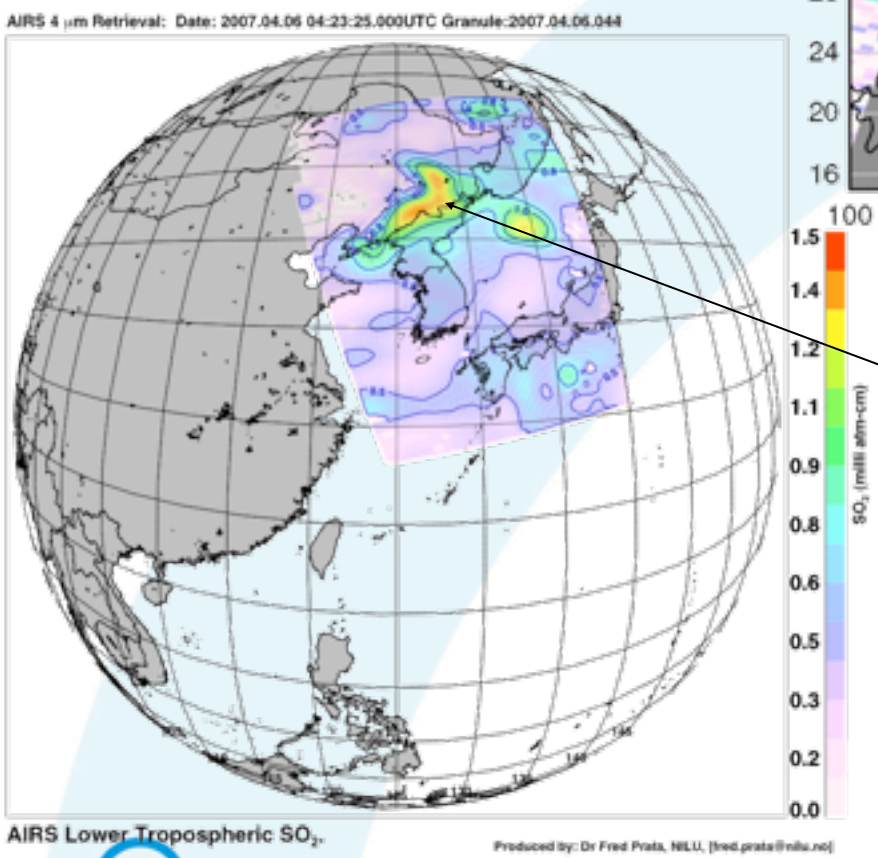

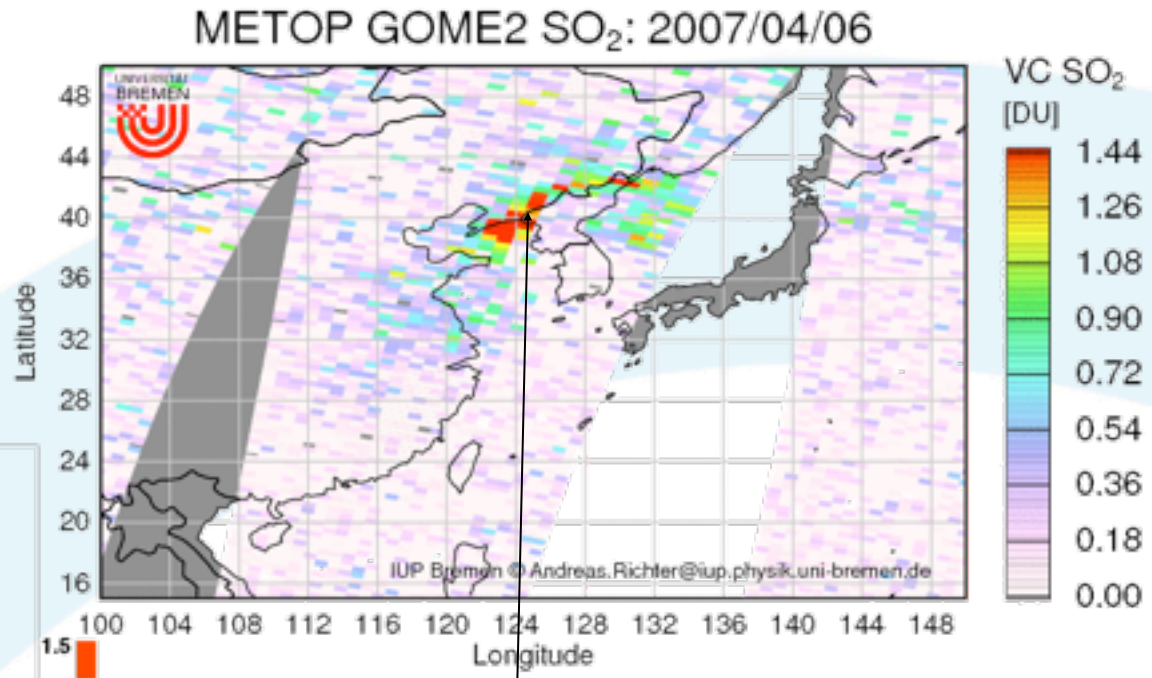

Anthropogenic SO_2 emissions

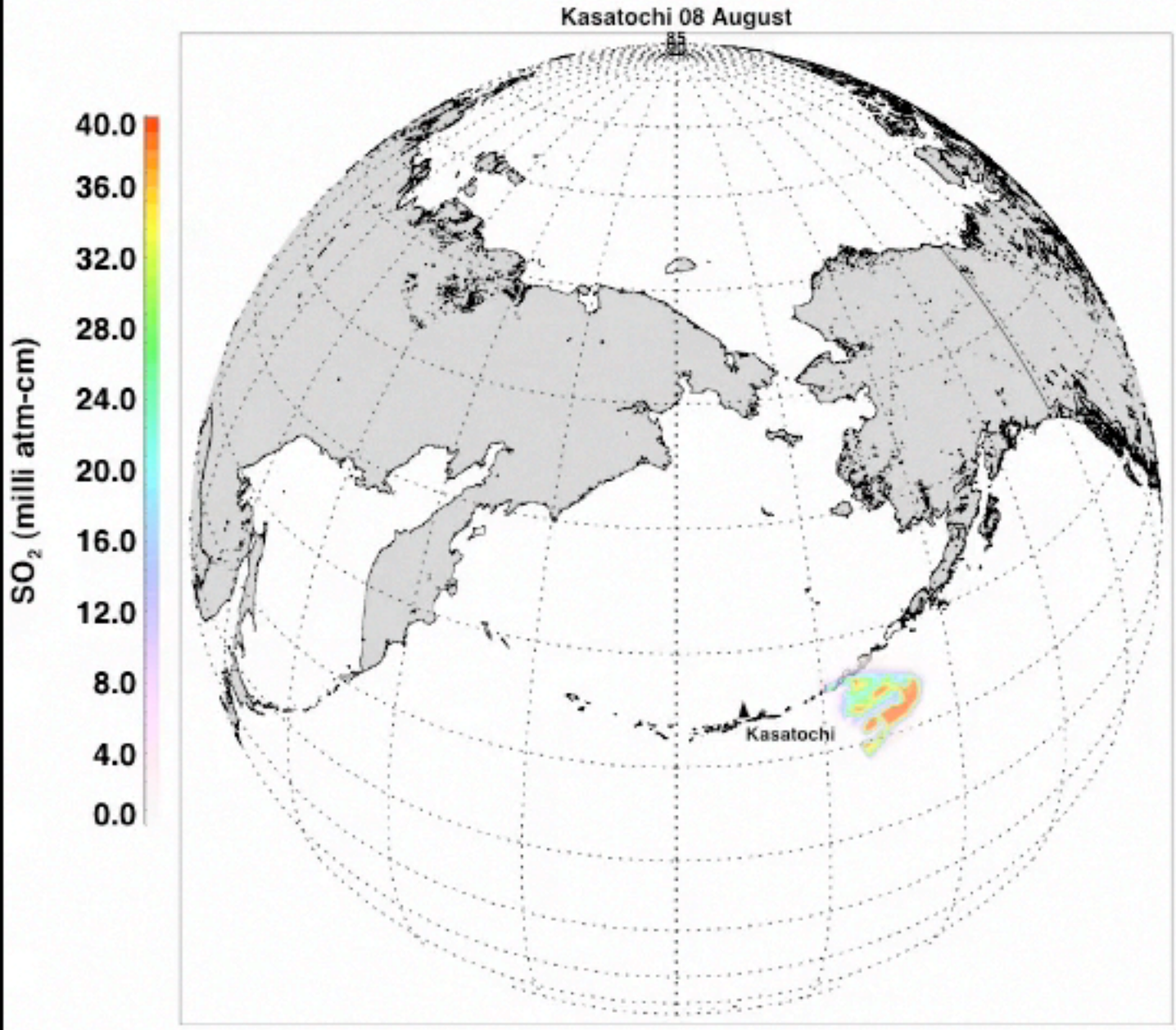
Kasatochi 08 August
85
40.0
36.0
32.0
28.0
24.0
20.0
16.0
12.0
8.0
4.0
0.0
SO2 (milli atm-cm)
Kasatochi

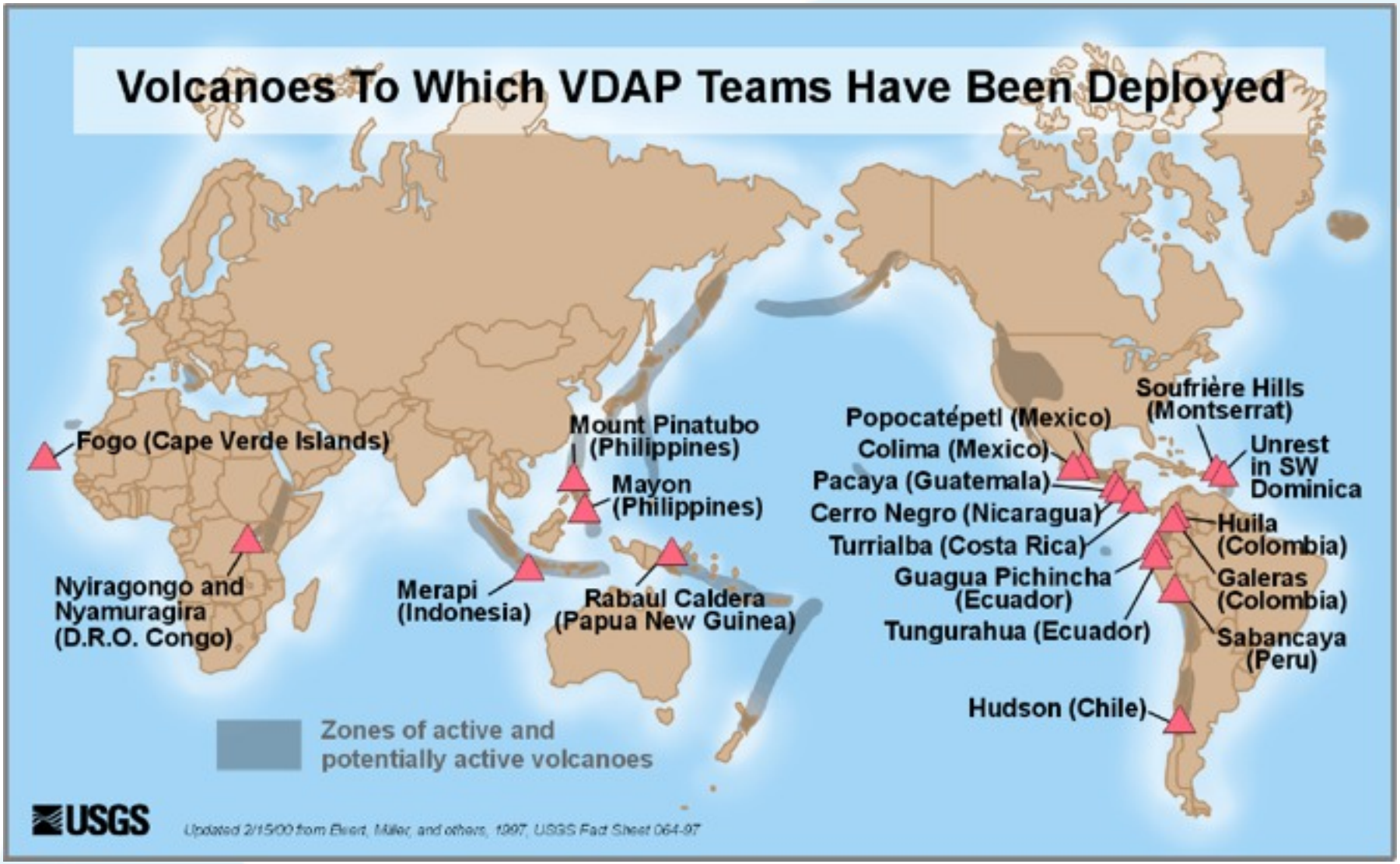
Volcanoes To Which VDAP Teams Have Been Deployed
Fogo (Cape Verde Islands)
Nyiragongo and Nyamuragira (D.R.O. Congo)
Merapi (Indonesia)
Mount Pinatubo (Philippines)
Mayon (Philippines)
Rabaul Caldera (Papua New Guinea)
Popocatépetl (Mexico)
Colima (Mexico)
Pacaya (Guatemala)
Cerro Negro (Nicaragua)
Turrialba (Costa Rica)
Guagua Pichincha (Ecuador)
Tungurahua (Ecuador)
Soufrière Hills (Montserrat)
Unrest in SW Dominica
Huila (Colombia)
Galeras (Colombia)
Sabancaya (Peru)
Hudson (Chile)
Zones of active and potentially active volcanoes
USGS
Updated 2/15/00 from Elliott, Miller, and others, 1997, USGS Fact Sheet 064-97

IASI – Dust detection (based on the concavity index)

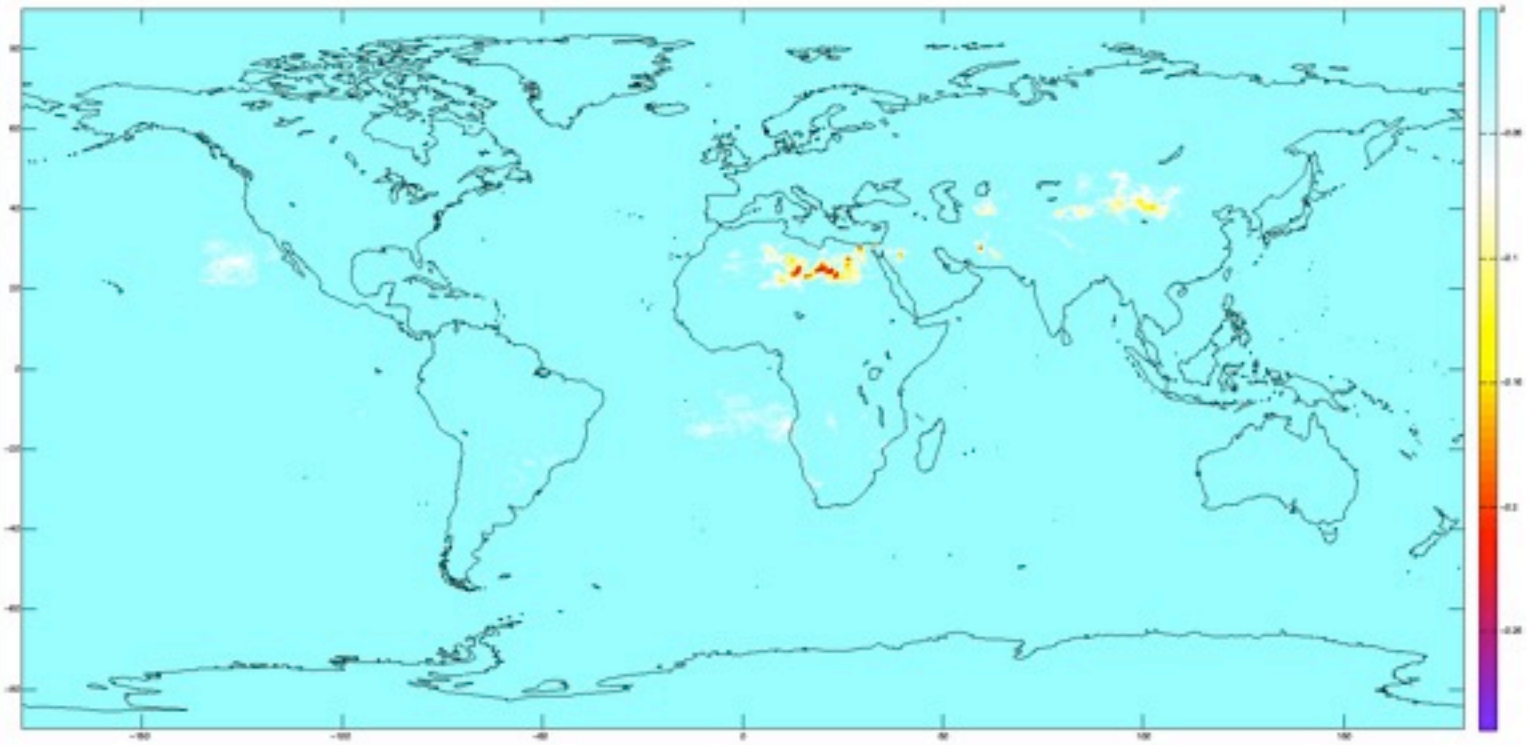

August 2008 pm.

(Courtesy Levien Clarisse)

Direct use of satellite SO_2 measurements

Climate sensitivity to volcanic forcing

$$DF = -A\ AOD(l)$$
$$AOD(l) = f(RH, l)\ Q_{ext}\ U_{SO_4}/C_{SO_4}$$

~SO_2 burden

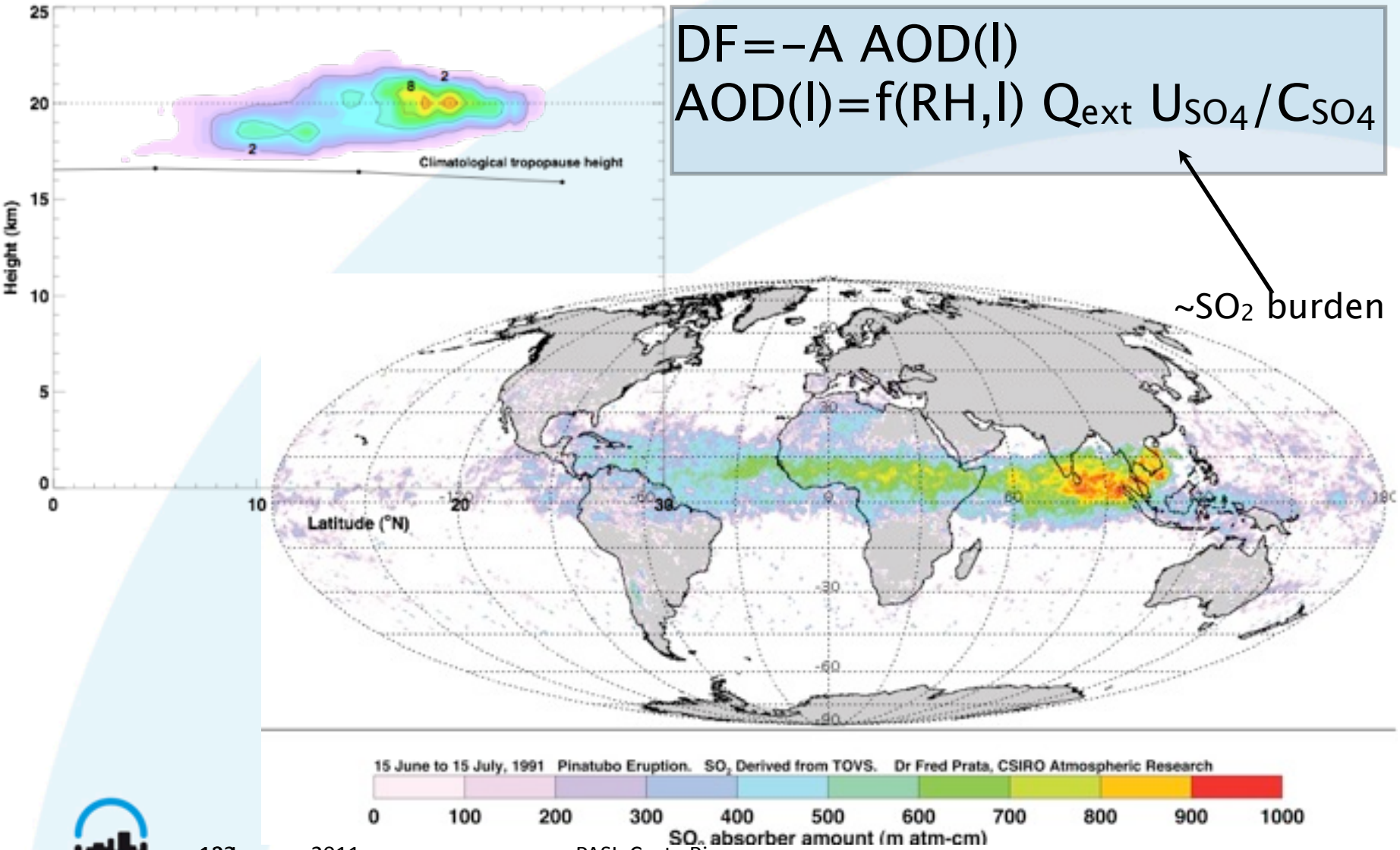

Other gases - HCl

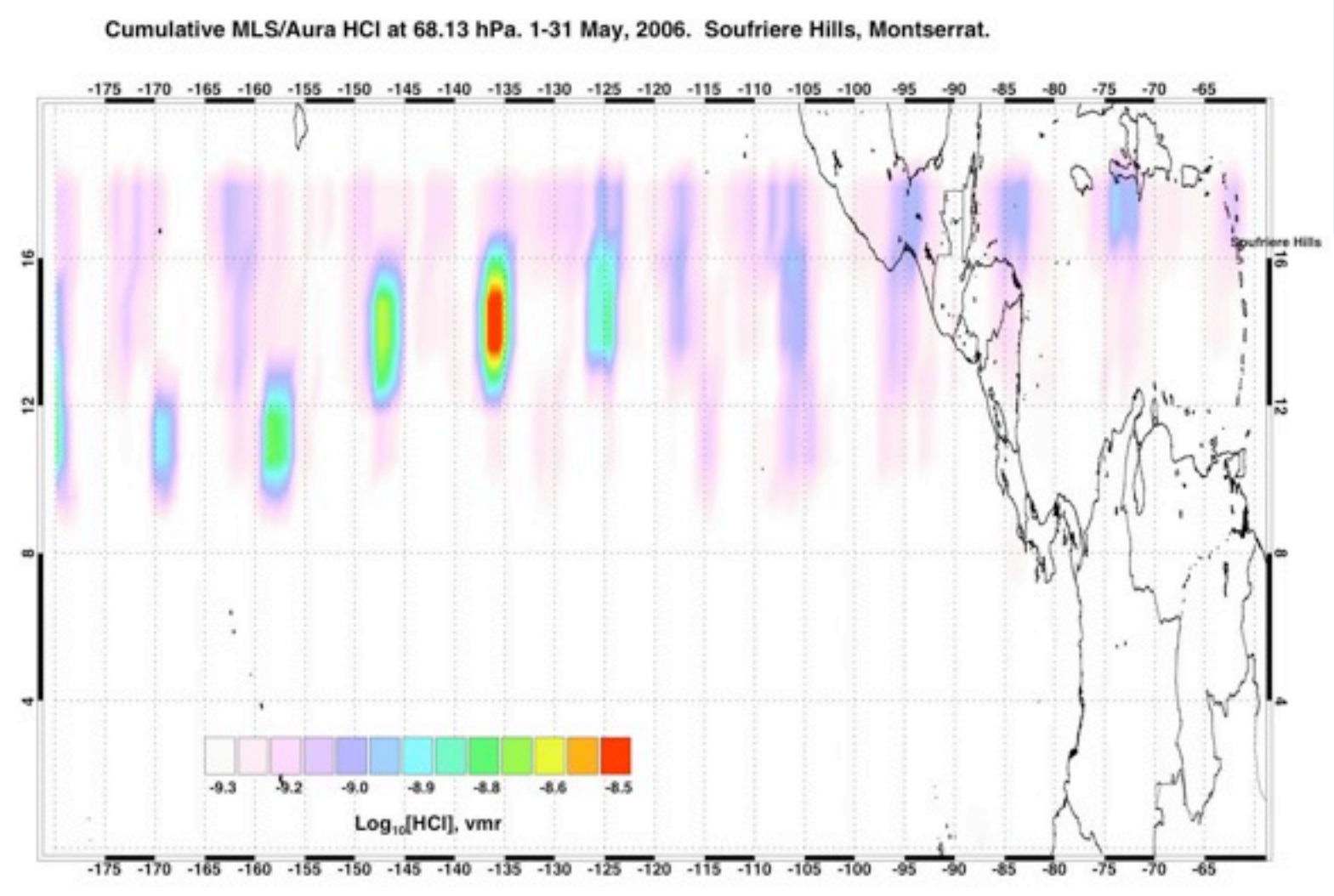

Prata, A. J., S. A. Carn, A. Stohl, and J. Kerkmann, 2007, Long range transport and fate of a stratospheric volcanic cloud from Soufriere Hills volcano, Montserrat, ***Atmos. Chem. Phys.,*** 7, 5093–5103.

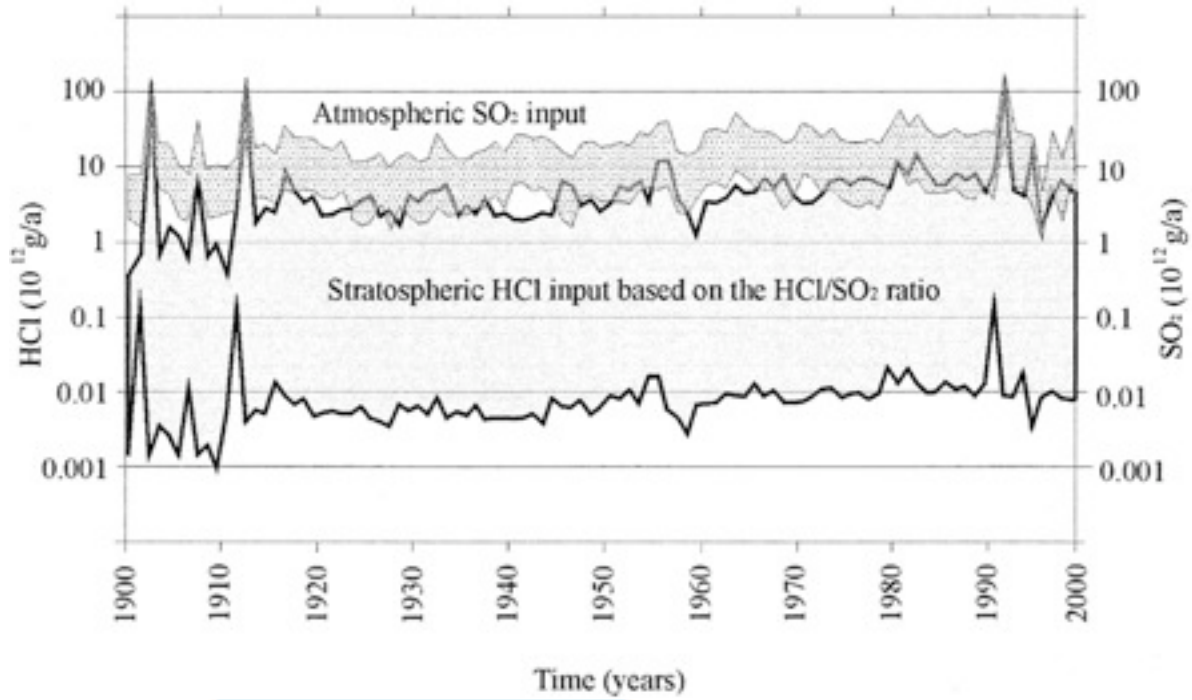

Assumes molar ratio of ~0.01 ($HCl:SO_2$)

Prata *et al*., (2007) find ~0.03-0.1 using MLS and AIRS data.

Annual global volcanic gas input into the atmosphere from 1972 to 2000 (this work)

	SO_2 (10^{12} g/yr)	H_2S (10^{12} g/yr)	HCl (10^{12} g/yr)	HF (10^{12} g/yr)	HBr (10^{9} g/yr)
Atmosphere	15.0–21.0	1.5–37.1	1.2–170	0.7–8.6	2.6–43.2
Stratosphere	2.4–4.0	0.1–5.0	0.1–12	0.03–0.4	0.04–0.07
Stratosphere with washout effect	2.1–3.2 (~25%)	0.01–3.8 (~25%)	$0.1–12\times10^{-3}$ (~99.99%)	$0.03–0.4\times10^{-3}$ (~99.99%)	$0.04–0.07\times10^{-3}$ (~99.99%)

Boundary layer SO_2 from AIRS

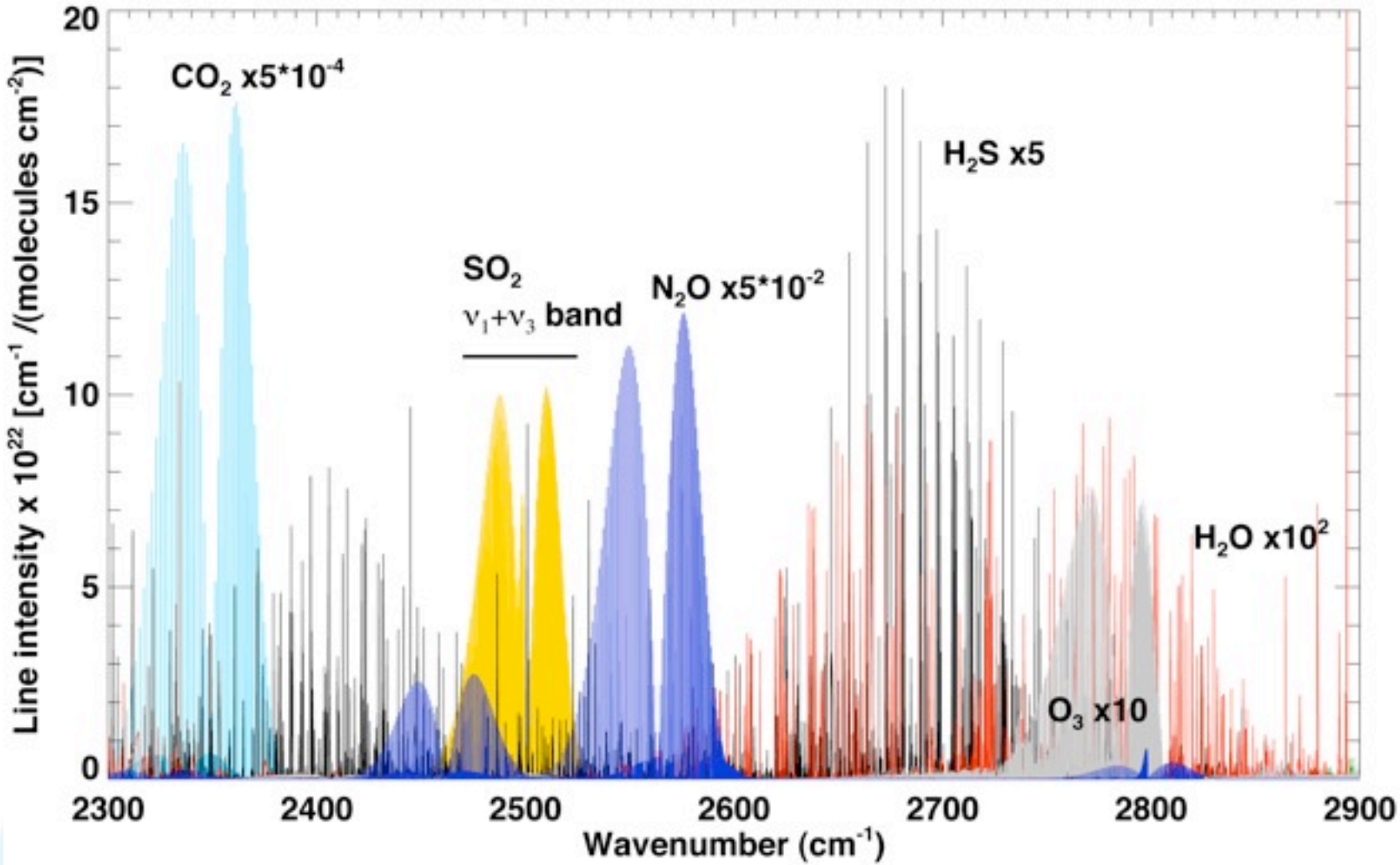

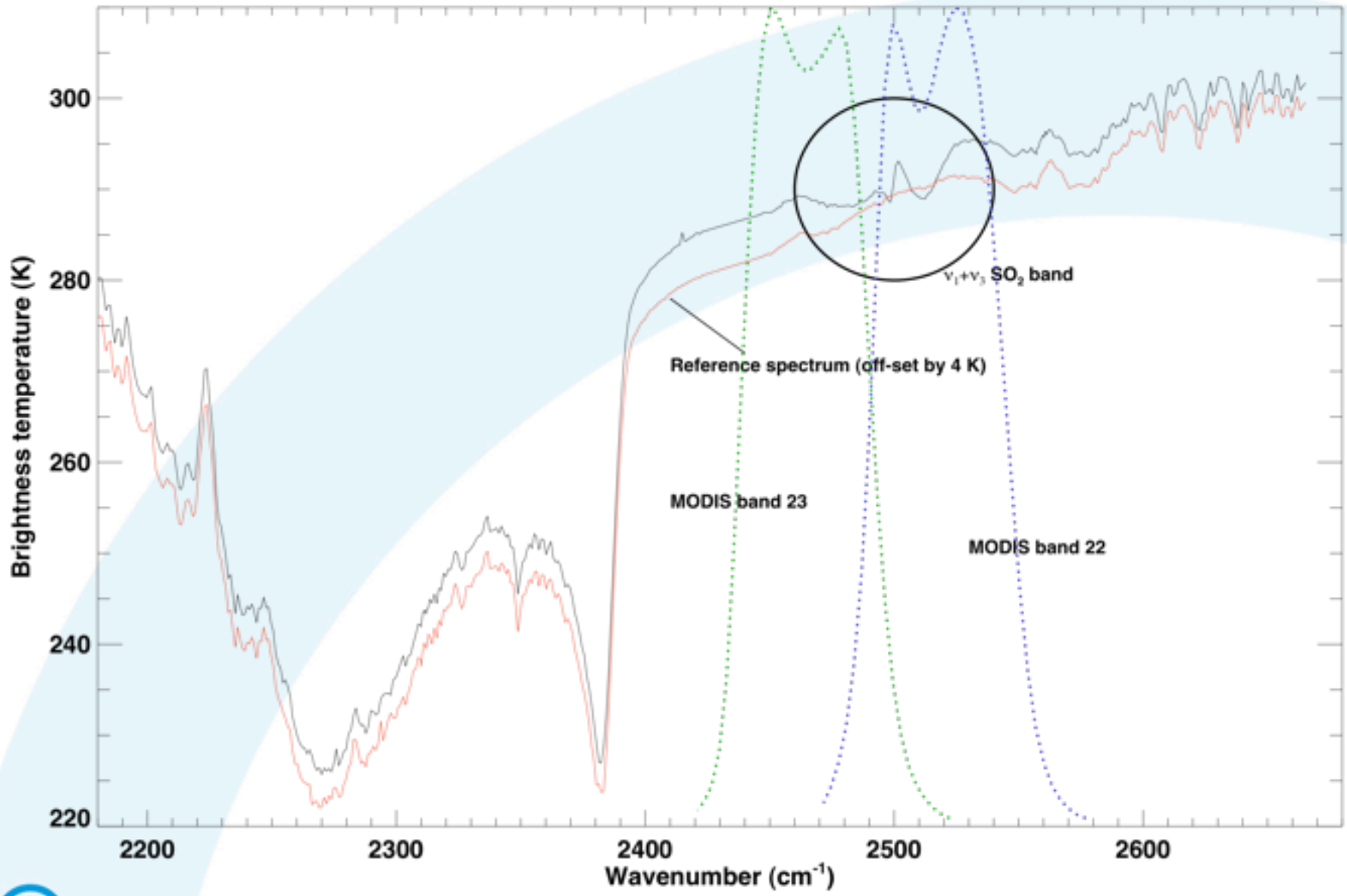
Brightness temperature (K)
300
280
260
240
220
2200
2300
2400
2500
2600
Wavenumber (cm^{-1})
$\nu_1+\nu_3$ SO_2 band
Reference spectrum (off-set by 4 K)
MODIS band 23
MODIS band 22

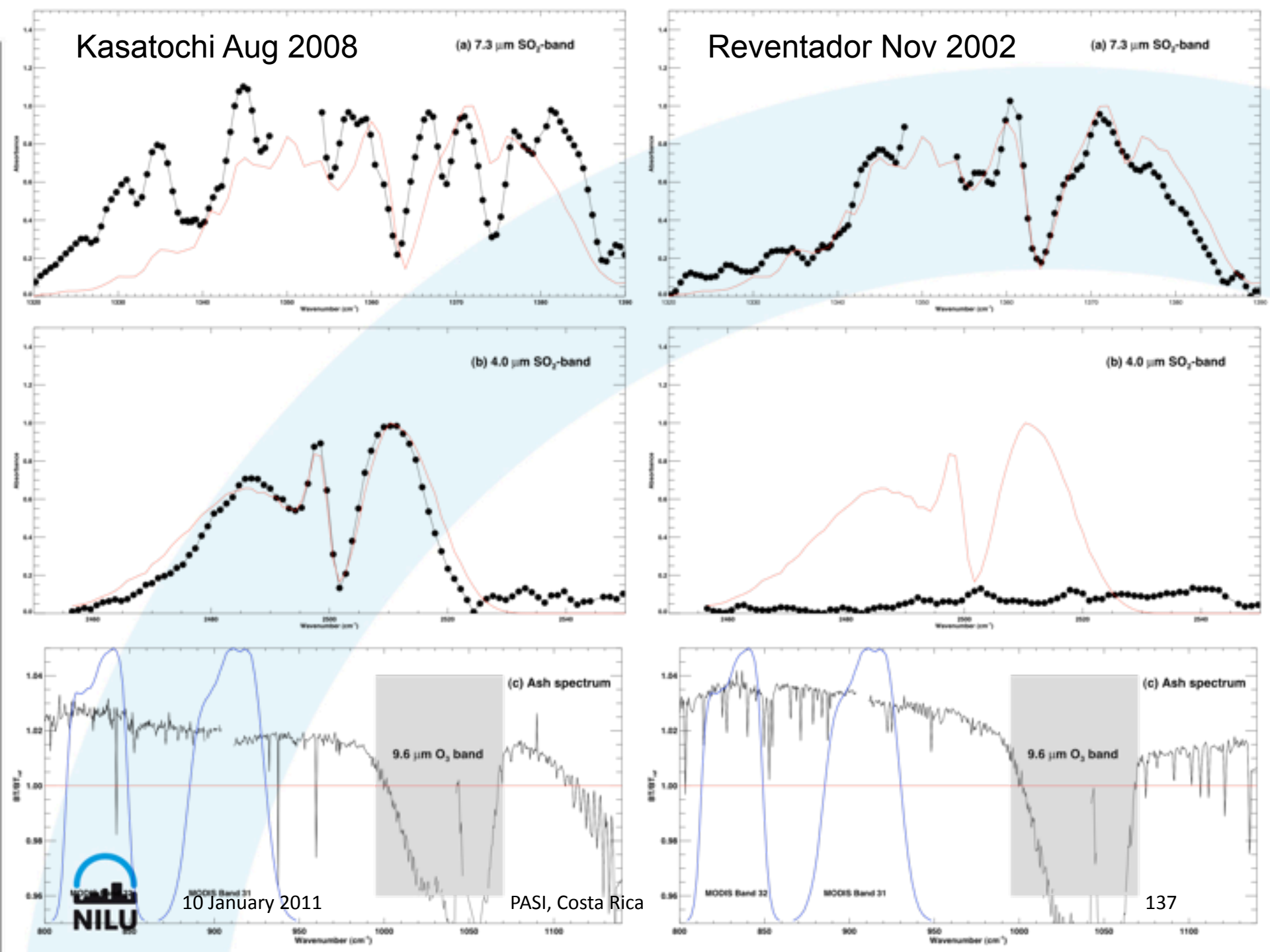
Kasatochi Aug 2008
(a) 7.3 μm SO2-band
(b) 4.0 μm SO2-band
(c) Ash spectrum
9.6 μm O3 band
MODIS Band 31
Reventador Nov 2002
(a) 7.3 μm SO2-band
(b) 4.0 μm SO2-band
(c) Ash spectrum
9.6 μm O3 band
MODIS Band 32
MODIS Band 31

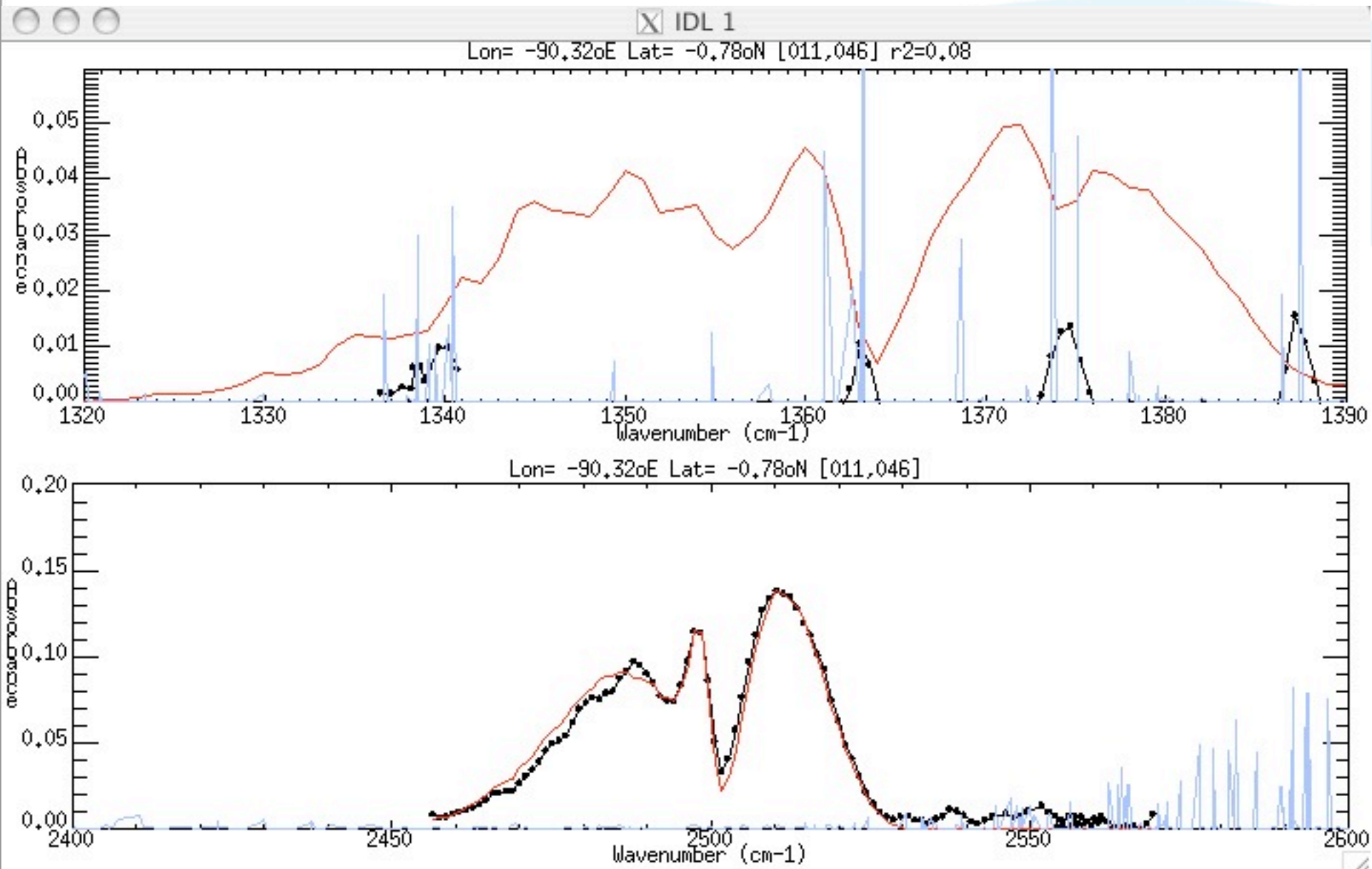
IDL 1
Lon= -90.32oE Lat= -0.78oN [011,046] r2=0.08
Absorbance
0.05
0.04
0.03
0.02
0.01
0.00
1320
1330
1340
1350
1360
1370
1380
1390
Wavenumber (cm-1)
Lon= -90.32oE Lat= -0.78oN [011,046]
Absorbance
0.20
0.15
0.10
0.05
0.00
2400
2450
2500
2550
2600
Wavenumber (cm-1)

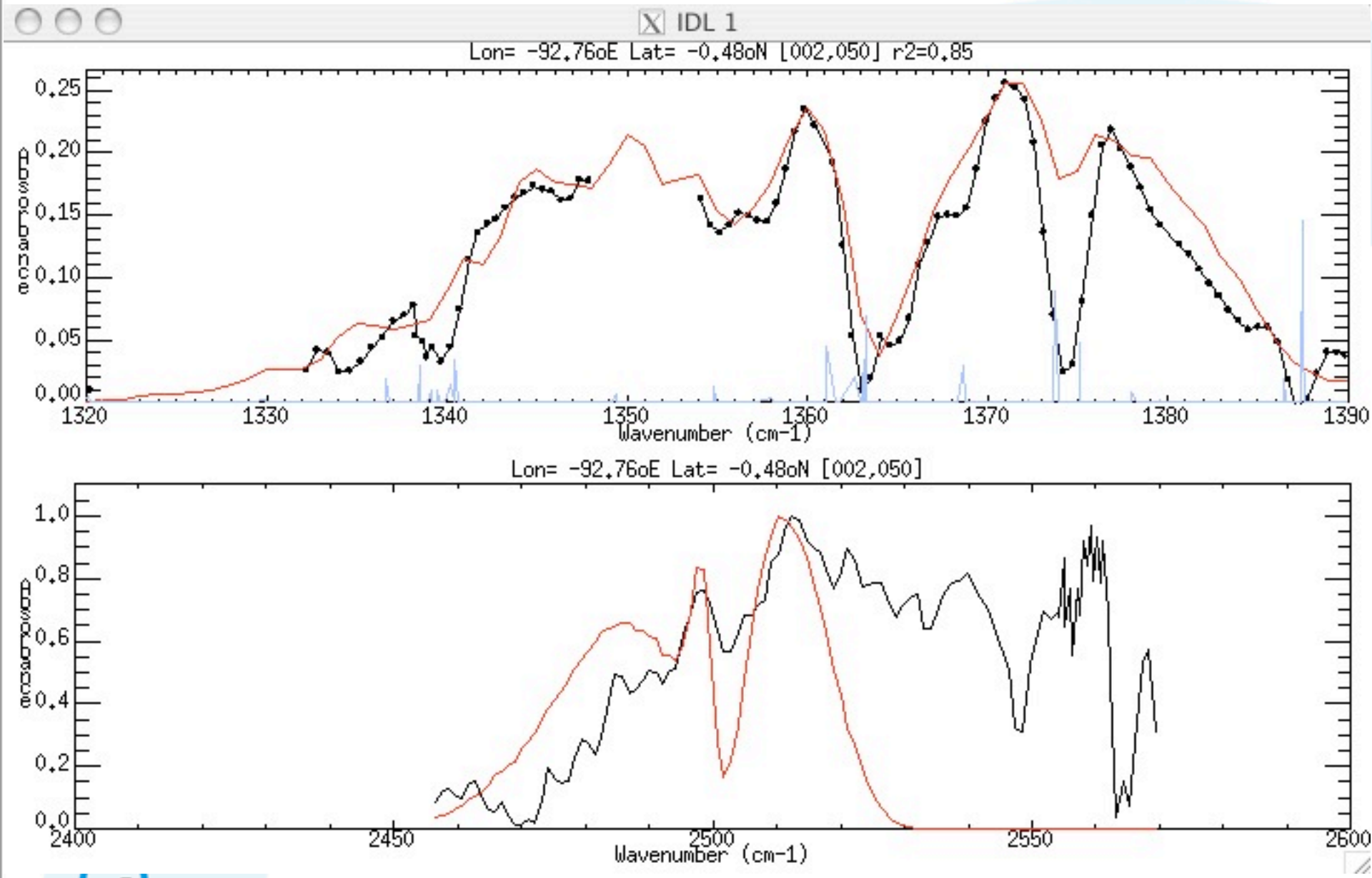
IDL 1
Lon= -92.76oE Lat= -0.48oN [002,050] r2=0.85
Absorbance
0.25
0.20
0.15
0.10
0.05
0.00
1320
1330
1340
1350
1360
1370
1380
1390
Wavenumber (cm-1)
Lon= -92.76oE Lat= -0.48oN [002,050]
Absorbance
1.0
0.8
0.6
0.4
0.2
0.0
2400
2450
2500
2550
2600
Wavenumber (cm-1)

Sierra Negra

23.10.2005

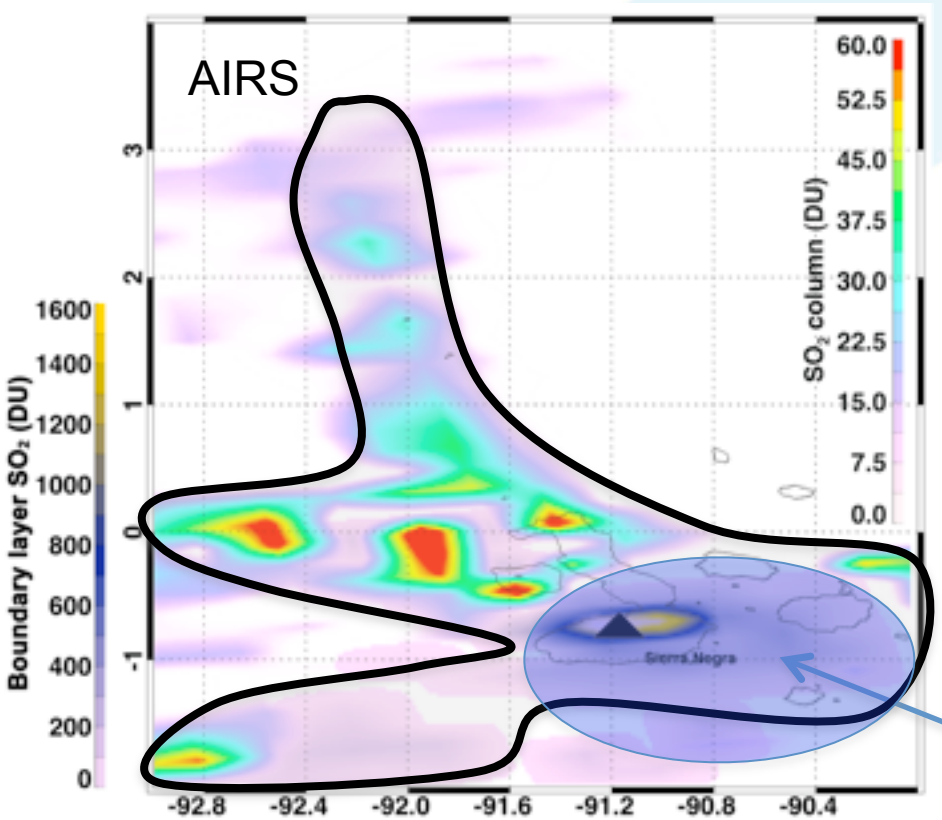

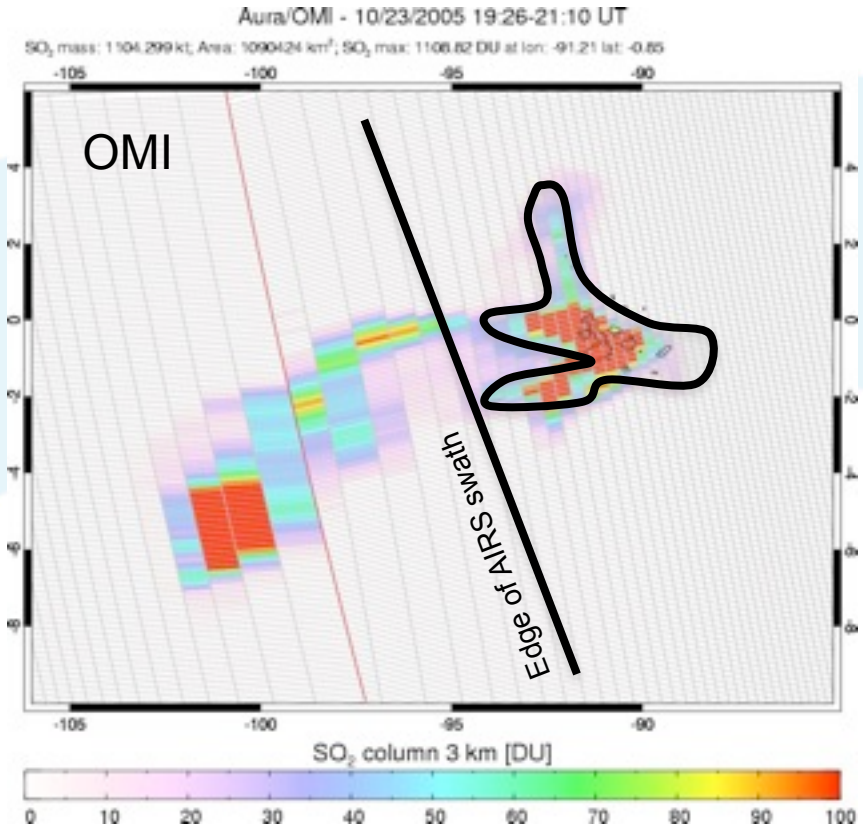

Boundary layer SO_2?

European volcano-related projects

Project	Lead (NILU involvement)	Funding (M€)	Funding Agency	Duration (yrs)
GlobVolcano	Italy (x)	0.8	ESA	3
Exupery	DLR (x)	0.3	ESA	3
SAVAA	NILU (✓)	0.5	ESA	3
MIA-VITA	BRGM-France (✓)	5	FP7	3
SAFER	French Consortium (✓)	23	FP7	5
PGP	Oslo U (✓)	5	NFR	5
NOVAC	Chalmers (x)	5	FP5	5

Further information

AIRS

Transport

OMI

SEVIRI

Aviation

UV imager

SO_2 Pinatubo

TOVS

- **Prata, A. J**., and C. Bernardo, 2007, Retrieval of volcanic SO_2 column abundance from Atmospheric Infrared Sounder data, ***J. Geophys. Res***., 112, D20204, doi: 10.1029/2006JD007955.
- **Prata, A. J.,** S. A. Carn, A. Stohl, and J. Kerkmann, 2007, Long range transport and fate of a stratospheric volcanic cloud from Soufri`ere Hills volcano, Montserrat, ***Atmos. Chem. Phys.,*** 7, 5093–5103.
- Carn, S. A., Krotkov, N. A., Yang, K., Hoff, R. M., **Prata, A. J**., Krueger, A. J., Loughlin, S. C., and P. F. Levelt, 2007, Extended observations of volcanic SO_2 and sulphate aerosol in the stratosphere, ***Atmos. Chem. Phys. Discuss***., 7, 2857–2871.
- **Prata, A. J**., and J. Kerkmann, 2007, Simultaneous retrieval of volcanic ash and SO_2 using MSG-SEVIRI measurements, ***Geophys. Res. Lett***. 34, L05813, doi:10.1029/2006GL028691.
- **Prata, A. J.**, 2008, Satellite detection of hazardous volcanic clouds and the risk to global air traffic, ***Nat. Hazards***, DOI 10.1007/s11069-008-9273-z.
- Tupper, A., I. Itikarai, M. S. Richards, **A. J. Prata**, S. Carn, and D. Rosenfeld, 2007: Facing the challenges of the International Airways Volcano Watch: the 2004/05 eruptions of Manam, Papua New Guinea. ***Weather and Forecasting***, Vol. 22, No. 1,175-191.
- Bluth, G. J. S., J.M. Shannon, I.M. Watson, **A.J. Prata** and V.J. Realmuto, 2007, Development